MOISTURE TRANSPORT PROCESSES AND CONTROL OF RELATIVE HUMIDITY IN REFRIGERATED FACILITIES

A thesis presented in partial fulfilment of the requirements for the degree of

Master of Engineering M.E

at Massey University, Palmerston North,

New Zealand.

Maumoon Sujau

2007

ABSTRACT

Increasingly air relative humidity (RH) is becoming an important design and operational variable for refrigerated facilities. An integrated dynamic model of the main heat and moisture transfer mechanism in a refrigerated facility was developed. Specific features of the model that enabled RH to be predicted were:

- Multiple air zones to represent variation of temperature and RH with position.
- A single zone evaporator model with dehumidification based on a straight line approach to the saturation condition at the surface temperature.
- Condensation and evaporation of water from surfaces and structures in the facilities.
- Evaporator defrost assuming that a fraction of the defrost heat melts frost and the rest heats the evaporator and refrigerant mass.
- Hot gas bypass with liquid refrigerant desuperheating to prevent the compressor operating into vacuum.
- Moisture sorption by packaging associated with the product.

The model was validated against data collected from a walk-in cool store 3.3m wide by 4.4m long by 3.0m high. The cool-store was cooled by an air cooled direct expansion HFC-134a refrigeration system with electric defrost, a suction line heat exchanger and electronic evaporation pressure regulating (EPR) valve for temperature control. To mimic the different design and operating conditions extra sensible and latent heat loads were provided by the cool store lights, up to 5 kW of electric heaters, and an ultrasonic humidifier.

For the validation room trials fan speed, coil size, sensible load, latent loads and temperature set point were varied. Other conditions were held constant as far as possible and the room was operated for at least two defrost cycles.

For the coolstore the model computed about 70 ordinary differential equations and more than 160 algebraic equations which were solved using Matlab 6.5, with the ODE45 solver.

The measured and predicted store air temperature, RH, refrigerant suction and discharge temperatures and pressures showed good agreement for most of the trials during both pull-down and the mainly steady-state operation between defrosts. Differences in measured and predicted RH and refrigeration system operating conditions were largely explained by uncertainty in model input data, measurements and calibration; and imprecision of the actual refrigeration control system and particularly the hot gas bypass capacity control and the expansion valves. This suggests that the model is a useful tool for the design and optimisation of passive or active RH control strategies for refrigerated stores.

Trials were also undertaken to quantify the effect of defrost frequency on the coolstore performance. Defrost efficiency and defrost duration were both proportional to defrost interval and doubled as defrost interval increased from 6 hours to 30 hours. For short defrost intervals; temperature control was poorer due to the frequent pull-downs. For longer defrost interval the room RH was lower and temperature control was poorer due to frost induced decline of evaporator performance. The optimal defrost interval for the particular cool store was 8 to 12 hours. Overall energy use did not change significantly due to the use of EPR temperature control and the low latent heat loads used.

ACKNOWLEDGEMENTS

I have received much help and guidance during this study project. First of all I would like to thank my supervisor Professor Donald Cleland, (Institute of Technology and Engineering, ITE, at Massey University) for taking me on as a post graduate student and for the help and discussions.

I would also like to thank the following persons for advice and assistance during the course of this project:

Dr Inge Merts, ITE, Massey University.
Dr John Bronlund, ITE, Massey University.
Dr Richard Love, Fresh Technologies, Massey University.
Dr Tony Paterson, ITE, Massey University.

Thanks for the assistance from the following during the experimental phase of the project that helped make data collection easier;

Mr. Bruce Collins, ITE, Massey University
Mr. Craig Bellhouse, ITE, Massey University
Mr. Leo Bolter, ITE, Massey University
Ms. Sue Nicholson, Fresh Technologies, Massey University.
Ms. Ann-Marie Jackson, ITE, Massey University

Thanks to Judd Refrigeration Ltd for the modifications to the refrigeration circuit to enable detailed monitoring of the coolstore.

Thanks to Massey University's Building Maintenance staff for the electrical modifications and installation of the electrical measuring sensors on the coolstore.

I would also like to acknowledge Fresh Technologies, Massey University for making available the coolstore used in this work.

Finally thanks to my eldest son *Masood* for helping me to debug the computer programme.

TABLE OF CONTENTS

LIST OF FIGURES

LIST OF TABLES

1 INTRODUCTION

Refrigeration is a widely accepted technology worldwide; historically it played an important role in the food industry as a preservation technology. The other areas of interest include comfort air-conditioning, industrial processes and heat pump technology with air-conditioning being the leading area of application due to demand for improved quality of living worldwide. Food refrigeration processes include chilling and freezing under controlled conditions and cool (>0°C) and cold (<-10°C) storage. There are alternative preservation technologies in the food industry but these technologies tend to change the product characteristics so refrigeration is likely to remain a key technology for a long time.

Temperature control has the highest priority in the operation of a food storage facility but increasingly improved control of air relative humidity (RH) and free moisture is being demanded. In particular, relative humidity affects the rate of evaporative water loss from unpackaged foods, and the strength of paper base packaging. Free moisture (condensation or ice) in an integrated facility is a concern from quality, food safety and operational safety perspectives. Air RH also influences the performance of evaporators due to frosting and the need for defrosting.

The overall objective of this research is to quantify the mechanisms for moisture transport in refrigerated facilities as the first stage of optimum design and control of facilities from an air RH perspective. The main focus will be refrigerated storage facilities (cool stores and cold stores) using air as the heat transfer medium.

2 LITERATURE REVIEW

2.1 INTRODUCTION

This chapter reviews the literature concerned with quantifying the transfer of moisture and control of air RH in refrigerated facilities. As shown in Figure 2-1 the effects of temperature and humidity are so intertwined that any attempt to quantify moisture transport must also consider other forms of energy transfer (e.g. sensible heat).

2.2 HEAT AND MOISTURE TRANSPORT IN REFRIGERATED STORAGE FACILITIES

Figure 2-1 shows the main heat and moisture transport mechanisms involved in refrigerated facilities (ASHRAE, 2001, Cleland *et. al.* 2002). These mechanisms are summarised in the following sections.

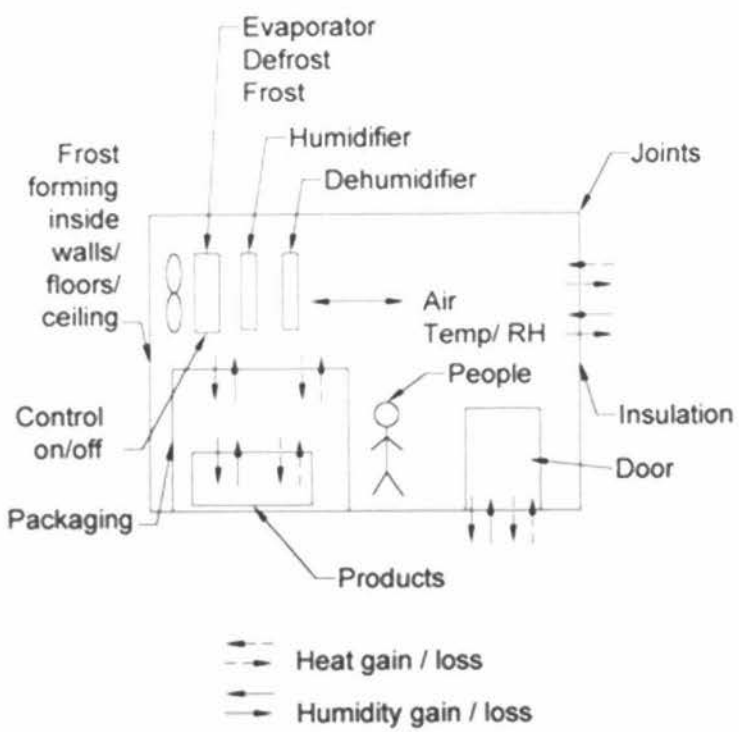

Figure 2-1: Schematic diagram of heat and moisture transport mechanisms in a refrigerated facility.

2.2.1 Evaporator

The evaporator is generally a finned tube air cooler with evaporating refrigerant in the tubes. As the air passes through the evaporator it is cooled and usually dehumidified. If the surface temperature is less than 0°C then frost forms. Frost build impedes air flow so eventually the evaporator must be defrosted. Defrosting inevitably results in some release of sensible heat and moisture back into the air. Therefore the evaporator involves heat and moisture heat transfer due to air cooling plus frosting and defrosting.

2.2.2 Frost / Condensate Formation on Inside Surfaces

The inner surfaces of a refrigerated facility comprises of all the partition walls, ceiling, floor and structures inside the room. If the temperature of room surfaces fall below the dew point temperature of the room air then condensation of water on the surfaces will occur and if it falls below 0°C, frost formation occurs. The condensation/frost may evaporate/sublime if the room air temperature decreases below the surface temperatures.

2.2.3 Air Infiltration

Infiltration of heat into cool stores/cold stores arises from exchange of warm and cold air through openings to the ambient due to natural convection. The common openings are doors, conveyor ports, cracks in walls and leaking gaskets in panel's joints or around doors. The main source of air infiltration is generally the door and open door access represents the biggest increase in refrigeration loads. Air infiltration involves transfer of both sensible heat and moisture (latent) loads.

2.2.4 Insulation

The walls, ceiling and floors in a refrigerated room act as a thermal resistance to heat transfer between outside ambient and low temperature conditions inside the room. The thermal behaviour of the surfaces depends on the thermal characteristics of the material in each of the layers of the surface. Low temperature applications such as food industry cool rooms are heavily insulated and these generally have low volumetric heat capacity but very high thermal resistance.

However many structures are made of concrete with significant thermal capacity. Steel or aluminium lining also have high thermal capacitance per unit volume.

2.2.5 People and Equipment Load

People or equipment working in the cool store/cold store adds heat loads. Heat and moisture loads from people are due to respiration, convection and radiation. Equipment includes lights, vehicles, and fan motors. Other than fans, equipment loads are generally considered as a small component of the total heat load, but these can have localised effects on the air and product temperature and relative humidity.

2.2.6 Product

There are two cases to consider for products. Firstly the product may enter the store at a higher temperature than the store air temperature and is cooled to the store air temperature. Secondly, there is the heat and moisture transfer once the product is close to storage temperature due to respiration, condensation or evaporation, and/or due to fluctuations in air temperature. The products can be either single product items or multiple product items stacked together.

2.2.7 Absorption / Desorption by Packaging

Packaging generally has negligible thermal capacity compared to that of the product. However packaging adds extra thermal resistance for heat transfer and acts as a source/sink for moisture.

2.2.8 Humidification

The ability to add moisture to the air to raise humidity is an important part of close control of air RH in some cool rooms. The need may be brought about by a change in the room RH conditions due to products and packaging, sensible heat loads or dehumidification in normal plant operation. Systems include steam humidifiers, spray foggers and ultrasonic humidifiers. Humidification generally adds both sensible and latent heat.

2.2.9 Temperature and RH Operating Point

The temperature is generally controlled by modulating the rate of sensible heat removal by the evaporator to match the rate of sensible heat entry by other mechanisms. If the refrigeration system is overloaded then temperature will increase above the set point until a new balance is reached between sensible heat entry and removal.

The moisture transport mechanisms can operate in either direction, although frosting or condensation on structures and the evaporators and absorption by packaging generally act to remove moisture, while air infiltration, defrost and product evaporative loss generally act to add moisture into a facility.

Figure 2-2 shows the relationship between entry and removal rates of moisture to a refrigerated air space and the air relative humidity of the facility. The RH in space varies to keep the rates of addition and removal the same. If the incoming moisture level is increased (e.g. with a humidifier) the RH in the space increases. On the other hand if the incoming moisture rate is lowered with constant removal rates the system moisture level decreases. Therefore RH can be controlled to the required level by the manipulation of a number of system parameters. Often this is not done so the RH floats depending on the moisture transfer balances.

2.2.10 Summary

The main mechanism for heat and moisture removal in an integrated facility is the evaporator. The performance of the evaporator is highly dependent on the performance of the mechanical refrigeration systems. Therefore to model heat and moisture transfer in a facility we must also model the mechanical refrigeration system.

In the following sections the literature related to quantifying (modelling) heat and moisture transport and refrigeration systems is reviewed. First, there is a broad discussion of modelling approach, then research on modelling integrated systems

(both the mechanical refrigeration system and the application it is refrigerating) is reviewed and finally the industrial mechanisms for heat and moisture transfer and component models are reviewed.

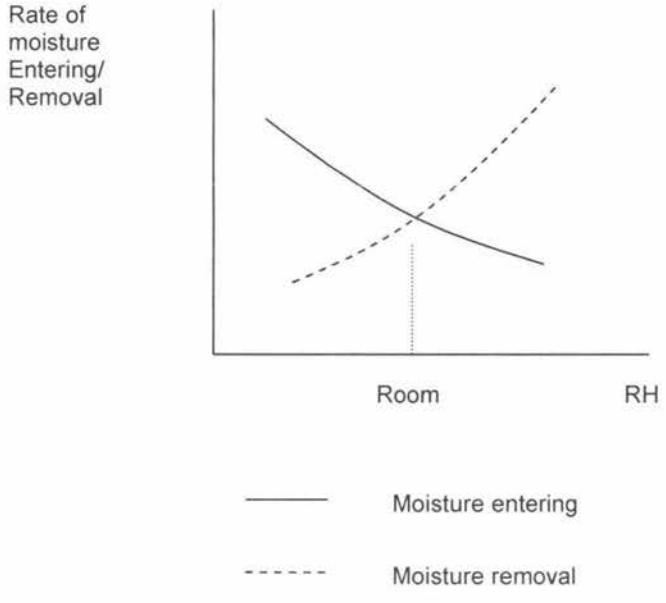

Figure 2-2: Rates of moisture entry and removal as a function of air relative humidity

2.3 MODELLING APPROACHES

The traditional design of cold storage facilities assume that a uniform temperature environment can be obtained in the conditioned space and product freezing and chilling times and refrigeration loads are evaluated on the basis of steady state conditions for a given set of external weather conditions. The actual heat load will increase above the mean for significant periods of time. The design should include some allowance for such peak loads or significant variations in operating conditions are inevitable. The control system in the facility is designed to maintain as closely as possible to the chosen steady state design conditions by following the time-variable performance of the plant (Cleland, 1990).

Experience shows that refrigeration facilities rarely perform at the expected design condition; often because transient performances are overlooked. Analysis of transient performance requires dynamic simulation.

Mathematical formulation of refrigeration systems can be based on either empirical (black box) or mechanistic (white box) approaches (Cleland, 1990). Empirical models assume system output variables based on input conditions without reference to internal operation of the system, thereby reducing the flexibility of the system as any changes to internal mechanisms often require a complete reworking of the model. Mechanistic models are based on fundamental laws and scientific principles to describe the internal working of the system. The advantages of mechanistic over empirical models are that they can be used for a wider range of systems applications or can be used beyond the limits of testing with greater confidence (Tanner, 1998).

Both modelling approaches often involve time and positional variability to describe a system. Time variability can be modelled by either step-wise steady-state modelling or full unsteady-state or dynamic modelling. The level of detail considered in dynamic models of refrigeration systems published vary to a large extend and those models with variables that are position-dependent show a broad range of complexity (Cleland *et al.* 1989). If positional-variability is required in detail then partial differential equations are considered. Otherwise the models can be formulated with ordinary differential equations or treated using simple lump-sum approach.

The accuracy of the model depends on the reliability of assumptions made and the quality of the information of system data input (Cleland, 1983). To include all physical effects in the model can be complicated and expensive; hence a simple model of the application incorporating most of the important effects can predict the

outputs as well as a more complete model where the input data is not accurately known.

Cleland (1990) proposed three groups, Type I, Type II and Type III, of refrigeration system models based on the level of detail and the balance between the mechanical refrigeration system and the application it serves.

Type I models consider the mechanical refrigeration system in detail, but use simple models of the refrigerated applications. The loads from the application are based only as a function of time and the interactions between the engine room and the application are largely ignored. The refrigeration system is modelled considering both thermodynamic and hydrodynamic aspects of the process.

Type II models consider the mechanical refrigeration plant in detail similar to Type I models but include complex models of the real dynamics of the refrigeration users and are usually the most complicated models.

Type III models include complex models of the real dynamics of the refrigeration users and use simple models for the mechanical refrigeration system (generally considers less hydrodynamic behaviour of the plant than Type I and II). These models are often described as 'thermal' models where as Type I and II referred to as 'mechanical' models.

2.4 OVERALL SYSTEM MODELS

Overall system models include both refrigeration system (compressor, evaporators, condensers, liquid receivers, pipe work, condensers and secondary refrigerant systems etc) and refrigeration applications (users). As refrigeration applications are the main source of time variability in plant performance, the total system dynamics cannot be modelled without considering the refrigeration system response to its applications. A refrigeration system will exhibit time–variability behaviour even with a constant cooling requirement at constant evaporation

temperature. The actual heat load over time profile is the result of interaction between mechanical plant and application. In general the installed mechanical plant will never accurately match the application. Therefore neither refrigeration applications nor refrigeration system can be modelled alone with independently derived time-variable heat loads. For accurate modelling both have to be considered simultaneously.

Refrigerant movement within the mechanical plant can be either modelled using algebraic equations assuming dynamics of refrigerant flow are of only negligible significance (quasi-steady state), or with differential equations based on unsteady state mass balance.

Cleland et al. (1982) developed a dynamic model for fish freezing and storage on board small fishing vessel and associated refrigeration system (compressor, condenser and evaporator). The air space within the hold was modelled as a single perfectly mixed zone; ordinary differential equations (ODE's) with lumped thermal capacity were used for product temperature, temperature of structures, ice thickness on the evaporator and freezing front position within fish. The compressor was modelled using algebraic equation. The model showed good agreement with measured data, although some lack of fit was found during loading times and close to start-ups.

Cleland (1983) developed a dynamic model for industrial refrigeration plants under variable load conditions (meat processing plant). The refrigeration applications included freezers, chillers and cold stores and controlled atmosphere work areas. The model used a combination of several ordinary differential and algebraic equations to describe the refrigeration plant and its interactions with its products for each application. It also takes into account a water vapour balance due to the wet nature of the applications by ODE's for air temperature and humidity. The air space was modelled as a single perfectly mixed zone. The model was validated by Cleland (1985) with data collected from a New Zealand meat processing plant with

a total refrigeration capacity of 2.5 MW. The air temperatures profile for freezing and chilling operations followed the same trends as the measured data except for immediately after step changes in plant operation.

The above model formed the basis for commercial computer simulation package RADS (Refrigeration Analysis, Design and Simulation) as described by Cleland (1985b) and Cornelius (1991). The RADS evaporator model assumes the air flow rate and heat transfer performance are independent of the extent of frosting, and humidity of air leaving the evaporator can be estimated by assuming a straight line approach of the air to the saturation condition at the mean evaporator surface temperature. The applications of RADS are heat load evaluations, multi-stage compression plant layout design, and simulation of the interactions between refrigeration systems applications and control systems.

Lovatt (1992) developed a computer program (RefSim) for complete environment simulation of industrial refrigeration systems. This was a major development for complete refrigeration systems. Most of the models were ODE's, and included moisture transfer models with single zones. Even though some of the models were based on the RADS package, an additional 16 new models were developed (Estrada-Flores, 1996). RefSim was found to be a flexible environment, which was general enough to simulate both simple and complex refrigeration systems. To test the whole simulation environment three refrigeration plants of different applications were surveyed to obtain data. RefSim predicted the measured data satisfactorily and was superior to those from other commercial refrigeration simulation packages. The differences between the predicted and measured values indicate that the uncertainties were more due to input data than model deficiencies.

Amos *et al.* (1993a) carried out steady-state analysis of sensible and latent heat entry and removal for a refrigerated cool store. The analysis was carried during four typical operating periods using the "Room" program of the RADS package (Cleland, 1985; Cornelius, 1991). The predicted RH was in good agreement with

the measured data. For the store studied the design and operational factors affecting RH the most were the evaporator surface area and the occurrence of precooling within the cool store. The next most significant factors were door management and floor insulation.

Kallu *et al.* (1993) developed a refrigeration modelling system applicable to the New Zealand meat industry, which accurately predicted the overall refrigeration system heat load and energy use versus time profiles for a "good practice" without resorting to an expensive and time consuming room-by-room analysis. "Good practice" was defined as the efficient use of the best refrigeration technology available to the industry at reasonable cost". The model was divided into four parts, prediction of product heat load, product related heat loads, base load heat loads and refrigeration system energy use. The forecasts were produced with very few plant-specific data, and virtually no room specific data. The model was validated against the modelled plant with a capacity of 250 beef animals per shift.

Amos (1995) developed a multi zone dynamic model to enable predictions of both the time and the positional variation of temperature and humidity in a large industrial apple cool store. The model used ordinary differential and algebraic equations to describe the refrigeration plant and its interactions with its products for the application. It estimated airflow between zones using fixed user defined pathways, and included water vapour transport as well as heat transfer; condensation on surfaces and water absorption by packaging. The frosting on the evaporator was modelled based on RADS, and assumed none of the heat supplied for defrost entered the cool store air. The product sub-model allowed movement of product batches during the simulation and accounted for differences in cooling rate within a batch. The model used a Proportional Integral (PI) control system. It was concluded that the use of 5 or 8 air zones appeared to be the best value between accuracy and complexity. The model was used to study the effects of design and operational features on cool store air temperature, humidity, product temperature and product weight loss.

Jakobsen (1995a, b, c) developed a dynamic simulation model of the behaviour of a domestic refrigerator and was validated against measurements on a 325 L unit. The model used ordinary differential and algebraic equations to describe the refrigeration plant and its interactions with refrigerated air space, ignoring frosting of the evaporator and air RH. The research included measurement of thermodynamic losses in the refrigeration cycle and various means of energy optimisation.

Becker *et al.* (1995) and Hasse *et al.* (1996) developed a mathematical model for dynamic processes in cold storage plants, which included mass and energy balance coupled with simple assumptions of heat and mass transfer. The model uses ordinary differential and algebraic equations to describe the refrigeration plant and its interactions with the application. The model consists of linked subsystems such as the cold-store air, goods, room structure, cold-store walls, evaporator, refrigerator and environment, and also included freezing of goods, frosting of the evaporator and the possibility of defrosting. The model was named SIMORES (Simulation Model of Refrigeration Systems) and was implemented using MATLAB as a numeric computation and visualization tool. The transient behaviour of the relative humidity and temperature was reported with two different controllers during the cooling period and for a defrosting period. Comparisons of the simulation to the experimental data for a medium-size cold store were in good agreement. The simulation model is suited for the investigation of the complex dynamic behaviour of cold stores and in the development of improved automation and control concepts.

Rossi *et al.* (1999) developed a dynamic model for air conditioners; the model involves set of ordinary differential equations for mass and energy conservation. The overall model also includes models for the compressor and expansion valve. The model captures the transient response during start up and shut down, and the results showed the effects of on/off cycling on cooling capacities and the

thermodynamic states of the refrigerant and air. It was validated for a 3 ton rooftop air conditioner.

Klein *et al.* (1999) developed a steady-state model for a 230 litre capacity domestic refrigerator. The model was based on basic conservation laws combined with experimental data for the compressor, the capillary tube-suction line heat exchanger and the cabinet heat gain. The results were consistent with the experimental data; however the model is system specific.

Jolly *et al.* (2000) developed a mathematical model of the refrigeration system in shipping containers for full load simulation of its steady state thermal performance. The key components such as compressor, evaporator, condenser and thermostatic expansion valve were modelled separately. These were coupled by the appropriate mass and energy transfer relationships to form the main model. The evaporator sub model considered the effect of changes in relative humidity of air. The cooling capacity tests were performed on a 40 ft full scale container housed in a temperature controlled environmental test chamber at an ambient temperature of 38°C. The results indicated good agreement with the experimental results and the simulation results fall within the 10% uncertainty of measurements. To increase the confidence level of the model it was recommended to validate at other ambient conditions and for different system configurations.

Lee *et al.* (2000) developed a steady state model for the performance analysis and simulation of an integrated automobile air conditioning system under various operating conditions. The model analyzed the performances of separate components and including a laminated type evaporator, a swash plate type compressor, a parallel flow type condenser, a receiver drier and externally equalized thermostatic expansion valve. The results indicate model of the integrated system was within 7% of the experimental results.

Koury *et al.* (2001) developed two numerical models to simulate the transient and steady state behaviour of a vapour compression refrigeration system. Time dependent partial differential equations of the system were obtained from the mass, energy and momentum balances for control volumes of the evaporator and condenser. Steady state models were applied to the components with low thermal inertia such as the compressor and expansion valve. The comparison between the terminal values of the transient model agrees with the predictions from the steady state model. The model could be used as an algorithm to control the refrigeration capacity and the degree of superheat of the system. The model did not include any moisture transfer as the evaporator was a water chiller.

Brooks (2001) developed a control strategy to schedule the supply of refrigeration to rooms containing frozen product to minimise electricity cost. The model used ordinary differential and algebraic equations to describe the refrigeration plant and its interactions with its products for the application. The total heat load included heat loads due to evaporator frosting. The results show the control strategy gave appropriate performance under a wide variety of potential operations and tariffs.

Bendapudi *et al.* (2005) developed a dynamic model of a centrifugal chiller system using the finite volume approach for both the evaporator and condenser (shell and tube heat exchangers). The overall system model also includes models of thermostatic expansion valve and centrifugal compressor. The model can be used to predict steady-state and transient performance under variety of loading conditions including start up and was validated using data from a 90 ton R134a centrifugal chiller. The prediction agreed well with measurements under most conditions in terms of the steady-state values and for the time constants of the transients.

Sieres *et al.* (2005) developed a window's based computer software for simulating vapour compression refrigeration system (SISREF). The programme can be self designed by the user and includes a library of different refrigerants and 10 different components; compressor, expansion device, condenser, evaporator, heat

exchanger, flash tank, direct intercooler flash tank, indirect intercooler flash tank, mixer and splitter. The main feature of the software is its user friendly interface, and the user can draw the system scheme by adding different components, connecting them and entering different input data. With these combinations different refrigeration system can be solved. The results are presented in the form of tables and the cycle diagrams drawn on log P – h or T – s thermodynamic charts. The software is intended to serve as a teaching aid.

2.5 COMPONENTS MODELLING

2.5.1 Air

Air is the most crucial component linking the source of heat and moisture transfer to the sink (the refrigeration system, particularly the evaporator) for any cool store or cold store.

Models of freezers, chillers and cold stores are based on the heat and moisture balances on the air in the application. There are methods that consider the actual air hydrodynamics due to forced convection (but not natural convection) and a more common modelling approach in complete models is the use of single perfectly mixed zone or several such zones with cross flow within them.

Single-Zone Models

Air can be treated as a perfectly stirred single-zone and often it is assumed that the change in density with temperature is negligibly small. One ordinary differential equation (ODE) is used for each of temperature and humidity by mass and energy balance. Cleland et al. (1982), Cleland (1983, 1985), Cleland (1985b) and Cornelius (1991), and Lovatt (1992) used a single fully mixed zone for representing air conditions in the room, meaning that any interaction with any other components model instantly affects the full room air volume.

Multi-Zone Model

In such models the cool store is split into a number of air zones. Air in each zone can be treated as a perfectly mixed. The main difficulties in multi zone model have been due to ill-defined boundary conditions between zones, with no physical barrier to stop air cross mixing. Hence there is a requirement for measurement or prediction of the rate of mixing between zones. The measurements and predictions of these flows between zones are difficult due to ill-defined air flow patterns, product stacking arrangements and the pattern of door openings in cold stores. Air transfers between zones have often been modelled as plug-flow along well defined air flow path (one dimensional plug flow) from the fan discharge to the intake.

Amos *et al.* (1993b) and Amos (1995) developed multi-zone models to quantify variations in air velocity, air temperature and relative humidity with position within a large New Zealand apple cool store. It was concluded that the most appropriate model for these type of cool store's would be a dynamic model in which a number of perfectly mixed zones are used to subdivide the air space into areas with large local heat sources.

Distributed (or Fluid Dynamics) Models

These models model the physical behaviour of a fluid, using conservation of mass, energy, momentum to express these as governing partial differential equations. Computational Fluid Dynamics (CFD) is a numerical technique for solving governing equations of fluid flow for a system with respect to both time and space discretisation and subject to appropriate boundary conditions. The airflow is predicted based on the Navier-Stokes equations for fluid flow using finite volume difference or control volume formulations in Computational Fluid Dynamics (CFD) packages.

Tassou *et al.* (1999) and ASHRAE (2001) provide outlines of the CFD technique and its application to refrigeration and HVAC industry. CFD is currently applied to

room air motion to predict parameters such as velocity and temperature distribution, air change effectiveness, and humidity for the comfort of the occupant. Other uses of CFD include external flow models to predict building infiltration, heat transfer rates for heating and cooling loads, and wind loads for structural design, and analyzing internal flows of non standard component.

Modelling based on CFD has been used by researchers and manufacturers of refrigerated display cabinets to investigate the performance of proposed design modifications, these models have been restricted to steady-state operating conditions (Xiang *et al.* 1998). CFD application to refrigeration industry has not yet gained wide acceptance due to the relatively small size of demand, high investment in software and the highly trained personnel required to make the application of CFD cost effective.

2.5.2 Evaporator

The evaporator is the main refrigeration system component linking the process and the refrigeration system. Other than direct cooling of a product, such as in a plate freezer, most evaporators cool air or liquids such as water, brine or glycol.

To maintain moderate or low temperatures in rooms, air is circulated through evaporator coil. In addition to the sensible loads, some moisture may be removed from air, either as liquid water or frost. This dehumidification process is an important characteristic of the air-water vapour mixture behaviour of air as it passes through an evaporator coils. The design of evaporator plays a crucial role in the performance of the system. There are a number of studies dealing with evaporator design and simulations. Crawford *et al* (1992) reviewed recommended procedures for the use of evaporators in refrigerated warehouses. The factors studied included evaporator design, effect of frost accumulation, defrost performance, fan effects, costs, air distribution and unit sizing. The results indicate main areas for future study was in the effect of frost, defrosting and air distribution.

Turaga *et al.* (1985) carried out a review of data and methods currently used in North America for the estimation of heat transfer and pressure drops for refrigerant evaporation (two phase flow) in the tubes and tube-bends of direct expansion coils (DX-coils). Generalized correlations of heat and momentum transfer phenomena on the refrigerant side of DX-coils are complex due to the continuously changing two-phase flow regimes and the presence of lubricating oil from the compressor. The results presented are limited in their accuracy and application to commercial coils. Further estimation of non-dimensional heat transfer and pressure drop coefficients for complete DX-coils (air cooling and de-humidifying applications) is presented. The review summarizes current estimation techniques for the case of smooth tubes in the absence and presence of oil.

Smith (1989) investigated the cooling of moist air at freezer temperatures by means of recirculatory air cooling systems calculated in accordance with the psychrometric procedure used by air-conditioning practitioners. It was found that:

- Airborne ice crystal forms during air-cooling process under certain operating conditions depending on the coil entering air temperature and moisture level.
- Room RH reduces at sensible heat ratios less than 1.0 with the lowering of coil surface temperature until a point is reached below which the RH ceases to reduce and increases instead.
- Under certain dry-bulb temperature and sensible heat ratio conditions room air can exist in a state of supersaturation regardless of coil design, refrigerant temperature, and circulated air rate.

The limiting of the coil surface temperature to its theoretical "psychrometric minimum" or to some higher temperature in order to avoid the psychrometric events stated above can be achieved by means of proper coil TD selection and subsequent refrigerant temperature control, except where load sensible heat ratio is fairly low. Use of dry surface type coils for the latter case requires raising the sensible heat ratio by additional means. Coil performance graphs and tabulations were prepared from calculations to avoid the low limit.

Smith (1992) investigated latent heat, equipment related load and applied psychrometrics at freezer temperatures. The heat loads created in the process of extracting moisture from air at freezer temperature were observed to be very large compared to the sensible heat gain from the moisture and may be very large compared to all other components of total refrigeration load. The high latent heat gain is common to most freezers with poor performance of the refrigeration system, very high RH and low coil refrigerant temperature.

Cleland (1990) reviewed the three most common models of evaporator and expansion valve combinations. These combinations are:

- Direct expansion evaporator with thermostatic expansion valve as a controlling device for refrigerant entry to the evaporator.
- Flooded evaporator with a level control device maintaining a constant liquid refrigerant level in the associated surge drum to control the entry of refrigerant to the evaporator.
- The liquid refrigerant is deliberately oversupplied to the evaporator by circulating pump from a liquid/vapour separator vessel usually with a throttling valve prior to the evaporator for the purpose of ensuring even refrigerant distribution. The pump system overcomes the pressure drop across this valve and a level control valve modulates entry of high pressure liquid refrigerant to the separator vessel.

The evaporator and control valve models vary in complexity for each group and are closely related. It was concluded that there is no point in using a detailed evaporator model with a simplistic control valve model. It was found a further development of models with increased complexity especially on the air side (including water vapour condensation) and refrigerant side would be an invaluable tool to designers of the refrigerant systems.

Jia *et al.* (1995) developed a general distributed parameter model to describe transient behaviour of evaporators. The model can predict distribution of the refrigerant velocity, void fraction, temperature, tube wall temperature, air

temperature and humidity for both the position and time domains. A two level iteration method was proposed to solve the numerical solutions instead of solving the non-linear equations simultaneously. The experimental work was carried out on a full-scale refrigeration system with R-134a as the working fluid. The results indicate that the model satisfactory predicted dynamic response compared to the experimental measurements, but underestimated the degree of superheat. The numerical method proposed was very stable and efficient.

Jia *et al.* (1999), Mithraratne *et al.* (2000), Mithraratne *et al.* (2001) and Liang *et al.* (2001) developed dynamic mathematical models to study the behaviour of dry expansion and counter flow water cooled evaporators. The models include two phase flows, thermostatic expansion valve (TEV) control, and complex refrigerant circuitry. Heat and refrigerant mass flows were described with algebraic and differential equations, but do not include moisture transfer modelling. The predictions of the simulation were in good agreement with the experimental data.

Ng *et al.* (1999) carried out experimental work to investigate an alternative low cost method to improve DX evaporator coil efficiency using TX valves under low TD (temperature difference) operating conditions. The method proposed was to install the SH (super heat) bulb for the TX valve after the SLHE (suction line heat exchanger) instead of the conventional method between the evaporator and SLHE. Results indicated the proposed method achieved stable operating conditions with lower TD and at the same time improved the evaporator performance compared to the conventional evaporator exit position. It is also shown that more precise selection of SLHE size is justified and best possible selection of SLHE will achieve improved evaporator performance and low TD operating range benefits without the risk of instability.

Kim *et al.* (2002) has reviewed the air-side thermal performance of finned tube heat exchangers, and further investigated airside performance of brazed aluminium heat exchangers under dehumidifying conditions. The experiments

evaluated heat transfer and pressure drop characteristics of wet surfaces for 30 samples of louvered fin heat exchangers with different geometrical parameters. The results of the test were compared to the dry surface heat exchangers in terms of sensible heat factor and friction factor as a function of Reynolds number based on louver pitch. The correlations for sensible heat factor and friction factor developed had root mean square errors of ±17% and ±14% respectively.

2.5.3 Frosting

The transfer of heat and moisture in an evaporator between air and a wetted surface, are shown in Figure 2-3. The dry bulb temperature of the air entering the section is T_i and its moisture content is H_i. The boundary layer of the air is in equilibrium with the water/ice on the surface. That is, it is saturated and at the same temperature as the surface, T_s, and the moisture content of the air at the surface is equal to the saturated humidity, H_s. The difference in temperature between the air and the wet surface creates a driving force for heat transfer. The water vapour pressure in air is proportional to the moisture content; H_i and the difference between H_i and H_s cause the transfer of water vapour between the bulk air and the boundary layer. It is generally accepted that the overall transfer process approximately follows close to a straight-line on the psychrometric chart (Figure 2-4). The straight-line law states the "the air path on the psychrometric chart drives towards the saturation line at the temperature of the wetted surface" (Stoecker, 1988).

If the temperature of the surface is below 0°C then frost will form rather than condensation. Otherwise the frosting and condensation processes are similar.

Industrial and commercial freezers for food distribution are subject to high frost formation inside and around the freezer doors, caused by the interchange of warm and cold air, especially when there are door openings. Essentially cold air from the freezer rushes out along the floor of the entrance, at the same time, warm and humid air rush into the freezer near the ceiling (Sherif *et al.*, 2001).

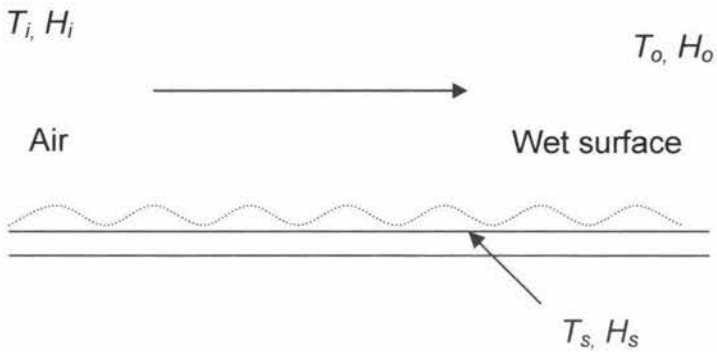

Figure 2-3: Heat and mass transfer between air and a wetted surface

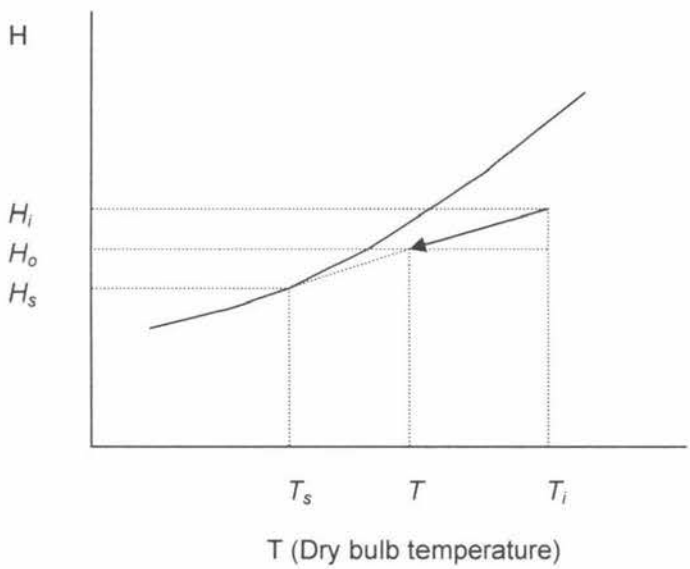

Figure 2-4: Psychrometric chart showing heat and mass transfer between air and wetted surface according to the straight line approach law

Sanders (1974) investigated the behaviour of air coolers with frost formation. It was concluded that the present state of knowledge was insufficient for an accurate theoretical approach to the process of frost formation in air coolers. A practical

approach would be to determine under accurately known circumstances the effect of frost formation on the behaviour of complete air coolers. The results of the investigation could be used to obtain operating characteristics of air coolers operating under conditions of frost formation, there by improving the functioning of cold stores.

Niederer (1976) investigated frosting effects on coil heat transfer under laboratory conditions, with refrigerant side cooling capacities based on ASHRAE Standard 25-68. The experiments were carried out with four different fin spacing coils with overfed liquid ammonia by mechanical pumps. The overfed ammonia eliminated superheat and kept the internal surface wet. The results indicate:

- Increase of heat transfer coefficient initially from frost accumulation and decrease of heat transfer coefficient by reduction in refrigerant flow were not the major causes of capacity variation when frost accumulated on the heat transfer surface.
- Decrease in heat transfer coefficient and the corresponding air cooler capacity was mainly to the reduced air flow.
- Wider fin spacing coils can operate for longer intervals between defrost periods at higher efficiency than closer fin spaced coils.
- Frost accumulation on the coil surface can adversely affect coil performances, it is recommended to provide sufficient equipment so that average capacity of the system will carry the design load.

Marinyuk (1980) investigated the effect of frost formation on heat transfer between a test cylinder and its gaseous environment. The main factors dealt within the study include total heat flux, the steady state convective heat transfer coefficient, and the mass of frost accumulating on the test cylinder and thermal conductivity of frost. The results indicate that the diffusion mechanisms of moisture transfer within the frost layer increases the frost density and thermal conductivity with time and that frost thermal conductivity is dependent on the formation temperature.

Kondepudi *et al.* (1993a, b) and Kondepudi *et al.* (1989) developed mathematical models to predict the performance of finned tube heat exchangers under frosting conditions. The frost model was detailed and included the heat exchanger characteristics, frost accumulation and its effect on energy transfer in relation to varying humidities, fin densities and ambient conditions. It was found that the analytical model under estimated the experimental results by 15% to 20% and these discrepancies could be improved by incorporating better frost thermal properties and airside heat transfer coefficients under frosting conditions Kondepudi *et al.* (1993 b).

O'Hagan (1994) carried out experimental investigations of the change in performance of a cooling coil under frosting conditions, and assessed the validity of the unfavourable frost formation theory proposed by Smith (1989). The theory states that unfavourable frost formation occurs when the line representing the temperature and humidity of the air passing through the coil, crosses the saturation line of the psychometric chart. This is more likely to occur under conditions of high relative humidity, low sensible heat ratio, and/or high refrigerant-to-air temperature difference. The frost formed under unfavourable conditions is low density and causes greater decline in coil performance for the same total frost accumulation than under favourable frosting conditions. Results confirmed the theory. Equations were developed to calculate the transition from favourable to unfavourable conditions. The measured rate of change of coil performance deterioration with frost formation appeared to be related to the lowest temperature on the coil surface rather than mean surface temperature. The types of frost formations were satisfactorily predicted using the refrigerant evaporation temperature as an approximation to the lowest coil surface temperature.

Fahlen (1995) developed a new methodology to investigate the variations in the frost density in frosted coils. The experimental method was based on continuously weighing the coil. The classic equations for pressure drop in dry coils provide a relation between pressure drop, flow rate and frost thickness, and with instant

value of the frost mass provides direct method to calculate frost density. The results with different air velocities, temperatures, humidities and cooling loads were similar to previously published data. The time dependence of frost growth shows the characteristic high density of frost at the start, density rapidly decreasing followed by a final increase. This method could be used to measure on line the effective density of the frost formed in ordinary coils.

Sheriff et *al.* (2001) investigated frost formation process on a finned-tube freezer coil. The frost formation theories were expressed using the results of the investigations and psychrometric theory, and a demarcation line was found to exist between snow like and more traditional frost like formation patterns. The benefit of the study was it could be used to develop a protocol that guides better refrigerating system design and more efficient operation.

Yun *et al.* (2002) developed a physical model of frost layer growth and frost properties with airflow over a flat plate at subfreezing temperature. An empirical correlation for average frost roughness was suggested from the experimental measurements. The flow patterns of airflow over the frost surface were shown to be turbulent. A modified Prandtl mixing-length scheme containing the effects of both frost roughness and turbulent boundary layer thickness was used to calculate the heat and mass transfer coefficients. The model can be used to estimate heat and mass transfer coefficients, frost thermal conductivity, frost thickness, frost mass concentration and frost density with relative to time and space. The results showed good agreement with basic trends of the test data taken from the literature.

Mago *et al.* (2005) investigated coil frosting issues at low freezer temperatures near saturation conditions. Extensive studies has been carried out on frost formation, very few studies looked into the formation mechanisms under supersaturated conditions while accounting for psychrometric effects. Frost formation under supersaturated conditions is in fact the result of superposition of

two distinct mechanisms. The first is diffusion-driven mechanism that results in transformation of water vapour into frost bypassing the liquid phase due to concentration (or humidity ratio) driving force between the free stream freezer air and the air in the boundary layer of the cold surface. This is the mechanism of frost formation under subsaturated conditions, and with higher humidity ratio in the free stream air and with lower the coil surface temperature, creates a larger driving force causing more rapid deposition of frost. The second mechanism is convection-driven and is the direct result of excess amount of moisture present in air beyond the saturation point at the existing air temperature, this can only exist either as suspended liquid droplets (mist) if the air is above freezing point of water or as suspended ice crystals if the air temperature is below freezing point.

Xia *et al.* (2005) investigated air-side thermal-hydraulic performance of louvered-fin, flat-tube heat exchangers with sequential frost growth cycles. The study included two different heat exchangers; both circuited in a cross-flow configuration, air flow horizontal and the tubes vertical. The first heat exchanger had a manifold at the top and the second had manifolds at the top and bottom of the heat exchanger. The performance under frosting conditions was periodic and repeatable after the third or fourth frosting cycle. This was due to the periodic distribution of liquid water at the end of defrost, and the roles of frost growth and water retention on the surface. The thermal-hydraulic performance depended on heat exchanger geometry for the two heat exchangers and further work was required for a broader range of geometry.

2.5.4 Defrost

Evaporator coils are prone to frost formation due to the water vapour in the air condensing and freezing when the surface temperature of the evaporator coil falls below 0°C. Frost accumulations deteriorate the coil performance by both reducing the airflow through the coil and insulating the surface thereby reducing the refrigerating capacity of the unit. Hence, evaporator coils need to be defrosted

periodically to maintain system performance and temperature control. Defrosting creates certain disadvantages (Machielsen *et al.*1989):

- The equilibrium condition in the refrigerated space is disturbed due to the non-continuous operation of the air cooler and causes deviations in the desired values of temperature and humidity.
- Formation of fog and ice at walls ceiling and on cooled goods, due to the chimney effect with electrical defrosting.
- Heating and also expansion of the refrigerated air can lead to high pressure in relation to the pressure outside and this effect is greater if the fans start immediately after the defrosting process. This can result in damage to the warehouse and in causing permanent leaks.

Sanders (1974) have found the following phases occurred during defrosting processes:

- The surface and frost layer is heated and reaches a temperature of 0°C, as soon as it reaches 0°C the frost melts and is absorbed into the frost layer.
- The saturated frost layer starts to melt from the wall or surface creating an air gap, while ice is formed on the surface exposed to refrigerated area.
- The air gap and ice layer becomes larger, when the heat transfer by conduction and radiation is greater than the free convection heat transfer, the ice melts completely.

The most widely used methods of defrosting industrial refrigeration systems are:

- Air
    - For small systems operating above 0°C, natural heating from the cool room space is used to melt the frost with the refrigeration system switched off.
    - Ducted ambient air is circulated through the coil to defrost the evaporator using dampers.
- Electric heating by electric heating elements threaded through the coil block.

- Water-spraying a high flow rate of water or anti-freeze solutions on the cooler surfaces to melt and wash the frost off (the water may be heated).
- Hot gas, evaporator internal heating by passing hot refrigerant vapour from the compressor discharge.
- Combined hot-gas/water defrosts.

The defrosting process in refrigeration systems is most frequently controlled by a preset time cycle; due to its simplicity, reliability and low cost. Timed defrost cycles have the disadvantage of operating unnecessary cycles when frost formation is low and reduces the energy efficiency of refrigeration system as well as the accuracy of the temperature control. On the other hand on demand systems only defrosts when necessary, thereby reducing the number of defrost cycles and the amount of energy used. Tassou *et al.* (1998) reviewed the demand defrost techniques, and found the techniques has not gained wide acceptance by the refrigeration industry for food retail sector in general, due to its excessive capital costs and reliability problems related to the complex and unreliable sensing methods.

Sanders (1974) investigated the theoretical defrosting process for a one dimensional case for hot gas and electrical defrosting methods. Results indicate the possibility of forming air gaps between the evaporator wall and frost layer is much greater for thick frost layers, in turn causing longer defrosting period. However thick frost layers improve the defrost efficiency. With small frost layer thicknesses it is less possible that air gaps will occur. It is more likely for the frost layer, saturated with melting water to stick to the evaporator wall. This could lead to shorter defrosting times on one hand or less favourable defrosting efficiencies to occur. Since the air gaps has detrimental effect on defrosting time it is not recommended that defrosting efficiency be restricted to a high value but the aim should be to avoid air gaps during the operation of air coolers. A lower defrosting efficiency with shorter defrosting time is more advantageous than a too long duration of the defrosting period (too long interruption of the operation) caused by

air gaps. Under certain circumstances complete defrosting of air coolers is impossible, particularly in the case of hot gas defrosting. It was concluded that the present state of knowledge was insufficient for an accurate theoretical approach to the process of defrosting of air coolers.

Niederer (1976) investigated defrosting effects on coil heat transfer with hot-gas and electric defrosting under laboratory conditions. The results indicate that only 15% to 25% of the heat required to defrost was in fact carried out by the condensate and the rest lost to the surrounding refrigerated space and to heat up the metal of the coil and cabinet of the air cooler. It is recommended that the heat load for defrosting of the coils must be considered in the initial design of heat load.

Stoecker *et al.* (1983) investigated the energy considerations in hot gas defrosting of industrial refrigeration coils. The tests were carried out on a laboratory R-22 system and in field tests of an ammonia system. It was shown that the pressure differences across the coil lower than currently used in industry can achieve satisfactory defrost. A hot gas pressure 100 kPa above the setting of the outlet pressure regulator was found to be adequate for R-22 and ammonia systems. A lower setting of the outlet pressure regulator can also lower the inlet pressure and still stays within the 100 kPa recommended pressure difference giving higher defrost efficiency. The drain control should remove liquid from the coil as rapidly as possible and prevent vapour from passing back to the suction line.

Cole (1989a) and Cole (1989b) investigated heat and mass transfer and fluid flow mechanisms involved in the hot gas defrost process in large commercial freezers with ammonia as the refrigerant. It was found that 80% of the energy required during defrosting is added into the refrigeration system as added load and less than 20% for defrosting. The maximum achievable defrost efficiency was in the range of 60% to 75% with different configuration of evaporators coils, different sizes and construction materials and the amounts of frost. The main losses are due to heat and mass transfer into air in the refrigerated space and refrigerant vapour bypass

into compressor suction. Designers or operators can minimize the above effects by controlling evaporator defrost relief pressure, hot gas supply pressure and defrost duration. Operating costs can also be minimized by preventing or minimizing the bypass of gas to the suction. Nomographs were produced with the results to estimate refrigeration loads due to heat losses and associated costs.

Machielsen *et al.* (1989) analysed the defrosting behaviour of frosted air coolers with forced air circulation based on Dutch Standard NEN 1876. Using the effective refrigeration capacity, two dimensionless numbers were derived to give the optimum cooling period before defrosting starts.

Ditchev *et al.* (1998) analysed various method of defrosting currently used and proposed a new efficient hot gas defrosting system. The method was validated under industrial operating conditions. It uses a special compact vapour transformer to regulate the temperature of refrigerant feeding into the evaporator with automated defrosting modes. The transformer is fed with hot gas from the compressor discharge through an internal heat exchanger on the suction line. This enables the condensed refrigerant to completely evaporate before entering the compressor.

The advantage of this system was:

- Its simple in design and highly reliable compared to conventional defrost system
- Fast and uniform defrosting of the whole heat exchanger surface.
- Smaller distance between the fins (3-4 mm) decreases the overall heat exchanger dimensions and related costs.
- Cold room temperature can be maintained very accurately due to fast and uniform defrosting, and all heat exchange surfaces are efficiently used.
- Compatible with all types of evaporators and water-and air-cooled condensers and can be employed in both new and existing refrigeration equipment.

- Defrosting time does not depend on the ambient conditions compared to the classical hot-vapour defrosting methods.

Tassou *et al.* (1998) also investigated demand defrosts control systems, by field measurements in supermarket multi-deck cabinets and controlled tests in a laboratory environmental test chamber. The parameters that could be used for defrost initiation were identified as:

- Environmental conditions of temperature and relative humidity. It was seen that the condensate increased with both ambient temperature and relative humidity.
- Duration of the previous defrost cycle. A short defrost cycle indicated a small frost built-up on the coil and slow frost growth operating conditions, whereas a long defrost cycle indicated a heavy frost built up on the coil and high rate of frost growth operating condition. Duration can indirectly indicate the optimum frequency of defrost for a given cabinet and operating conditions.
- Divergence between the air temperatures just after the coil and the air temperature at some point in the test chamber after a period of operation between defrosts. This divergence was mainly due to the reduction in the air flow through the coil arising from excessive frost built-up.

Additional work is required to validate the strength of these parameters, in terms of repeatability, both in laboratory and actual supermarket conditions.

Argaud (1999) compared experimentally the two main methods to initiate defrost, using a time delay and using the temperature difference between the air and the evaporator for reversible air/water heat pumps. Under most favourable system conditions for France such as air at +3°C with relative humidity 85%, where the frosting is relatively important the two methods gave virtually the same starting time. With dryer conditions the second method improved the energy savings by 10%.

Hoffenbecker *et al.* (2005) developed a mathematical model for a frosted coil to determine the energy requirement for hot gas defrosting. The model was scaled-up based on a single fin surface. The model predicts defrosting time for complete melt of the accumulated frost and the sensible and latent heat load transfer to conditioned space during defrosting. Predictions compared well with actual defrost cycle field measurements and to the results previously published studies. The results from the analysis for the present model showed an optimum hot gas temperature as a function of accumulated mass and density of frost on the evaporator. The other interesting outcome was the model predicted that the mass of moisture re-evaporated back to the space increases with decreasing hot gas temperature. This behaviour was due to the prolonged defrosting time to complete the full melt of accumulated frost. The results from this model indicate the defrosting energy can be minimized by reducing defrosting time.

Mago *et al.* (2005) investigated experimentally coil defrosting issues at low freezer temperatures near saturation conditions with hot gas. The study compares defrosting in supersaturation and subsaturations conditions. One method suggested was to use dampered coils, this increased the defrost efficiency by up to 43%. The other method was to use higher coil-face velocities, where the frost had a crystal structure that makes it more likely to collect in the melt pan during defrosting than to sublimate back into the freezer space. Lower coil-face velocities during defrosting was likely to result in significant amount of moisture transfer to the freezer space and/or a structural collapse of chunks of frost on the freezer floor, resulting in a smaller amount of collected melt and a correspondingly smaller defrosting efficiency.

2.5.5 Air Infiltration

Air infiltration through open doors into refrigerated facilities significantly affects the design, operation and performance of such systems. The warm moist air entering the room need to be conditioned to the desired conditions, this additional heat load

increases the capital and operating costs of the system. The moisture from the moist air deposits as frost on the evaporator reduces the efficiency of the system and has to be removed periodically by defrosting and may also deposits as ice or condensate on the floors, walls, ceiling and products creating a safety hazard and unpleasant environment thereby reducing productivity.

Infiltration reducing devices such as air curtains, strip curtains, impact doors, fast operating doors, and vestibules reduce doorway infiltration in cold storage facilities and hence refrigeration load.

Gosney *et al.* (1975) investigated heat and enthalpy gains through cold room doorways continuously open and opened on various timed cycles. The experimental work was carried out using two scale models of different sizes to represent cold room with carbon dioxide as a tracer gas to predict air flow and air exchanges. The model developed predicted air interchange more accurate than previous research work.

Hendrix *et al.* (1989) investigated infiltration heat gains through cold storage room doorways in particular to natural convection process, viscous, thermal effects and transient behaviour, and to verify the predictive ability of existing analytical models and door way protection devices. The field trials were carried out on full size working cold storage rooms with wide ranging operating conditions. The practical importance of the results indicates knowledge of steady-state doorway air velocities and temperatures may simply be used to determine cold room infiltration heat gain. The results also indicated the Gosney and Olama model predicted the closest to the experimental results. Good agreement was found with those previously published on door protective devices.

Cleland (1990), Amos (1995) and Estrada-Flores (1996) reviewed air infiltration through open doors for refrigerated facilities. Using Tamm's equation a theoretical estimate can be predicted for air infiltration through open doors; experimental

measurements have shown that the prediction is normally higher than what occurs in practice (Cleland 1990).

Downing *et al.* (1993) investigated the level of effectiveness of cold-storage door protective devices based on the model by Gosney *et al.* (1975) for air exchange for an unprotected doorway under actual operating conditions. The tests were conducted with tracer gas decay method on eight different protective devices commonly used in industry. The results indicate the effectiveness can vary from 80% for air curtains, to greater than 90% for strip curtains and greater than 95% for vestibule combinations.

Tso *et al.* (2002) investigated heat and mass transfer characteristics of the body of a refrigerated truck for cases without an air curtain, with a fan air curtain and with plastic strip curtain. The results indicate air curtains were more effective than plastic strip curtains and can reduce the infiltration heat load by 11%. The air curtains were less effective with ambient temperatures >40°C. The comparison of experimental and simulation results indicate good agreement.

Cleland *et al.* (2004) developed an empirical model for the modifications of the ASHRAE Handbook model based on Gosney and Olama model to predict the rate of infiltration through doors into refrigerated buildings. Chen *et al* (2002), East et *al.* (2002) and East et *al.* (2003) measured door air infiltration for a wide range of door opening scenarios. The modelled equation predicted accurately.

2.5.6 Humidifiers

Humidifiers are used when the desired RH is greater than the value the refrigeration facility naturally achieves. There is a number of commercially available hardware for this requirement. These include steam humidifiers, fogging humidifiers and ultra sonic humidifiers.

1. Steam humidifiers

The steam humidification process is achieved by directly injecting steam (water vapour under pressure and high temperature) in to the air stream. Usually the steam source for this type of humidifier is at a constant supply pressure from a central steam boiler at low pressure and hence a quick response to humidification is achieved. Boiler treatment chemicals discharged into the air stream could contaminate the quality of air, therefore chemicals should be checked for safety and care should be taken to avoid contamination from water or steam supplies. A humidity controller/ sensor are used to modulate a control valve to introduce steam into the air stream. The disadvantage of the steam humidifier is the addition of extra sensible heat load from the steam to the room (ASHRAE, 2000).

2. Fogging humidifiers

Fogger use high-pressure water atomisation via a series of pumps and manifolds equipped with nozzles. The droplet size is inversely proportional to the square root of the pressure ratio. The pressure in fogging systems varies between 69 and 137.9 bars. High-pressure fogging uses excess heat from the treated space to evaporate the water; so it is more energy efficient than steam humidifier and is attractive to mid sized and large commercial and industrial applications (Houston, 2000).

3. Ultrasonic humidifiers

In ultrasonic humidifiers the moisture is generated by transforming electrical energy into mechanical (acoustical) energy via a piezoelectric transducer, which oscillates at a frequency of 1.65 MHz. Typical ultrasonic humidifier system control includes water conductivity-measuring devices to reduce problem with impurities. The very small diameter water nebula generated allows quick evaporation of the droplets in the air stream. This feature is extremely important when trying to maintain tight humidity control such as in process and lab applications. Ultrasonic humidifiers give an instantaneous response to calls for humidification with a contaminant free environment, and

better energy efficiency compared to more conventional methods (Shahid, 1995).

2.5.7 Insulation

If room air temperature changes it affects the rate of heat transfer through surfaces causing a temperature change in the surfaces. The simplest approach to modelling surfaces could be to ignore the temperature change on the surfaces and to use a quasi-steady state model based on the temperature difference across the surface and the resistance to heat flow of the material, assuming negligible thermal capacity. Amos (1995) and Estrada-Flores (1996) reviewed models of building shells for refrigerated facilities.

Extensive work has been carried out into studying dynamic behaviour of walls in air-conditioned buildings, and limited research on the thermal behaviour of low temperature refrigerated room, walls, ceiling and floor (Estrada-Flores *et al.* 1995).

Estrada-Flores *et al.* (1995) modelled sandwich panel type walls using two models of different complexity. The models were validated using predictions from an accurate finite element computer programme, which represented a fully distributed scheme (DDD), across a wide range of external and internal heat transfer conditions. It was found a model using two differential equations, which included thermal capacity of external metal layers and insulation resistance was more accurate than an algebraic model with only insulation resistance. The advantages of increasing the level of complexity were negligible. With increase in insulation resistance both models were significantly less accurate.

Estrada-Flores (1996) and Estrada-Flores *et al.* (2001) developed wall models for low temperature applications assuming each wall layer could be represented by one of five possible thermal behaviours: null, resistance only, capacity only, alternating resistance and capacity (lumped) or fully distributed resistance and capacity. A number of practical models for each of the four common low

temperature wall types were studied by comparing them with the simulated performance from a finite element model. The resistance was the main factor affecting the mean heat flow entering a room. It was recommended that metal layers be represented by capacity only model, thin insulation layers by resistance only models, thicker insulation layers by lumped or fully distributed models, and concrete layers by lumped or fully distributed models and the recommended number of zones within a lumped or distributed model for a layer rises as the amplitude of the expected repeating temperature cycle for that layer increases.

East et *al.* (2002) measured thermal insulation quality of refrigerated buildings. It was found the insulation thermal conductivity for a 21 year-old expanded polystyrene sandwich (EPS) panel store was 1.43 times higher than the nominal value, which confirms the deterioration over time (the factor for a similar 2 year old store was 1.23). The surface temperature measured on a similar store with and without weather shields showed that the weather-shield significantly reduced the day time peak heat loads but did not had a huge impact on the daily average heat load.

2.5.8 Product and Packaging

Products can be stored for extended periods of time in bulk-stacked packages within cool storage facilities, and their life depends on temperature, quantity of water loss (i.e. affected by air relative humidity), and the composition of the atmosphere nearby. The desired bulk storage environment can be created in the refrigerated space, but packaging system design can modify the local in-package environment.

Modelling requires understanding of the heat and mass transfer processes within the commodity, between the packaging and both the commodity and the external environment, with or without atmosphere modification. Even though products are the main purpose of refrigeration system, less attention has been given to these

components, and model are less developed and simpler than those used for refrigeration system components (Lovatt, 1990).

Lovatt (1990), Amos (1995) and Tanner (1998) presented wide-ranging reviews of heat and mass transfer models of product and packaging in refrigerated facilities.

Lovatt (1992) developed a model for food product to predict heat release profile during chilling and freezing, this being the main contributor for mean and peak heat loads in industrial refrigeration plants. The model was made up of ordinary differential equations (ODE) and tested against finite difference (FD) calculations for a range of product shapes and cooling conditions. The results indicate the model predicted within 10% of FD calculations and had a 10% margin of error compared with experimental freezing of meat cartons. The model was found to be well suited for freezing products but less effective for chilling product.

Jamieson *et al.* (1993) used a simple model for heat conduction with convection at the surface with effective thermal properties and heat transfer coefficients to predict cooling of pallets of cheese in cool stores. The results indicate there was little effect of differences in air velocity on the cooling rate of cheese; chimneystack arrangements on pallets gave 40% faster cooling rates than the solid pallet stacks, with 12% less product. The difference between the measured and predicted temperature profile reflected the uncertainties of input data. The model can be used for more general application of cooling palletised products without ventilation of air through the products.

Amos *et al.* (1993c) investigated the effect of both product position within a pre-cooling stack and pallet-stacking configuration on cooling rates for a multi-row forced-air pre-cooling system. It was found that cooling rates in a staggered pallet stack configuration was 30% faster on average than for an in-line configuration. The standard design methods of packaging to maximize forced air pre-cooling of bulk stacked packaged products were to allow: high percentage of vents, good

alignment of vents, tight and precise assembly of containers onto pallets. Containers without high levels of ventilation should be spaced on pallets to allow sufficient airflow through the pallets and close positioning of pallets to minimise gaps. A spread out pallet stacking arrangement reduces air bypassing around pallets in multiple row stacking systems.

Lin *et al.* (1993), Lin *et al.* (1996a) & Lin *et al.* (1996b) developed empirical methods for predicting chilling times applicable to a range of regular and irregular two-dimensional and three dimensional shapes capable of predicting both thermal centre and mass average temperatures involving simple algebraic expressions. The regular shape model was tested against equivalent analytical solutions. The irregular shape two-dimensional model was tested against finite element numerical method and the three-dimensional model tested against eight geometric shapes experimentally. The results were sufficiently accurate taking into account data uncertainties involved in chilling of many regular geometric shapes for practical purposes.

Eagleton *et al.* (1994) investigated the application of two common moisture-sorption isotherm models GAB and BET, initially developed for food materials, to fibreboard components of packaging for transport of fresh apples. Moisture-sorption and desorption isotherms were constructed from samples conditioned at temperature 1°C and 40°C and relative humidity between 43% and 95%. The results indicate GAB isotherm was more appropriate for the range of temperature and humidities studied than the BET isotherm. The developed isotherms and the fitted model are useful tool for predicting the water vapour interactions that occur among the transpiring fresh products, the hygroscopic fibreboard packaging, and the high humidity environments of storage of products.

Amos (1995) developed a multi-zoned conduction and convection model of an apple carton to predict apple temperature and weight loss, air temperature, enthalpy and humidity, and packaging temperature with position and time within

the carton. The model was tested against measured data and found to be a good fit for air and apple temperatures but insufficient data was available for testing of humidity and weight loss sub-models. Accurately predicting patterns of airflow within the carton was difficult; therefore measurements to determine airflow patterns were required before predictions could be made for alternative packaging systems.

Tanner (1998) developed a dynamic generalized mathematical model for design of horticultural food packages exposed to refrigerated conditions, which included sub models, to predict key in-package heat and mass transfer processes. The dynamic simulation consisted of two components, the pre-cooling (heat transfer) model and bulk storage (mass transfer) model. In addition a quasi-steady state weight loss model was developed. The models were experimentally tested, the results confirmed predictions and measurements within likely data uncertainties for mass loss, packaging moisture uptake and relative humidity difference to the external environment. A single zone model was found to be adequate for all test data even though the model was developed to support multi-zone use. The models have significant potential for wider application to the design of horticultural packaging and prediction of heat and mass transfer characteristics in horticultural packaging systems.

Witt *et al.* (1999) developed a two-zone, lumped-parameter heat transfer model between palletized product and its surrounding cool store air. The model was validated using a finite difference model and measurements for a pallet in a cool store. The results indicated that empirical adjustment was required for systems with significant ventilation through the pallet. The model was found to be reliable, as part of an overall cool store simulation system.

Campanone *et al.* (2002) developed a heat transfer model for foods, which allowed the possibility of internal heat generation, variable physical properties, composite materials, surface water evaporation and convective and/or radiative boundary

conditions, either constant or time varying. A numerical method was developed using the Crank-Nicolson scheme, and the model was validated against exact solutions and experimental data for the refrigeration of various foods. It can be used to simulate for a wide range of refrigeration foods under diverse types of operating conditions in refrigeration.

2.6 AIR SPACE RELATIVE HUMIDITY

The RH in cool store is determined by the balance between the rate of moisture entry and the rate of moisture removal. The design and operation of cool store can significantly affect this balance and hence the resulting RH (Amos *et al.*, 1993a). Tanner (1998) reviewed modelling of airspace relative humidity.

Amos *et al.* (1993a) analysed steady state sensible and latent heat entry and heat removal during four typical operational periods over the apple season on a large apple cool store. The predicted values of RH were similar to the measured values in the cool store. The evaporator surface area and the occurrence of pre-cooling within the cool store were the design and operational factors having greatest effect on the RH. The other significant factors were door protection and management, and floor insulation.

Tso *et al.* (2001) found that using an electronic expansion valve with adjustable superheat setting with hot gas by pass control or suction modulation control could provide relative humidity control in cargo space in a more energy efficient way, than the re-heat system currently used in reefers.

Gupton (2001) examined the principles involved in controlling humidity in air-conditioned buildings. The fundamental issues outlined would help owners and managers to communicate more effectively with their consulting engineers about efficient and cost effective operation of these systems.

2.7 CONTROL OF REFRIGERATION SYSTEM

The efficiency and power consumption of refrigeration systems depends on a number of variables, which include:

1. Refrigeration load.
2. Temperature at which the load is controlled.
3. Ambient conditions (influence the heat rejection).
4. Design and control of the plant.

Control technology has been rapidly developed to satisfy the complex human requirements in the refrigeration industry. The control systems must match the supply and demand to achieve the optimum energy efficiency of a refrigeration plants, and with proper thermal designs should facilitate the desired level of control. Other important key parameters include the way measurements and controls are implemented in relation to the bulk fluid conditions. The static and dynamic accuracies of sensors must be greater than the precision of the control action (James *et al.* 1993).

Janssen *et al.* (1992) analysed both numerically and experimentally, the losses associated with the on/off control of domestic refrigeration equipment. The results indicated an efficiency increase of 10-18% for the continuously running system (one compressor) compared with an on/ off system.

James *et al.* (1993) investigated concepts for closed and open loop control systems for air-conditioning systems using mathematical models. The model was based on a simple R22 direct expansion (DX) air cooling and dehumidifying system with a semi-hermetic reciprocating compressor and a frequency inverter to control the compressor speed and hence the capacity. Tests for the dynamic behaviour of the plant were carried out by changing compressor speed, from a minimum of 850 rpm to a maximum of 1450 rpm. The plant and model responses appear coincident at low frequencies, however at higher frequencies, differences increase. For the closed loop controller a simple PID control algorithm was used,

and showed the controller achieving both control and accuracy and sensitivity for the plant, however reliable measurements were essential. The open loop control showed that good set point accuracy was achieved together with a rapid reaction to changes in the set point or operating conditions, however controller diagnostic routines were essential since a fault will result in the loss of set point accuracy.

Chan *et al.* (1998) investigated modern supermarket refrigeration systems consisting of multi-compressor refrigeration racks in which the compressors were arranged in parallel and cycle on and off to satisfy the load. The effect of floating suction and head pressures and the influence of on/off control parameters on the efficiency and stability of the system were investigated. A model of the system incorporating frosting on the evaporator coils, geometric characteristics of the components and controls were developed based on the TRNSYS simulation environment. The model was validated using experimental results from the laboratory and found to perform well. The results showed an improvement in energy utilisation of about 23% on multi-compressor refrigeration rack when the bandwidth on the control of the suction pressure was reduced from 27.6 kPa (g) to 13.8 kPa (g). The narrow bandwidth tends to lead to high compressor cycling rates, which could be overcome by the introduction of variable speed control. The results also indicated better COP, energy efficiency and more uniform control of the suction pressure with variable control than for the on/off control.

Yaqub *et al.* (2000) investigated capacity control of a vapour compression refrigeration system by injecting hot gas and liquid refrigerant into the compressor suction (hot gas bypass). The study investigated three different by-pass methods for refrigerant HFC-134a:

- Injection from compressor discharge to suction side.
- Injection of liquid and hot gas to the suction side.
- Injection of hot gas into the evaporator.

The model used a finite difference approximation, to model variations in the condenser and evaporator temperatures with respect to capacity and external fluid

inlet temperatures. Compressor discharge temperatures increased significantly with hot-gas by pass (without any liquid injection). Injecting hot gas directly into the evaporator inlet has the highest COP at a given capacity ratio and gives the lowest compressor discharge temperatures and the by-pass mass fraction of the refrigerant.

Manske *et al.* (2001) developed a mathematical model for an existing large two-temperature level cold storage distribution facility. The system was made up of a combination of single-screw and reciprocating compressors, an evaporative condenser and a combination of liquid overfeed and direct expansion evaporators. The simulation was in agreement with the experimental data recorded from the system. The study mainly focused on the methods, analysis and the results related to condenser sizing and head pressure control. It was concluded that operating head pressures that minimize the energy costs of the system were found to be a linear function of the outdoor wet-bulb temperatures and presented a methodology for implementing the optimum control strategy. The annual simulation of the performance of the system carried out show a reduction of 11% in energy consumption as a result of the recommended design and control changes.

Tso *et al.* (2001) developed a mathematical model to compare the performance of the hot gas by pass control and suction modulation control in refrigerated shipping containers. The factors examined were compressor power draw, coefficient of performance and the sensible heat factor of evaporator coil against variations in container load, set point and ambient temperatures. The results show that suction modulation control was more energy efficient and that performance of the evaporator was found to be unaffected by either method of control. The sensible heat ratio of the evaporator was found to have a strong influence by the superheat setting. Higher superheat setting causes temperature difference between coil and circulating air to increase resulting in higher mass transfer. By means of electronic expansion valve with adjustable superheat setting it may be possible to provide humidity control with higher energy efficiency than the current practice of reheat

systems. One possible setback with low setting of superheat in evaporator is the liquid flooding back to the compressor. Results indicate this wasn't the case with evaporator on partial load, further experimental and simulation will be required to determine a safe operating envelope to avoid flooding back.

2.8 REFRIGERANT THERMODYNAMIC PROPERTY

Both designer's and plant user's need computer data-base covering thermodynamic properties of common refrigerants, with high accuracy, consistent with reasonable access time to check performance (Chan *et al.* 1981a). Chan *et al.* (1981 a, b, c) developed computer subroutines for calculation of common refrigerant properties.

Cleland (1994) developed polynomial curve-fit equations for thermodynamic properties for refrigerant R134a; this was an extension of the Cleland (1986) work which gave alternative computer routines for evaluation of refrigerant thermodynamic properties in the form of curve fitted equations for R22 and R717 among other refrigerants. The equations can be applied with greater computation speed for applications in the area of dynamic simulation and were found to be accurate for estimating properties for many practical situations, but should not be seen as a general replacement for the Chan and Haselden routines (Cleland 1986).

3 RESEARCH OBJECTIVES

The literature reviews gives an overview of the existing work carried out by researchers in the refrigeration areas relating to moisture transport mechanisms. The majority of researchers have carried out extensive studies on modelling the refrigeration system components, with emphasis on temperature control and energy use in refrigerated facilities. Most models have considered heat transfer in detail but little on the combined heat transfer and moisture transport. There has been limited research into mechanisms affecting the relative humidity and how to model them. A model of a complete refrigeration system including considerations of application of moisture transport would be a useful aid for refrigeration systems design and operating engineers.

Taking the above factors into consideration the detailed objectives of this study were to:

1. Formulate a dynamic model of heat and mass transfer processes in a cold storage facility to predict temperature and relative humidity.
2. Measure performances of cold room for a range of heat and moisture loads and operating conditions.
3. Use the experimental data to calibrate and validate the model.

Defrosting is the main mechanism for removal of frost from the refrigeration facility. The literature reviews showed that there is little information on defrost efficiency and its impact on temperature and RH control. Therefore a fourth objective was to:

4. Investigate the effect of defrost frequency on the defrost efficiency, cold room air temperature and relative humidity and refrigeration system energy efficiency.

4 COOL STORE MODEL DEVELOPMENT

A key objective of the research project is to develop mathematical models of heat transfer and water vapour (mass) transport in a cool store and to incorporate them into a computer simulation model. In this chapter appropriate component models are selected and formulated. The model was developed as generally as possible so that it could be applied more widely than the cool store studied experimentally. Section 2 and Figure 2-1 give general description of the main mechanisms for heat and mass transfer.

4.1 AIR ZONE

The air space was divided into multiple zones of arbitrary size to allow spatial variation in conditions to be modelled. A full distributed (e.g. CFD) model was considered too complex to use especially if the moisture transport mechanisms are to be included. Each zone was assumed to be perfectly mixing, so temperature and humidity are constant within the zone. For simplicity it was also assumed that each zone has constant volume and constant density of air. Given that temperature and RH are controlled, large changes in density are not likely so this is justified. The only exception is calculation of natural convection of air between zones.

Figure 4-1 shows the air zone components associated with heat and moisture transport mechanisms. All calculations were done using an unchanging dry air basis.

The unsteady-state energy balance for the i^{th} air zone is:

$$F_{a,buffer} . M_i . \frac{dh_i}{dt} = \phi_{air \to i} + \phi_{d \to i} + \phi_{s \to i} + \phi_{st \to i} + \phi_{fl \to i} + \phi_{hg \to i} + \phi_{pr \to i} + \phi_{hu \to i} \qquad (4\text{-}1)$$

Where:

M_i = Mass of dry air in the i^{th} zone (kg).

h_i = Enthalpy of air in the i^{th} zone (J/kg).

$\phi_{d\rightarrow i}$ = Energy flow into the i^{th} zone through doors (W).

$\phi_{s\rightarrow i}$ = Energy flow into the i^{th} zone through surfaces (W).

$\phi_{fl\rightarrow i}$ = Energy flow into the i^{th} zone through the floor (W).

$\phi_{st\rightarrow i}$ = Energy flow into the i^{th} zone from structures (W).

$\phi_{pr\rightarrow i}$ = Energy flow into the i^{th} zone from products (W).

$\phi_{h\,g\rightarrow i}$ = Energy flow into the i^{th} zone from heat generators (W).

$\phi_{hu\rightarrow i}$ = Energy flow into the i^{th} zone from humidifiers (W).

$\phi_{air\rightarrow i}$ = Energy flow to the i^{th} zone due to forced and natural convection of air from other air zones and the evaporators (W).

$F_{a,buffer}$ = Correction factor for room air mass thermal buffering.

Similarly, the water vapour balance for the air in the i^{th} zone is:

$$F_{a,buffer}.M_i.\frac{dH_i}{dt} = m_{air\rightarrow i} + m_{d\rightarrow i} + m_{s\rightarrow i} + m_{st\rightarrow i} + m_{fl\rightarrow i} + m_{pr\rightarrow i} + m_{hg\rightarrow i} + m_{hu\rightarrow i} \quad (4\text{-}2)$$

Where:

H_i = Absolute humidity of i^{th} zone air (kg water vapour / kg dry air).

$m_{d\rightarrow i}$ = Mass of water vapour entering the i^{th} zone through doors (kg/s).

$m_{s\rightarrow i}$ = Mass of water vapour entering the i^{th} zone through surfaces (kg/s).

$m_{fl\rightarrow i}$ = Mass of water vapour entering the i^{th} zone through the floor (kg/s).

$m_{st\rightarrow i}$ = Mass of water vapour entering the i^{th} zone from structures (kg/s).

$m_{pr\rightarrow i}$ = Mass of water vapour entering the i^{th} zone from products (kg/s).

$m_{h\,g\rightarrow i}$ = Mass of water vapour entering the i^{th} zone from heat generators (kg/s).

$m_{hu\rightarrow i}$ = Mass of water vapour entering the i^{th} zone due to humidifiers (kg/s).

$m_{air\rightarrow i}$ = Mass of water vapour entering the i^{th} zone due to forced and natural convection from adjacent air zones and the evaporators

(kg/s).

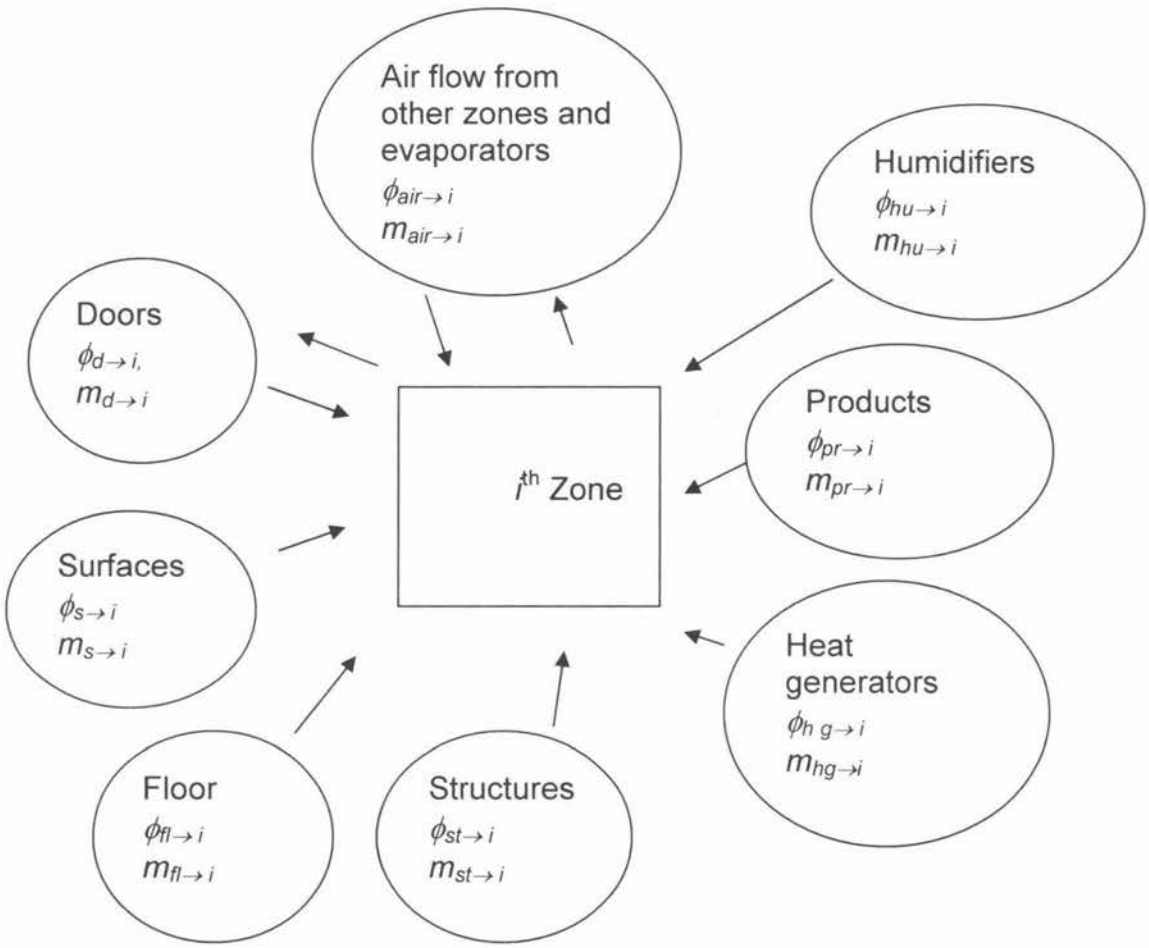

Figure 4-1: Conceptual model of heat and mass transfer for the i^{th} air zone

The mass of air in the room can be divided up between zones so:

$$M_i = F_i . V_{ro} . \rho_a \tag{4-3}$$

$$\sum_{i=1}^{I} F_i = 1 \tag{4-4}$$

Where:

F_i = Fraction of the air in the room that the i^{th} zone contains.

V_{ro} = Room volume (m^3).

ρ_a = Density of air (kg/m^3).

Equation 1 and 2 can be used to calculate enthalpy and absolute humidity in the zone. The temperature of the zone can be estimated using the following equation based on the equation for enthalpy of air as a function of temperature and humidity.

$$T_i \approx \frac{h_i - H_i.h_{fg}}{c_a + H_i.c_v} \qquad (4\text{-}5)$$

Where:

T_i = Temperature of the i^{th}zone (°C).

h_{fg} = Latent heat of evaporation for water at 0°C (J/kg).

c_a = Specific heat capacity of dry air (J/kg K).

c_v = Specific heat capacity of water vapour (J/kg K).

4.2 HEAT AND WATER VAPOUR FLOW DUE TO AIR FLOW

Airflow in a cool store is primarily due to the natural convection due to localised density differences and forced convection due to fans. It was assumed that the natural and forced convection components were additive but independent. Hence energy and water vapour mass flow into the i^{th} zone is made up of the following components (Figure 4-2):

- Energy and mass flow due to natural convection from neighbouring zones.
- Energy and mass flow due to forced convection from neighbouring zones.
- Energy and mass flow directly to/from fans and
- Energy and mass flow directly to/from evaporators.

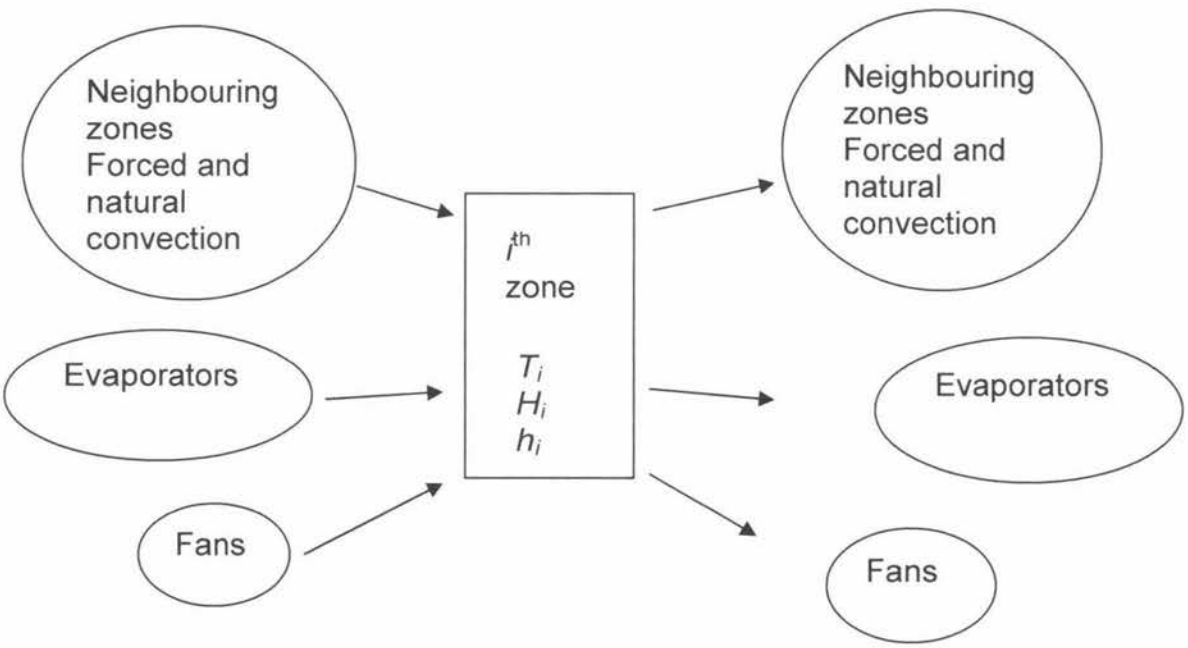

Figure 4-2: Air zone mass balance due to air flow

$$\phi_{air \to i} = \phi_{nc,i} + \phi_{for,i} \tag{4-6}$$

$$m_{air \to i} = m_{nc,i} + m_{for,i} \tag{4-7}$$

Where:

$\phi_{nc,i}$ = Heat flow to the i^{th} zone due to natural convection from other zones (W).

$\phi_{for,i}$ = Heat flow to the i^{th} zone due to forced convection from fans, evaporators and other zones (W).

$m_{nc,i}$ = Water vapour to i^{th} zone due to natural convection from other zones (kg/s).

$m_{for,i}$ = Water vapour flow to i^{th} zone due to the forced convection from fans, evaporators and other zones (kg/s).

4.2.1 Natural Convection with Adjacent Zones

Natural convection was assumed to take place across the boundary with up to *N* other zones and occur in both directions in a balanced manner. The heat and water vapour flow due to natural convection can be expressed as follows:

$$\phi_{nc,i} = \sum_{n=1}^{N} u_{n\to i} \cdot \rho_a \cdot \frac{A_{i,n}}{2} \cdot (h_n - h_i) \tag{4-8}$$

$$m_{nc,i} = \sum_{n=1}^{N} u_{n\to i} \cdot \rho_a \cdot \frac{A_{i,n}}{2} \cdot (H_n - H_i) \tag{4-9}$$

Where:

$A_{i,n}$ = Area of interface between the i^{th} zone and the n^{th} neighbouring zone (m^2).

$u_{n\to i}$ = Air velocity between the n^{th} neighbouring zone and the i^{th} zone (m/s).

h_n = Enthalpy of air in n^{th} zone associated with i^{th} zone (J/kg).

H_n = Absolute humidity of air in n^{th} zone associated with i^{th} zone (kg water vapour / kg dry air).

The natural convection velocity of air between i^{th} zone and other zones was calculated using the model developed by Amos (1995).

$$u_{n\to i} = 0.134 . |(T_i - T_n)|^{0.5} \tag{4-10}$$

Where:

T_n = Air temperature of the n^{th} zone associated with i^{th} zone (°C).

During implementation, the calculation was done for all air zones but $A_{i,n}$ was set to 0 for non-adjacent zones.

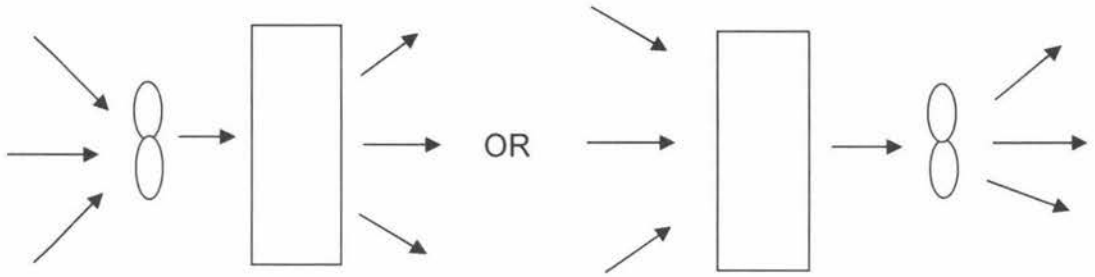

Figure 4-3(a): Single fan supplying or drawing air from an evaporator.

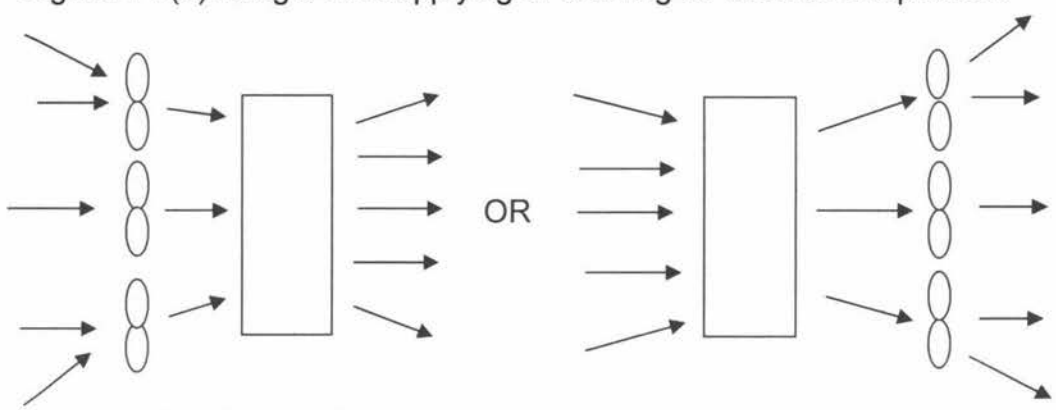

Figure 4-3 (b): Multiple fans supplying or drawing air from an evaporator.

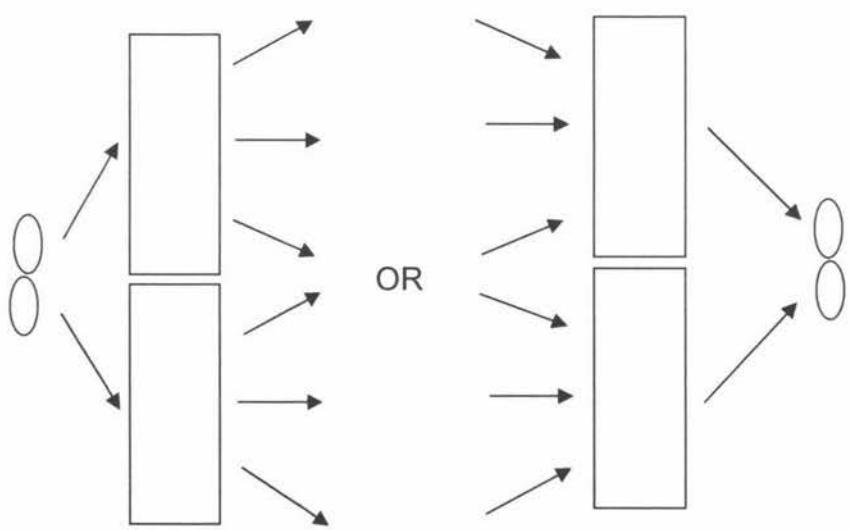

Figure 4-3(c): Single fan supplying or drawing air from multiple evaporators

4.2.2 Forced Convection

All forced convection is due to fans. In practice fans can draw air from a location that can encompass more than one air zone, from other fans and from one or more evaporators (induced draught) and at the same time discharge into a number of air zones, other fans or evaporators (forced draught). Fans may be single speed, dual speed or may have continuously variable speed. Frost can accumulate on evaporators causing pressure drops across the coil which can affect air velocity and air distribution.

A generic model that covers all the possibilities becomes quite complicated and would probably need to involve an in-depth fundamental approach of the air hydrodynamics. The most common configuration of fans and evaporators in a cold store is:

1. Single or multiple fans supplying air to or drawing air from an evaporator. One or more fans may serve a single evaporator, but each fan is uniquely linked with only one evaporator. (Figure 4-3 (a) or (b)).
2. Fans supplying air to or drawing air from single or multiple air zones without an evaporator.

A less common configuration would involve each fan supplying more than one evaporator (Figure 4-3 (c)). In such a case if the evaporators frost unevenly, the distribution of air coming from/passing to the fan will change, which would significantly increase the level of complexity of a model for such a configuration. To limit model complexity, the configuration shown in Figure 4-3 (c) was modelled assuming that all evaporators served by a single fan, frost at the same rate and could be modelled lumped together as one large evaporator rather than multiple evaporators (i.e. same as Figure 4-3(a)).

Hence the model allowed multiple fans, evaporators and zones with the constraint that each fan could only draw air from or discharge air to a single evaporator as shown in Figure 4-4 and Figure 4-5.

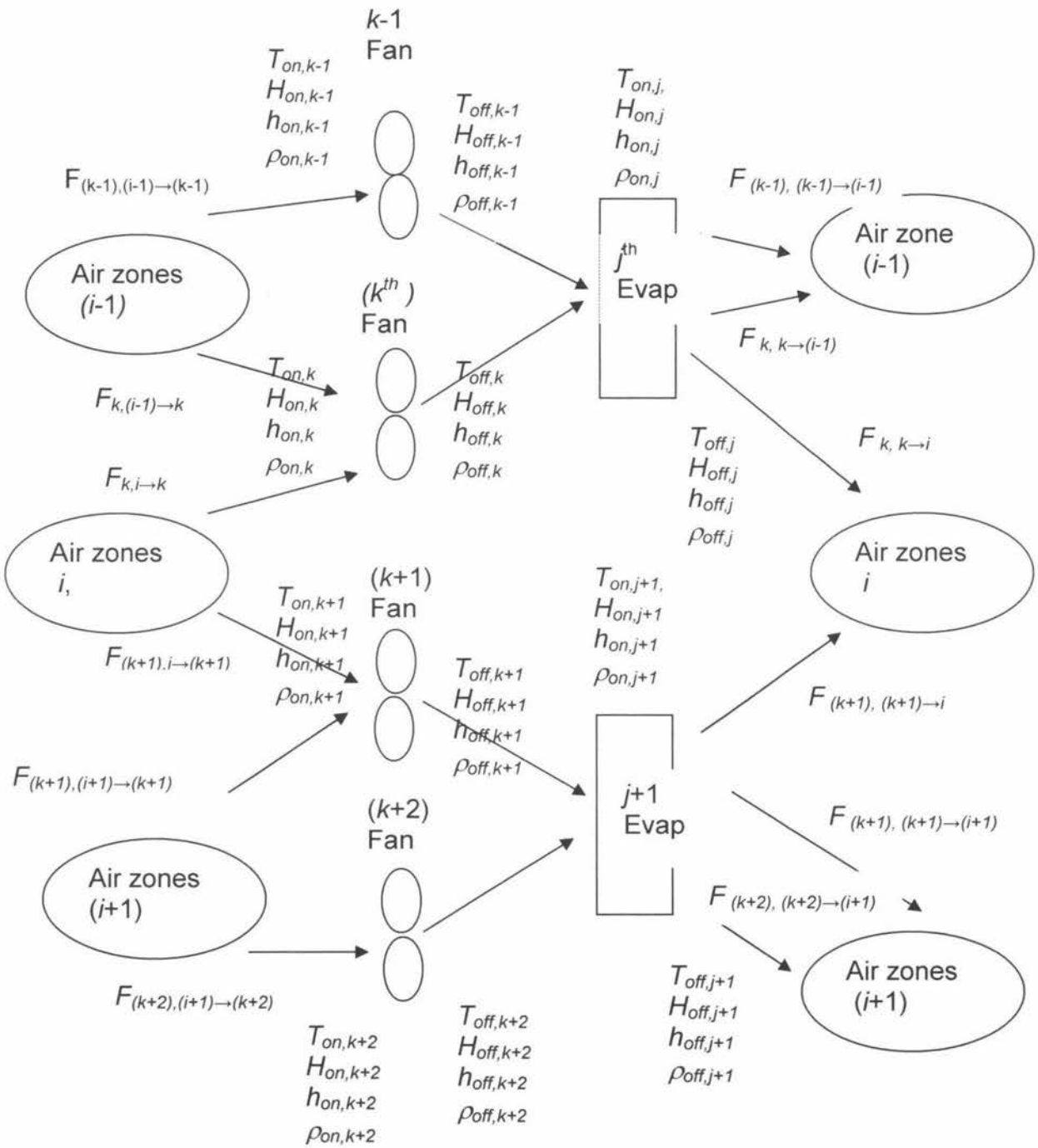

Figure 4-4: General airflow pattern for forced draught fans.

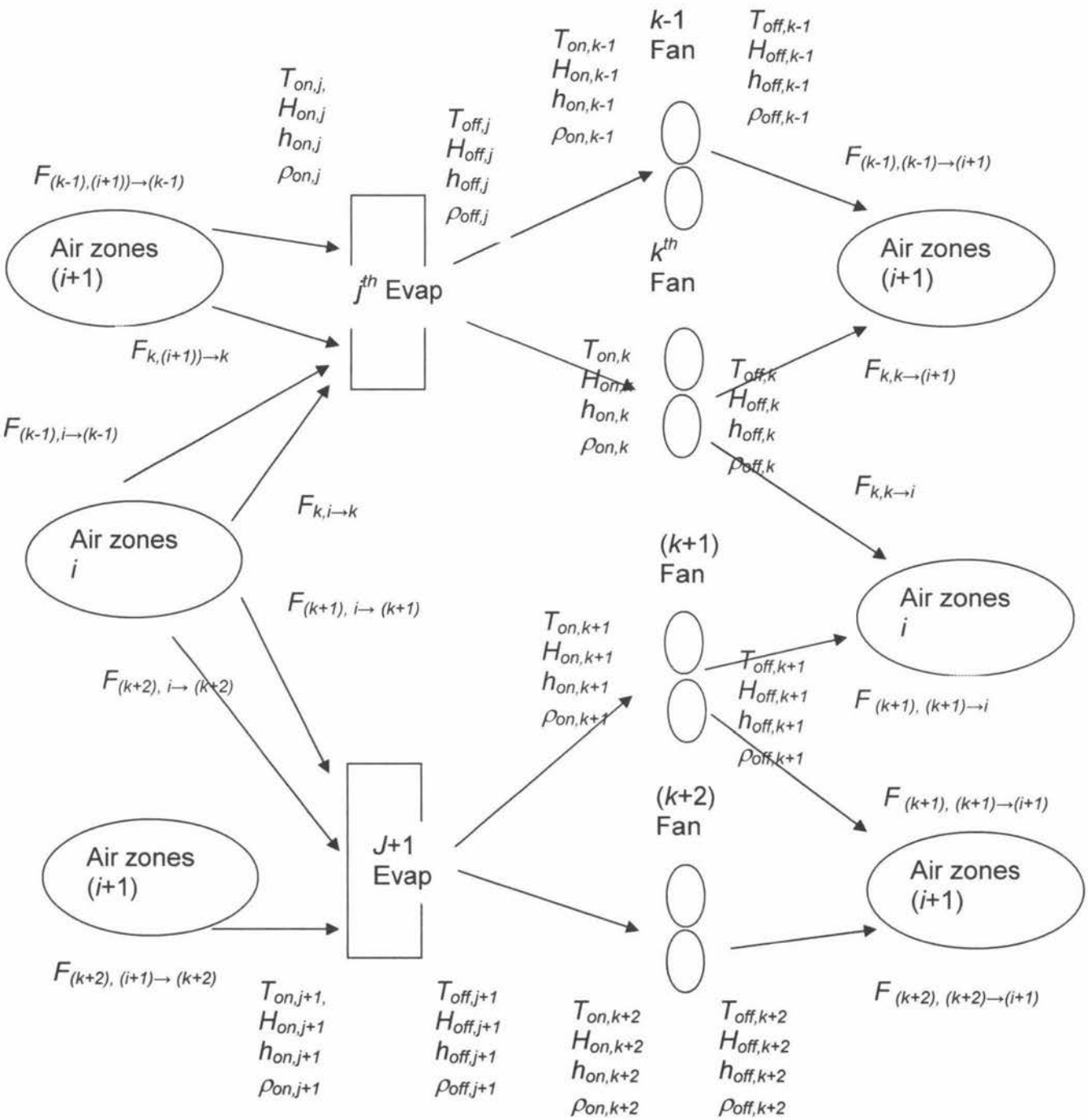

Figure 4-5: General airflow pattern for induced draught fans

Fans arranged in series were not allowed (they must be modelled as a single fan). Fans not associated with an evaporator (i.e. they can draw and discharge to air

zones) can be modelled by including a dummy evaporator with zero surface area (and hence no cooling capacity).

Given these restrictions the air flow from the fan can be modelled as depending on only:

- Fan speed setting.
- Mass of ice deposited on the surface of the associated evaporator as the rest of the air pathway will not change significantly.

The evaporators can either be induced draught (fans downstream) or forced draught (fans upstream). For forced draught (blow through), all fan energy was assumed to immediately transfer to the air passing onto the evaporator and the temperature of this air is slightly increased relative to that of the entering air. The energy flow from the fan into the air depends on the fan rating and speed and will be totally sensible heat.

The other requirement of forced convection is to define the airflow pathways between zones. It was decided that these would be predefined based on the air flow through each fan. That is, the flow through each fan is assumed to follow a unique pathway between zones that are independent of but additional with the flow from other fans. The flow between any two zones due to a particular fan is defined as a fraction of the total air flow rate from that fan. Thus separate air pathways need to be defined for each and every fan in the facility and are summed to get the total air flow between zones and that of evaporators.

The defined air pathways for the air zones can be started with those zones from which fans or evaporators draw air and finished with those zones into which fans or evaporators discharge air. The total mass flows of air into the i^{th} zone can be expressed by summing the contribution of each fan.

The sign conventions used in the model are:

- All flows entering the i^{th} zone are positive.
- All flows leaving the i^{th} zone are negative.
- All fractions are positive (i.e. flows leaving zone *i* are considered in the context of the flow entering zone n).
- Obviously, there must be an overall air mass balance for each zone.

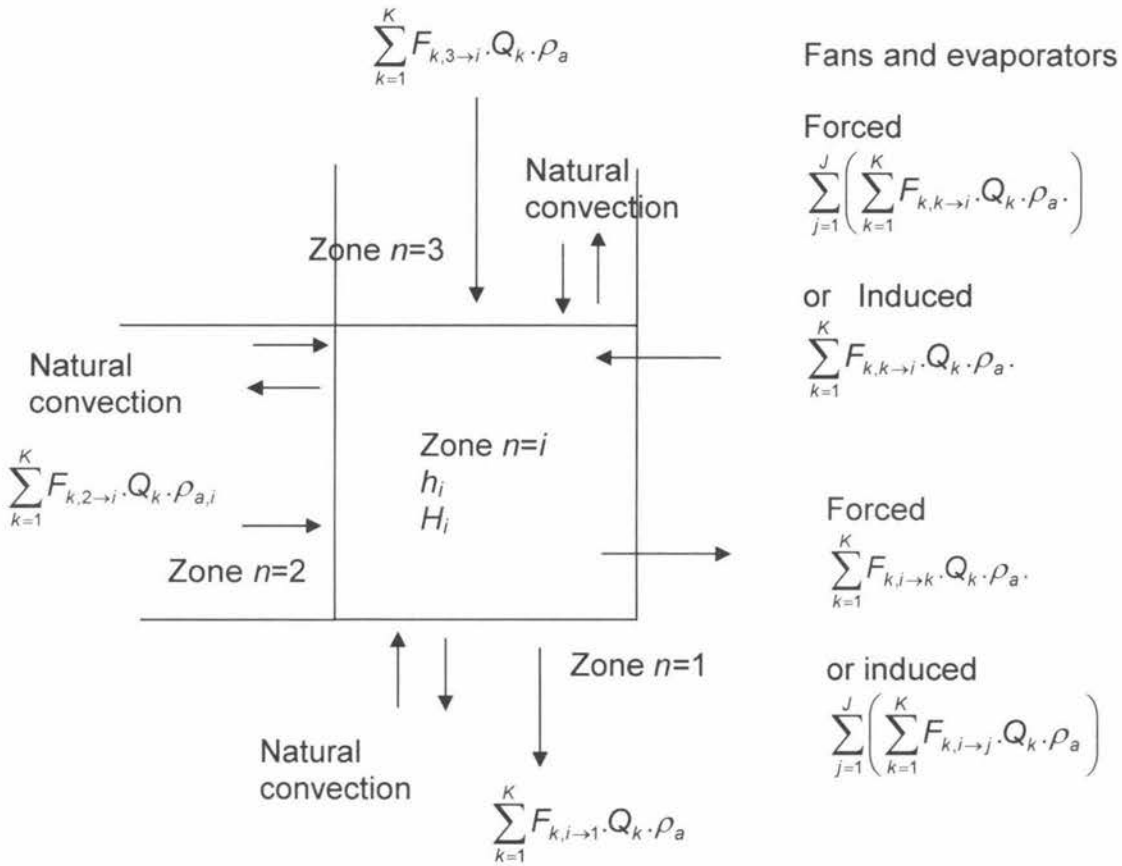

Figure 4-6: Forced convection airflows for the i^{th} zone.

Figure 4-6 shows an example of possible air flows for a zone. The heat entries to a zone by forced convection are the sum of the air flows from:

- Fans. Up to *K* fans that are associated with that zone.
- Evaporators. Up *J* evaporators that are associated with that zone.

- Forced convection flow from up to *N* neighbouring zones.

The heat flows due to forced convection to i^{th} zone can be expressed as follows:

$$\phi_{for\to i} = (\sum_{j=1}^{J}\sum_{k=1}^{K} F_{k,j\to i}.Q_k.\rho_a.h_{off,j} - \sum_{k=1}^{K} F_{k,i\to k}.Q_k.\rho_a.h_i$$

$$+ \sum_{n=1}^{N}\sum_{k=1}^{K} F_{k,n\to i}.Q_k.\rho_a.h_n - \sum_{n=1}^{N}\sum_{k=1}^{K} F_{k,i\to n}.Q_k.\rho_a.h_i).(forced)$$

$$+ (\sum_{k=1}^{K} F_{k,k\to i}.Q_k.\rho_a.h_{off,k} - \sum_{j=1}^{J}\sum_{k=1}^{K} F_{k,i\to k}.Q_k.\rho_a.h_i$$

$$+ \sum_{n=1}^{N}\sum_{k=1}^{K} F_{k,n\to i}.Q_k.\rho_a.h_n - \sum_{n=1}^{N}\sum_{k=1}^{k} F_{k,i\to n}.Q_k.\rho_a.h_i).(1-forced)) \qquad (4\text{-}11)$$

Where:

forced = 1 for forced draught fan

forced = 0 for induced draught fan

Where:

$F_{k,j\to i}$ = Fraction of k^{th} fan flow into zone *i* from the j^{th} evaporator.

$F_{k,i\to k}$ = Fraction of k^{th} fan flow coming from zone *i*.

$F_{k,i\to j}$ = Fraction of k^{th} fan flow passing from i^{th} zone to j^{th} evaporator.

$F_{k,k\to i}$ = Fraction of k^{th} fan flow passing to zone *i*.

$F_{k,i\to n}$ = Fraction of k^{th} fan flow passing from zone *i* to zone *n*.

$F_{k,n\to i}$ = Fraction of k^{th} fan flow passing from zone *n* to zone *i*.

Q_k = Flow rate of the k^{th} fan with frosting (m^3/s).

$h_{off,j}$ = Enthalpy of air leaving j^{th} evaporator (J/kg).

$h_{off,k}$ = Enthalpy of air leaving k^{th} fan (J/kg).

To maintain a balance of flow in the i^{th} zone, the net flows (mass) to i^{th} zone must be equal to zero. Hence necessary conditions are that:

$$\sum_{i=1}^{I} F_{k,i\to k} = 1 \tag{4-12}$$

$$\sum_{i=1}^{I} F_{k,k\to i} = 1 \tag{4-13}$$

$$F_{k,k\to i} + \sum_{n=1}^{N} F_{k,n\to i} = F_{k,i\to k} + \sum_{n=1}^{N} F_{k,i\to n} \tag{4-14}$$

Similarly the water vapour flows due to forced convection to i^{th} zone can be expressed as follows:

$$\begin{aligned} m_{for\to i} = &(\sum_{j=1}^{J}\sum_{k=1}^{K} F_{k,j\to i}.Q_k.\rho_a.H_{off,j} - \sum_{k=1}^{K} F_{k,i\to k}.Q_k.\rho_a.H_i \\ &+ \sum_{n=1}^{N}\sum_{k=1}^{K} F_{k,n\to i}.Q_k.\rho_a.H_n - \sum_{n=1}^{N}\sum_{k=1}^{K} F_{k,i\to n}.Q_k.\rho_a.H_i).(forced) \\ &+ (\sum_{k=1}^{K} F_{k,k\to i}.Q_k.\rho_a.H_{off,k} - \sum_{j=1}^{J}\sum_{k=1}^{K} F_{k,i\to k}.Q_k.\rho_a.H_i \\ &+ \sum_{n=1}^{N}\sum_{k=1}^{K} F_{k,n\to i}.Q_k.\rho_a.H_n - \sum_{n=1}^{N}\sum_{k=1}^{k} F_{k,i\to n}.Q_k.\rho_a.H_i).(1-forced)) \end{aligned} \tag{4-15}$$

Where:

$H_{off,\,j}$ = Absolute humidity of air leaving j^{th} evaporator (kg/kg).

$H_{off,k}$ = Absolute humidity of air leaving k^{th} fan (kg/kg).

Figure 4-7 and Table 4-1 and Table 4-2 shows a possible air flow path way for a system with 5 zones, 2 evaporators and 2 fans. To meet the condition of equation (4-14) for the example in Table 4-1 and Table 4-2:

$$\sum Columns = \sum Rows$$

During implementation the flow fraction for the following has to be defined.

- Every zone to zone combination
- Every fan to zone combination
- Every evaporator to zone combination.
- Every fan to evaporator combination.

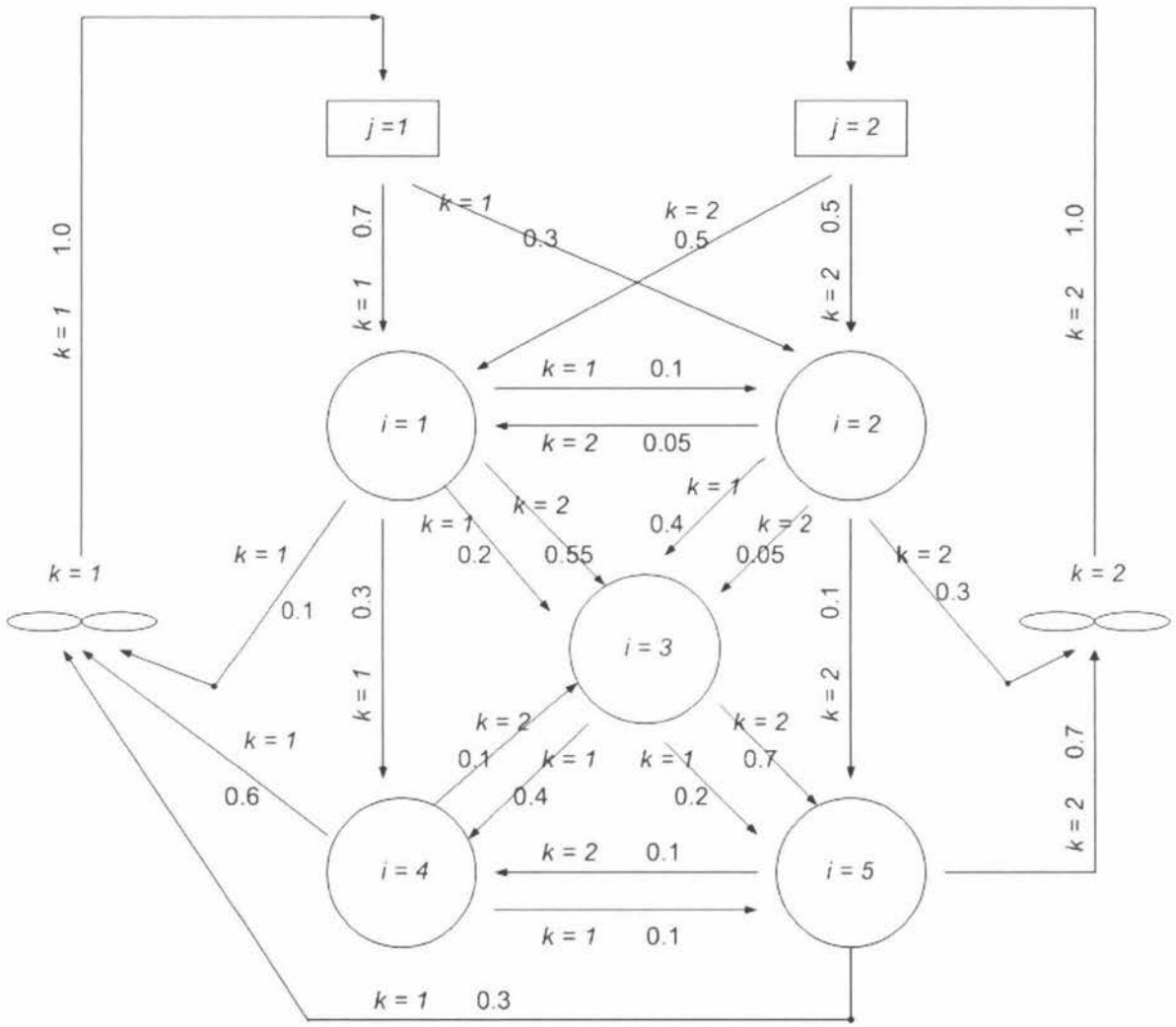

Figure 4-7: Flow pattern in a 5 air zone, 2 fan, 2 evaporator example with forced draught fans, showing non zero positive air flow fractions only.

Table 4-1: Air flow fractions for fan (k = 1), for the example in Figure 4-7

$F_{source \rightarrow sink}$			Source								
			Zones					Evaporators (j)		Fans (k)	
			1	2	3	4	5	1	2	1	2
Sink	Zones	1	0	0	0	0	0	0.7	0	0	
		2	0.1	0	0	0	0	0.3	0	0	
		3	0.2	0.4	0	0	0	0	0	0	
		4	0.3	0	0.4	0	0	0	0	0	
		5	0	0	0.2	0.1	0	0	0	0	
	Evaporators (j)	1	0	0	0	0	0	0	0	1.0	
		2	0	0	0	0	0	0	0	0	
	Fans (k)	1	0.1	0	0	0.6	0.3	0	0	0	
		2									

Table 4-2: air flow fractions for fan (k = 2), for the example in Figure 4-7

$F_{source \rightarrow sink}$			Source								
			Zones					Evaporators (j)		Fans (k)	
			1	2	3	4	5	1	2	1	2
Sink	Zones	1	0	0.05	0	0	0	0	0.5		0
		2	0	0	0	0	0	0	0.5		0
		3	0.55	0.05	0	0.1	0	0	0		0
		4	0	0	0	0	0.1	0	0		0
		5	0	0.1	0.7	0.1	0	0	0		0
	Evaporators (j)	1	0	0	0	0	0	0	0		0
		2	0	0	0	0	0	0	0		1.0
	Fans (k)	1									0
		2	0	0.3	0	0	0.7	0	0		

4.2.3 Fans

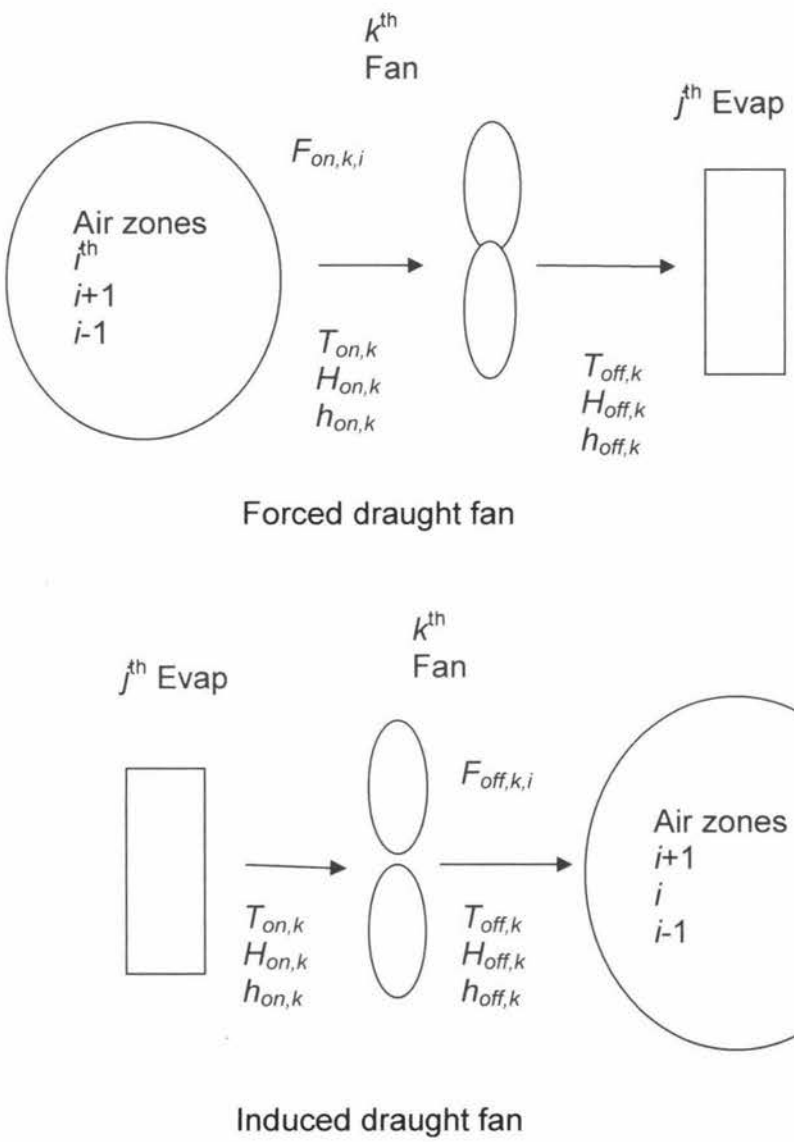

Figure 4-8: Airflow pattern through the k^{th} fan.

The airflow pattern for forced and induced draught airflow through the k^{th} fan is shown in Figure 4-8. The enthalpy of air onto the k^{th} fan from air zones (forced draught) or from evaporators (induced draught) can be expressed as follows:

$$h_{on,k} = \frac{\sum_{i=1}^{I} F_{k,i\to k}.Q_k.h_i}{\sum_{i=1}^{I} F_{k,i\to k}.Q_k}.(forced) + h_{off,j}.(1-forced) \qquad (4\text{-}16)$$

Where:

$h_{on,k}$ = Enthalpy of air on to k^{th} fan (J/kg)

The enthalpy of air leaving the k^{th} fan can be estimated by assuming that all the fan electrical energy is transferred to heat energy and thus to the air stream at the fan:

$$h_{off,k} = h_{on,k} + \frac{\phi_k}{Q_k.\rho_a} \qquad \text{if } Q_k \neq 0 \qquad (4\text{-}17)$$

$$h_{off,k} = h_{on,k} \qquad \text{if } Q_k = 0 \qquad (4\text{-}18)$$

Where:

ϕ_k = k^{th} fan power (W).

$h_{off,k}$ = Enthalpy of air leaving k^{th} fan (J/kg).

The heat energy released by the k^{th} fan can be expressed as follows assuming fan power is not affected by evaporator frosting:

$$\phi_k = \phi_{k,full}\left[\frac{N_k}{N_{k.full}}\right]^3.SwitchFan_k \qquad (4\text{-}19)$$

Where:

$\phi_{k,full}$ = Rated power of k^{th} fan at full speed (W).

$N_{k\,full}$ = Full speed of k^{th} fan (rpm).

N_k = Actual speed of k^{th} fan (rpm).

$SwitchFan_k$ = Switch indicating if fan k is on (1) or off (0).

Since there is no moisture release by the fan the humidity will be same as the incoming humidity. So:

$$H_{on.k} = \frac{\sum_{i=1}^{I} F_{k,i\to k}.Q_k.H_i}{\sum_{i=1}^{I} F_{k,i\to k}.Q_k}.(forced) + H_{off,j}.(1-forced) \qquad (4\text{-}20)$$

$$H_{off,k} = H_{on,k} \qquad (4\text{-}21)$$

Where:

$H_{off,k}$ = Absolute humidity of air leaving k^{th} fan (kg/kg)

$H_{on,k}$ = Absolute humidity of air on to k^{th} fan (kg/kg)

The expressions for the airflows through the k^{th} fan for forced and induced draught flows with frosting can be expressed as follows:

$$Q_k = Q_{ini.k}.\left(\frac{N_k}{N_{k,full}}\right).F_{fr,j}.SwitchFan_k \qquad (4\text{-}22)$$

Where:

$Q_{ini,k}$ = Rated flow of k^{th} fan without frosting (m^3/s).

$F_{fr,j}$ = Factor for airflow decline with frost accumulation on the j^{th} evaporator.

4.2.4 Evaporators

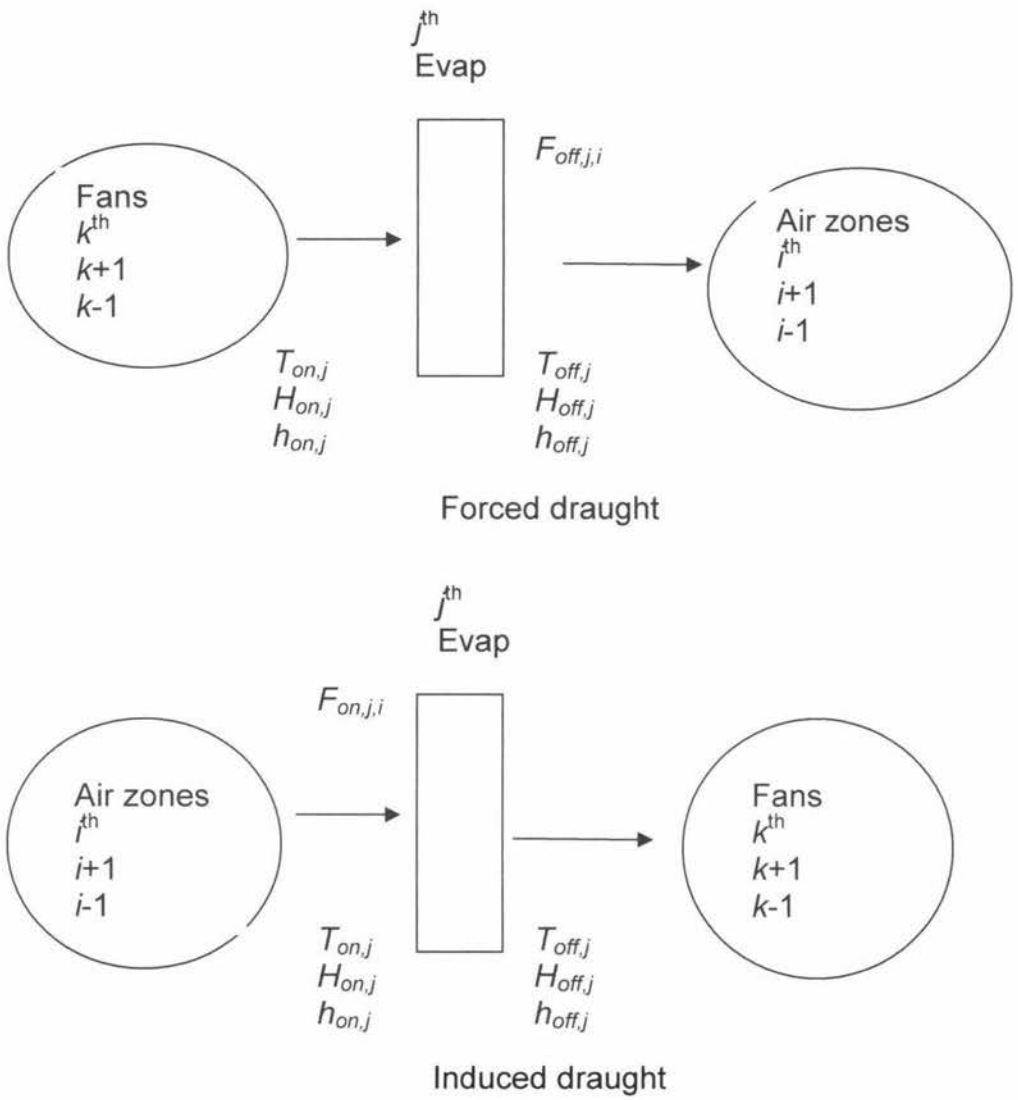

Figure 4-9: Airflow pattern through the j^{th} evaporator.

The airflow pattern for forced and induced draught airflow through the j^{th} evaporator is shown in Figure 4-9. The expressions for airflow through the j^{th} evaporator with frosting can be expressed as follows:

$$Q_j = \sum_{k=1}^{K} Q_k . F_{kj \to k} . (1 - forced) + \sum_{k=1}^{K} Q_k . F_{kk \to j} . (forced) \quad (4\text{-}23)$$

Where:

Q_j = Air flow rate through the j^{th} evaporator with frosting (m^3/s).

The enthalpy of air on to the j^{th} evaporator from air zones or fans can be expressed as:

$$h_{on,j} = \frac{\sum_{k=1}^{K} Q_k . F_{k,k \to j} . h_{off,k}}{\sum_{k=1}^{k} Q_k . F_{k,k \to j}} . (forced) + \frac{\sum_{k=1}^{K} \sum_{i=1}^{N} F_{k,i \to k} . Q_k . h_i}{\sum_{k=1}^{K} \sum_{i=1}^{N} F_{k,i \to k} . Q_k} . (1 - forced) \quad (4\text{-}24)$$

Where:

$h_{on,j}$ = Enthalpy of air on to the j^{th} evaporator (J/kg).

Similarly the humidity of air onto the j^{th} evaporator (forced draught or induced draught) can be expressed as:

$$H_{on,j} = \frac{\sum_{k=1}^{K} Q_k . F_{k,k \to j} . H_{off,k}}{\sum_{k=1}^{k} F_{off,k,j} . Q_k . F_{k,k \to j}} . (forced) + \frac{\sum_{k=1}^{K} \sum_{i=1}^{N} F_{k,i \to k} . Q_j . H_i}{\sum_{k=1}^{K} \sum_{i=1}^{N} F_{k,i \to k} . Q_j} . (1 - forced) \quad (4\text{-}25)$$

The temperature of air can be estimated using the equivalent of equation (4-5):

$$T_{on,j} = \frac{h_{on,j} - H_{on,j} h_{fg}}{c_a + H_{on,j} c_v} \quad (4\text{-}26)$$

The humidity of air leaving j^{th} evaporator can be estimated using the straight-line approach as proposed by Stoecker *et al.* (1982):

$$H_{off.j} = H_{on.j} + \left[\frac{T_{off.j} - T_{on.j}}{T_{on.j} - T_{s,j}}\right]\left(H_{on.j} - H_{sa,j}\right) \quad (4\text{-}27)$$

Where:

$H_{sa,j}$ = Saturated air humidity at j^{th} evaporator surface temperature (kg/kg).

$T_{s,j}$ = Surface temperature of the j^{th} evaporator coil (°C).

The temperature of air leaving the j^{th} evaporator can be expressed using the standard heat exchanger model for sensible heat transfer based on the temperature of the surface of the evaporator.

$$T_{off.j} = T_{s,j} + \left(T_{on,j} - T_{s,j}\right)e^{-\left(\frac{U_{a,j}.A_{s,j}.Switch_{ref,j}.Switch_j}{m_{a,j}.(c_a + H_{on,j}.c_v)}\right)} \quad (4\text{-}28)$$

Where:

$m_{a,j}$ = Mass of air passing through the j^{th} evaporator (kg/s).

$U_{a,j}$ = Heat transfer coefficient from the air to the j^{th} evaporator surface (W/m^2K).

$A_{s,j}$ = Effective air-side surface area of the j^{th} evaporator (m^2).

$Switch_{ref,j}$ = Switch to control refrigeration supply to the j^{th} evaporator. (0 = off, 1 = on).

$Switch_j$ = Solenoid valve for isolating the j^{th} evaporator. (0 = off, 1 = on).

The surface temperature of the j^{th} evaporator can be estimated as follows:

$$T_{s,j} = T_{on.j} - \frac{U_{o,j}}{U_{a,j}}.\left(T_{on.j} - T_{ref,j}\right) \quad (4\text{-}29)$$

Where:

$$\frac{1}{U_{o,j}.A_{s,j}} = \frac{1}{U_{a,j}.A_{s,j}} + \frac{1}{U_{ref,j}.A_{ref,j}} \quad (4\text{-}30)$$

$$A_{s,j} = A_{a,outj} + \eta_{fin}.A_{fin,j} \quad (4\text{-}31)$$

Where:

$U_{o,j}$ = Overall heat transfer coefficient from air to refrigerant for the j^{th} evaporator (W/m^{2}K).

$U_{ref,j}$ = Refrigerant side heat transfer coefficient for the j^{th} evaporator (W/m^{2}K).

$A_{ref,j}$ = Area of the j^{th} evaporator on the refrigerant side (m^2).

$A_{fin,j}$ = Area of the j^{th} evaporator fins (m^2).

η_{fin} = Fin efficiency.

Refrigerant side and air to evaporator surface heat transfer coefficient for the j^{th} evaporator is given by:

$$U_{ref,j}A_{ref,j} = \frac{F_{UAEvap,j}.UA_{o,refer}}{Ra} \quad (4\text{-}32)$$

$$U_{a,j,refer}A_{s,j} = \frac{F_{UAEvap,j}.UA_{o,refer}}{(1-Ra)} \quad (4\text{-}33)$$

Where:

$UA_{o,refer}$ = Design overall heat transfer coefficient from air to refrigerant for the evaporator (W/K).

Ra = Ratio of overall heat transfer coefficient for the evaporator to refrigerant side heat transfer coefficient under no frost condition.

$F_{UAEvap,j}$ = Heat transfer correction factor for the j^{th} evaporator.

The enthalpy of air leaving j^{th} evaporator can be expressed as:

$$h_{off,j} = T_{off,j}(c_a + H_{off,j}.c_v) + H_{off,j}.h_{fg} \quad (4\text{-}34)$$

During defrosting the fans are stopped and hence airflow through the evaporator due to fans will be zero but a significant amount of flow continues due to natural convection.

$$m_{a,j} = Q_j.\rho_a.(1 - Switch_{de,j}) + m_{j,nc}.Switch_{de,j} \quad (4\text{-}35)$$

$$m_{j,nc} = u_{nc,j}.\rho_a.A_j \quad (4\text{-}36)$$

Where:

$m_{j,nc}$ = Mass of air through j^{th} evaporator due to natural convection (kg/s).

$Switch_{de,j}$ = Defrost switch for j^{th} evaporator (0 = off, 1 = on).

$u_{nc,j}$ = Velocity of air through j^{th} evaporator due to natural convection (m/s).

A_j = Face area of the j^{th} evaporator (m^2).

The velocity of air flowing through the evaporator can be estimated as:

$$u_j = \frac{m_{a,j}}{\rho_a.A_j} \quad (4\text{-}37)$$

Where:

u_j = Velocity of air through j^{th} evaporator (m/s).

The velocity of air flowing through the evaporator by natural convection was estimated using the model proposed by Amos (1995).

$$u_{nc,j} = 0.134.\left|T_{on,j} - T_{s,j}\right|^{0.5} \quad (4\text{-}38)$$

The air side heat transfer coefficient for the j^{th} evaporator can be calculated by using the correlation of the form given by Brooks (2001):

$$U_{a,j} = U_{a,j,refer}.\left(\frac{u_j}{u_{j,refer}}\right)^a \quad (4\text{-}39)$$

Where:

$u_{j,refer}$ = Reference velocity of air flowing through j^{th} evaporator (m/s).

a = Value depending on the evaporator design.

$U_{a,j,refer}$ = Air side heat transfer coefficient for j^{th} evaporator at reference air flow (W/m^2K).

The two general approaches to modelling the decline in air flow rate through evaporator with frost mass are either a linear decline or an exponential decline. Both models were considered. The linear model (O'Hagan 1994) is the reduction in performance as follows:

$$F_{fr,j} = \left(1 - M_{fr,j} R_{Q,j}\right) \tag{4-40}$$

Where:

$M_{,fr,j}$ = Mass of frost on the j^{th} evaporator (kg).

R_{Qj} = Fractional airflow decline with frost accumulation (1/kg).

The exponential model is:

$$F_{fr,j} = e^{-\frac{M_{fr,j}}{F_j}} \tag{4-41}$$

Where:

F_j = Frosting constant (kg)

The rate of mass of ice deposited on the j^{th} evaporator is given by the sum of loss or gain of moisture by condensation/evaporation plus losses of frost due to melting during defrost.

The following conditions apply:

If $M_{fr,j} <= 0$ and $T_{sj} <= 0$ (no frost and surface below 0 °C so frost can form)

$$\frac{dM_{fr,j}}{dt} = \max\left(0, \left[m_{a,j}.\left(H_{on.j} - H_{off.j}\right) - \left(\frac{\phi_{to,de,j}.\eta_{de}.Switch_{de,j}}{h_{lat,fr}}\right)\right]\right) \quad (4\text{-}42)$$

Else if $M_{fr,j}$ <= 0 and T_{sj} >= 0 (no frost and surface below 0 °C so condensation only)

$$\frac{dM_{fr,j}}{dt} = 0 \quad (4\text{-}43)$$

Else if $M_{fr,j}$ >= 0 and T_{sj} <= 0 (frost present and surface below 0 °C so frost can form)

$$\frac{dM_{fr,j}}{dt} = m_{a,j}.\left(H_{on.j} - H_{off.j}\right) - \left(\frac{\phi_{to,de,j}.\eta_{de}.Switch_{de,j}}{h_{lat,fr}}\right) \quad (4\text{-}44)$$

Else if $M_{fr,j}$ >= 0 and T_{sj} >= 0 (frost present and surface above 0 °C so frost will melt)

$$\frac{dM_{fr,j}}{dt} = \min\left(m_{a,j}.\left(H_{on.j} - H_{off.j}\right) - \left(\frac{\phi_{to,de,j}.\eta_{de}.Switch_{de}}{h_{lat,fr}}\right) - Cond_{Drain,j}\right) \quad (4\text{-}45)$$

Else

$$\frac{dM_{fr,j}}{dt} = 0 \quad (4\text{-}46)$$

Where:

$h_{lat,fr}$ = Latent heat of melting (J/kg).

$Cond_{Drain,j}$ = Maximum evaporator condensate drain rate (kg/s).

This model assumes that when the evaporator is defrosting then frost will form or melt depends on the energy balance and that when frost is melting there is a maximum rate that the condensate can drain off the evaporator.

4.2.5 Door Model

The air infiltration through doors often represents more than half the total heat loads for refrigerated stores (coldstores) and it is often the main source of frost on cooling coils. Optimal design and operation of such facilities require accurate prediction of the air infiltration rates. The considerations include:

- Increases the operating costs of the refrigeration system related to the higher heat and moisture loads.
- Increases the capital costs of the refrigeration system related to the higher heat and moisture loads.
- The temperature fluctuations of the cold room may adversely affect product quality or loss of capacity.
- Moisture in the warm air results in fogging, icing of the floor, walls, and product and frosting of the evaporators.

The Chen *et al.* (2002) model was used to evaluate the heat load due to air infiltration through each door. The model includes consideration of:

Air tightness (infiltration rate when door is closed)
Door infiltration when door is open
Effect of door open time
Effect of forklift traffic
Effect of door protection

The total heat and mass flow entry to a zone is the sum of the flow from up to D doors that open into that zone.

$$\phi_{d\to i} = \sum_{d=1}^{D} \phi_d \tag{4-47}$$

$$m_{d\to i} = \sum_{d=1}^{D} m_d \tag{4-48}$$

The average heat load and moisture transfer due to infiltration of air due to a door can be expressed as follows:

$$\phi_d = Q_{av,\inf} \cdot \rho_{a,i} (h_{out} - h_i) \quad (4\text{-}49)$$

$$m_d = Q_{av,\inf} \cdot \rho_{a,i} (H_{out} - H_i) \quad (4\text{-}50)$$

Where:

ϕ_d = Total heat load through door (W).

m_d = Total moisture load through door (kg/s).

$\rho_{a,i}$ = Density of air in the i^{th} zone (kg/m^3).

$Q_{av,inf}$ = Average air infiltration rate (m^3/s).

h_{out} = Enthalpy of the air outside the door (J/kg).

H_{out} Humidity of air outside the door (kg/kg).

The average effect of the door can be represented as a weighted sum of the air infiltration when the door is open, the door is closed, and if open the effect of forklift entering:

$$Q_{av,inf} = Q_{inf,cl}(1 - F_{op}) + Q_{inf,op} \cdot F_{op} + Q_{tr} \cdot F_{op} \quad (4\text{-}51)$$

Where:

$Q_{inf,cl}$ = Air infiltration rate when door is closed (air tightness) (m^3/s).

F_{op} = Fraction of time the door is open.

$Q_{inf,op}$ = Air infiltration rate through an open door without traffic (m^3/s).

Q_{tr} = Extra air infiltration rate due to forklift traffic (m^3/s).

$Q_{inf,cl}$ is the air leakage rate when the doors are closed and depends on number of factors such as external wind speed and directions etc and is generally slow compared to the infiltration when the door is open. Therefore $Q_{inf,cl}$ is assumed to be a constant for a particular store and is expressed for the door closed period as:

$$Q_{\inf,cl} = Q_{se} \cdot L_{se} \quad (4\text{-}52)$$

Where:

Q_{se} = Air interchange through seals (m^3/s m).

L_{se} = Length of door seals (m).

The door infiltration when the door is open is given by:

$$Q_{inf,op} = Q_{Tam}.F_{Tam}.F_{pro} \quad (4\text{-}53)$$

Where:

Q_{Tam} = Air infiltration rate calculated from Gosney and Olama modified Tamm's equation (m^3/s).

F_{Tam} = Tamm's equation correction factor for unprotected door.

F_{pro} = Door protection correction factor.

The door protection correction factor is related to the effectiveness:

$$F_{pro} = (100 - E_{pro})/100 \quad (4\text{-}54)$$

Where:

E_{pro} = Effectiveness of door protection (%).

The flow through an open door is given by Gosney and Olama modified Tamm's equation:

$$Q_{Tam} = 0.67w.y\sqrt{2g.y(1-z)/(1+z^{1/3})^3} \quad (4\text{-}55)$$

Where:

w = Door width (m).

y = Door height (m).

g = Gravitational acceleration (m/s^2).

z = Ratio of warm air density to cold air density = $\rho_{a,out}/\rho_i$

$\rho_{a,out}$ = Density of air outside the door (kg/m^3)

For a typical 3m high forklift doors (between 1.8 and 2.8 m wide) with strip curtain protection with each forklift carrying $1m^3$ pallets, then Q_{tr} is related to the temperature difference across the door by (Cleland *et al*, 2002):

$$Q_{tr} = 0.44(T_{out} - T_i)^{1.8} \quad (4\text{-}56)$$

Where:

T_{out} = Temperature outside the door (°C).

4.2.6 Surface Model

A surface is defined as any planar solid structure, which separates the i^{th} zone air from other zones or from ambient air outside the cool store. Examples of surfaces are insulated walls and ceiling within a cool or cold store (Figure 4-10). The main methods of energy transfer through surfaces are due to convection and radiation on the outside surfaces, convection on the inside surfaces, conduction through the surfaces, energy accumulation on the materials of the surfaces and moisture deposition/evaporation on the inside surfaces.

There are a number of models with varying complexity for modelling surfaces. Surfaces can be treated as resistance only, capacity only, resistance plus capacity (lumped distributed models) or null characteristics (Estrada-Flores *et al,* 1995). In all these models it was assumed thermal properties are not temperature dependent and that each wall layer is internally homogeneous.

For a sandwich panel type wall (Figure 4-10) the resistance only model would not give an accurate energy loading on the air zone since the thermal capacity of the materials of the surfaces are ignored. Therefore a resistance plus capacity (lumped thermal capacity) model would give a better prediction for energy load into

the air zone with two ODE's for inside and outside metal surface temperatures and allows the buffering effect of the surface mass to be taken into account.

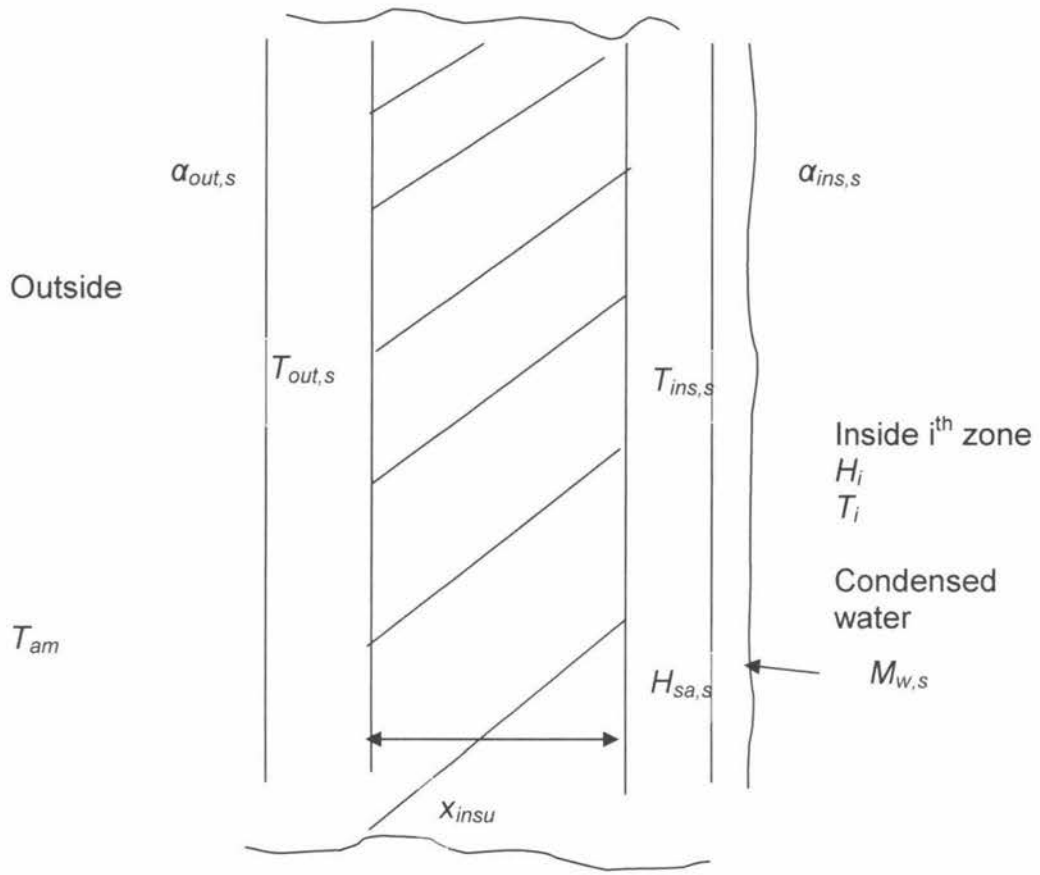

Figure 4-10: Cross section of a typical surface

Since a surface can be common to a number of air zones, a factor is inserted to distinguish the portion of area associated with the particular zone. The model is based on the following assumptions:

Negligible resistance and significant thermal capacity for the metal layers on the inside and external surfaces.

Resistance only for the insulation.

Water vapour condenses on to the inner metal surface only.

The total heat and mass flow entry to a zone is the sum of the flows from up to S surfaces that are associated with that zone.

$$\phi_{s\to i} = \sum_{s=1}^{S}\left(\phi_{ins,s\to i} - \phi_{w,s}\right) \tag{4-57}$$

$$m_{s\to i} = -\sum_{s=1}^{S}\left(\frac{dM_{w,s}}{dt}\right)_i \tag{4-58}$$

Where:

$\phi_{ins,s\to i}$ = Convective heat flow from the inside surface to the i^{th} air zone (w).

$\phi_{w,s}$ = Heat flow to the surface due to water transfer from air zone (W).

$M_{w,s}$ = Mass of condensed water/ice on the inside surface (kg).

For each surface the outside surface temperature is given by:

$$F_{out,s,buffer} M_{out,s} . c_{out,s} . \left[\frac{dT_{out,s}}{dt}\right] = \phi_{out,am\to s} - \phi_{cond} \tag{4-59}$$

Where:

$M_{out,s}$ = Mass of outer surface (kg).

$c_{out,s}$ = Specific heat capacity of outer surface (J/kg K).

$T_{out,s}$ = Outside surface temperature (°C).

$\phi_{out,am\to s}$ = Energy flow to the outer surface from outside air (W).

ϕ_{cond} = Energy flow from outer surface to inside surface by conduction (W).

$F_{out,s,buffer}$ = Correction factor for thermal buffering for the outer metal surface.

The inside surface temperature is given by:

$$\left(M_{s,w}.c_w + F_{ins,s,buffer}M_{ins,s}.c_{ins,s}\right)\left[\frac{dT_{ins,s}}{dt}\right] = \phi_{cond} - \sum_{i=1}^{N}\phi_{ins,s\to i} + \sum_{i=1}^{N}\phi_{w,s} - c_w T_{ins,s}\frac{dM_{w,s}}{dt} \quad (4\text{-}60)$$

Where:

$M_{ins,s}$ = Mass of inside surface (kg).

$c_{ins,s}$ = Specific heat capacity of inner surface (J/kg K).

c_w = Specific heat capacity of water (J/kg K).

$T_{ins,s}$ = Inside surface temperature (°C).

$F_{ins,s,buffer}$ = Correction factor for thermal buffering for the inner metal surface.

The energy flow due to conduction is given by:

$$\phi_{cond} = \frac{\lambda_{insu}}{x_{insu}}.F_{ef,insu}.A_s(T_{out,s} - T_{in,s}) \quad (4\text{-}61)$$

Where:

A_s = Surface area of the surface (m^2).

λ_{insu} = Thermal conductivity of the insulation (W/m K).

x_{insu} = Insulation thickness (m).

$F_{ef.insu}$ = Insulation effectiveness factor

Some of the outside surfaces can be exposed to sun; hence the model takes into account energy flow due to both convection and radiation. The convection and radiation mechanisms can be combined and expressed in terms of convection style equation with sol-air temperature. The condensation/evaporation of water vapour on the outside surface is considered very unlikely and hence is ignored. The energy flow from outside ambient conditions to the outside surface due to convection and solar radiation is given by:

$$\phi_{out,am\to s} = \alpha_{out,s}.A_s(T_{sol} - T_{out,s}) \quad (4\text{-}62)$$

Where:

$\alpha_{out,s}$ = Convective heat transfer coefficient for the outside face (W/m^{2}K).

T_{sol} = Sol-air temperature for the outside face of the surface (°C).

The sol-air temperature is given by:

$$T_{sol} = T_{am} + \frac{SolRad.\varepsilon_{out,s}}{\alpha_{out,s}} \quad (4\text{-}63)$$

Where:

T_{am} = Ambient temperature (°C).

$SolRad$ = Solar radiation incident on the outside surface (W/m^2).

$\varepsilon_{out,s}$ = Emissivity of the outside face of the surface.

The energy flow from the inside surface to associated air zones due to convection is given by:

$$\phi_{ins,s\rightarrow i} = \alpha_{ins,s}.F_{s,i}.A_s(T_{ins,s} - T_i) \quad (4\text{-}64)$$

Where:

$\alpha_{ins,s}$ = Convective heat transfer coefficient for the inside faces (W/m^{2}K).

$F_{s,i}$ = Fraction of the surface associated with i^{th} zone.

The energy flow to surface due to water deposition is given by:

$$\phi_{w,s} = \left(\frac{dM_{w,s}}{dt}\right)_i (h_{fg} + c_v T_i) \quad (4\text{-}65)$$

For both condensation and evaporation of water to occur from the surface the sensible heat component of the enthalpy of water deposited is always equal to that of the water vapour in the air zone.

Assuming water only condenses or evaporates from the surface and is not absorbed, the rate of deposition for the s^{th} surface associated with i^{th} zone and conditions are as follows:

$$\left(\frac{dM_{w,s}}{dt}\right)_i = k_s.F_{s,i}.A_s.F_{e.co,s}(H_i - H_{sa,s}) \qquad (4\text{-}66)$$

Where:

k_S = Mass transfer coefficient for water vapour to the surface from the zone air (kg/m^2 s).

$F_{e,co,s}$ = Evaporation correction factor for the surface.

$H_{sa,s}$ = Saturation humidity of water or ice at surface temperature $T_{ins,s}$ (kg/kg).

The term $F_{e,co,s}$ is an empirical factor depending on the area for evaporation which may be different from the surface area due to formation of water droplets rather than a uniform film of water. The relationships are:

If $M_{w,s} = 0$ and $H_{sa,s} > H_i$, then $F_{e,co,s} = 0$

If $M_{w,s} = 0$ and $H_{sa,s} \leq H_i$, then $F_{e,co,s} = 1.0$

If $M_{w,s} > 0$ and $H_{sa,s} > H_i$, then $F_{e,co,s} = A_e/A_s$

If $M_{w,s} > 0$ and $H_{sa,s} \leq H_i$, then $F_{e,co,s} = 1.0$

Where:

A_e = Evaporation area (m^2).

For the s^{th} surface the water condenses or evaporators due to all associated zones can be expressed as:

$$\left(\frac{dM_{w,s}}{dt}\right) = \sum_{i=1}^{N}\left(\frac{dM_{w,s}}{dt}\right)_i \qquad (4\text{-}67)$$

The mass transfer coefficient for water transfer was estimated by the Lewis relationship:

$$k_s = \frac{\alpha_{ins,s}}{c_a + H_i.c_v} \tag{4-68}$$

4.2.7 Floor Model

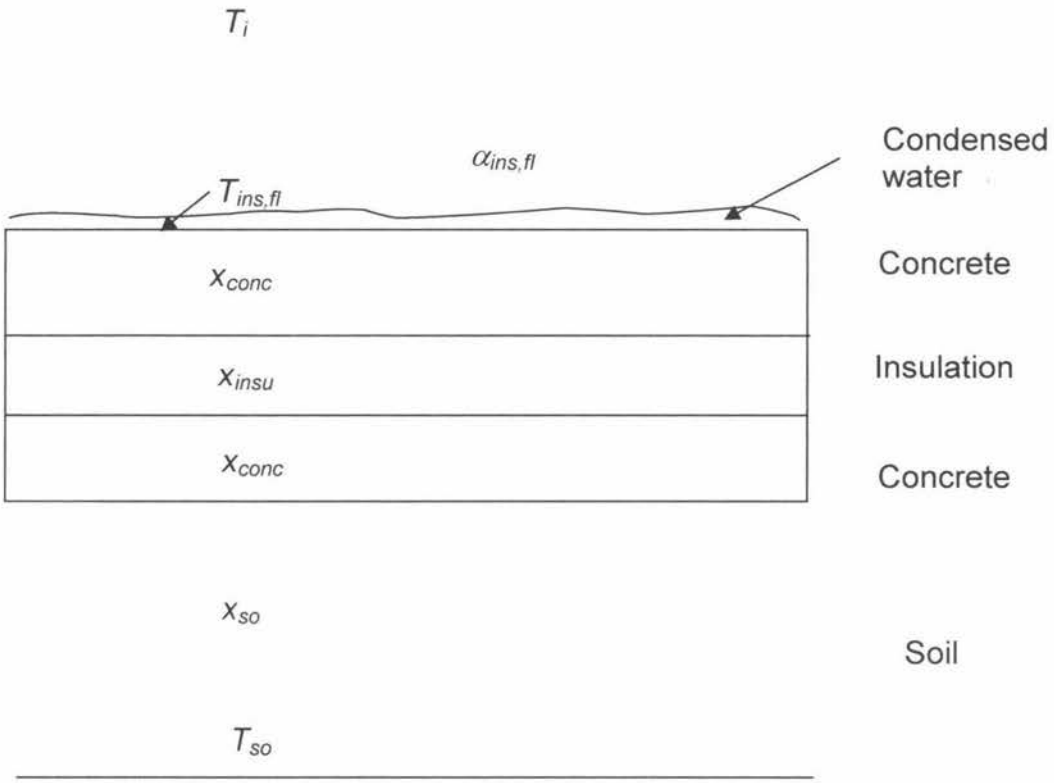

Figure 4-11: A typical floor cross section

Figure 4-11 shows a typical floor cross section for a refrigerated store. It has an insulation layer sandwiched between an upper and a lower layer of concrete. It was assumed that the floor thermal mass was located at the top surface of the floor slab. The floor model can be modelled similar to the surface model except the outside ambient air temperature is replaced by under floor soil temperature and the solar radiation term is eliminated. The conduction component was considered through the soil and the lower concrete slab and insulation, and water vapour condenses onto the floor.

Since a floor can be common to a number of zones, a factor is inserted to distinguish the portion of area associated with each air zone. The total heat and mass flow entry to a zone is the sum of the flow from up to *Fl* floors that are associated with that zone.

$$\phi_{fl\rightarrow i} = \sum_{fl=1}^{Fl} \left(\phi_{ins,fl\rightarrow i} - \phi_{w,fl}\right) \tag{4-69}$$

$$m_{fl\rightarrow i} = -\sum_{fl=1}^{Fl} \frac{dM_{w,fl}}{dt} \tag{4-70}$$

Where:

$\phi_{ins,fl\rightarrow i}$ = Convective heat flow from the inside floor surface to the i^{th} air zone (w).

$\phi_{w,fl}$ = Heat flow to the floor surface due to water transfer from air zone (W).

$M_{w,fl}$ = Mass of condensed water on the floor (kg).

The inside floor surface temperature is given by:

$$(F_{fl,buffer}.M_{fl}.c_{fl} + M_{w,fl}.c_w)\frac{dT_{ins,fl}}{dt} = U_{fl}.F_{fl}.A_{fl}(T_{so} - T_{ins,fl}) - \sum_{i=1}^{N}\phi_{ins,fl} + \sum_{i=1}^{N}\phi_{w,fl} - c_w.T_{ins,fl}.\frac{dM_{w,fl}}{dt} \tag{4-71}$$

Where:

M_{fl} = Floor mass (kg).

c_{fl} = Specific heat capacity of floor (J/kg K).

U_{fl} = Heat transfer coefficient from the deep soil to the position where the thermal mass is located (W/m^2K).

A_{fl} = Area of floor (m^2).

T_{so} = Soil temperature underneath the floor (^oC).

$T_{ins,fl}$ = Floor surface temperature (°C).

$F_{fl,buffer}$ = Correction factor for thermal buffering for the floor.

The overall heat transfer coefficient (U_{fl}) takes into account thermal resistance through the soil from the position where soil temperature was measured and through the lower floor slab and through insulation to the lower surface of the top floor slab. The overall heat transfer coefficient (U_{fl}) is expressed as follows:

$$U_{fl} = \frac{1}{\frac{x_{conc}}{\lambda_{conc}} + \frac{x_{insu}}{\lambda_{insu}.F_{ef.insu}} + \frac{x_{so}}{\lambda_{so}}} \quad (4\text{-}72)$$

Where:

x_{conc} = Thickness of the concrete layer (m).

λ_{conc} = Thermal conductivity of concrete (W/m K).

x_{insu} = Thickness of the insulation layer (m).

λ_{insu} = Thermal conductivity of insulation layer (W/m K).

x_{so} = Thickness of the soil below concrete slab to temperature measurement position (m).

λ_{so} = Thermal conductivity of soil (W/m K).

The energy flow from the floor surface to all associated air zones due to convection is given by:

$$\phi_{ins,fl\rightarrow i} = \alpha_{ins,fl}.F_{fl,i}.A_{fl}.(T_{ins,fl} - T_i) \quad (4\text{-}73)$$

Where:

$\alpha_{ins,fl}$ = Convective heat transfer coefficient from air zone to floor (W/m^{2}K).

$F_{fl,i}$ = Fraction of the floor associated with the i^{th} zone.

Using the same analogy as for the surface the energy flow to the floor due to water deposition is given by:

$$\phi_{w,fl} = \left(\frac{dM_{w,fl}}{dt} \right)_i (h_{fg} + c_v T_i) \tag{4-74}$$

For both condensation and evaporation of water to occur from the floor the sensible heat component of the enthalpy of water deposited is always equal to that of the water vapour in the air zone.

Assuming water only condenses or evaporates from the floor and is not absorbed, the rate of deposition for the fl^{th} surface associated with i^{th} zone and conditions are as follows:

$$\left(\frac{dM_{w,fl}}{dt} \right)_i = k_{fl} . F_{fl,i} . A_{fl} . F_{e,co,fl} (H_i - H_{sa,fl}) \tag{4-75}$$

Where:

k_{fl} = Mass transfer coefficient for water vapour to the floor surface from the zone air (kg/m^2 s).

$H_{sa,fl}$ = Saturation humidity of water at floor surface temperature $T_{ins,fl}$ (kg/kg).

$F_{e,co,fl}$ = Evaporation correction factor for the floor.

The term $F_{e,co,fl}$ is an empirical factor depending on the area for evaporation which may be different from the surface area due to formation of water droplets rather than a uniform film of water. The relationships are:

If $M_{w,fl} = 0$ and $H_{sa,fl} > H_i$, then $F_{e,co,fl} = 0$

If $M_{w,fl} = 0$ and $H_{sa,fl} \leq H_i$, then $F_{e,co,fl} = 1.0$

If $M_{w,fl} > 0$ and $H_{sa,fl} > H_i$, then $F_{e,co,fl} = A_e/A_{fl}$

If $M_{w,fl} > 0$ and $H_{sa,fl} \leq H_i$, then $F_{e,co,fl} = 1.0$

For the fl^{th} floor the water condenses or evaporators due to all associated zones can be expressed as:

$$\frac{dM_{w,fl}}{dt} = \sum_{i=1}^{N}\left(\frac{dM_{w,fl}}{dt}\right)_i \tag{4-76}$$

The mass transfer coefficient for water transfer was estimated by the Lewis relationship given by:

$$k_{fl} = \frac{\alpha_{ins,fl}}{c_a + H_i.c_v} \tag{4-77}$$

4.2.8 Structures Model

Structures are fittings in cool or cold stores other than surfaces, floors, and products with significant thermal mass and heat capacity. Most structures are metallic and have high thermal conductivity and large surface area to volume ratios. They provide thermal buffering and water condense or evaporates from surfaces.

The structures can be modelled similar to the surface model. Since structures can be common to a number of zones, a factor is inserted to distinguish the portion of area associated with the particular zone.

The total heat and mass flow entry to a zone is the sum of the flow from structures up to *St* structures that are associated with that zone.

$$\phi_{st\to i} = \sum_{st=1}^{St}\left(\phi_{st} - \phi_{w,st}\right) \tag{4-78}$$

$$m_{st\to i} = -\sum_{st=1}^{St}\frac{dM_{w,st}}{dt} \tag{4-79}$$

Where:

ϕ_{st} = Convective heat flow from the st^{th} structures to the air zone (W).

$\phi_{w,st}$ = Heat flow to the structure due to water transfer from the air zone (W).

$M_{w,st}$ = Mass of condensed water on the structure (kg).

The temperature of the structure is given by:

$$(F_{st,buffer}.M_{st}c_{st} + M_{w,st}c_w)\frac{dT_{st}}{dt} = -\sum_{i=1}^{N}\phi_{st} + \sum_{i=1}^{N}\phi_{w,st} - c_w.T_{st}\frac{dM_{w,st}}{dt} \quad (4\text{-}80)$$

Where:

M_{st} = Mass of structures mass (kg).

c_{st} = Specific heat capacity of structures (J/kg K).

T_{st} = Structures temperature (°C).

$\alpha_{i,st}$ = Convective heat transfer coefficient from the air zone to the structures (W/m^{2}K).

A_{st} = Surface area of the structures (m^2).

$F_{st,buffer}$ = Correction factor for thermal buffering for the structures.

The energy flow from the structures to associated air zones due to convection is given by:

$$\phi_{st} = \alpha_{i,s}.F_{st,i}.A_{st}(T_{st} - T_i) \quad (4\text{-}81)$$

Where:

$F_{st,i}$ = Fraction of the structures in the i^{th} zone.

Using the same analogy as for the surface the energy flow to structures due to water deposition is given by:

$$\phi_{w,st} = \left(\frac{dM_{w,st}}{dt}\right)_i (h_{fg} + c_v T_i) \quad (4\text{-}82)$$

For both condensation and evaporation of water to occur from the structure the sensible heat component of the enthalpy of water deposited is always equal to that of the water vapour in the air zone. Assuming water only condenses on or evaporates from the structure and is not absorbed, the rate of deposition for the st^{th} surface associated with i^{th} zone and conditions are as follows:

$$\left(\frac{dM_{w,st}}{dt}\right)_i = k_{st}.F_{st,i}.A_{st}.F_{e.co,st}(H_i - H_{sa,st}) \qquad (4\text{-}83)$$

Where:

k_{st} = Mass transfer coefficient for water vapour to the structures from the zone air (kg/m^2 s).

$F_{e,co,st}$ = Evaporation correction factor for the structures.

$H_{sa,st}$ = Saturation humidity of water or ice at structures temperature $T_{,st}$ (kg/kg).

The term $F_{e,co,st}$ is an empirical factor depending on the area for evaporation which may be different from the surface area due to formation of water droplets rather than a uniform film of water.

If $M_{w,st} = 0$ and $H_{sa,st} > H_i$, then $F_{e,co,st} = 0$

If $M_{w,st} = 0$ and $H_{sa,st} \leq H_i$, then $F_{e,co,st} = 1.0$

If $M_{w,st} > 0$ and $H_{sa,st} > H_i$, then $F_{e,co,st} = A_e/A_{st}$

If $M_{w,st} > 0$ and $H_{sa,st} \leq H_i$, then $F_{e,co,st} = 1.0$

For the st^{th} structure the water condenses or evaporators due to all associated zones can be expressed as:

$$\frac{dM_{w,st}}{dt} = \sum_{i=1}^{N}\left(\frac{dM_{w,st}}{dt}\right)_i \qquad (4\text{-}84)$$

The mass transfer coefficient for water transfer was estimated by the Lewis relationship:

$$k_{st} = \frac{\alpha_{i,st}}{c_a + H_i.c_v} \tag{4-85}$$

4.2.9 Heat Generator Model

Heat generators can be defined as any devices, which give out a heat load to the air zones. Such devices include: people, forklifts and lights etc. The total heat and mass flow entry to a zone is the sum of the flow from up to *Hg* heat generators that are associated with that zone.

$$\phi_{hg\rightarrow i} = \sum_{hg=1}^{Hg} \phi_{hg}.Switch_{HG}.F_{hg,i} \tag{4-86}$$

$$m_{hg\rightarrow i} = \sum_{hg=1}^{Hg} m_{hg}.Switch_{HG}.F_{hg,i} \tag{4-87}$$

Where:

ϕ_{hg} = Heat generator total heat load (W).

m_{hg} = Rate of water vapour added by the heat generator (kg/s).

$Switch_{HG}$ = Switch indicating if the heat generator is operating. (1 = on, 0 = off)

$F_{hg,i}$ = Fraction of heat generator associated with i^{th} zone.

The heat load from heat generator can be expressed as follows:

$$\phi_{hg} = \phi_{hg,sen} + \phi_{hg,la} \tag{4-88}$$

Where:

$\phi_{hg,sen}$ = Heat generator sensible heat load (W).

$\phi_{hg,la}$ = Heat generator latent heat load (W).

$$m_{hg} = \frac{\phi_{hg,la}}{(h_{fg} + c_v T_i)} \tag{4-89}$$

4.2.10 Humidifier Model

Humidifiers can be defined as any device, which adds moisture to the air zones. The total heat and mass flow entry to a zone is the sum of the flow from up to *Hu* humidifiers that are associated with that zone.

$$\phi_{hu \to i} = \sum_{hu=1}^{Hu} \phi_{hu} . Switch_{hu} . F_{hu,i} \tag{4-90}$$

$$m_{hu \to i} = \sum_{hu=1}^{Hu} m_{hu} . Switch_{hu} . F_{hu,i} \tag{4-91}$$

Where:

ϕ_{hu} = Humidifier total heat load (W).

m_{hu} = Rate of water vapour added by the humidifier (kg/s).

$Switch_{hu}$ = Switch indicating if the humidifier is operating. (1 = on, 0 = off)

$F_{hum,i}$ = Fraction of humidifier associated with i^{th} zone.

The heat load from humidifier can be expressed as follows:

$$\phi_{hu} = (\phi_{hu,sen} + \phi_{hu,la}) \tag{4-92}$$

Where:

$\phi_{hu,sen}$ = Heat generator sensible heat load (W).

$\phi_{hu,la}$ = Heat generator latent heat load (W).

$$m_{hu} = \frac{\phi_{hu,la}}{(h_{fg} + c_v T_i)} \tag{4-93}$$

For ultrasonic humidifier the water at room temperature is sprayed into the air stream as tiny water droplets and hence the latent heat load is given by:

$$\phi_{hu,lat} = m_{hu}.c_w.T_i \quad (4\text{-}94)$$

Where:

c_w = Specific heat capacity of water (J/kg K).

If there is on/off control of the humidifier:

If $H \leq H_{sp}$ then $Switch_{hu} = 1$

$H \geq H_{sp} + DB_{hu,set}$ then $Switch_{hu} = 0$

H_{sp} is the absolute humidity that the zone is controlled to maintain.

Alternatively if a PID controller is used for the humidifier it can be expressed as follows:

$$Switch_{hu} = \max\left(1, \left(Pf_{hu}.(H_{sp} - H_{on,j}) + \frac{1}{I_{hu}}.\int(H_{sp} - H_{on,j})dt + D_{hu}.\frac{dH_{on,j}}{dt}\right)\right) \quad (4\text{-}95)$$

Where:

H_{sp} = Absolute humidity set point (kg/kg).

$H_{on,j}$ = Absolute humidity of air on to j^{th} evaporator ((kg/kg).

$DB_{hu,set}$ = Dead band for the humidifier.

Pf_{hu} = Proportional constant for the humidifier.

I_{hu} = Integral constant for the humidifier.

D_{hu} = Derivative constant for the humidifier.

4.2.11 Product and Packaging

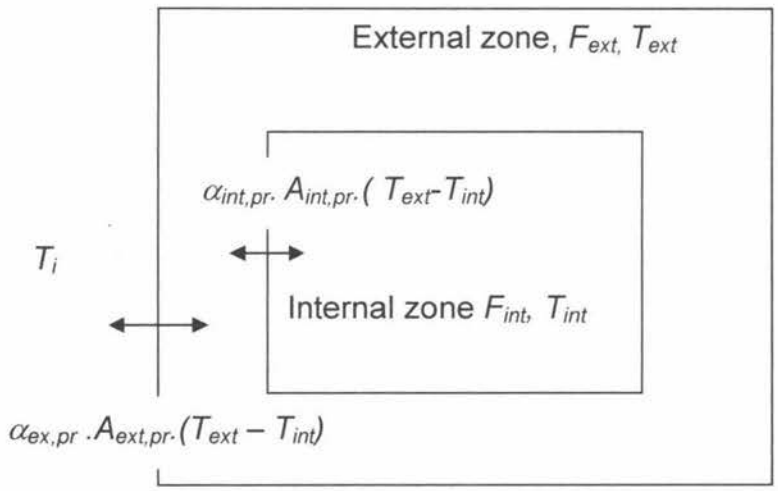

Figure 4-12: Two zone product model used to simulate product heat transfer.

Figure 4-12 shows the two zone product model for heat transfer between the product and the air (Witt *et al*, 1999). The products are potentially the highest source of thermal capacitance in a refrigerated facility. A product model should be able to represent both precooling and bulk storage of product, and needs to include a range of mechanisms including conduction within the product; convection, radiation, evaporation from product surface to the air, heat generation within the product and heat and mass transfer for packaging associated with the product, particularly the adsorption of moisture by paper based materials (Amos, 1995). The Witt *et al* (1999) model was found to be the simplest model to simulate the cooling and buffering characteristics of products. Model features are:

- Two product zones to give accuracy for both pull-down heat transfer and buffering heat transfer during storage.
- Lumped-parameter heat transfer between the product and cool store air with fluctuating temperature.

- Conduction heat transfer within the solid product.
- Convection heat transfer outside the surface of the solid product.
- Respiration and evaporation of water vapour from fruit surface assumed negligible or modelled as pseudo-convection (Amos, 1995).
- Absorption of water by packaging associated with the product.

Each product batch is assumed to exist in a single air zone only. The total heat and mass flow entry to an air zone is the sum of the flow from solid products up to *Pr* solid products that are associated with that zone.

$$\phi_{pr\rightarrow i} = -\sum_{pr=1}^{Pr}\left(\phi_{ex,pr} + \phi_{w,ex,pr}\right).B_{pr.bat} \tag{4-96}$$

Where:

$\phi_{ex,pr}$ = Heat transfer rate from air zone to the outside of a solid product item (W).

$\phi_{w,ex,pr}$ = Heat transfer rate due to water condensing on the outer surface (W).

$B_{pr,bat}$ = Number of product item in each batch.

$$m_{pr\rightarrow i} = -\sum_{pr=1}^{Pr}\frac{dM_{w,pack,pr}}{dt}.B_{pr.bat} \tag{4-97}$$

Where:

$M_{w,pack,pr}$ = Amount of moisture in packaging associated with each product item (kg/s).

The equation for the temperature in the outside zone of each product batch is:

$$(M_{w,pack,pr}.c_w + F_{ex,pr}.M_{pr}.c_{ef,pr})\frac{dT_{ex,pr}}{dt} = \phi_{ex,pr} - \phi_{\text{int},pr} + \phi_{w,ex,pr}$$
$$- c_w.T_{ex,pr}.\frac{dM_{w,pack,pr}}{dt} \tag{4-98}$$

Where:

M_{pr} = Mass of solid product in each item (kg).

$F_{ex,pr}$ = Mass fraction allocated to the external product zone.

$c_{ef,pr}$ = Effective specific heat capacity of the solid product (J/kg K).

$T_{ex,pr}$ = Temperature of outside product zone (°C).

$\phi_{int,pr}$ = Heat transfer rate to inside zone (W).

The heat transfer due to convection between the outside product zone and the i^{th} zone is:

$$\phi_{ex,pr} = \alpha_{ex,pr} . A_{ex,pr} . (T_i - T_{ex,pr}) \quad (4\text{-}99)$$

Where:

$A_{ex,pr}$ = Outside surface area of the solid product item (m^2).

$\alpha_{ex,pr}$ = Effective heat transfer coefficient between the solid product item and the air (W/m^2K)

The heat transfer between the outside and inside zones was modelled as pseudo-convection.

$$\phi_{int,pr} = \alpha_{int,pr} . A_{int,pr} . (T_{ex,pr} - T_{int,pr}) \quad (4\text{-}100)$$

Where:

$\alpha_{int,pr}$ = Effective heat transfer coefficient between solid product external and internal zones (W/m^2K)

$A_{int,pr}$ = Surface area of the product inside zone (m^2).

$T_{int,pr}$ = Temperature of inside product zone (°C).

The ODE for the temperature of the inside zone for the product item is:

$$\left(1-F_{ext,pr}\right)M_{pr}c_{ef,pr}\frac{dT_{\text{int},pr}}{dt}=\phi_{\text{int},pr} \tag{4-101}$$

Where:

$F_{ext,pr}$ = Mass fraction allocated to the outer product zone.

The energy flow due to absorption/desorption of moisture by the packaging is:

$$\phi_{w,ex,pr}=\left(\frac{dM_{w,pack,pr}}{dt}\right).(h_{fg}+c_vT_i) \tag{4-102}$$

The amount moisture in the packaging is given by:

$$M_{w,pack,pr}=\left(\frac{mc_{pack,pr}}{100-mc_{pack,pr}}\right).M_{dry,pack,pr} \tag{4-103}$$

Where:

$mc_{pack,pr}$ = Packaging moisture content of the pr^{th} product batch (%).

$M_{dry,pack,pr}$ = Mass of dry packaging associated with each product item (kg).

Therefore the rate of change of moisture in the package associated with each product item is given by differentiating equation (4-103).

$$\left(\frac{dM_{w,pack.pr}}{dt}\right)=\left(\frac{100.\dfrac{dmc_{pack,pr}}{dt}}{\left(100-mc_{pack,pr}\right)^2}\right).M_{dry,pack,pr} \tag{4-104}$$

The rate of change of moisture content of the packing associated with each product item is:

$$\frac{dmc_{pack,pr}}{dt}=k_{mc}.\left(EMC_{pack,i}-mc_{pack,pr}\right) \tag{4-105}$$

Where:

$EMC_{pack,i}$ = Equilibrium package moisture content for packaging in the associated air zone (%).

k_{mc} = Rate constant for water absorption or desorption (s^{-1}).

The equilibrium moisture content at a given RH can be estimated from the moisture sorption isotherm of packaging material. A commonly applied model is GAB isotherm (Eagleton *et al,* 1994) and an isotherm based on this model from paper-based packaging materials is:

$$EMC_{pack,i} = \frac{\frac{RH_i}{100}}{\frac{k_{GAB}}{x_{mGAB}}\left(\frac{1}{c_{GAB}}-1\right)\cdot\left(\frac{RH_i}{100}\right)^2+\left(\frac{\left(1-\frac{2}{c_{GAB}}\right)}{x_{mGAB}}\right)\cdot\left(\frac{RH_i}{100}\right)+\left(\frac{1}{x_{mGAB}}\right)\cdot\left(\frac{c_{GAB}}{k_{GAB}}\right)} \quad (4\text{-}106)$$

Where:

c_{GAB} = GAB isotherm constant.

k_{GAB} = GAB isotherm constant.

x_{mGAB} = GAB isotherm constant.

RH_i = RH of the i^{th} zone.

The constants for the heat transfer between the external and internal zone can be estimated by (Witt *et al,* 1999);

$$\alpha_{ins,pr}.A_{ins,pr} = \frac{E}{3}.\frac{V_{pr}.\beta^2.\lambda_{pr}}{X^2{}_{pr}} \quad (4\text{-}107)$$

Where:

E = Shape factor for the product item.

V_{pr} = Volume of each solid product item (m^3).

λ_{pr} = Effective thermal conductivity of the product (W/m K).

X_{pr} = Shortest distance between the surface and centre of the product

item (m).

β is the first root of:

$$\beta \cot \beta + (Bi - 1) = 1 \qquad (4\text{-}108)$$

Where

$$Bi = \frac{\alpha_{ex,pr} . X_{pr}}{\lambda_{pr}} \qquad (4\text{-}109)$$

Where:

Bi = Biot number

M_{pr}, $c_{ef,pr}$ and λ_{pr} can be estimated from the physical data for the products. The ratios of external zone to internal zones mass fraction are given by (Witt *et al.* 1999):

$$\frac{F_{ex,pr}}{(1 - F_{ext,pr})} = 5.431 - 5.309 e^{(-0.1438 Bi^{-0.7068})} \qquad \text{for Bi} < 50 \qquad (4\text{-}110)$$

$$\frac{F_{ex,pr}}{(1 - F_{ext,pr})} = 0.20 \qquad \text{for Bi} \geq 50 \qquad (4\text{-}111)$$

Using the methodologies of Jamieson *et al* (1993), the effective thermal properties of the product can be estimated by assuming that each product has two parts:

1. External packaging with trapped air item that affects the value of $\alpha_{ex,pr}$.
2. Mixture of internal packaging, product, and air that effect $c_{ef,pr}$ and λ_{pr}.

The external packaging provides thermal resistance between the air zone and the product and the effective surface heat transfer coefficient takes into account the convection from the packaging surface to the air, radiation from the packaging

surface to surrounding objects, acting in parallel; plus conduction through the external packaging layers and trapped air in series (Jamieson *et al*,1993).

$$\frac{1}{\alpha_{ex,pr}} = \frac{1}{\alpha_a} + \sum \frac{x_{pack}}{\lambda_{pack}} + \frac{x_a}{\lambda_a} \qquad (4\text{-}112)$$

Where:

$\alpha_{ex,pr}$ = Heat transfer coefficient between outside surface and zone air (W/m^2 K).

α_a = Heat transfer coefficient due to convection or combined convection, evaporation and radiation (W/m^2 K).

x_{pack} = Thickness of external packaging (m).

x_a = Thickness of air trapped (m).

λ_{pack} = Thermal conductivity of external packaging (W/m K).

λ_a = Thermal conductivity of trapped air (W/m K).

Jamieson *et al* (1993) approximated convective heat transfer between the air and the packaging surface using:

$$\alpha_a = 25 u_a^{0.25} \qquad (4\text{-}113)$$

Where:

u_a = Velocity of air stream over the product item (m/s).

The effective thermal conductivity for the pallet can be estimated by the series model (Jamieson *et al*, 1993):

$$\lambda_{pr} = \frac{1}{\frac{\sum_b F_b}{\lambda_b}} \qquad (4\text{-}114)$$

Where:

λ_b = Thermal conductivity of product b^{th} component (W/m K).

F_b = Volume fraction of the b^{th} product component.

The effective specific heat capacity of the product is given by:

$$c_{ef,pr} = \sum F_{pr}.c_{pr} \quad (4\text{-}115)$$

Where:

c_{pr} = Specific heat capacity of product component (J/kg K).

F_{pr} = Mass fractions of product component.

4.3 REFRIGERANT SIDE COMPONENTS

To complete the cold store model the refrigeration components performance need to be predicted. Figure 4-13 shows a schematic of the refrigeration system. The basic cycle is a single stage direct expansion system with a single compressor but with number of evaporators with suction line heat exchangers (SLHE). Compressor control possibilities are on/off based on suction pressure, on/off based on room temperature and hot gas by pass to prevent low suction pressure.

The modelling approach described by Amos (1995) was adopted except that:

- More detailed models of the evaporators that included the effects of frosting and defrosting were used.
- The hot gas bypass control option was added.
- Suction line heat exchangers were added to include subcooling/ superheating of the refrigerant entering/leaving the evaporators.

Room air temperature control is by either evaporator pressure regulator (EPR) on the evaporators or on/off solenoids controlling liquid feed to each evaporator.
General assumptions of the model are:

- Pressure drop (ΔP) was constant
- Heat losses from pipes are negligible

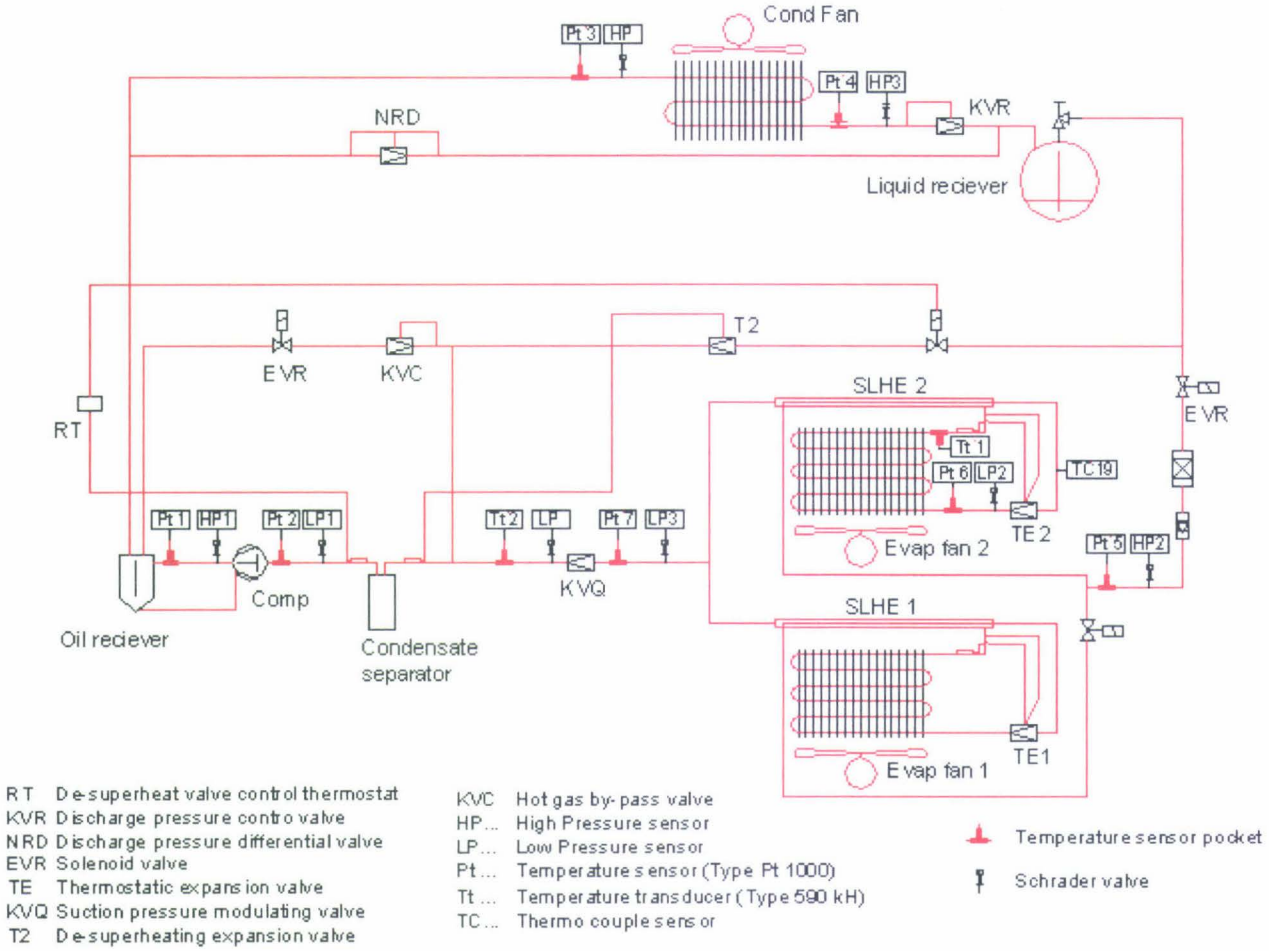

Figure 4-13: Schematic of the refrigerant circuit and experimental measuring locations.

- Negligible refrigerant hold up in pipes and compressor
- Constant super heat at the exit from the evaporator.
- Constant sub cooling of the refrigerant exiting the condenser

4.3.1 Evaporator Model (Refrigerant-side)

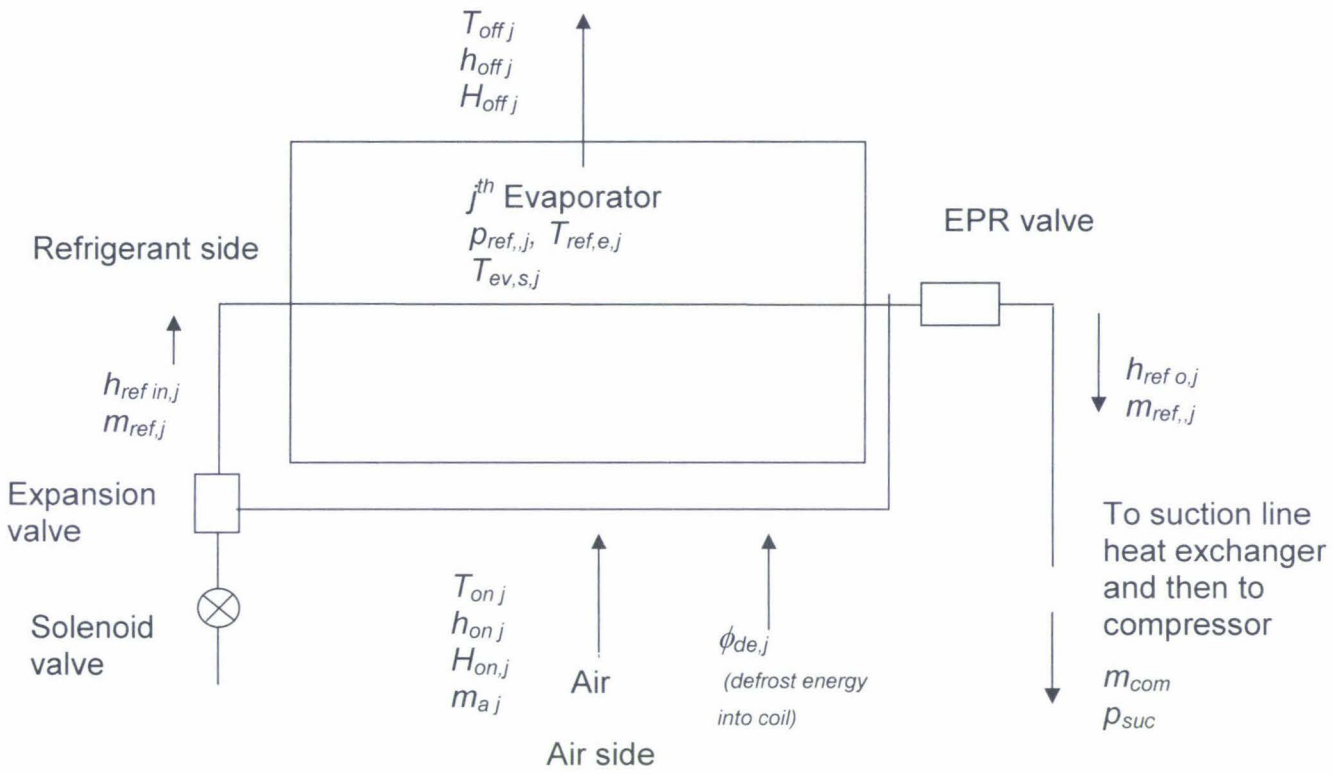

Figure 4-14: Schematic of the evaporator showing model nomenclature.

Figure 4-14 shows a schematic diagram for the evaporator. Three possible single zone approaches to modelling the refrigerant side of the evaporator are:

1. Use of an ODE for the compressor suction condition and algebraic equations for the refrigerant evaporation temperature in the evaporator.

2. Use of an ODE for refrigerant evaporation temperature in the evaporator and algebraic equations for the compressor suction conditions based on flow through the EPR valve.
3. Use of an ODE for both refrigerant evaporation temperature in the evaporator and suction condition of the compressor.

The third modelling approach was chosen because it is most appropriate for multiple evaporators. A multi-zone evaporator model was considered too complex given the uncertainty in many of the application heat loads. It was assumed that there were no heat losses in the evaporator.

The refrigerant evaporation temperature for the j^{th} evaporator can be determined from an energy balance considering heat transfer from the air, change in heat transfer rate due to frosting, energy removed by the refrigerant and heat addition due to defrost:

$$\frac{d(M_{fr,j}.c_{fr} + F_{Evapbuffer}.Mc_j.).T_{ref,j}}{dt} = \phi_{a,j} - \phi_{ref,j} + \phi_{de,j}.(1-\eta_{de}).Switch_{de,j} \qquad (4\text{-}116)$$

Where:

$M_{fr,j}$ = Mass of frost on the j^{th} evaporator (kg/s).

Mc_j = Thermal buffering capacity of the j^{th} evaporator (W/K).

$T_{ref,j}$ = Temperature of evaporating refrigerant in j^{th} evaporator (°C)

$\phi_{a,j}$ = Total heat transfer from the air stream to the j^{th} evaporator (W).

$\phi_{ref,j}$ = Total heat transfer to refrigerant in the j^{th} evaporator (W).

$\phi_{de,j}$ = Total heat load due to defrost of the j^{th} evaporator (W).

c_{fr} = Specific heat capacity of frost (J/kg K).

$F_{Evapbuffer}$ = Correction factor for thermal buffering for the evaporator.

$Switch_{de,j}$ = Switch for defrost coil. (1 = on, 0 = off)

η_{de} = Defrost efficiency

Using the chain rule the equation can be decoupled to give:

$$(M_{fr,j}.c_{fr} + F_{Evapbuffer}.Mc_j.)\frac{dT_{ref,j}}{dt} = \phi_{a,j} - \phi_{ref,j} + \phi_{de,j}.(1-\eta_{de}).Switch_{de,j}$$
$$- c_{fr}.T_{ref,j}.\frac{dM_{fr,j}}{dt} \quad (4\text{-}117)$$

The heat flow from the air to the evaporator is a combination of sensible and latent heat and is given by:

$$\phi_{a.j} = m_{a.j}(h_{on,j} - h_{off,j}) = m_{a,j}.\left(c_p.(T_{on,j} - T_{off,j}) + h_{fg}.(H_{on,j} - H_{off,j})\right) \quad (4\text{-}118)$$

The energy flow from the evaporator to the refrigerant is:

$$\phi_{ref.j} = m_{ref,j}.\left(h_{ref,out,j} - h_{ref,in,j}\right)Switch_{ref,j} \quad (4\text{-}119)$$

Where:

$m_{ref,j}$ = Mass flow of refrigerant through the j^{th} evaporator (kg/s).

$h_{ref.out,\ j}$ = Enthalpy of refrigerant at the j^{th} evaporator outlet (J/kg).

$h_{ref.in\ j}$ = Enthalpy of refrigerant at the j^{th} evaporator inlet (J/kg).

Section 4.3.2 shows how the enthalpy of refrigerant was evaluated.

A method is needed to estimate the refrigerant flow through each of the j^{th} evaporators which may have different evaporating temperatures. It was decided that the flow rate would be estimated pro-rata to the suction line pressure drop.

Since evaporator pressure is a function of saturated temperature of the refrigerant (refer to Section 4.4.1), the pressure drop across the suction line for each evaporator can be estimated using suction pressure and pressure drop across the evaporator pressure regulator (EPR) valve:

$$P_{ref,j} = f_1(T_{ref,j}) \quad (4\text{-}120)$$

$$\Delta P_j = P_{ref,j} - P_{suc} + \Delta P_{EPR} \quad (4\text{-}121)$$

Where:

ΔP_j = Suction line pressure drop for the j^{th} evaporator (Pa).

$P_{ref,j}$ = Refrigerant pressure in the j^{th} evaporator (Pa).

P_{suc} = Compressor suction pressure (Pa).

ΔP_{EPR} = Pressure drop across EPR valve (Pa).

The volume of refrigerant flow through the j^{th} evaporator can be estimated relative to define volumetric flow at a known reference pressure drop.

$$Q_{ref,j} = \left(abs\left(\frac{\Delta P_j}{\Delta P_{std,j}} \right) \right)^{\frac{1}{3}} . Q_{std,j} \tag{4-122}$$

Where:

$Q_{std,j}$ = Reference volume flow for the j^{th} evaporator (m^3/s).

$P_{std,j}$ = Reference pressure drop across the j^{th} evaporator (Pa).

Thus the refrigerant mass flow through the j^{th} evaporator is:

$$m_{ref,j} = \frac{Q_{ref,j}}{v_{ref,Out,j}} \tag{4-123}$$

Where:

$v_{ref,Out,j}$ = Specific volume of refrigerant at j^{th} evaporator outlet (m^3/kg).

4.3.2 Suction Line Heat Exchanger (SLHE)

Figure 4-15 shows a schematic for the suction line heat exchanger (SLHE). The SLHE was modelled as a simple heat exchanger with constant effectiveness. The sub cooled liquid refrigerant from the condenser is further cooled by the suction line heat exchanger (SLHE) to heat the refrigerant vapour leaving the evaporator to the suction of the compressor. Since the model consists of multiple evaporators with multiple SLHE, all the outlet vapour from the SLHE's will mix at the suction

condition. The enthalpy of refrigerant vapour leaving the evaporator is a function of evaporator pressure and temperature (refer to Section 4.4.4).

$$T_{ref,out,j} = T_{ref,j} + SH \tag{4-124}$$

$$h_{ref,out,j} = f_4(P_{ref,j}, T_{ref,out,j}) \tag{4-125}$$

Where:

$T_{ref,out,j}$ = Refrigerant temperature at the j^{th} evaporator outlet (°C).

SH = Evaporator super heat (°C).

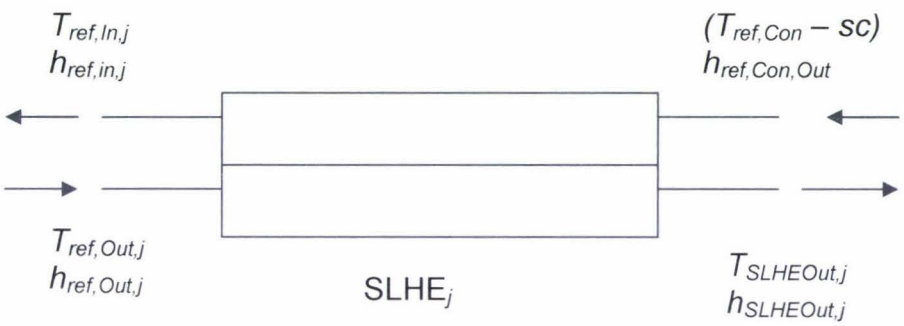

Figure 4-15: Schematic of the suction line heat exchanger.

The enthalpy of the liquid refrigerant entering the j^{th} evaporator can be estimated using the enthalpy of refrigerant at j^{th} evaporator outlet and temperature of liquid refrigerant at the condenser outlet by an energy balance over the SLHE:

$$h_{ref,in,j} = h_{ref,Con,Out} - h_{SLHEOut,j} + h_{ref,Out,j} \tag{4-126}$$

Where:

$h_{ref,Con,Out}$ = Enthalpy of liquid refrigerant at condenser outlet (J/kg).

$h_{SLHEOut,j}$ = Enthalpy of super heated refrigerant vapour at the SLHE outlet (J/kg).

It is assumed that the mass flow rates on the liquid and vapour sides of the SLHE are equal then:

$$T_{SLHEOut,j} = T_{ref,Out,j} + \varepsilon_{SLHE}.\left(T_{ref,conOut} - T_{ref,Out,j}\right) \quad (4\text{-}127)$$

Where:

$T_{ref,Con,Out}$ = Temperature of subcooled refrigerant leaving condenser (°C).

ε_{SLHE} = Heat transfer effectiveness factor for the heat exchanger (SLHE).

Enthalpy of refrigerant leaving SLHE outlet is a function of suction pressure and temperature of refrigerant at SLHE outlet (refer to Section 4.4.4).

$$h_{SLHEOut,j} = f_4(P_{Suc}, T_{SLHEOut,j}) \quad (4\text{-}128)$$

Enthalpy of refrigerant leaving the condenser is a function of condensing pressure and the temperature of liquid refrigerant at condenser outlet (refer to Section 4.4.2).

$$T_{ref,Con,Out} = T_{ref,Con} - SC \quad (4\text{-}129)$$

$$h_{ref,Con,Out} = f_3(T_{ref,Con,Out}) \quad (4\text{-}130)$$

Where:

$T_{ref,Con}$ = Refrigerant temperature at condenser (°C).

$h_{ref,Con,Out}$ = Enthalpy of refrigerant at condenser outlet (J/kg).

SC = Condenser sub cooling (°C).

The total heat transfer from liquid to vapour refrigerant in the j^{th} evaporator SLHE is given by:

$$\phi_{SLHEOut,j} = m_{ref,j}.\left(h_{SLHEOut,j} - h_{ref,Out,j}\right) \quad (4\text{-}131)$$

Where:

$\phi_{SLHEOut,j}$ = Total heat transfer from the liquid to vapour refrigerant in the j^{th}

evaporator SLHE (W).

4.3.3 Hot Gas Bypass

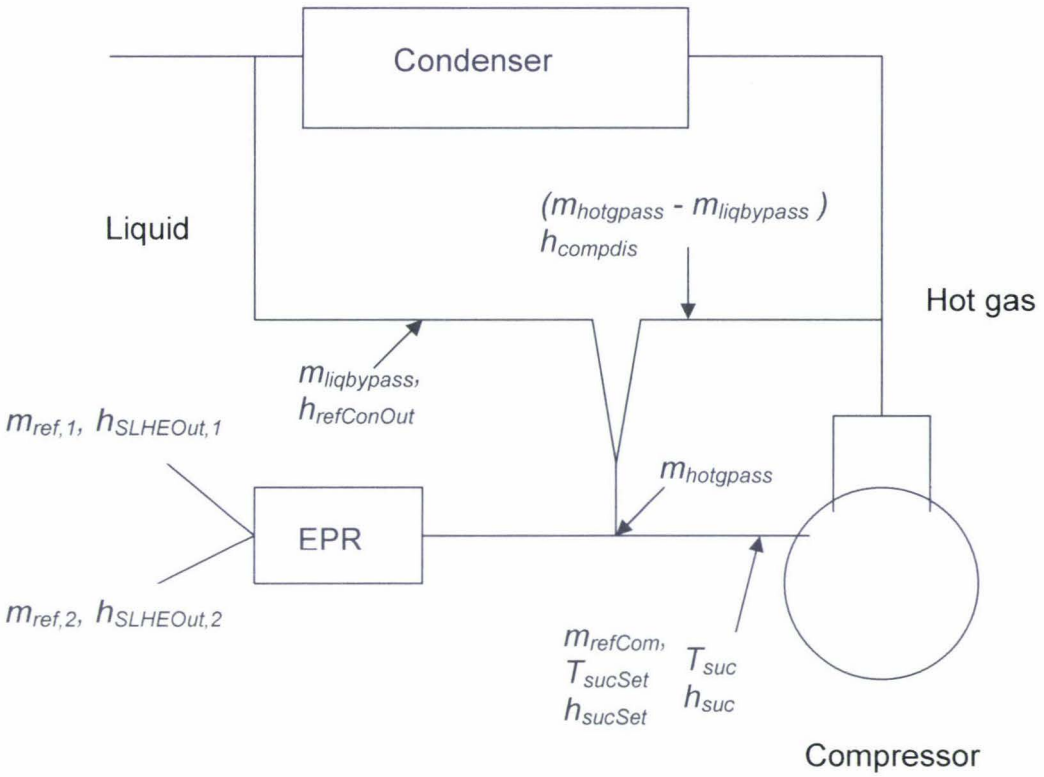

Figure 4-16: Schematic diagram showing the hot gas by pass area of the refrigeration circuit

Figure 4-16 shows a schematic of a hot gas bypass circuit with dual evaporators feeding to one EPR valve at the compressor suction. If the suction pressure falls too low the compressor would cut out on low pressure to prevent vacuum operation. The hot gas bypass acts to avoid vacuum operation. However with hot gas bypass, the higher suction temperature can lead to high discharge pressure and temperature. To control the suction pressure and temperature a controlled

flow rate of liquid refrigerant from the condenser exit and hot gas from the discharge line is mixed at the entrance to the suction line (hot gas by pass). The flow rate of liquid is controlled by thermostatic expansion valve to ensure that the suction temperature is at or below a set point. The flow rate of hot gas is controlled by a solenoid valve fed by a differential pressure sensor which activates when the suction pressure falls below the suction pressure setpoint.

The energy balance on the compressor suction gives:

$$\left(\sum_{j=1}^{NEvaps} m_{ref,j}.h_{SLHEOut,j}\right) + m_{liqbypass}.h_{refConOut} + \left(m_{hotgpass} - m_{liqbypass}\right)h_{comdis} = \left(\left(\sum_{j=1}^{NEvaps} m_{ref,j}\right) + m_{hotgpass}\right).h_{sucSet} \quad (4\text{-}132)$$

Rearranging the above equation gives the mass flow rate of liquid refrigerant by passed into the suction line for a given suction temperature set point (T_{sucSet}). The value of liquid refrigerant has to be a positive quantity and hence is expressed as:

$$m_{liqbypass} = max\left(0, \frac{\left(\left(\left(\sum_{j=1}^{NEvaps} m_{ref,j}\right) + m_{hotgpass}\right).h_{sucSet} - \left(\sum_{j=1}^{NEvaps} m_{ref,j}.h_{SLHEOut,j}\right) - m_{hotgpass}.h_{Comdis}\right)}{\left(h_{refConOut} - h_{Comdis}\right)}\right) \quad (4\text{-}133)$$

Where:

h_{sucSet} = Enthalpy of refrigerant at set suction temperature and corrected suction pressure (J/kg).

h_{Comdis} = Enthalpy of refrigerant at compressor discharge (J/kg).

$h_{refConOut}$ = Enthalpy of refrigerant at condenser outlet (J/kg).

The enthalpy of refrigerant at the set suction temperature is a function of set temperature and suction pressure (refer to Section 4.4.4):

$$h_{sucSet} = f_4(P_{suc}, T_{sucSet}) \tag{4-134}$$

The mass of hot gas bypass can be expressed as:

$$m_{hotgpass} = \frac{Q_{hotgpass}}{v_{suc}} \tag{4-135}$$

Where:

$Q_{hotgpass}$ = Volume of hot gas bypass (m^3/s).

The maximum flow rate of hot gas bypass cannot exceed the refrigerant flow through compressor at any given time and is:

$$Q_{hotgpassMax} = \eta_{Com,vol} \cdot Q_{Com} \tag{4-136}$$

The volume of hot gas bypass can be expressed in being proportional to the difference between suction pressure and setpoint suction pressure and the suction pressure deadband. If suction pressure is less than the sum of the suction pressure setpoint and the deadband the volume of hot gas bypass is:

$$Q_{hotgpass} = min\left(\left(Q_{hotgpassMax} \cdot F_{hotgpassMax} \right), \left(\frac{Q_{hotgpassMax} \cdot \left(P_{hotgpass} + DB_{hotgpass} - P_{suc} \right)}{F_{hotgpass}} \right) \right) \tag{4-137}$$

Where:

$DB_{hotgpass}$ = Dead band for the suction pressure (Pa).

$P_{hotgpass}$ = Hot gas bypass pressure setpoint (Pa).

$F_{hotgpassMax}$ = Correction factor for maximum allowable hot gas bypass.

$F_{hotgpass}$ = Proportional factor for hot gas bypass.

If suction pressure is greater than the sum of suction pressure setpoint and the deadband the volume of hot gas bypass is:

$$Q_{hotgpass} = 0 \tag{4-138}$$

4.3.4 Compressor Model

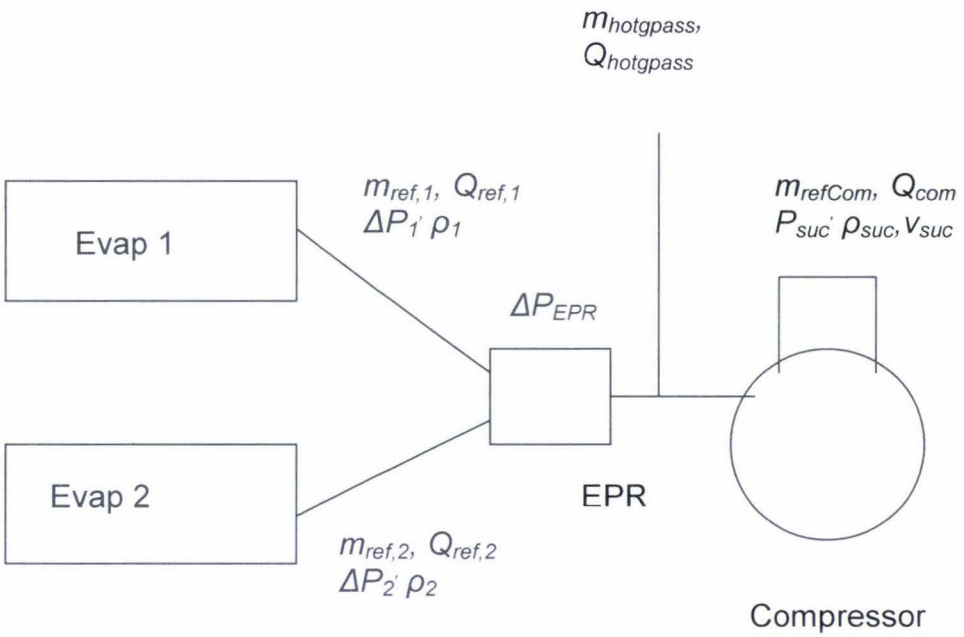

Figure 4-17: Refrigerant flow from two evaporators to the compressor

Figure 4-17 shows a schematic of the refrigeration system low pressure side. The temperature of refrigerant vapour entering the compressor suction is a function of enthalpy and pressure (refer to Section 4.4.4):

$$T_{suc} = f_4(h_{suc}, P_{suc}) \tag{4-139}$$

Where:

P_{suc} = Compressor suction pressure (Pa).

h_{suc} = Enthalpy of refrigerant vapour at compressor suction (J/kg).

A mass balance on the compressor suction gives:

$$V_{suc} \cdot \frac{d\rho_{suc}}{dt} = \sum_{j=1}^{J} (m_{ref,j}) + m_{hotgpass} - Q_{com} \cdot \eta_{comvol} \cdot \rho_{suc} \quad (4\text{-}140)$$

Where:

$m_{hotgpass}$ = Liquid plus hot gas by pass into suction line (kg/s).

ρ_{suc} = Density of refrigerant at suction condition (kg/m^3).

V_{suc} Volume of the compressor suction (m^3)

Applying universal gas laws, the density of the refrigerant can be expressed in terms of pressure.

$$\rho = P \cdot \frac{MW}{R.T} \quad (4\text{-}141)$$

Where:

MW = Molecular weight of refrigerant

R = Universal gas constant

Hence the rate of change of refrigerant density can be expressed in terms of rate of change of pressure.

$$\frac{d\rho}{dt} = \frac{MW}{R.T} \cdot \frac{dP}{dt} \quad (4\text{-}142)$$

Since density of refrigerant at compressor suction and SLHE outlets are approximately equal, equation (4-140) can be re-expressed as:

$$k_{sucpressure} \cdot F_{sucbuffer} \cdot \frac{dP_{suc}}{dt} = \sum_{j=1}^{J} Q_{ref,j} + Q_{hotgpass} - Q_{com} \cdot \eta_{comvol} \cdot Switch_{com} \quad (4\text{-}143)$$

Where:

$k_{sucpressure}$ = Thermal buffering constant for the compressor suction.

$F_{sucbuffer}$ = Correction factor for thermal buffering for suction pressure.

$Switch_{com}$ = Compressor switch (1 = on, 0 = off).

If refrigerant flow exists in the suction then the suction enthalpy is given by:

$$h_{suc} = \frac{\sum_{j=1}^{J} m_{ref,j}.h_{SLHEOut,j} + \left(m_{hotgpass} - m_{liqbypass}\right).h_{Comdis} + m_{liqbypass}.h_{refConOut}}{\left(\sum_{j=1}^{J} m_{ref,j} + m_{hotgpass}\right)} \quad (4\text{-}144)$$

If there is no flow through the evaporator ($m_{ref,j}$ = 0) the following conditions is defined to obtain suction enthalpy.

$$h_{suc} = \frac{\sum_{j=1}^{J} h_{SLHE,j}}{J} \quad (4\text{-}145)$$

The mass flow through compressor is:

$$m_{refCom} = \frac{Q_{com}\eta_{Com,Vol}}{v_{suc}}.Switch_{Com} \quad (4\text{-}146)$$

Where:

Q_{Com} = Compressor swept volume (m^3/s).

$\eta_{Com,vol}$ = Compressor volumetric efficiency.

v_{suc} = Specific volume of refrigerant entering the compressor suction (m^3/kg).

The enthalpy of vapour leaving the compressor can be calculated by assuming all compressor input energy transfer to the vapour except for some defined heat losses:

$$h_{Comdis} = h_{suc} + \frac{\Delta h_{Comdis}}{\eta_{ComIsen}} - \frac{\phi_{Comloss}}{m_{refCom}} \quad (4\text{-}147)$$

Where:

$h_{Com,dis}$ = Enthalpy of refrigerant at compressor discharge (J/kg).

h_{suc} = Enthalpy of refrigerant at suction (J/kg).

Δh_{Comdis} = Change in enthalpy due to compression (J/kg).

$\eta_{ComIsen}$ = Compressor isentropic efficiency.

$\phi_{Comloss}$ = Heat loss from compressor surface to ambient air (W).

The temperature of compressor discharge is a function of discharge enthalpy and condenser pressure (refer to Section 4.4.4):

$$T_{Comdis} = f_4(h_{Comdis}, P_{ref,Con}) \tag{4-148}$$

Where:

$P_{ref,Con}$ = Condenser pressure (Pa).

Condenser pressure is a function of saturated refrigerant temperature of the condenser; hence discharge pressure can be expressed in terms of the following (refer to Section 4.4.1):

$$P_{ref,Con} = f_1(T_{ref,Con}) \tag{4-149}$$

$$P_{Comdis} = P_{ref,Con} + \Delta P_{disline} \tag{4-150}$$

Where:

$\Delta P_{disline}$ = Pressure drop across the compressor discharge line (Pa).

The heat loss from the compressor surface can be expressed as:

$$\phi_{Comloss} = (UA)_{Com} . F_{UA,Com} . (T_{Comdis} - T_{am}) \tag{4-151}$$

Where:

$(UA)_{Com}$ = Heat transfer coefficient between compressor outer surface and ambient air (W/k).

$F_{UA,Com}$ = Correction factor for compressor heat transfer.

T_{am} = Ambient air temperature (°C).

4.3.5 Condenser Model

For the condenser the model derived by Cleland (1983) and Cleland *et al.* (1982) was used. The enthalpy of refrigerant at condenser outlet is estimated assuming that subcooling in the condenser is constant. The condenser temperature can be expressed in terms of an ODE:

$$(Mc_{Con}.F_{Conbuffer}).\frac{dT_{refCon}}{dt} = \phi_{refCon} - \phi_{airCon} \quad (4\text{-}152)$$

Where:

ϕ_{refCon} = Total heat transfer to refrigerant in the condenser (W).

ϕ_{airCon} = Total heat transfer to air in the condenser (W).

Mc_{Con} = Thermal buffering capacity of condenser (W/K).

$F_{Conbuffer}$ = Correction factor for thermal buffering of the condenser.

The heat rejected by the refrigerant is given by:

$$\phi_{refCon} = (m_{refCom} - (m_{hotgpass} - m_{liqbypass})).(h_{Comdis} - h_{refConOut}) \quad (4\text{-}153)$$

The heat rejected to surrounding medium from the condenser is given by:

$$\phi_{airCon} = (UA)_{Con}.F_{UACon}.(T_{refCon} - T_{am}) \quad (4\text{-}154)$$

Where:

$(UA)_{Con}$ = Product of overall heat transfer coefficient and heat transfer area (W / K).

F_{UACon} = Correction factor for condenser overall heat transfer coefficient.

T_{am} = Ambient temperature (C)

4.3.6 Evaporator and Compressor Control

The evaporator control can be carried out by an EPR valve with a PID controller or simply by an on/off switch for the refrigerant solenoid valve. In either case the

control mechanism can be based on air-on or air-off temperature of the air stream through the evaporator.

A PID controller for the system with an EPR valve (air-on basis) can be expressed as follows:

$$\Delta P_{EPR} = Pf_{EPR} \cdot (T_{sp} - T_{on,j}) + \frac{1}{I_{EPR}} \cdot \int (T_{sp} - T_{on,j}).dt + D_{EPR} \cdot \frac{dT_{on,j}}{dt} \qquad (4\text{-}155)$$

Where:

ΔP_{EPR} = Pressure drop across the EPR valve (Pa).

T_{sp} = Air temperature set point (°C).

Pf_{EPR} = Proportional response factor for the EPR valve.

I_{EPR} = Integral response factor for the EPR valve.

D_{EPR} = Differential response factor for the EPR valve.

A minimum and a maximum value of ΔP_{EPR} are set in the model. In case of ΔP_{EPR} calculated to be less than minimum set value, ΔP_{EPR} is set to the minimum value. If it is calculated to be greater than the maximum set value then ΔP_{EPR} is set for the maximum set value and the integral term in equation (4-155) is set to zero.

Alternatively, a simple on/off evaporator controller can be expressed in terms of temperature of air on to the evaporator. The controller can switch the refrigerant solenoid valve ($Switch_{ref,j}$) in the following manner:

If $T_a \leq T_{a,\,set}$ then $Switch_{ref,j} = 0$

$T_a > T_{a,\,set} + DB_{a,set}$ then $Switch_{ref,j} = 1$

And $\Delta P_{EPR} = \Delta P_{EPR,\,min}$

Where:

$T_{a,\,set}$ = Control set temperature (°C).

$DB_{a,set}$ = Deadband limit for solenoid control (°C).

T_a is the temperature that the evaporator is controlled to maintain and can be that of air entering ($T_{on,j}$) or leaving ($T_{off,j}$) the evaporator or the air zone temperature (T_i) depending on where the control thermostat is located.

The compressor can be switched on/off depending on the compressor suction pressure and different status with the following conditions:

If $P_{suc} \leq LP_{cutout}$ or $Switch_{de,j} = 1$ then $Switch_{Com}$=0

If $P_{suc} > LP_{cutout} + DB_{LPcutout}$ and $Switch_{de,j} \neq 1$ then $Switch_{Com}$=1

Where:

LP_{cutout} = Set low pressure cut out (Pa).

$DB_{LPcutout}$ = Dead band limit for compressor suction pressure (Pa).

If defrosting all fans are switched off as well as the compressor being switched off.

If $Switch_{de,j} = 1$ then $SwitchFan_k$ = 0 (4-156)

If $Switch_{de,j} = 0$ then $SwitchFan_k$ = 1 (4-157)

Most defrost systems are initiated on a fixed time basis, and use a combination of time or temperature termination because such systems are simple and reliable. The defrost coil can be switched depending on the duration of defrosting time and surface temperature of the evaporator coil with the following conditions:

If $t_{elaps} \geq t_{deRep}$ and $t \leq (t_{deRep} + t_{deDur})$ and $T_{sj} \leq T_{sjdefrostoff}$ then $Switch_{de,j}$ =1

If $t_{elaps} \geq t_{deRep}$ and $t \leq (t_{deRep} + t_{deDur})$ and $T_{sj} \geq T_{sjdefrostoff}$ then $Switch_{de,j}$ =0

If $t_{elaps} \leq t_{deRep}$ or $t \geq (t_{deRep} + t_{deDur})$ then $Switch_{de,j}$ =0

Where:

t_{elaps} = Time since last defrost (s).

t_{deRep} = Defrost repeating interval (s).

t_{deDur} = Maximum allowable time for defrosting (s).

$T_{sjdefrostoff}$ = Evaporator surface temperature setpoint for defrosting (°C).

4.4 REFRIGERANT PROPERTIES FOR R134A

The refrigeration system modelled uses refrigerant R134a. In order to evaluate energy transfer in the refrigeration system it is necessary to calculate the refrigerant thermodynamic properties at different operating conditions. The polynomial curve-fits for refrigerant thermodynamic properties for R134a developed by Cleland (1992) were used to evaluate the refrigeration system model.

4.4.1 Vapour Pressure and Saturation Temperature for R134a (f_1 & f_2)

The refrigerant vapour pressure and saturation temperature is:

$$P_{sat} = f_1(T_{sat}) = \exp\left(21.51297 - \frac{2200.9809}{246.61 + T_{sat}}\right) \quad (4\text{-}158)$$

$$T_{sat} = f_2(P_{sat}) = \left(\frac{-2200.9809}{\ln(P_{sat}) - 21.51297}\right) - 246.61 \quad (4\text{-}159)$$

Where:

P_{sat} = Absolute saturated pressure of refrigerant (Pa).

T_{sat} = Saturated temperature of refrigerant (°C).

4.4.2 Liquid Enthalpy for R134a (f_3)

The polynomial curve fit for liquid refrigerant based on ASHRAE enthalpy datum is:

$$h_L = f_3(T_L) = 50952 + 1335.29T_L + 1.70650T_L^2 + 7.6741\times10^{-3}T_L^3 \quad (4\text{-}160)$$

Where:

h_L = Enthalpy of liquid refrigerant (J/kg).

T_L = Temperature of liquid refrigerant (°C).

The range of applicability is equation (4-160) is (-40°C ≤ T_L ≤ 70°C).

4.4.3 Saturated Vapour Enthalpy for R134a

The polynomial curve fit for saturated vapour enthalpy for R134a based on ASHRAE enthalpy datum is:

$$h_v = 249455 + 606.163 \times T_{sat} - 1.05644 \times T_{sat}^2 - 1.82426 \times 10^{-2} T_{sat}^3 \quad (4\text{-}161)$$

Where:

h_v = Enthalpy of saturated vapour (J/kg).

The range of applicability for equation (4-161) is (-40°C ≤ T_L ≤ 70°C).

4.4.4 Superheated Vapour Enthalpy for R134a (f_4)

Super heated vapour at pressure P and temperature T_{SH} the degree of super heat is given by:

$$\Delta T_{SH} = T_{SH} - T_{sat} \quad (4\text{-}162)$$

The polynomial curve fit for super heated vapour enthalpy for R134a based on ASHRAE enthalpy datum is:

$$h_{SH} = f_4(P_{sat}, T_{SH}) = h_v \begin{pmatrix} 1 + 3.48186 \times 10^{-3}.\Delta T_{SH} + 1.6886 \times 10^{-6}.\Delta T_{SH}^2 \\ + 9.2642 \times 10^{-6}.\Delta T_{SH}^2.T_{sat} - 7.698 \times 10^{-8}.\Delta T_{SH}^2.T_{sat} \\ + 1.7070 \times 10^{-7}.\Delta T_{SH}.T_{sat}^2 - 1.2130 \times 10^{-9}.\Delta T_{SH}^2.T_{sat}^2 \end{pmatrix} \quad (4\text{-}163)$$

Where:

h_{SH} = Enthalpy of super heated vapour (J/kg).

T_{SH} = Temperature of super heated refrigerant (°C)

4.4.5 Saturated Vapour-specific Volume for R134a

The polynomial curve fit for saturated vapour specific volume is:

$$v_v = \exp\left(-12.4539 + \frac{2669.0}{273.15 + T_{sat}}\right) \times \begin{pmatrix} 1.01357 + 1.06736 \times 10^{-3}.T_{sat} \\ -9.2532 \times 10^{-6}.T_{sat}^2 \\ -3.2192 \times 10^{-7}.T_{sat}^3 \end{pmatrix} \quad (4\text{-}164)$$

Where:

v_v = Specific volume of saturated vapour (m^3/kg).

4.4.6 Superheated Vapour-specific Volume for R134a (f_5)

The polynomial curve fit for super heated vapour specific volume for R134a is:

$$v_{SH} = f_5(P_{sat}, T_{SH}) = v_v \begin{pmatrix} 1 + 4.7881 \times 10^{-3}.\Delta T_{SH} - 3.965 \times 10^{-6}.\Delta T_{SH}^2 \\ +2.5817 \times 10^{-5}.\Delta T_{SH}.T_{sat} - 1.8506 \times 10^{-7}.\Delta T_{SH}^2.T_{sat} \\ +8.5739 \times 10^{-7}.\Delta T_{SH}.T_{sat}^2 - 5.401 \times 10^{-9}.\Delta T_{SH}^2.T_{sat}^2 \end{pmatrix} \quad (4\text{-}165)$$

Where:

v_{SH} = Specific volume of super heated vapour (m^3/kg).

4.4.7 Enthalpy Change for Isentropic Compression for R134a (f_6)

4.4.7.1 No Vapour Superheat at Suction

Enthalpy change in isentropic compression for R134a with no vapour super heat at suction is:

$$\Delta h = f_6(P_{comdis}, P_{SucCom}, \Delta T_{comp}, \Delta T_{SH}, T_{SatSuc})$$

$$= \frac{c}{c-1}.P_{SucCom}v_{SucCom}.\left(\left(\frac{P_{Comdis}}{P_{SucCom}}\right)^{\left(\frac{c-1}{c}\right)} - 1\right) \quad (4\text{-}166)$$

Where:

Δh = Enthalpy change in isentropic compression for R134a (J/kg).

The saturated suction and discharge temperature corresponding to suction and discharge pressure can be calculated using equation (4-159) and the temperature change due to compression is:

$$\Delta T_{comp} = T_{SatComdis} - T_{SatSuc} \tag{4-167}$$

The curve fit for c is:

$$\begin{aligned} c = c_{il} &= 1.06469 - 1.6907\times10^{-3}.T_{SatSuc} - 8.560\times10^{-6}.T_{SatSuc} \\ &- 2.135\times10^{-5}.T_{SatSuc}.\Delta T_c - 6.1730\times10^{-7}.T_{SatSuc}^2.\Delta T_c \\ &+ 2.0740\times10^{-7}.T_{SatSuc}.\Delta T_c^2 + 7.720\times10^{-9}.T_{SatSuc}^2.\Delta T_c^2 \\ &- 6.103\times10^{-4}.\Delta T_c \end{aligned} \tag{4-168}$$

4.4.7.2 Vapour Superheat at Suction

If the suction vapour is at P_{Suc} and temperature T_{Suc} the suction superheat is:

$$\Delta T_{SH} = T_{Suc} - T_{SatSuc} \tag{4-169}$$

The curve fit equation for c for equation (4-166) for vapour with superheat at suction is:

$$c = c_{il}.\begin{pmatrix} 1 + 1.1757\times10^{-3}.\Delta T_{SH} - 1.814\times10^{-5}.\Delta T_{SH}^2 + 4.121\times10^{-5}.\Delta T_{SH}^2.T_{SatSuc} \\ - 8.093\times10^{-7}.\Delta T_{SH}^2.T_{SatSuc} \end{pmatrix} \tag{4-170}$$

The value of c_{il} is found from equation (4-168).

4.5 AIR HUMIDITY

The model given by Cleland et al (2002) based on ideal gas laws were used for the calculation of air absolute humidity:

$$P_{to} = P_v + P_g \tag{4-171}$$

Using molecular weight of water as 18 and the mean molecular weight of dry air 29 the following equation can be obtained.

$$H = \frac{18.P_v}{29.(P_{to} - P_v)} \quad (4\text{-}172)$$

Where:

P_v = Partial pressure of water vapour (Pa).

P_{to} = Total air (atmospheric) pressure (Pa).

P_g = Partial pressure of dry air (Pa).

Saturation humidity can be expressed:

$$H_w = \frac{18P_w}{29(P_{to} - P_w)} \quad (4\text{-}173)$$

Where:

H_w = Saturated humidity (kg water vapour / kg dry air).

P_w = Vapour pressure of water vapour (Pa).

The vapour pressure of water vapour can be expressed in terms of dry bulb temperature is as follows:

If $T < 0^oC$

$$P_w = e^{(28.7775 - \frac{6071.67}{(T+271.511)})} \quad (4\text{-}174)$$

If $T > 0^oC$

$$P_w = e^{(23.4795 - \frac{3990.56}{(T+233.833)})} \quad (4\text{-}175)$$

Relative humidity is expressed as follows:

$$RH = \frac{P_v}{P_w}.100 \qquad (4\text{-}176)$$

Where:

RH = Relative humidity (%).

4.6 NUMERICAL IMPLEMENTATION

Matlab 6.5 was used to carry out the computer simulation of the model presented above. The ODE's were solved using the ODE45 solver package incorporated in the package based on an explicit Runge-Kutta formula. The CD accompanying this thesis contains the computer programme written for Matlab 6.5.

The input data for operating parameters and SI data was previously prepared on an Excel spread sheet called "Matrix" and included on the CD. The output of the model simulation was saved onto six output data files (outdata1 to outdata 6) at required time intervals by changing time step on the input data (for the simulations 30 second interval was used). Table 4-3 give the details of output data for the six files at each time step.

Computation time was roughly proportional to simulation time. For example, on a 3.0 GHz PC with 512 MB of RAM, it took 9.4 hours computation time to simulate 47 hours of actual time for the for the cool room described in chapter 5. The cool store model involved 2 air zones and 2 evaporators with 4 induced draught fans. The moisture and heat loads were mimicked by an ultrasonic humidifier and with electrical heaters. The model for this situation comprised about 70 ordinary differential equations and more than 160 algebraic equations.

Table 4-3: List of out put data from the programme (files outdata 1 to outdata6).

Outdata 1

t	Time (s).
h_i	Enthalpy of air zones (J/kg).
H_i	Absolute humidity of air zones (kg water vapour / kg dry air).
T_i	Temperature of the air zones (^oC).
RH_i	Relative humidity of air zones (%).
$\phi_{air \rightarrow i}$	Energy flow to the air zones due to forced and natural convection of air from other air zones and the evaporators (W).
$m_{air \rightarrow i}$	Mass of water vapour entering the air zones due to forced and natural convection from adjacent air zones and the evaporators (kg/s).
$h_{off,\,j}$	Enthalpy of air leaving evaporators (J/kg).
$h_{on,j}$	Enthalpy of air on to the evaporators (J/kg).
$H_{off,\,j}$	Absolute humidity of air leaving evaporators (kg/kg).
$H_{on,j}$	Absolute humidity of air on to the evaporators (J/kg).
$T_{off,\,j}$	Temperature of air leaving evaporators (^{o}C).
$T_{on,j}$	Temperature of air on to the evaporators (^{o}C).
$RH_{off,\,j}$	Relative humidity of air leaving evaporators (%).
$RH_{on,j}$	Relative humidity of air on to the evaporators (%).
$m_{a,,j}$	Mass of air passing through the evaporators (kg/s).
$T_{s,j}$	Surface temperature of the evaporator coils (^{o}C).

Outdata 2

t	Time (s).
$\phi_{a,\,j}$	Total heat transfer from the air stream to the evaporators (W).
$\phi_{ref,\,j}$	Total heat transfer to refrigerant in the evaporators (W).
$\phi_{de,j}$	Total heat load due to defrost of the evaporators (W).
$\phi_{a,\,j,\,to}$	Total heat transfer from the air stream to all evaporators (W).
$\phi_{ref,\,j,\,to}$	Total heat transfer to refrigerant to all evaporators (W).

Table 4-3: Continued.

$\phi_{de,j,\,to}$	Total heat load due to defrost all the evaporators (W).
$F_{fr,j}$	Frosting factor
$m_{ref,j}$	Mass flow of refrigerant through the evaporators (kg/s).
m_{refCom}	Mass flow of refrigerant through the compressor (kg/s).
$Q_{ref,j}$	Volume of refrigerant flow through the evaporators (m^3/s).
$Q_{ref,j,to}$	Volume of refrigerant flow through all the evaporators (m^3/s).
$T_{ref,In,j}$	Temperature of liquid refrigerant at evaporator inlets (°C)
$T_{ref,j}$	Temperature of evaporating refrigerant in evaporators (°C)
T_{suc}	Suction temperature (°C)
$T_{sat,suc}$	Saturated suction temperature (°C)
T_{refcon}	Condenser temperature (°C)
T_{Comdis}	Discharge temperature (°C)
$T_{sat,Comdis}$	Saturated discharge temperature (°C)
T_{Comsur}	Compressor surface temperature (°C)
$T_{refconOut}$	Refrigerant temperature at condenser outlet (°C)
$T_{ref,Out,j}$	Temperature of refrigerant at evaporator outlets (°C)
$T_{SLHEOut,j}$	Temperature of refrigerant at SLHE outlets (vapour) (°C)
Outdata 3	
t	Time (s).
$P_{ref,,j}$	Refrigerant pressure in the evaporators (Pa).
ΔP_j	Suction line pressure drop for the evaporators (Pa).
P_{suc}	Compressor suction pressure (Pa).
ΔP_{EPR}	Pressure drop across EPR valve (Pa).
$P_{ref,Con}$	Condenser pressure (Pa).
$\eta_{Comlsen}$	Compressor isentropic efficiency
$\eta_{Com,vol}$	Compressor volumetric efficiency.
$\phi_{Comloss}$	Heat loss from compressor surface to ambient air (W).
$Switch_{ref,j}$	Switch to control refrigerant supply to the evaporators.
$Switch_{Com}$	Compressor switch.

Table 4-3: Continued.

$Switch_{def,j}$	Switch for defrost coils
$Switch_{fan}$	Switch for fans
$Switch_{d}$	Switch for door opening
$\phi_{d,i}$	Total heat load through door to zones (W).
$m_{d,i}$	Total moisture load through door to zones (kg/s).
$\phi_{hg,i}$	Heat generator total heat load to zones (W).
$\phi_{hu,i}$	Humidifier total heat load to zones (W).
Outdata 4	
t	Time (s).
$\phi_{s\rightarrow i}$	Total heat flow from the surfaces to the air zones (w).
$\phi_{fl\rightarrow i}$	Total heat flow from the floor to the air zones (w).
$\phi_{st\rightarrow i}$	Total heat flow from the structures to the air zones (w).
$m_{hg\rightarrow i}$	Total moisture flow from the heat generators to the air zones (kg/s).
$m_{hu\rightarrow i}$	Total moisture flow from the humidifiers to the air zones (kg/s).
$m_{s\rightarrow i}$	Total moisture flow from the surfaces to the air zones (kg/s).
$m_{fl\rightarrow i}$	Total moisture flow from the surfaces to the air zones (kg/s).
$m_{st\rightarrow i}$	Total moisture flow from the structures to the air zones (kg/s).
$M_{w,s}$	Mass of condensed water/ice on the inside surface (kg).
$M_{w,fl}$	Mass of condensed water/ice on the floor surface (kg).
$M_{w,st}$	Mass of condensed water/ice on the structures (kg).
$UA_{o,j}$	Overall heat transfer coefficient from air to refrigerant for the evaporators (W/K).
$U_{a,j}$	Heat transfer coefficient from the air to the evaporator surface (evaporators) (W/m^2K).
$U_{o,j}$	Overall heat transfer coefficient from air to refrigerant for the evaporators (W/m^2K).
u_j	Velocity of air through evaporators (m/s).

Table 4-3: Continued.

$Q_{hotgpass}$	Volume of hot gas bypass (m^3/s).
$\phi_{pr\rightarrow i}$	Total heat flow from the products to the air zones (w).
$m_{pr\rightarrow i}$	Total moisture flow from the products to the air zones (w).
Outdata 5	
t	Time (s).
$T_{ins,s}$	Inside surface temperature (°C).
$T_{out,s}$	Outside surface temperature (°C).
$T_{ins,fl}$	Floor surface temperature (°C).
T_{st}	Structures temperature (°C).
$T_{ex,pr}$	Temperature of outside product zone (°C).
$T_{int,pr}$	Temperature of inside product zone (°C).
$mc_{pack,pr}$	Packaging moisture content of the pr^{th} product batch (%).
$M_{w,pack,pr}$	Amount of moisture in packaging associated with each product item (kg/s).
Outdata 6	
t	Time (s).
$\phi_{sen,to}$	Total sensible heat load (w).
$\phi_{lat,to}$	Total latent heat load (w).
$\phi_{s,\ sen}$	Total sensible heat load from surfaces (w).
$\phi_{s,lat}$	Total latent heat load from surfaces (w).
$\phi_{fl,\ sen}$	Total sensible heat load from floor (w).
$\phi_{fl,lat}$	Total latent heat load from floor (w).
$\phi_{st,\ sen}$	Total sensible heat load from structures (w).
$\phi_{st,lat}$	Total latent heat load from structures (w).
$\phi_{d,\ sen}$	Total sensible heat load through doors (w).
$\phi_{d,lat}$	Total latent heat load through doors (w).
$\phi_{pr,\ sen}$	Total sensible heat load from products (w).

Table 4-3: Continued.

$\phi_{pr,lat}$	Total latent heat load from products (w).
$\phi_{de,\ sen}$	Total sensible heat load from defrost coils (w).
$\phi_{fan,\ sen}$	Total sensible heat load from fans (w).
$\phi_{hg,sen}$	Total sensible heat load from heat generators (w).
ϕ_{Com}	Compressor power

5 EXPERIMENTAL METHODS

5.1 INTRODUCTION

Measurements of the performance of a small walk-in cool room and its associated refrigeration system were made in order to provide model validation data. The cool room was operated for a range of artificial sensible and latent heat loads (some constant and some variable) in order to provide data across a wide range of conditions.

In addition some trials were under taken for a range of defrost frequency settings in order to both provide further validation data and to investigate the effect of defrost frequency on defrost efficiency,

5.2 COOL STORE DESCRIPTION

Figure 5-1 and Figure 5-2 shows the cooling coils and the condensing unit for the cool room. Figure 5-3 shows the cool room location inside the post harvest laboratory in Massey University's Ag Engineering Building. The cool room was 3.3 m wide by 4.4 m long by 3.0 m high with the walls, ceiling and floor constructed from 150 mm thick sandwich insulation panels, and a 1.2 m by 2.4 m hinged door protected by a strip curtain. The walls and ceiling panels had steel cladding on the inner and outer surfaces. The floor panel is polystyrene insulated panel with steel cladding on the inner surface. The store was lit with 450 W of lighting and cooled by two cooling coils via an air cooled HFC-134a refrigeration system, with a nominal capacity of 7.6 kW at -10°C evaporation temperature and 40°C condensation temperature. The coils had a nominal sensible heat transfer rating of 640 W/K each and had two induced draft variable speed 73 W fans each, 2 kW electric defrost elements. Refrigerant feed was controlled by a thermostatic expansion (TX) valve and each evaporator coil also had a suction line heat exchanger. One coil of the system could be isolated from the system (fans remain on) by a liquid feed solenoid valve if required. The air temperature of the room was controlled by an electronic evaporation pressure regulating (EPR) valve.

Figure 5-1: Cooling coils for the cool room.

Figure 5-2: Air cooled condensing unit.

The fans had a single speed potentiometer to regulate the fan speed of all four fans. Time between defrosts (defrost interval) was controlled by a time clock ranging from 2 to 30 hour intervals and defrost was terminated based on coil surface temperature or time (whichever was shortest). Table 5-1 gives the details of the major components installed on the refrigeration system.

Table 5-1: Details of major refrigeration system components

Components	Make and Model
Condensing unit	APV 13440X
Compressor	DWM – Copeland Model: DLL40X (Semi accessible)
Evaporator	Comprex S4/3 PED (2 off)
Expansion valve	Sporlan QVE -2 - C
Temperature and humidity control	Carel RTH 640
Humidity sensor	Carel SSDOHH (Humidity sensor)
Temperature sensor	Carel SSTOOB (Temperature sensor)
Defrost control	Carel S90 – DP10000
Over temperature safety switch	MSK80R
Evaporator pressure valve	Danfoss KVQ22 / EKS67
Solid state reheat relay	SSR/1500
Reheat controller	QLD Control Co Model 1HV4002
Alarm temperature	Carel CR7224 (set for temperature)
Alarm humidity	Carel CR7224 (set for humidity)
Refrigerant	R134a
Fan speed control	Carrier generic

5.3 EXPERIMENTAL SET-UP

To measure the variations of cool room temperature, relative humidity, refrigerant temperature, pressure and electrical power consumptions, a 64 channel HP Agilent data logger was used to record all measured data simultaneously through out the experimental period. Figure 4-13 & Table 5-2 gives the details of temperature and pressure sensor locations in the refrigerant circuit. Figure 4-13, Figure 5-4 & Table 5-2 gives the temperature and RH sensor locations for the cool room. Figure 5-4 shows the thermopile arrangement that was to measure evaporator and condenser air temperature change.

The fixed sensors included:

- Coil air off temperature and air-on temperature using thermocouples and thermopiles to obtain differential temperature.
- Coil air-on RH and room RH using RH Hycal Ceramic SIL sensors and the stores RH control probe (Carel SSDOHH).
- Ambient RH using a Hycal Ceramic SIL sensor.
- Temperature of walls and air zones using thermocouples (Type T) and temperature transducers (590kH).
- Refrigerant temperature at various locations in the circuit using PT1000 sensors.
- Refrigerant pressure at 6 locations using Danfoss AKS 32 low and high pressure transducers.
- Power consumption of the compressor, evaporator fan, condenser fan and defrost coil using power (kW) and current transducers (Carrel T-1W3 and Carrel T-1LC).

A handheld vane anemometer was used to measure the cooling coil air velocities before and after the experimental trial as follows:

- Evaporator fan air flow measurements for 100% and 50% settings.
- Condenser fan flow measurement.

Artificial sensible heat load was provided by up to 5 kW electric heating elements and the lighting system. A handheld clip on ammeter and multi-meter was used to measure the current and voltage of the electric heaters before and after the experimental trial. The lighting load was estimated by their indicated power outputs based on the number of lights working during the experimental trial.

Artificial latent load was provided by a Stutz ENS 1200 ultrasonic humidifier (maximum output of 0.47 kg/hr). The water supply tank (25 litres) for the humidifier was weighed before and after each trial to obtain the water consumption during the trial. The evaporator condensate and, for defrost, melt amounts were measured by

weighing the collected melts on a regular basis. Masses were measured using standard laboratory scales with accuracy of ± 0.01 kg.

Air velocities, sensible heat loads and moisture loads were assumed to be constant throughout the trials.

5.4 SENSOR CALIBRATIONS

The RH sensors were calibrated to within ±3% RH, against four saturated salt solutions of known RH: Sodium chloride (75%), Potassium Chloride (87%), Potassium Nitrate (94%) and Magnesium Nitrate (54%). The sensors were located above the saturated salt solutions in an air tight jar; left hanging (without touching the salt solution) for a minimum of 24 hours and output voltage of the sensors were recorded during the period. The calibration is obtained by plotting output voltage verses known RH for the saturated solution. Appendix A gives the calibration curves for the four sensors. The temperature sensors were calibrated against ice and boiling point of water (within ±0.1 ^{o}C) and pressure sensors calibrated against a standard dead weight pressure gauge calibrator (±0.1 bar). Appendix B gives the calibration graphs for the six pressure sensors. The electrical power transducers were calibrated against known electrical loads (±0.01 kW). The weighting scale was accurate to within ±0.01 kg.

Table 5-2: Details of measuring sensors and transducers.

	Channel No.	Sensor ID	Measurements	Ratings	Sensor or Transducer Type
Power consumption (kW, KVA)	117	kW1	Compressor kW	3 kW	Carrel T-1W3
	118	V1	Phase voltage (Phase R)	230 V	230V/10V step down transformer
	116	I1	Compressor current (Phase R, for kVA)	5.1 A per phase	CT Ganz MAK62/30
	112	I2	Condenser fan current (Phase Y)	1.56 A (2x180 W / 230 V)	Carrel T-1LC
	113	I3	Evaporator fan current (Phase Y)	1.3 A (2x146 W / 230 V)	Carrel T-1LC
	115	I4	Defrost coil current (Phase R)	22 A (2x2530 W / 230 V)	Carrel T-1LC
	114	I5	Reheat coil current (Phase R)	13.04 A (2x1500 W / 230 V)	Carrel T-1LC
Voltage	316	UH	Voltage (for humidifier control)	0 to 10 V	
Temperature (Refrigerant R134a)	301	Pt1	Compressor discharge	HP (0 to 80^{0}C)	Pt 1000 temperature sensor
	302	Pt2	Compressor suction	LP (-30 to 20^{0}C)	
	303	Pt3	Condenser inlet	HP (0 to 80^{0}C)	
	304	Pt4	Condenser outlet	HP (0 to 80^{0}C)	
	305	Pt5	Expansion valve inlet	HP (0 to 80^{0}C)	
	306	Pt6	Evaporator 2 inlet after TEV 2	LP (-30 to 20^{0}C)	
	307	Pt7	Evaporator outlet (inlet to EPR valve)	LP (-30 to 20^{0}C)	
	119	TC19	SLHE 2 Liquid outlet		Thermocouple (Type T class 1)
	201	Tt1	Evaporator 2 superheat (near sensing bulb 2 for TEV2)	LP (-30 to 20^{0}C)	590kH temperature transducer
	202	Tt2	Outlet of EPR valve	LP (-30 to 20^{0}C)	

Table 5-2: Continued

	Channel No.	Sensor ID	Measurements	Ratings	Sensor Type
Pressure (Refrigerant R134a)	216	HP1	Compressor discharge	HP 0 to 25/30 bar g (with schrader valve)	Danfoss AKS 32, version 0 to 5V, High pressure transmitters
	217	HP2	Expansion valve inlet	HP 0 to 25/30 bar g (with schrader valve)	
	218	HP3	Condenser outlet	HP 0 to 25/30 bar g (with schrader valve)	
	213	LP1	Compressor suction	LP –1 to 5 bar g (with schrader valve)	Danfoss AKS 32, version 0 to 5V, Low pressure transmitters
	214	LP2	Evaporator 2 inlet after TEV 2	LP –1 to 5 bar g (with schrader valve)	
	215	LP3	EPR valve inlet (Evaporator outlet)	LP –1 to 5 bar g (with schrader valve)	
Temperature	318	TP2	Evaporator 1 air differential temperature (air on and air off) (^{0}C)		Thermopile 8 junctions
	319	TP3	Evaporator 2 air differential temperature (air on and air off) (^{0}C)		Thermopile 8 junctions
	310	TP5	Condenser air off (^{0}C)		Thermopile 8 junctions
	101	TC1	Evaporator 2 air on (^{0}C)		Thermocouple (Type T class 1)
	102	TC2	Evaporator 1 air on (^{0}C)		Thermocouple (Type T class 1)
	103	TC3	Coil surface (Evap 2) (^{0}C)		Thermocouple (Type T class 1)
	104	TC4	Coil surface (Evap 1) (^{0}C)		Thermocouple (Type T class 1)
	105	TC5	Wall (back) (^{0}C)		Thermocouple (Type T class 1)
	106	TC6	Wall (Opposite to Tt6, Adjacent to Room 4) (^{0}C)		Thermocouple (Type T class 1)
	107	TC7	Ambient (near door, above) (^{0}C)		Thermocouple (Type T class 1)

Table 5-2: Continued

	Channel No.	Sensor ID	Measurements	Ratings	Sensor Type
Temperature	108	TC8	Product (^{0}C)		Thermocouple (Type T class 1)
	109	TC9	Product (^{0}C)		Thermocouple (Type T class 1)
	110	TC10	Ambient air (between cool store back wall & room back wall) (^{0}C)		Thermocouple (Type T class 1)
	111	TC11	Wall (Opposite to Tt5, Adjacent to Room 1) (^{0}C)		Thermocouple (Type T class 1)
	203	Tt3	Air (^{0}C)		590kH temperature transducer
	204	Tt4	Air (^{0}C)		
	205	Tt5	Air (^{0}C)		
	206	Tt6	Air (^{0}C)		
Air Humidity	207	RH1	Air on evaporators (%)		RH Hycal Ceramic SIL
	208	RH2	Zone 2 (%)		RH Hycal Ceramic SIL
	209	RH3	Zone 1 (%)		RH Hycal Ceramic SIL
	210	RH4	Ambient (%)		RH Hycal Ceramic SIL
Current			Extra sensible	Measure current	Clip on ammeter
			Extra latent heat	Measure current	Clip on ammeter
Air velocity			Evaporator air off velocity.	Measure air velocity	Analogue vane anemometer (Air flow Development Ltd, Serial No. M20411)
			Condenser air off velocity.	Measure air velocity	Analogue vane anemometer (Air flow Development Ltd, Serial No. M20411)
Mass			Measure melt / condensate amount	Measure weight of condensate	Weighting machine

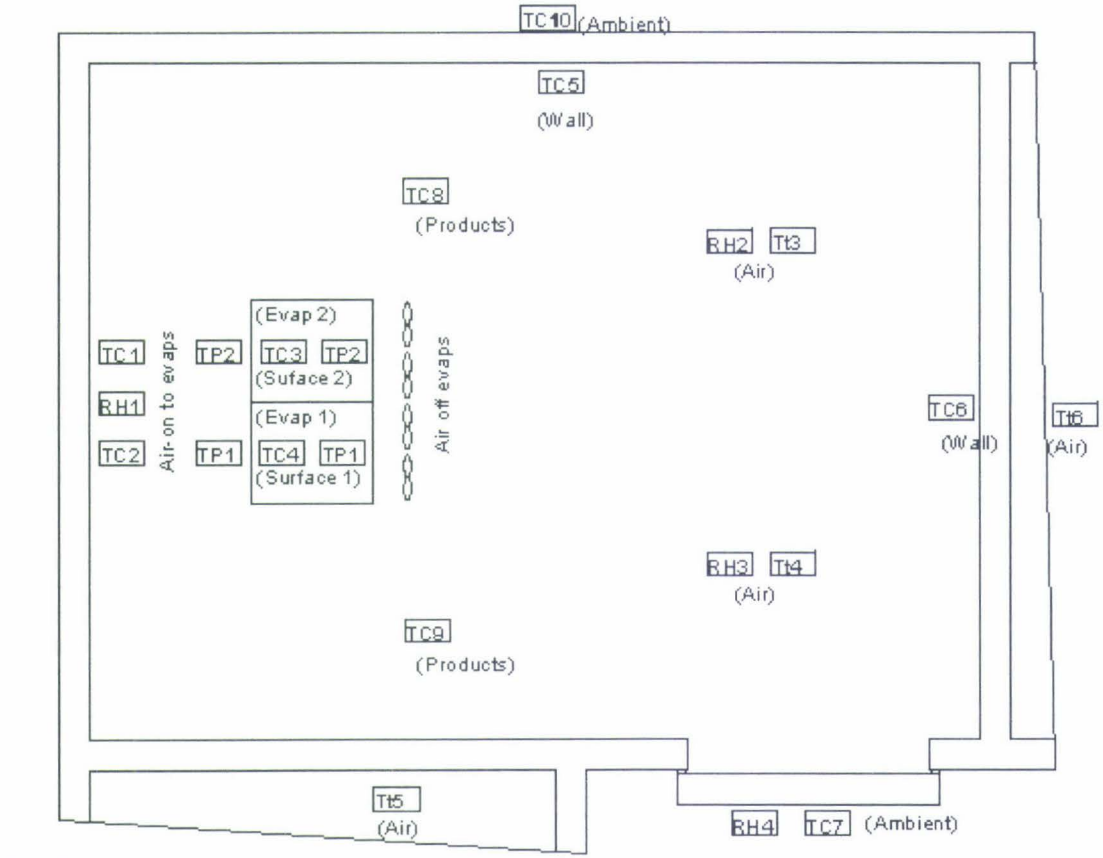

Figure 5-3: Temperature and RH sensor locations in the cool room

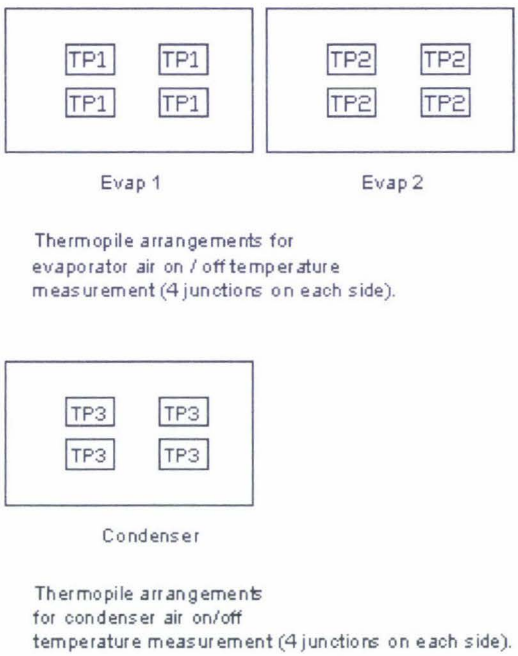

Figure 5-4: Thermopile arrangement for the evaporators & condenser

5.5 EXPERIMENTAL PLAN

Table 5-3 gives the operating conditions for the trials. Three types of experimental trials were carried out on the cool room.

1. Trials to estimate key model parameters.
2. Trials to show the effect of different defrosting frequency (1 to 6 defrost per day) on RH level, temperature control and defrost efficiency. For these trials conditions were held constant as far as possible (frost accumulation led to gradual change in evaporator performance over time between defrosts).
3. Trials to provide model validation data. These were unsteady state (dynamic) trials where the change in conditions with time including defrost periods were explicitly measured. The factors that were varied between trials were:
    - Fan speed
    - Coil size (one or two evaporator coils active)
    - Sensible heat load
    - Latent heat load
    - Temperature set point

For each trial the room was operated for at least two hours or until steady-state conditions had been achieved and the monitoring continued for at least two defrost cycles. The sampling interval on the data logger was 30 seconds.

During the trials there were few door openings and little personnel activity and the store held only very small amounts of kiwifruit. Table 6-1, Table 6-7 to Table 6-13 give the total length of each trial and the value of each variable.

Table 5-3: List of experimental trials.

Trial Number	Defrost Interval (Hours)	Temperature setpoint (C)	Lights (kW)	Extra Sensible Heat Load (kW)	Moisture added (kg/hour)	Evaporator Coil Size (%)	Evaporator Fan Speed (%)	Packaging (Trays of Kiwi fruit)
Pull Down								
1	X	0.5	0.45	0	0	100	100	0
Frosting Case								
2	12	1.6	0.45	3.0	0.31	100	100	0
3	16	1.6	0.45	3.0	0.31	100	100	0
4	24	1.6	0.45	3.0	0.29	100	100	0
5	6	1.6	0.45	3.0	0.29	100	100	0
6	30	1.6	0.45	3.0	0.29	100	100	0
7	8	1.6	0.45	3.0	0.30	100	100	0
8	8	1.6	0.45	5.0	0.45	100	100	0
9	24	1.6	0.45	5.0	0.39	100	100	0
10	16	1.6	0.45	5.0	0.41	100	100	0
11	30	1.6	0.45	5.0	0.41	100	100	0
12	12	1.6	0.45	5.0	0.47	100	100	0
13	6	1.6	0.45	5.0	0.43	100	100	0
Dynamic Trials								
14	6	1.6	0.45	2.0/1.0/ 2.0/2.0	0.33	100/100/ 100/50	100	0
15	12	1.6	0.45	3.0/3.0/ 3.0/3.0/2.0	0	100	100/50	0
Steady State Trial								
16	8	1.6	0	0	0	100	100	288

6 MODEL VALIDATION

6.1 INTRODUCTION

This chapter describes the validation of the cool room model formulated in Section 4. The validation was performed in three stages.

1. Calibration of key model parameters.
2. Comparison of predictions with measured data for the trials with a range of operating conditions.
3. Sensitivity analysis.

Predictions were computationally intensive so it was not practical to run all experimental trials for the validation. Therefore the 7 trials chosen were selected to represent a wide range of conditions. Table 6-1 gives the list of simulation and corresponding experimental trials used for parameter calibrations and model validation. Simulation trials 1-4 were used for parameter calibration whereas trials 5, 6 and 7 were used for validation of the calibrated model.

Table 6-1: Simulation trials

	Simulation 1	Simulation 2	Simulation 3	Simulation 4	Simulation 5	Simulation 6	Simulation 7
Experimental Trial No.	1	13	2	6	14	15	16
Defrost intervals (hrs)	Pull down	6	12	30	6	12	8
Length of trial (hrs)	2	15	26	62	11.2	47.2	17.8

6.2 PARAMETER VALUES

Many of the parameter could be based on physical measures or reasoning. Other's need to be calibrated using the experimental data.

6.2.1 Physical Measures

6.2.1.1 Room Data

Table 6-2 and Table 6-3 give the physical parameters of the room, the initial room temperature and relative humidity used for the simulations. Since the cool room under study was a small room, to simplify the input data it was divided into two equal zones along the length (Figure 5-3). The initial temperature and RH of each air zone was assumed to be the same as the initial room temperature and RH.

Table 6-2: Room parameter data

Parameter / Variable	**Symbol**	**Unit**	**Value**
Number of air zones.	*NZones*	-	2
Number of surfaces	*NSurfaces*	-	5
Number of floors	*NFloors*	-	2
Number of structures	*NStrucs*	-	3
Number of evaporators.	*NEvaps*	-	2
Number of fans.	*NFans*	-	4
Number of doors	*Ndoors*	-	1
Forced or induced draught. (For forced draught Forced = 1, for Induced draught, Forced = 0)	*forced*		0
Length		m	4.4
Width		m	3.3
Height		m	3
Density of air	ρ_{air}	kg/m^3	1.3
Specific heat capacity of water vapour	C_v	J/kg K	1.86×10^3
Specific heat capacity of water	C_w	J/kg K	4.18×10^3
Specific heat capacity of dry air (J/kg K).	C_a	J/kg K	1.01×10^3
Latent heat of water vapour (J/kg).	h_{fg}	J/kg	2.50×10^6
Latent heat of frost (J/kg).	h_{latfr}	J/kg	3.35×10^5
Specific heat capacity of frost	C_{fr}	J/kgK	2.04×10^3
Atmospheric pressure (Pa)	P_t	Pa	1.01×10^5
Gas constant.	R_{gas}	J/kg mole K	8.31×10^3
Dead band for temperature	DB_{set}	C	1.5
Room RH% setpoint for humidifier	RH_{set}	%	120
Zone1 (fraction of room volume associated with zone)	F_1	-	0.5
Zone2 (fraction of room volume associated with zone)	F_2	-	0.5

Table 6-3: Room and ambient air temperature and relative humidity data.

Parameter / Variable	Symbol	Unit	Simulation 1	Simulation 2	Simulation 3	Simulation 4	Simulation 5	Simulation 6	Simulation 7
Ambient temperature	T_{am}	°C	17	17	13.6	13	18	20	13
Ambient RH	RH_{am}	%	58.2	50	50	51.8	60	55	58
Set room temperature	$T_{a,set}$	°C	0.5	1.6	1.6	1.6	1.6	1.6	1.6
Surface 1 outside temperature	$T_{out,1}$	°C	4.5	5.5	5	5.9	5	5	5.8
Surface 2 outside temperature	$T_{out,2}$	°C	15.5	14.2	13.6	12	18	20	13.8
Surface 3 outside temperature	$T_{out,3}$	°C	15.5	14.2	13.6	12	18	20	13.8
Surface 4 outside temperature	$T_{out,4}$	°C	15.5	1.6	1.7	1.6	1.6	17	15
Surface 5 (ceiling) outside temperature	$T_{out,5}$	°C	17	17	13.6	13	18	20	13
Under floor temperature	T_{soil}	°C	10	10	10	10	10	10	10
Initial room temperature	T_{ini}	°C	14.2	4.8	1.6	1.6	1.6	2.5	1.6
Initial room RH	RH_{ini}	%	70.2	75.6	82.6	75	88.9	82	94

Table 6-4 gives the air flow pathway fractions for the four fans for each of the evaporators and associated zones within the cool store used for the seven simulation trials. Figure 6-1 shows air flow pathways for the four fans (Fan 3 pathways are symmetrical to Fan 2 and Fan 4 pathways are symmetrical to Fan 1). These were arbitraly set based on intuitive analysis of the physical configurations of the room.

For natural convection the associated zones partition areas are given in Table 6-5.

Table 6-4: Air flow fractions between zones, evaporators and fans ($F_{k,i\rightarrow n}$, $F_{k,k\rightarrow j}$, $F_{k,k\rightarrow i}$, $F_{k,i\rightarrow j}$).

Sink	Source																			
	Zone1				Zone2				Evap1				Evap2				Fans			
	Fan 1	Fan 2	Fan 3	Fan 4	Fan 1	Fan 2	Fan 3	Fan 4	Fan 1	Fan 2	Fan 3	Fan 4	Fan 1	Fan 2	Fan 3	Fan 4	Fan 1	Fan 2	Fan 3	Fan 4
Zone 1	0	0	0	0	0	0	0.1	0.1	0	0	0	0	0	0	0	0	0.8	0.6	0.4	0.2
Zone 2	0.1	0.1	0	0	0	0	0	0	0	0	0	0	0	0	0	0	0.2	0.4	0.6	0.8
Evap 1	0.7	0.5	0	0	0.3	0.5	0	0	0	0	0	0	0	0	0	0	0	0	0	0
Evap 2	0	0	0.5	0.3	0	0	0.5	0.7	0	0	0	0	0	0	0	0	0	0	0	0
Fan 1	0	0	0	0	0	0	0	0	1	0	0	0	0	0	0	0	0	0	0	0
Fan 2	0	0	0	0	0	0	0	0	0	1	0	0	0	0	0	0	0	0	0	0
Fan 3	0	0	0	0	0	0	0	0	0	0	0	0	0	0	1	0	0	0	0	0
Fan 4	0	0	0	0	0	0	0	0	0	0	0	0	0	0	0	1	0	0	0	0

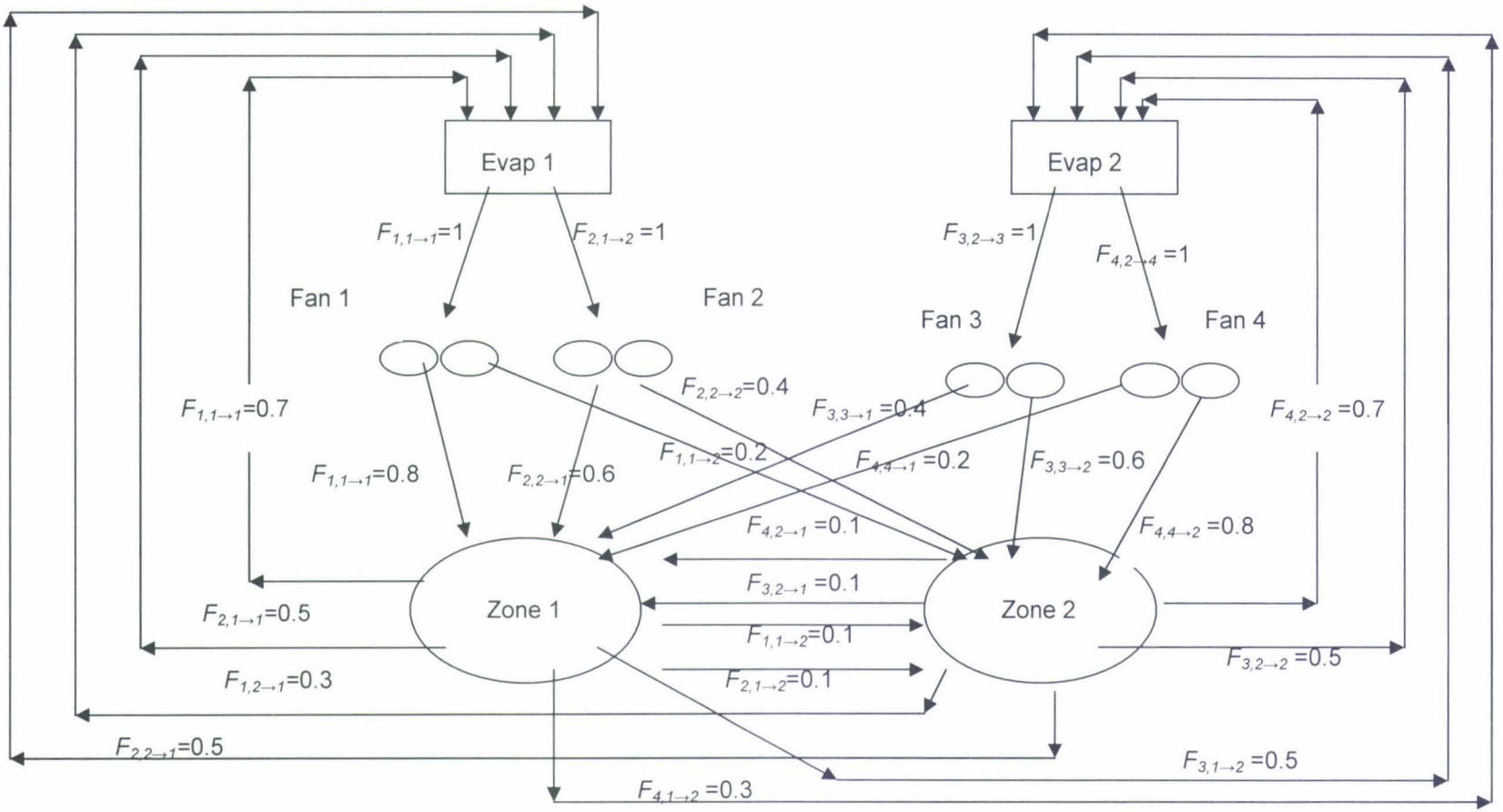

Figure 6-1: Air flow fractions between zones, evaporators and fans for the four fans.

Table 6-5: Areas associated with zone partition for natural convection.

		Symbols	Units	Source	
				Zone 1	Zone 2
Sink	Zone 1	$A_{1,2}$	m^2	0	14.52
	Zone 2	$A_{2,1}$	m^2	14.52	0

6.2.1.2 Door, Heat Generator and Humidifier

The room consist of a single door located in zone 1. The door open duration was set at 10 seconds and the frequency of the opening was the same as the defrost intervals, for the different trials. Since the room was a walk in cool room, folklift heat loads were not modelled and people load was considered insignificant. Table 6-6 gives door, heat generator and humidifier load fractions for the zones and the door physical data. Table 6-7 to Table 6-12 gives door opening times, input electrical heat loads and moisture loads, and timings for the various trials.

Table 6-6: Door, heat generator and humidifier data

Parameter / Variable	Symbol	Units	Value
Infiltration through door seals	Q_{se}	m^3/s	2.2×10^{-4}
Factor for Tamm's Equation	F_{Tam}	-	0.85
Factor for door protection	F_{pro}	-	0.92
Width of door	w	m	1.2
Height of door	y	m	2.35
Acceleration due to gravity	g	m/s^2	9.81
Door opening duration	t_{dOp}	s	10
		Zone 1	Zone 2
Fraction of door associated with each zone	$F_{d,i}$	1	0
Fraction of electric heater 1 associated with zones (2.53 kW)	$F_{hg,i}$	1	0
Fraction of room lights associated with zones (450 W)	$F_{hg,i}$	0.5	0.5
Fraction of electric heater 2 associated with zones (2.53 kW)	$F_{hg,i}$	0	1
Fraction of humidifier associated with each zone	$F_{hu,i}$	0.5	0.5

Table 6-7: Operating times for heat generators, humidifier, door and defrosting times for simulation 1 (pull down)

	Period
Time period (hrs)	0 to 2
Electrical heater 1 (W)	0
Room lights (W)	450
Electrical heater 2 (W)	0
Humidifier sensible heat (W)	0
Humidifier moisture load (kg/s)	0
Door	Closed during trial
Defrosting (hrs)	No defrosting

Table 6-8: Operating times for heat generators, humidifier, door and defrosting times for simulation 2 (6 hour defrost interval)

	Period
Time (hrs)	0 - 15
Electrical heater 1 (W)	2530
Room lights (W)	450
Electrical heater 2 (W)	2530
Humidifier Sensible heat (W)	65
Humidifier Moisture load (kg/s)	1.27×10^{-4}

Door	Closed during the trial		
Defrosting (hrs)	0	6.2	12.5

Table 6-9: Operating times for heat generators, humidifier, door and defrosting times for simulation 3 (12 hour defrost interval)

	Period
Time (hrs)	0 - 26
Electrical heater 1 (W)	1553
Room lights (W)	450
Electrical heater 2 (W)	1553
Humidifier sensible heat (W)	65
Humidifier moisture load (kg/s)	9.1×10^{-5}

Door	Open for 10 s at the start of trial		
Defrosting (hrs)	0	12.3	24.7

Table 6-10: Operating times for heat generators, humidifier, door and defrosting times for simulation 4 (30 hour defrost interval)

	Period
Time (hrs)	0 - 62
Electrical heater 1 (W)	1553
Room lights (W)	450
Electrical heater 2 (W)	1553
Humidifier sensible heat (W)	65.00
Humidifier moisture load (kg/s)	8.16×10^{-5}

Door	Closed during trial		
Defrosting (hrs)	0	30.7	61.6

Table 6-11: Operating times for heat generators, humidifier, door and defrosting times for simulation 5 (dynamic)

	Period 1	Period 2	Period 3	Period 4
Time (hrs)	0 – 3.1	3.1 - 5	5 – 7.1	7.1 – 11.2
Electrical heater 1 (W)	1035	517.5	1035	1035
Room lights (W)	450	450	450	450
Electrical heater 2 (W)	1035	517.5	1035	1035
Humidifier sensible heat (W)	65	65	65	65
Humidifier moisture load (kg/s)	9.52×10^{-5}	9.97×10^{-5}	9.03×10^{-5}	2.11×10^{-4}
Door (hrs)	-	3.1	5	7.1
Defrosting (hrs)	0	-	6	-
Evaporator 1	ON	ON	ON	OFF
Evaporator 2	ON	ON	ON	ON
Fan 1 (speed ratio)	Full	Full	Full	Full
Fan 2 (speed ratio)	Full	Full	Full	Full
Fan 3 (speed ratio)	Full	Full	Full	Full
Fan 4 (speed ratio)	Full	Full	Full	Full

Table 6-12: Operating times for heat generators, humidifier, door and defrosting times for simulation 6 (dynamic)

	Period 1	Period 2	Period 3	Period 4	Period 5	Period 6	Period 7	Period 8
Time (hrs)	0 – 3.3	3.3 – 5.3	5.3 – 7.3	7.3 – 22.2	22.2 – 24.3	24.3 – 26.3	26.3 – 28.8	28.8 – 47.2
Electrical heater 1 (W)	1553	1553	1553	1553	1553	1035	1035	1553
Room lights (W)	450	450	450	450	450	450	450	450
Electrical heater 2 (W)	1553	1553	1553	1553	1553	1035	1035	1553
Humidifier sensible heat (W)	0	65	65	65	65	65	65	65
Humidifier moisture load (kg/s)	0	1.01×10^{-4}	1.29×10^{-4}	1.29×10^{-4}	9.09×10^{-5}	1.12×10^{-4}	1.17×10^{-4}	1.33×10^{-4}
Door (hrs)	0	3.3	5.3	12.4	22.2	24.3	26.3	28.8
Defrosting (hrs)	0	-	-	12.4	22.2	-	-	28.8 & 41.2
Evaporator 1	ON	ON	ON	ON	OFF	ON	ON	ON
Evaporator 2	ON	ON	ON	ON	ON	ON	ON	ON
Fan 1 (speed ratio)	Full	Full	50%	Full	Full	Full	50%	Full
Fan 2 (speed ratio)	Full	Full	50%	Full	Full	Full	50%	Full
Fan 3 (speed ratio)	Full	Full	50%	Full	Full	Full	50%	Full
Fan 4 (speed ratio)	Full	Full	50%	Full	Full	Full	50%	Full

Table 6-13: Operating times for heat generators, humidifier, and door and defrosting times for simulation 7 (8 hour defrost interval)

	Period
Time (hrs)	0 - 17.8
Electrical heater 1 (W)	0
Room lights (W)	0
Electrical heater 2 (W)	0
Humidifier sensible heat (W)	0
Humidifier moisture load (kg/s)	0

Door opening (hrs)	-	-	16.5
Defrosting (hrs)	0	8.2	16.5

6.2.1.3 Evaporators and Fans

Table 6-14 and Table 6-15 give the input data for the evaporator and fans. The evaporator superheat was set to 1.5°C. Defrosting intervals for the simulations were 6 hourly, 12 hourly and 30 hourly for steady state trials plus two dynamic runs with 6 hourly and 12 hourly defrost intervals.

Table 6-8 to Table 6-12 gives the defrost initiation times for the simulation trials. The defrost termination was based on a set value of 10°C for the evaporator surface or to a maximum value of 0.5 hours which ever occurs first with a defrost efficiency of 50%.

Table 6-11 and Table 6-12 give the evaporator and fans speed setting during the dynamic trial runs. For simulation run 1 to 4 the two evaporators were switched on and the four fans speed set to full speed (100%). The evaporator and fan data was obtained from manufacturer's data sheets.

Table 6-14: Evaporator data (identical for both evaporators)

Parameter / Variable	Symbol	Units	Value
Overall heat transfer coefficient (manufacturer's)	$UA_{a,ref,j}$	W/K	640
Effective airside surface area of evaporator	$A_{s,j}$	m^2	33.4
Face area of evaporator	A_j	m^2	0.3
Reference velocity of air flowing through evaporator	$u_{j,refer}$	m/s	2.6
Mass of evaporators	M_j	kg	30
Refrigerant solenoid valve	*Switchref*		1
Superheat setting	*SH*	°C	1.5
Factor for evaporator's air flow	*a*	-	0.5
Defrost heater	$\phi_{to,de,j}$	W	2300
Defrost efficiency	η_{def}	%	50
Defrost switched off evaporator surface temperature	$T_{sjdefrostoff}$	°C	10
Evaporator (assumed to be copper)	C_j	J/kgK	385
Evaporator pressure drop (standard)	ΔP_{std}	Pa	3.5×10^{4}
Evaporator volume flow (standard)	Q_{std}	m^3/s	3.13×10^{-3}

Table 6-15: Fan data (identical for four fans)

Parameter / Variable	Symbol	Units	Value
Fan design flow	*Q_ini*	m^3/s	0.39
Fan power	ϕ_k	W	73

6.2.1.4 Compressor and Condenser

Table 6-16 gives the compressor and condenser unit data. The refrigeration system consists of a single semi-hermetic reciprocating compressor with an air cooled condenser (with two fans) unit. The sub-cooling on the condenser was set to 2.5°C. The compressor isentropic and volumetric efficiencies used were obtained from curve fit equations based on manufacturer's data in terms of pressure ratios and discharge temperature for the particular condensing unit.

The expression for the curve fit equation for the volumetric efficiency is:

$$\eta_{ComVol} = 1.033578473 - 3.8410148\times10^{-2}.(PR) - 5.25897\times10^{-4}.(PR)^2 + 1.21921\times10^{-4}.(PR)^3 - 5.92571\times10^{-6}.(PR)^4 - 2.000652\times10^{-3}.T_{Comdis} + 2.90237\times10^{-4}.(PR).T_{Comdis} - 1.19826\times10^{-6}.(PR).(T_{Comdis})^2 \quad (6\text{-}1)$$

Where:

PR = Ratio of discharge pressure to suction pressure

The expression for the curve fit equation for the isentropic efficiency is:

$$\eta_{ComIsen} = 1.80343423\times10^{-1} + 2.12064784\times10^{-1}.(PR) - 4.8668914\times10^{-2}.(PR)^2 + 4.192276\times10^{-3}.(PR)^3 - 1.31113\times10^{-4}.(PR)^4 + 3.36362\times10^{-4}.T_{Comdis} + 7.1599\times10^{-4}.(PR).T_{Comdis} - 5.67136\times10^{-6}.(PR).(T_{Comdis})^2 \quad (6\text{-}2)$$

Table 6-16: Compressor and condenser data

Parameter / Variable	Symbol	Units	Value
Refrigerant sub cooling	SC	°C	2.5
Refrigerant pressure drop across discharge line	$\Delta P_{disline}$	Pa	1.5×10^{4}
Thermal mass of condenser	M_{Con}	kg	40
Specific heat capacity of condenser (assumed to be copper)	C_{Con}	J/kg.K	385
Heat transfer rating for condenser	UA_{Con}	W/K	450
Compressor swept volume	Q_{com}	m^3/s	5.03×10^{-3}
Correction factor for the compressor swept volume	$F_{ComVolEff}$	-	1
Heat transfer coefficient for the compressor surface	UA_{com}	W/ K	7
Fraction as heat losses for compressor	X_{com}	-	0.85
Low pressure cut out	LP_{cutout}	Pa	4.0×10^{4}
Dead band for the low pressure cut out	$DB_{LPcutout}$	Pa	1.0×10^{4}
Compressor switch	$Switch_{com}$	-	1
Factor for the hotgas bypass	$F_{hotgpass}$	-	7.5×10^{4}
Factor for the hotgas bypass (maximum)	$F_{hotgpassMax}$	-	1
Dead band for hot gas bypass	$DB_{hotgpass}$	Pa	5.0×10^{4}
Pressure at which hot gas bypass activates.	$P_{hotgpass}$	Pa	1.0×10^{5}
Suction temperature setpoint	$T_{sucComSet}$	C	-2
Hot gas leakage rate	$Q_{hotgpassLeak}$	m^3/s	5.0×10^{-4}
Control type (1 = PID, 0 = ON/OFF)	$Controller$	-	1
PID Proportional factor	k_P	-	3.0×10^{5}
PID Integral factor	k_I	-	7.5×10^{-4}
PID Derivative factor	k_D	-	5
Min pressure drop allowed on EPR valve	Δ_{EPRMin}	Pa	3.0×10^{4}
Max pressure drop allowed on EPR valve	Δ_{EPRMax}	Pa	2.5×10^{6}

6.2.1.5 Room Surfaces

Table 6-17 gives the input data for the surfaces. Table 6-3 gives the input data for the ambient and room outside surface temperatures for the trials. The initial temperature of the inner metal surfaces was assumed to be same as initial room temperature. The ambient temperature variation was small and hence the simulation was carried out assuming ambient conditions were constant.

Table 6-17: Surface data

Parameter / Variable	Symbol	Units	Value
Surface location factor for zone1 (surface 1)	$F_{1,1}$	-	1
Surface location factor for zone2 (surface 1)	$F_{1,2}$	-	0
Surface location factor for zone1 (surface 2)	$F_{2,1}$	-	0.5
Surface location factor for zone2 (surface 2)	$F_{2,2}$	-	0.5
Surface location factor for zone1 (surface 3)	$F_{3,1}$	-	0
Surface location factor for zone2 (surface 3)	$F_{3,2}$	-	1
Surface location factor for zone1 (surface 4)	$F_{4,1}$	-	0.5
Surface location factor for zone2 (surface 4)	$F_{4,2}$	-	0.5
Surface location factor for zone1 (surface 5)	$F_{5,1}$	-	0.5
Surface location factor for zone2 (surface 5)	$F_{5,2}$	-	0.5
Thickness of insulation	x_{insu}	m	0.150
Thickness of outer metallic layer	$x_{outermetal}$	m	5.0×10^{-4}
Thickness of inner metallic layer	$x_{innermetal}$	m	5.0×10^{-4}
Density of outer metallic layer (Incropera *et al.* 1985)	$\rho_{outermetal}$	kg/m^3	7854
Density of inner metallic layer (Incropera *et al.* 1985)	$\rho_{innermetal}$	kg/m^3	7854
Specific heat capacity of outer layer (Incropera *et al.* 1985)	C_{outs}	J/kg.K	446
Specific heat capacity of inner layer (Incropera *et al.* 1985)	C_{ins}	J/kg.K	446
Convective heat transfer coefficient for inside surface.	α_{inss}	$W/m^2.K$	7
Convective heat transfer coefficient for outer surface.	α_{outs}	$W/m^2.K$	7
Insulation effectiveness	F_{efinsu}	-	1.5
Thermal conductivity of insulation (Incropera *et al.* 1985)	λ_{insu}	W/m.K	0.027
Area (surface 1)	A_1	m^2	14.5
Area (surface 2)	A_2	m^2	9.9
Area (surface 3)	A_3	m^2	14.5
Area (surface 4)	A_4	m^2	9.9
Area (surface 5)	A_5	m^2	14.5

6.2.1.6 Floor

Table 6-18 gives the floor input data. The input data for the under floor temperatures are given in Table 6-3. The floor was divided into two sections along the length such that the two parts share equally with the zones. The initial temperature of the inner metal surface floor is assumed to be the same as the initial room temperature.

Table 6-18: Floor input data

Parameter / Variable	**Symbol**	**Units**	**Value**
Floor location factor for zone1 (floor 1)	$F_{1,1}$	-	0.5
Floor location factor for zone2 (floor 1)	$F_{1,2}$	-	0.5
Floor location factor for zone1 (floor 2)	$F_{2,1}$	-	0.5
Floor location factor for zone2 (floor 2)	$F_{2,1}$	-	0.5
Thickness of concrete	x_{conc}	m	0.15
Thickness of soil layer at which temperature taken.	x_{soil}	m	1.5
Thickness of insulation	x_{insu}	m	0.15
Thickness of inner metallic layer	$x_{innermetal}$	m	5.0×10^{-4}
Density of inner metallic layer (Incropera *et al.* 1985)	$\rho_{innermetal}$	kg/m^3	7854
Specific heat capacity of inner layer (Incropera *et al.* 1985)	C_{ins}	J/kg.K	446
Convective heat transfer coefficient for inside surface.	α_{inss}	W/m^2.K	7
Insulation effectiveness	F_{efinsu}		1.5
Thermal conductivity of insulation (Incropera *et al.* 1985)	λ_{insu}	W/m.K	0.027
Thermal conductivity of concrete (Incropera *et al.* 1985)	λ_{conc}	W/m.K	1.4
Thermal conductivity of soil (Incropera *et al.* 1985)	λ_{soil}	W/m.K	0.52
Area (floor 1)	A_{fl}	m^2	7.26
Area (floor 2)	A_{fl}	m^2	7.26

6.2.1.7 Structures

Table 6-19 gives the input data for the structures. The room had three steel racks for stacking goods. The structures were located in the middle and either side of the store, the middle structure shares the two zones. The area and mass of structures were approximated from physical measurements and geometric considerations.

Table 6-19: Structure input data

Parameter / Variable	**Symbol**	**Units**	**Value**
Structure location factor for zone1 (structure 1)	$F_{1,1}$	-	1
Structure location factor for zone2 (structure 1)	$F_{1,2}$	-	0
Structure location factor for zone1 (structure 2)	$F_{2,1}$	-	0.5
Structure location factor for zone2 (structure 2)	$F_{2,2}$	-	0.5
Structure location factor for zone1 (structure 3)	$F_{3,1}$	-	0
Structure location factor for zone2 (structure 3)	$F_{3,2}$	-	1
Specific heat capacity of structures (Incropera *et al.* 1985)	C_{ins}	J/kg.K	446
Convective heat transfer coefficient for structure.	α_{st}	$W/m^2.K$	7
Area	A_{st}	m^2	10
Mass	M_{st}	kg	50

6.2.1.8 Products

Table 6-19 gives the input data for the products. The room was stacked with 288 trays of kiwi fruit for simulation trial 7. The trays were loaded into 6 stacks (4 × 50 and 2 × 44 trays). The initial temperatures of the products were assumed to be same as the initial room temperature.

Table 6-20: Product input data

Parameter / Variable	Symbol	Units	Value
Number of stacks	*NProd*	-	6
Product location factor for zone 1 stack 1	$F_{1,1}$	-	1
Product location factor for zone 2 stack 1	$F_{1,2}$	-	0
Product location factor for zone 1 stack 2	$F_{2,1}$	-	1
Product location factor for zone 2 stack 2	$F_{2,2}$	-	0
Product location factor for zone 1 stack 3	$F_{3,1}$	-	0
Product location factor for zone 2 stack 3	$F_{3,2}$	-	1
Product location factor for zone 1 stack 4	$F_{4,1}$	-	0
Product location factor for zone 2 stack 4	$F_{4,2}$	-	1
Product location factor for zone 1 stack 5	$F_{5,1}$	-	1
Product location factor for zone 2 stack 5	$F_{5,2}$	-	0
Product location factor for zone 1 stack 6	$F_{6,1}$	-	0
Product location factor for zone 2 stack 6	$F_{6,2}$	-	1
Number of batches in zone 1	B_{prbat}	-	1
Number of batches in zone 2	B_{prbat}	-	1
Specific heat capacity of products	C_{pr}	J/kg.K	4000
Thermal conductivity of product	λ_{pr}	W/mK	0.5
Shortest distance between surface and centre of product	X_{pr}	m	0.1
Thickness of packaging	x_{pr}	m	5.0×10^{-3}
Initial outside temperature of products	T_{prInEx}	°C	1.6
Initial inside temperature of products	$T_{prInIns}$	°C	1.6

Table 6-20: Continued.

Parameter / Variable	Symbol	Units	Value
Stack 1 to 4 mass	M_{pr}	kg	134
Stack 5 to 6 mass	M_{pr}	kg	100
Stack 1 to 4 dry package mass	$M_{drypack}$	kg	20
Stack 5 to 6 dry package mass	$M_{drypack}$	kg	17.6
Exposed surface area stack 1 to 4	A_{expr}	m^2	6.8
Exposed surface area stack 5 to 6	A_{expr}	m^2	6.8
Volume solid product (stack 1-4)	V_{pr}	m^3	0.5
Volume solid product (stack 5-6)	V_{pr}	m^3	0.44
Equivalent heat transfer dimensionality	E_{pr}	-	1.3
First root of Equation (4-108)	β	-	1.3
Velocity of air stream	u_a	m /s	0.5
Thickness of trapped air	x_a	m	1.0×10^{-2}
Thermal conductivity of trapped air	λ_a	W/m k	2.6×10^{-2}
GAB isotherm constant	X_{mGAB}	-	6.65×10^{-2}
GAB isotherm constant	C_{GAB}	-	5.49×10^{4}
GAB isotherm constant	K_{GAB}	-	7.33×10^{-1}
Rate constant for water absorption or desorption	k_{mc}	s^{-1}	1.0×10^{-6}
Initial Moisture content of packaging	$mc_{pack,pr}$	%	6

6.2.2 Calibrated Parameter Values

Model parameters that needed to be calibrated were:

- Thermal buffering correction factor for the room air ($F_{a,buffer}$).
- Correction factor for evaporator heat transfer coefficient ($F_{UA,Evap}$).
- Frost performance deterioration factor for the evaporator ($F_{fr,j}$).
- Ratio of heat transfer from air to refrigerant ($Ra_{a\rightarrow ref}$).
- Thermal buffering correction factor for evaporator ($F_{Evap,\ buffer}$).
- Suction line heat exchanger effectiveness factor (ε_{SLHE}).
- Thermal buffering correction factor for the suction pressure ($F_{sucbuffer}$).
- Correction factor for condenser heat transfer coefficient ($F_{UA,Con}$).

- Thermal buffering correction factor for the condenser ($F_{Conbuffer}$).
- Correction factor for compressor surface heat transfer coefficient ($F_{UA,Com}$).
- Correction factor for heat transfer coefficient for surfaces, floor and metal structures (F_{UAInS}, F_{UAOutS}, F_{UAFl}, F_{UASt},).
- Thermal buffering correction factor for surfaces, floor and metal structures ($F_{InSbuffer}$, $F_{OutS,buffer}$, $F_{Fl,buffer}$, $F_{St,buffer}$).

Table 6-21 gives the calibrated values for the above parameters. The calibrated parameter values were obtained using simulation trials 1, 2, 3 and 4. Thermal buffering factors for room air mass, evaporator mass and suction pressure were primarily calibrated using the simulation 1 pull down period and during the defrosting period for simulation 2 and 3. The evaporator heat transfer coefficient correction factor was calibrated using simulations 2 and 3 where high and low sensible heat loads were used. Simulation 4 was used to calibrate the evaporator frost deterioration factor because it had a relatively high latent heat load. The parameter values were not fully optimised. Rather they were arbitrarily chosen until the shapes and general trend of the predictions broadly matched the measurements. The long run time for the simulation meant that the use of mathematical optimisation techniques was not practical. The heat transfer correction factor for the condenser, surfaces, floor and structures and buffering factors for thermal masses for the inside, outside metal surfaces and metal structures were kept at 1.0, since the predicted results shows similar trend to the measured values.

Table 6-21: Calibrated parameter values

Parameter / Variable	Symbol	Unit	Value
Thermal buffering correction factor for room air thermal mass	$F_{a,buffer}$	-	6.5
Heat transfer correction factor for the evaporator	F_{UAEvap}	-	0.85
Ratio of heat transfer from air to refrigerant	$Ra_{a\rightarrow ref}$	-	0.5
Frost performance deterioration factor for the evaporator	$F_{fr,j}$	-	7.5
Heat transfer effectiveness factor for SLHE	ε_{SLHE}	-	0.3
Thermal buffering correction factor for evaporator thermal mass	$F_{Evapbuffer}$	-	3.5
Thermal buffering correction factor for suction pressure	$F_{Sucbuffer}$	-	0.5
Heat transfer correction factor for condenser	F_{UACon}	-	1
Thermal buffering correction factor for the condenser thermal mass	$F_{Conbuffer}$	-	3
Correction factor for the heat transfer coefficient for the compressor surface.	F_{UAcom}	-	1.9
Correction factor for heat transfer coefficient for inner surfaces	F_{UAInS}	-	1
Correction factor for heat transfer coefficient for outer surfaces	$F_{UAOutSur}$	-	1
Thermal buffering correction factor for the inside metal thermal mass of surfaces	$F_{InSbuffer}$	-	1
Thermal buffering correction factor for outside metal thermal mass of surfaces	$F_{OutS,buffer}$	-	1
Correction factor for heat transfer coefficient for floor	F_{UAFl}	-	1
Thermal buffering correction factor for inside metal thermal mass of floor.	$F_{Flbuffer}$	-	1
Correction factor for heat transfer coefficient for structures	F_{UASt}	-	1
Thermal buffering correction factor for structures thermal mass	$F_{Stbuffer}$	-	1

6.2.2.1 Thermal Buffering Factors

The room air thermal mass buffering factor was difficult to calibrate because a number of factors influence the room thermal mass and changes to one factor influences the other factors. These include evaporator mass, mass of metal

structures in the room, metal surfaces on the walls and floors. To calibrate the buffering factor the initial pull down during the start up of the refrigeration system and the pull down after the defrosting were used. The rate of change of temperature for room air, saturated refrigerant temperature for the evaporator, evaporator surface temperature and rate of change of suction pressure were the key measurement that were compared with the predictions.

Figure 6-2 compares the measured and predicted values of temperature, RH, saturated refrigerant temperature for the evaporator and evaporator surface temperature for simulation 1. Simulation 1 was a two hour trial where the room was cooled from ambient conditions to 0.5°C set point as shown in Figure 6-2. During the run both evaporators were switched on and fans were at full speed, with room lights switched off and no other extra sensible or latent heat load added. The predicted curves follow a broadly similar pull down to the measured data even though at a higher value. The experiment and simulation took almost same time to reach the lowest saturated refrigerant evaporation temperature. Once the pulldown was complete, due to the actual plant controller being less precise than the model controller, the measured values were found to fluctuate whereas the predicted values were very stable. In particular, cycling of the hotgas bypass control and instability of the thermostatic expansion (TX) valve affected the actual performance. Overall there was reasonable agreement between predicted and measured refrigerant evaporation temperature and the air temperature. Predicted air-on RH was about 8% higher than the measured values and zone RH was 12-14% higher than the measured values. Refrigerant hydrodynamics affects the refrigerant circuit, which the model does not attempt to predict, and may explain some of the differences during start-up and pull-down.

Figure 6-3 and Figure 6-4 compares the measured and predicted values of air temperature and RH, saturated refrigerant temperature of the evaporator and evaporator surface temperature for simulation 2 and 3 during a defrost period. The predicted value during defrosting and pull down after the defrost termination

follows similar trends to the measured values. For both simulations the measured and predicted defrost termination points are very close, but there was a slight shift in the predictions indicating predicted defrost termination was shorter than the measured case. Again there was a cyclic pattern in the measured values due to imperfect hot gas bypass and expansion valve control but there was close agreement on average with the predicted values which tend not cycle due to "perfect" control.

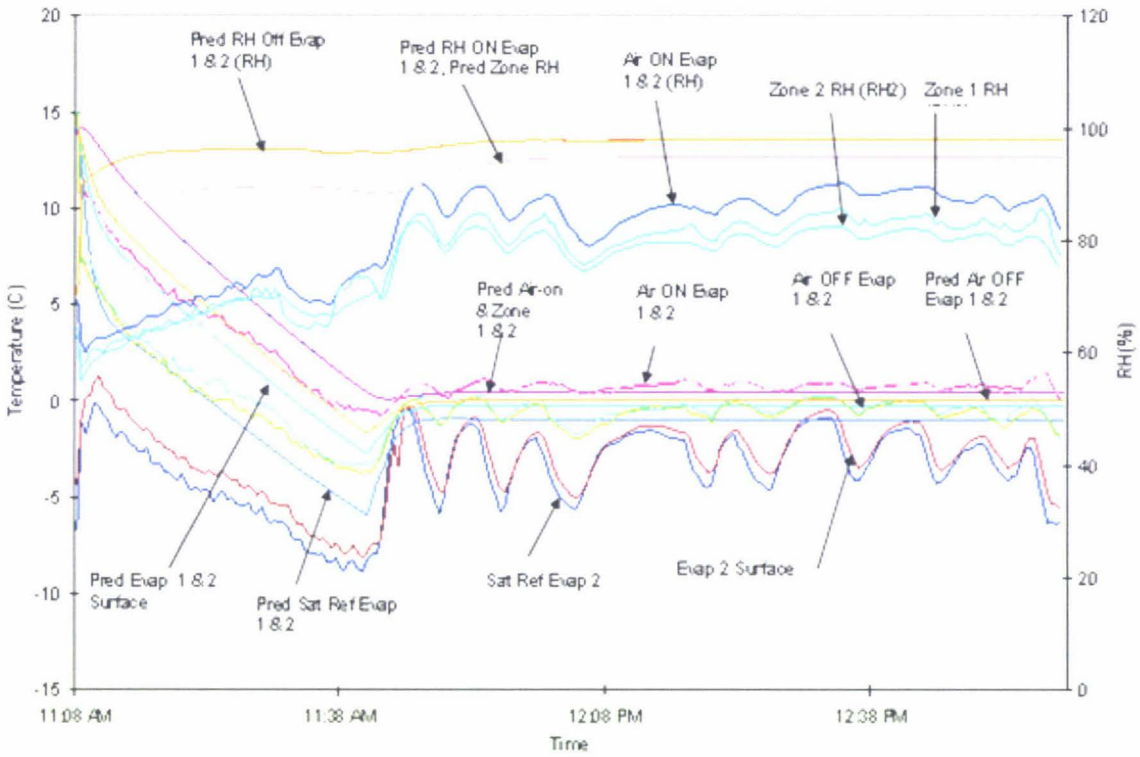

Figure 6-2: Comparison of predicted and measured temperatures and RH for simulation 1 (experimental trial 1, pull down).

Overall, changes in the thermal buffering factors may result in improvements for some simulations and poorer predictions for other simulations, so further optimization was difficult to justify.

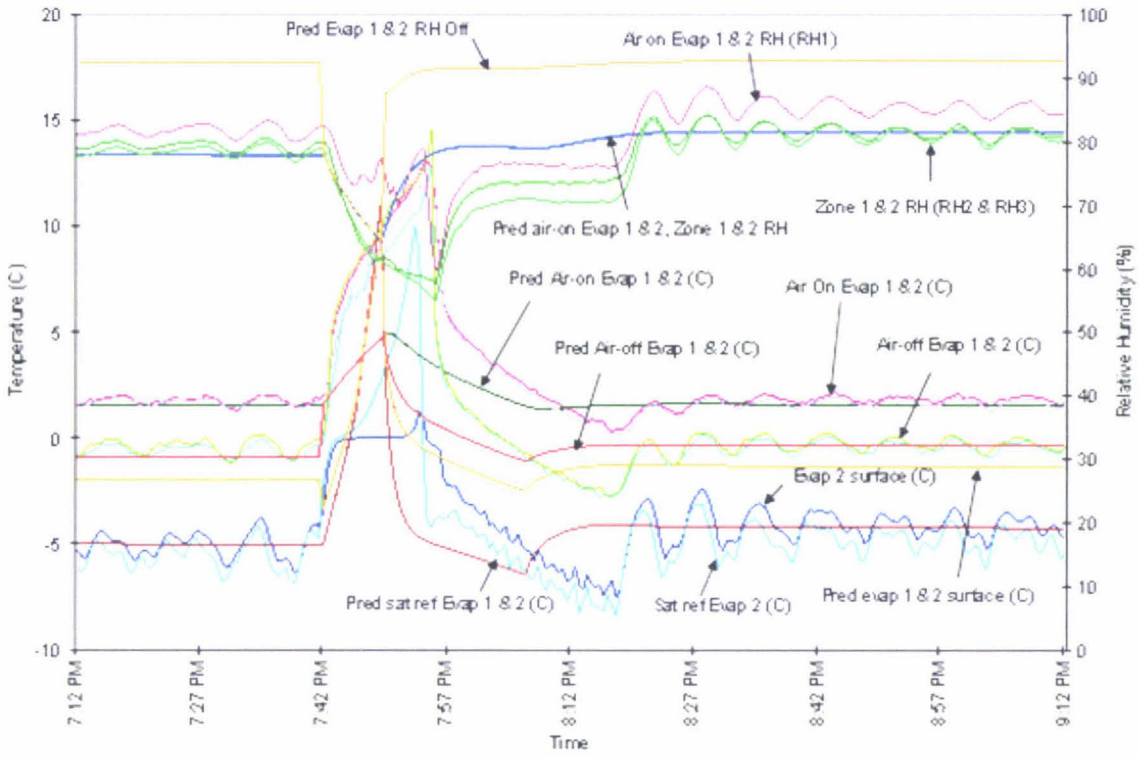

Figure 6-3: Comparison of predicted and measured temperatures and RH for simulation 3 (experimental trial 2, defrosting).

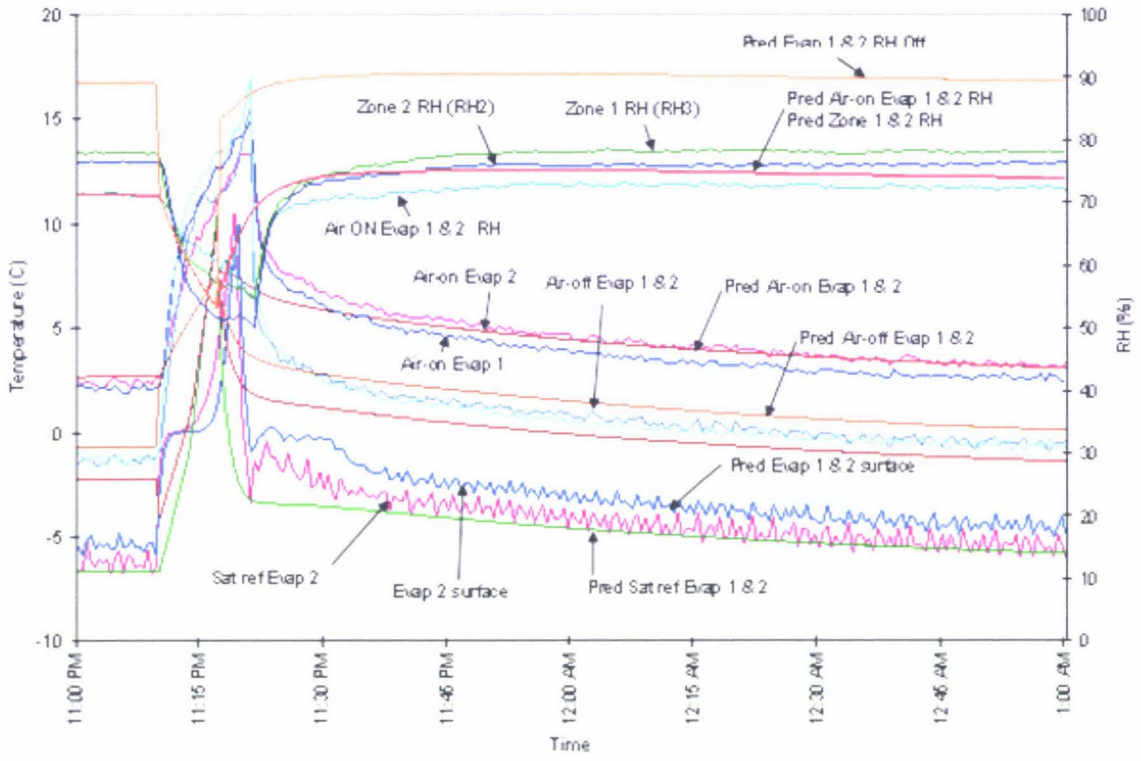

Figure 6-4: Comparison of predicted and measured temperatures and RH for simulation 2 (experimental trial 13, defrosting).

Figure 6-5 to Figure 6-7 shows the comparison of the measured and predicted results for the refrigerant pressure and temperature for the low pressure side for simulation 1, 2 and 3 during initial pull down and during defrosting. During defrosting refrigerant pressure and temperature both rise rapidly for both predicted and measured cases. In the measured case there was a distinct rapid rise and flattening and then further rise, whereas the predicted had a rapid rise only. The flattening on the measured data was probably due to the melting of frost at constant temperature. Clearly the model for the defrost mechanism could be improved so that the frost melting influences the predicted air and refrigerant conditions. The predicted pull down after the defrost termination was rapid, but in the measured case was an almost vertical drop followed by a period with a gradual decline. Again, this probably reflected the hydrodynamics effects of the refrigerant as the evaporator was rewetted after defrosting that were not fully modelled.

Overall, the predicted temperature and pressure for the low pressure side closely follow the measured values except for the simulation 2 where the predicted suction temperature is slightly lower than the measured suction temperature and simulation 3 where the predicted suction temperature is slightly higher. For simulation 1 the measured suction temperature was cycling. It is apparent that the cycling was due to activation of the hot gas bypass resulting in liquid injection into the suction line but the desuperheating control was unstable leading to cycling.

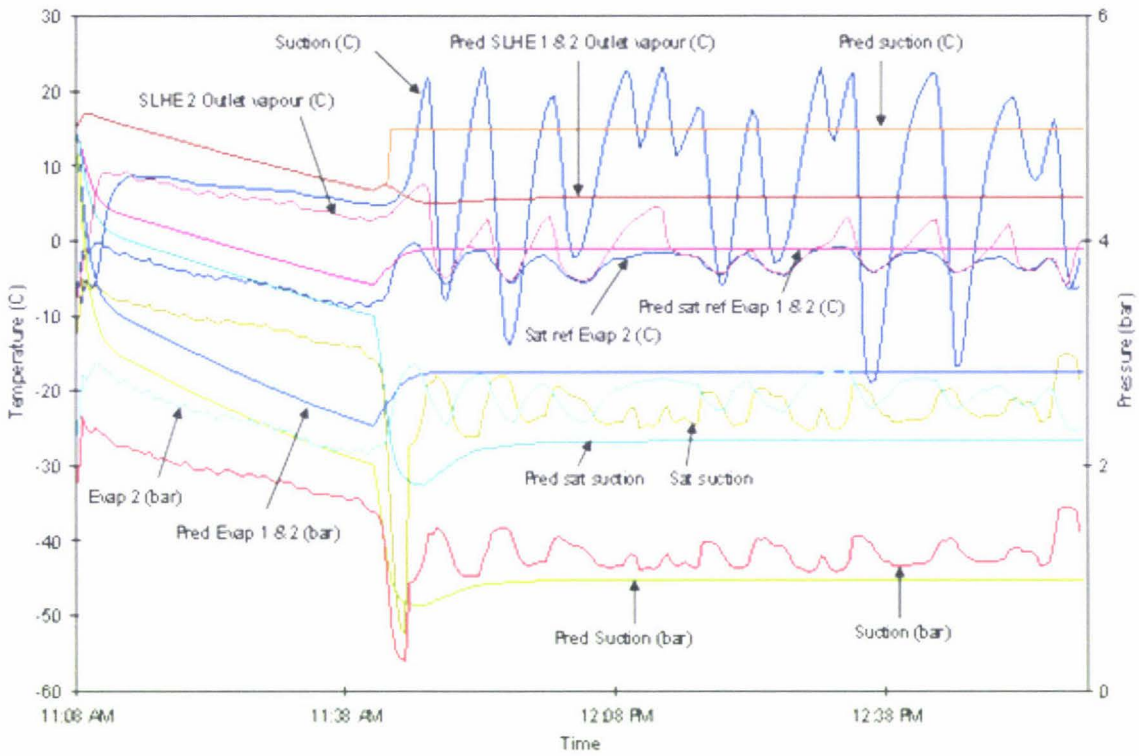

Figure 6-5: Comparison of predicted and measured refrigerant pressure and temperature for the low pressure side for simulation 1 (experimental trial 1)

For simulation 3 due to the predicted shorter defrost termination time the pull down time after the defrost was also shorter whereas for simulation 2 the pulldown was very similar to the measured values due to the high sensible heat loads during the pulldown.

The thermal buffering correction factor of 0.5 for the compressor suction improved the model stability, gave reasonable computational speed and gave a similar suction pressure gradient to that of the measured values during pull down.

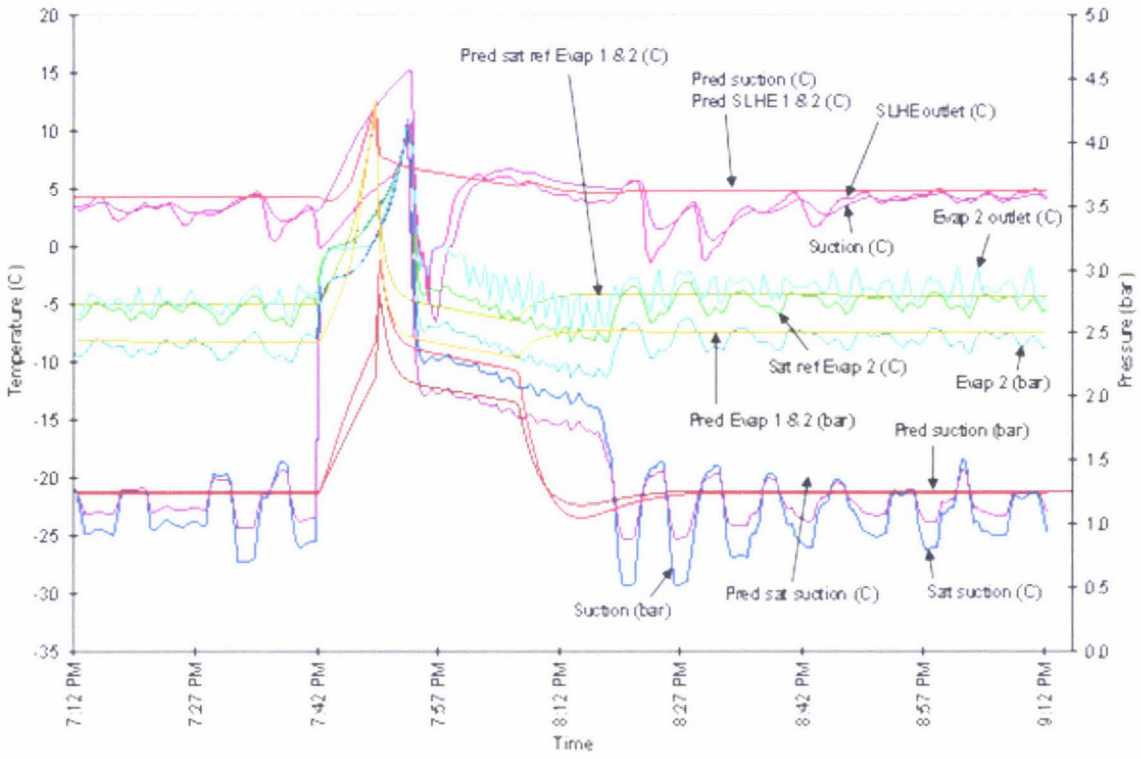

Figure 6-6: Comparison of predicted and measured refrigerant pressure and temperature for the low pressure side for simulation 3 (experimental trial 2)

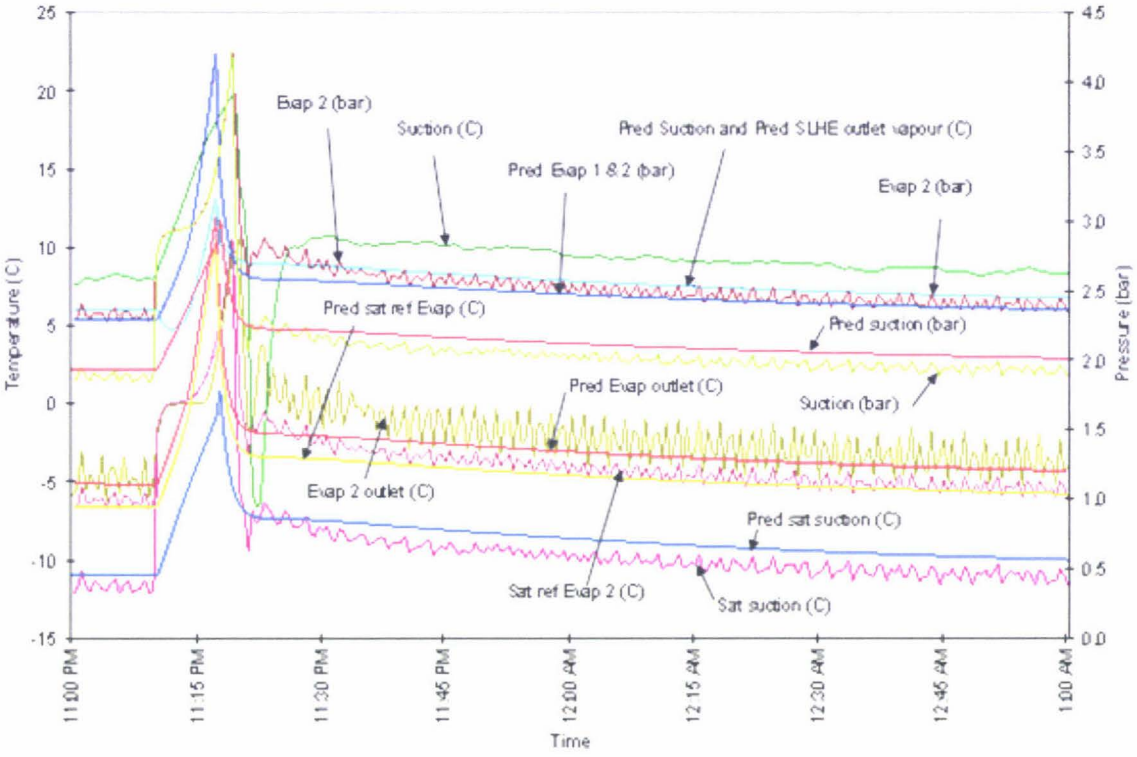

Figure 6-7: Comparison of predicted and measured refrigerant temperature and pressure for the low pressure side simulation 2 (experimental trial 13, defrosting).

Figure 6-8 to Figure 6-10 compares the measured and predicted values for the refrigerant pressure and temperature for the high pressure side for the simulations 1, 2 and 3 during initial pull down and during defrosting. For simulation 1 the predicted discharge pressure was initially higher and then reduced to a constant value, slightly lower than the measured values. The predicted discharge temperature was slightly higher than the cycling measured values. Again the cycling was due to the imprecise control of the hot gas bypass and/or due to the evaporator thermostatic expansion (TX) valve.

During defrost both predicted and measured temperature and pressure fell rapidly and once defrosting was terminated and the compressor started the temperature and pressure both rose rapidly. The predicted discharge temperature for the

simulation 3 was found to be higher than the measured values, whereas for the simulation 2 was very close. Overall, the predicted temperature and pressure for the high pressure side had a reasonable fit to the measured values.

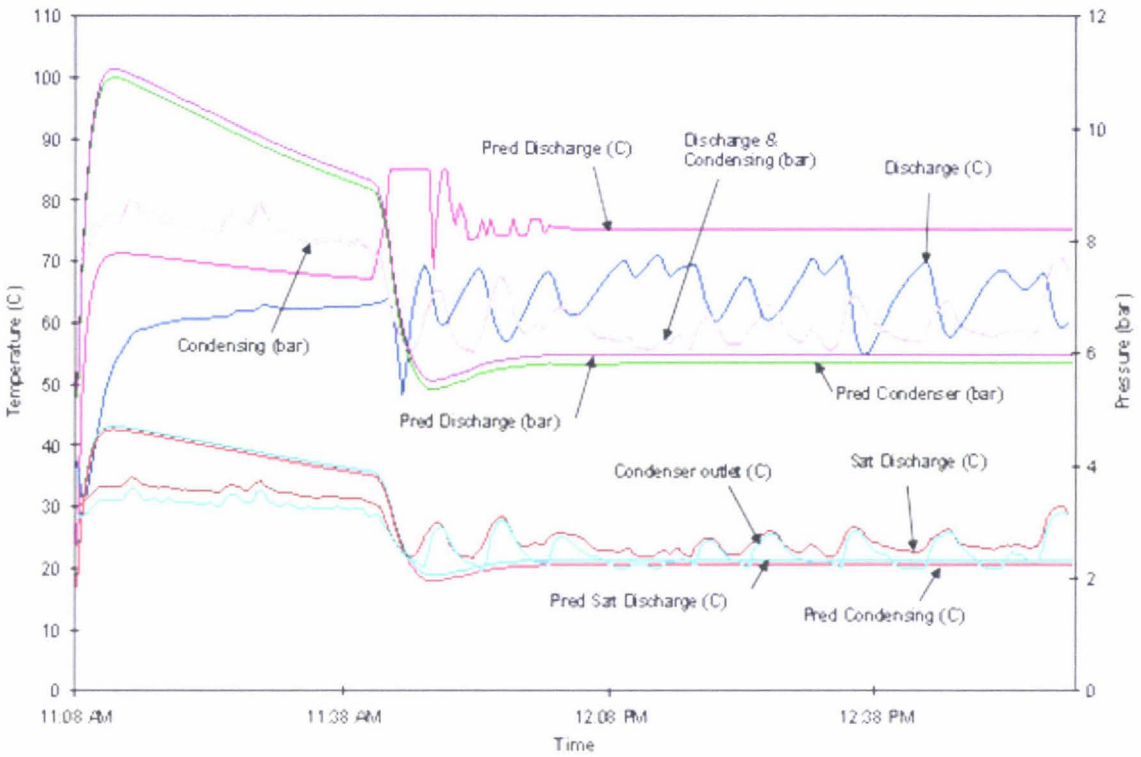

Figure 6-8: Comparison of predicted and measured refrigerant pressure and temperature for the high pressure side for simulation 1 (experimental trial 1).

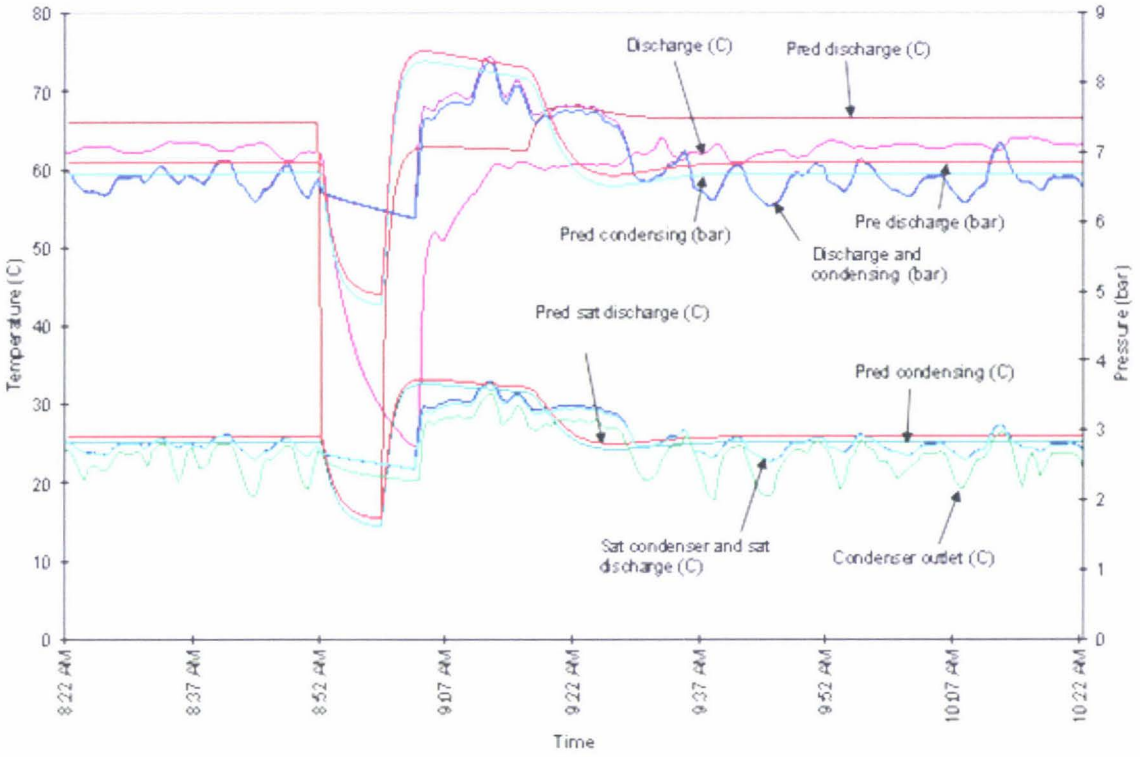

Figure 6-9: Comparison of predicted and measured refrigerant pressure and temperature for the high pressure side for simulation 3 (experimental trail 2, defrosting).

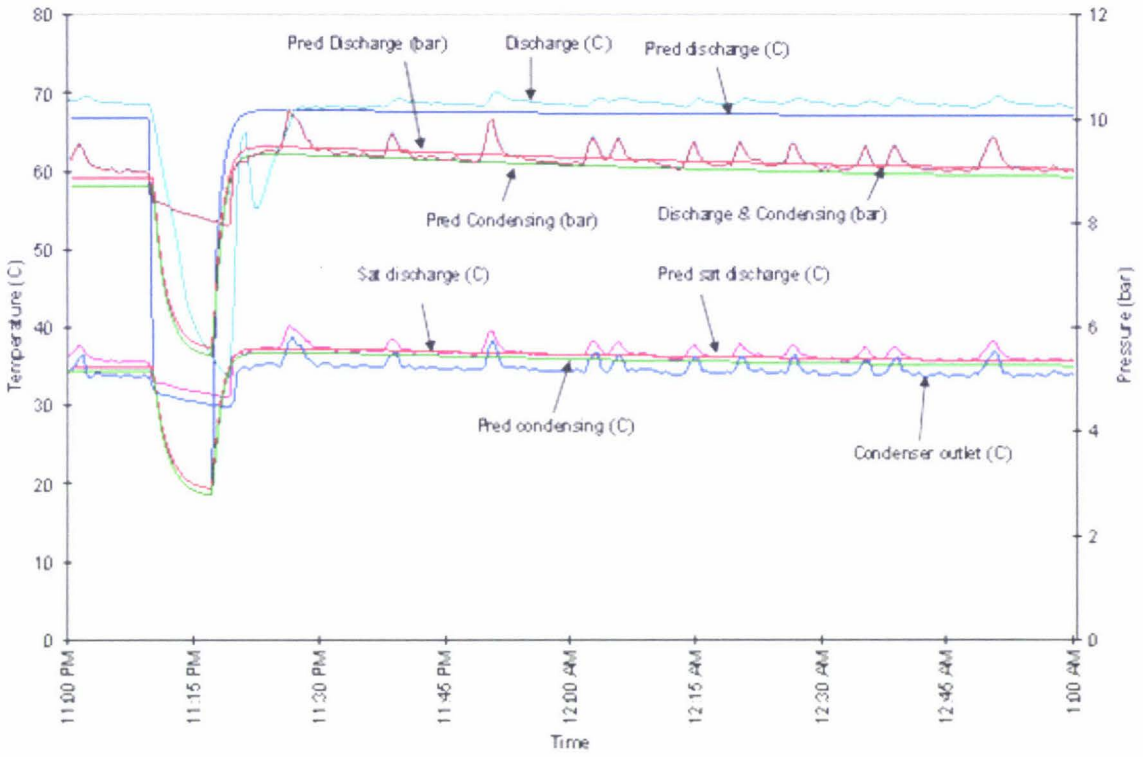

Figure 6-10: Comparison of predicted and measured temperature and pressure for the high pressure side for simulation 2 (experimental trial 13, defrosting).

Figure 6-11 compares the measured and predicted results for the surface temperatures for simulation 1 during initial pull down. The predicted pull down of the surface temperature follow a very similar pattern to that of the measured values after an initial lag. The assumption of negligible internal resistance to heat transfer in the metal surface and thermal capacity of the insulation are obviously not quite right but overall the difference is small. At steady state the measured values were slightly higher than the predicted values but the off-set was quite small. Overall the predicted surface temperatures follow to a similar trend to the measured values.

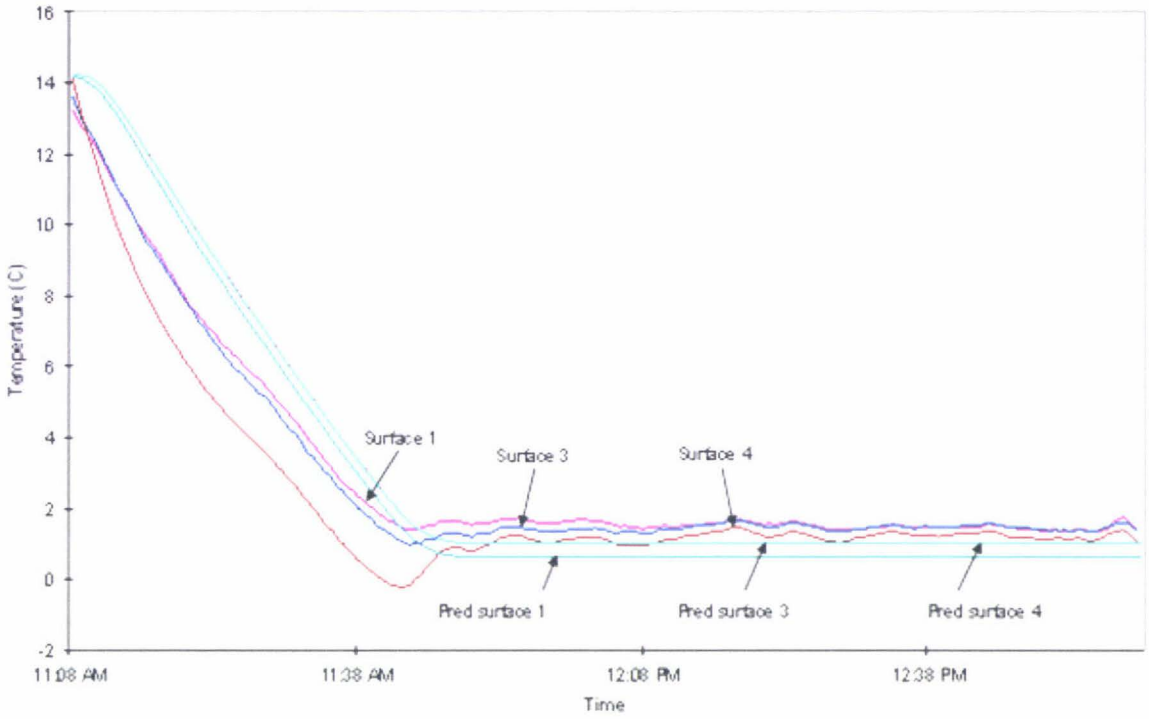

Figure 6-11: Comparison of predicted and measured surface temperatures for simulation 1 (experimental trial 1, pull down).

Figure 6-12 shows the predicted and measured surface temperatures before and after a defrost for simulation 3. The surface temperatures increases rapidly during defrosting and was rapidly cooled once the defrosting was terminated and compressor started. At steady state conditions the differences between the predicted and measured surface temperatures were small. One reason for the lag in the measured values compared with the predicted values was the shorter defrosting time for the predicted case and the thermal buffering values used.

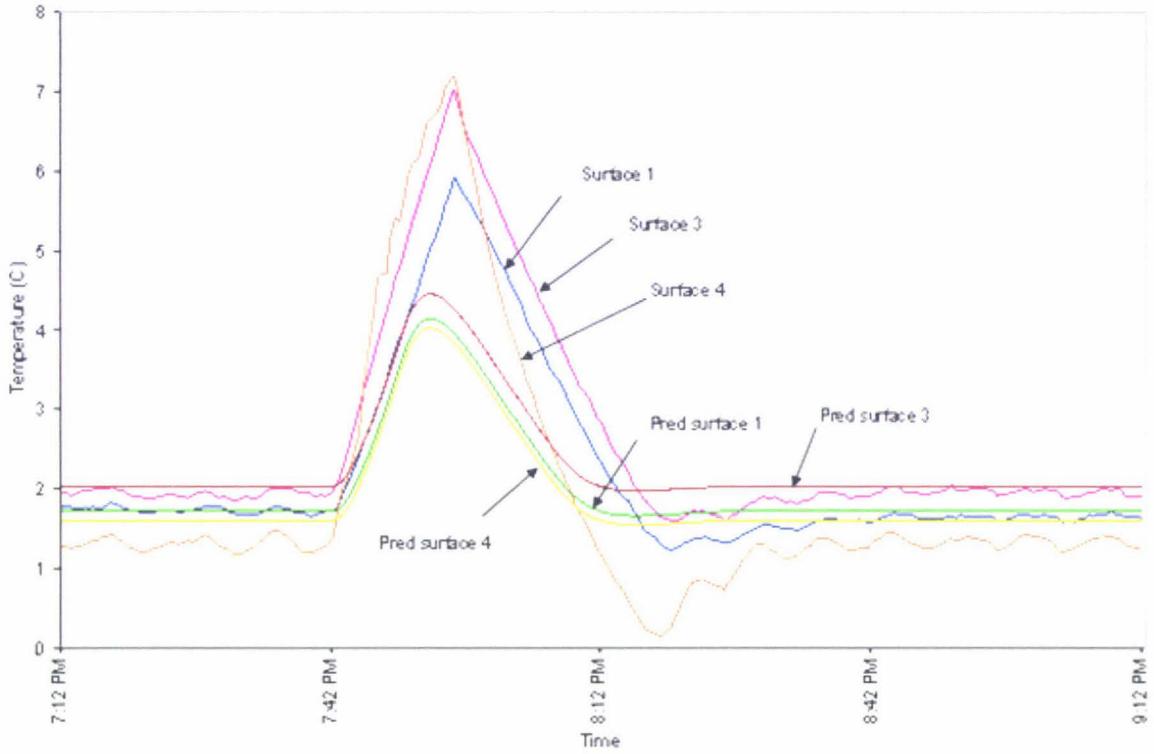

Figure 6-12: Comparison of predicted and measured surface temperature for simulation 3 (experimental trial 2, defrosting).

Figure 6-13 shows the predicted and measured surface temperatures before and after during defrosting for the simulation 2. The predicted values were consistently higher than the measured values suggesting either the thermal mass correction factor was too low and/or the surface heat transfer coefficient was too low. Given the heat transfer between the surfaces and the air was a relatively minor mechanism further optimisation of these parameters was not justified.

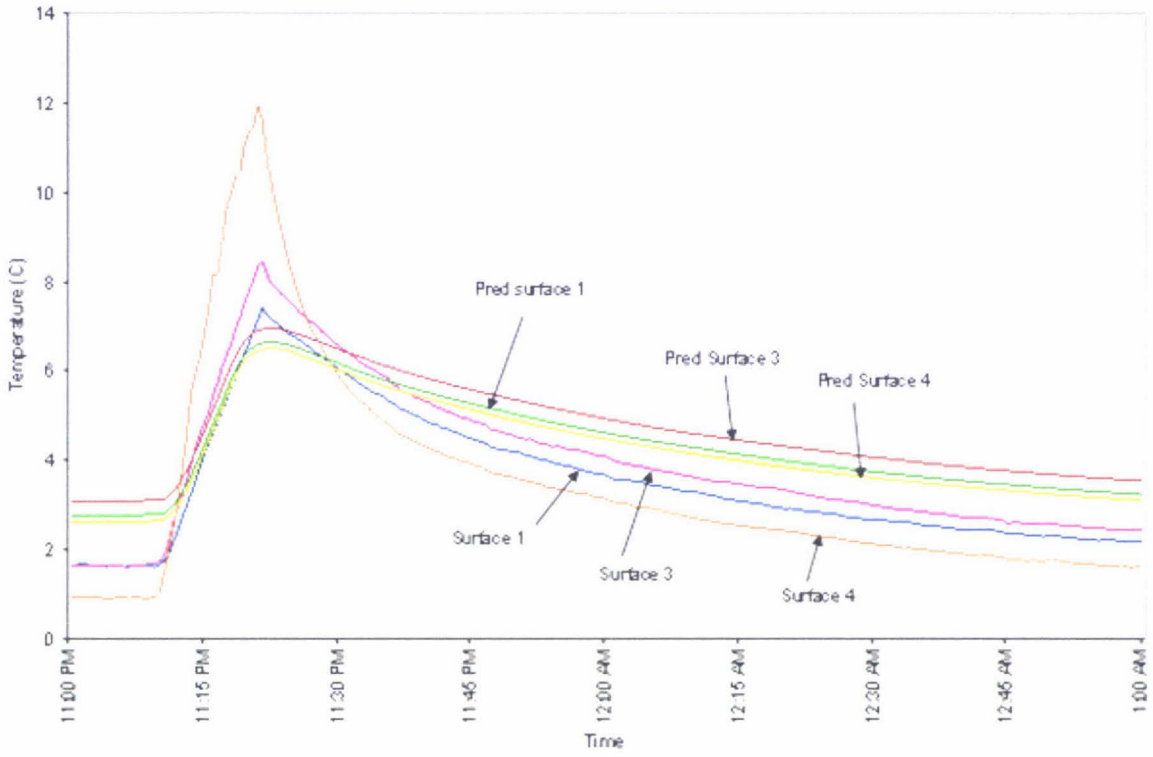

Figure 6-13: Comparison of predicted and measured surface temperature for simulation 2 (experimental trial 13, defrosting).

Figure 6-14 and Figure 6-15 compares the predicted and measured surface temperature for simulation 2 and 3. Overall predicted surface temperature were slightly higher than the measured values indicating less heat was transferred from the surfaces to the air space than in the predictions or that there was a significant difference in the temperature probe calibration. Since the temperature difference between predicted and measured values were small there was no reason to adjust the thermal buffering factor for the surfaces and floor and heat transfer coefficient correction factor.

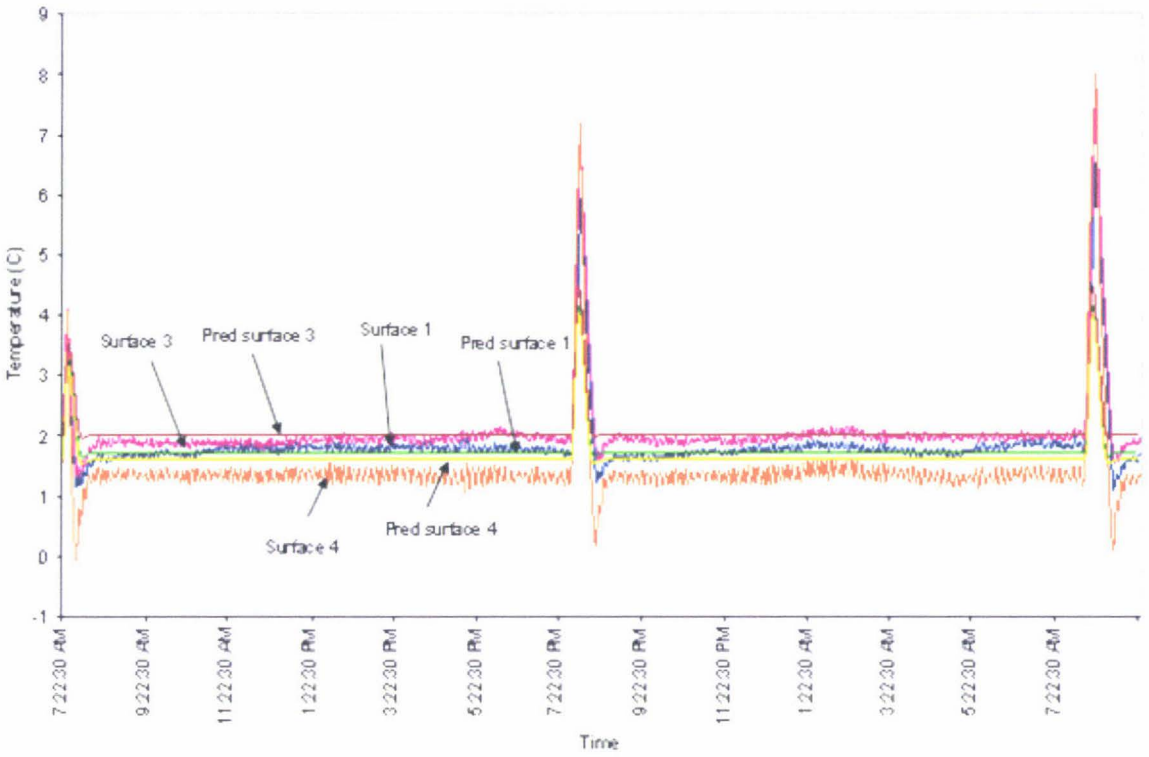

Figure 6-14: Comparison of predicted and measured surface temperature for simulation 3 (experimental trial 2)

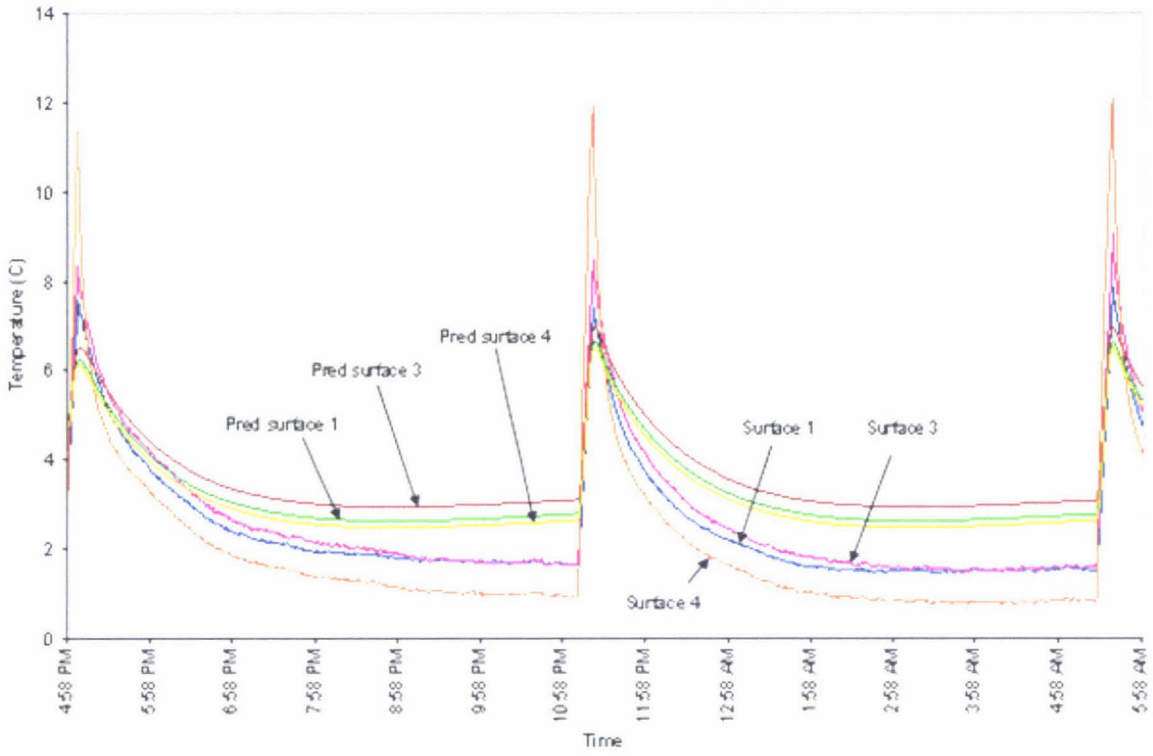

Figure 6-15: Comparison of predicted and measured surface temperature for simulation 2 (experimental trial 13).

6.2.2.2 Correction Factor for Evaporator Heat Transfer

Figure 6-16 and Figure 6-17 compares the experimental values to the predicted values for the room air temperature, evaporator surface temperature, air-on and air-off evaporators and saturated refrigerant temperature in the evaporator and RH for simulations 3 and 2 (12 hour and 6 hour defrost intervals). Except for the evaporator surface temperatures and the cycling in the measured values (probably due to imprecise control of the evaporator thermostatic expansion valve) the predicted temperatures closely follow the measured values.

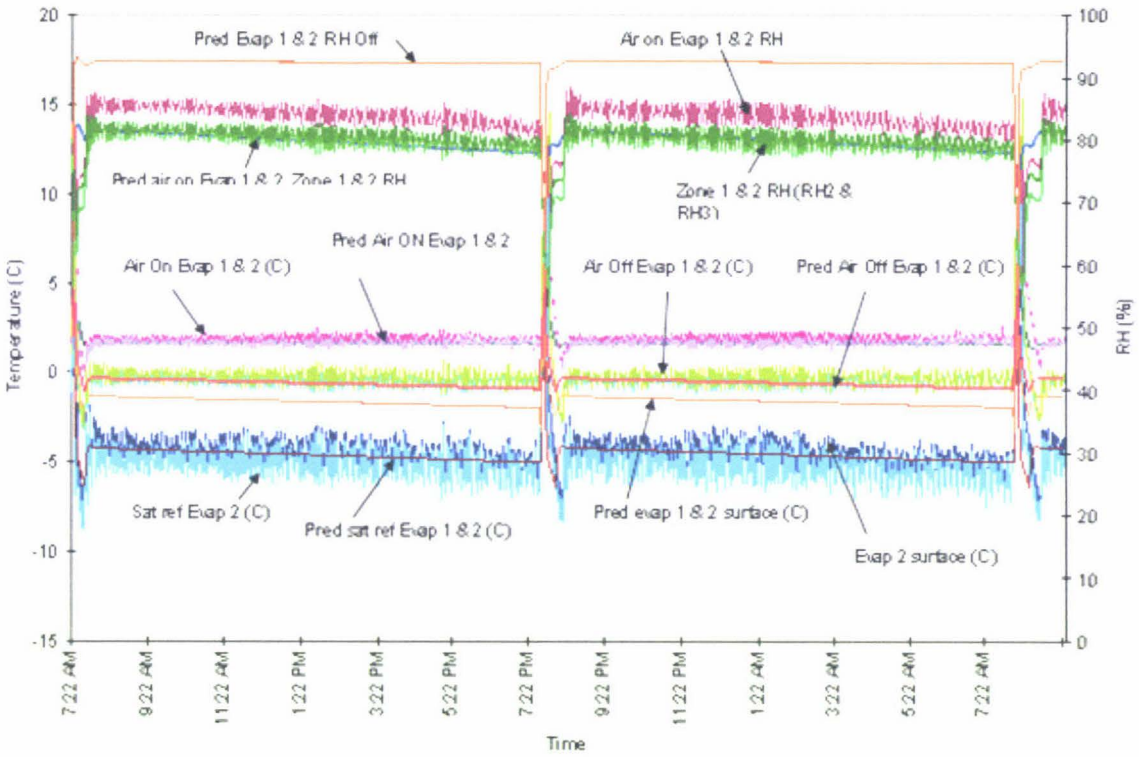

Figure 6-16: Comparison of predicted and measured temperature and RH for simulation 3 (experimental trial 2) with low sensible heat load.

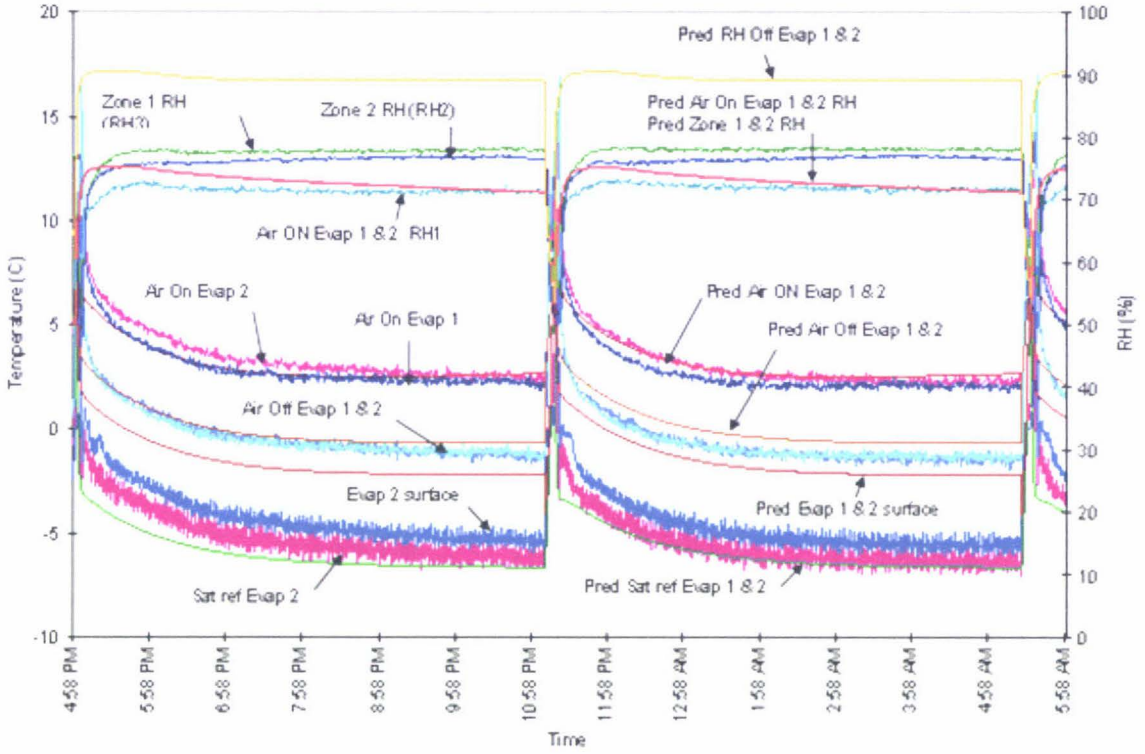

Figure 6-17: Comparison of predicted and measured temperature and RH, simulation 2 (experimental trial 13) with high sensible heat load.

The predicted evaporator surface temperature was consistently higher than the measured values. A possible reason is that the evaporator surface temperature sensor was located in "evaporator 1" end tube sensor pocket and hence measured refrigerant saturated evaporation temperature and not the actual fin surface temperature where air-side heat transfer was occurring. The measured evaporator surface temperature and saturated refrigerant temperature was differed by only about 0.5°C for the two trials. The other reason for higher predicted surface temperature was the value of overall to refrigerant side heat transfer coefficient ratio (0.5). If this value was lower then a closer fit of surface temperature would be achieved, but RH prediction would also be affected.

The predicted RH for the evaporator's air-off was higher than the predicted RH for the evaporator's air-on values consistent with dehumidification by the coil. The predicted air-on RH for the evaporator's has an error of -4% to 1.5% whereas for

the air zones the error was -4.5% to 0.5%. These differences are small given that RH measurement was ±3% at best. The predicted air-off RH was consistently higher than the measured zone values. This difference is probably because the zone measurements were not immediately at the evaporator exit, so significant mixing at the air-off air would have occurred. Table 6-22 and Table 6-23 give the average temperature and relative humidity for the trials.

Figure 6-18 and Figure 6-19 compares measured and predicted values for refrigerant pressure and temperature of the low pressure side for the simulation 3 (low sensible heat load) and 2 (high sensible heat load). The predicted values for evaporator pressure, saturated refrigerant temperature of the evaporator, evaporator outlet superheat conditions and suction line heat exchanger outlet (superheated vapour) closely agree with the measured values apart from the cycling in the measured values which was probably due to the control of the evaporator thermostatic expansion (TX) valve.

Table 6-22: Average measured and predicted air side temperatures, RH and evaporation temperature for simulation 3

		Measured Average	Predicted Average	Difference
Air off temperature (°C)	Evap 1	-0.09	-0.54	-0.19
	Evap 2	-0.34	-0.53	-2.66
Air on temperature (°C)	Evap 1	2.04	1.65	-0.39
	Evap 2	1.80	1.65	-0.15
Evaporator saturated refrigerant temperature (°C)	Evap 1		-4.54	
	Evap 2	-4.98	-4.54	0.44
Evaporator surface temperature (°C)	Evap 1		-1.57	
	Evap 2	-4.43	-1.57	2.86
Air-on RH (%)	Evap 1	83.54	79.73	-3.81
	Evap 2		79.72	-3.82
Evap 1 RH off (%)			92.31	
Evap 2 RH off (%)			92.30	
Zone 1 RH (RH3) (%)		79.37	79.77	0.40
Zone 2 RH (RH2) (%)		80.13	79.68	-0.45

Table 6-23: Average measured and predicted air side temperatures, RH and evaporation temperature for simulation 2

		Measured Average	Predicted Average	Difference
Air off temperature (°C)	Evap 1	-0.26	0.09	0.35
	Evap 2	-0.25	0.09	0.35
Air on temperature (°C)	Evap 1	2.99	3.15	0.16
	Evap 2	3.40	3.15	-0.25
Evaporator saturated refrigerant temperature (°C)	Evap 1		-5.82	
	Evap 2	-5.17	-5.82	-0.65
Evaporator surface temperature (°C)	Evap 1		-1.45	
	Evap 2	-4.31	-1.44	2.87
Air on RH (%)	Evap 1	71.38	72.80	1.42
	Evap 2		72.78	1.40
Evap 1 RH off (%)			89.04	
Evap 2 RH off (%)			89.03	
Zone 1 RH (RH3) (%)		77.26	72.84	-4.41
Zone 2 RH (RH2) (%)		75.73	72.74	-2.99

The difference in fit for different sensible heat loads suggests that the evaporator heat transfer model may be slightly too simplistic (e.g. refrigerant side heat transfer coefficient may vary significantly with temperature difference rather than being constant).

However, overall the good fits for air temperature, air RH and refrigerant low side pressure and temperature suggests the values for the evaporator heat transfer are reasonable.

For simulation 3 (low sensible heat load) the predicted suction temperature follows the measured values; whereas the simulation 2 (high sensible heat load) the predicted suction temperature was slightly higher. The good agreement for the compressor suction temperature suggests that the calibrated value for the suction

line heat exchanger effectiveness was reasonable. Table 6-24 and Table 6-25 give the average values of temperature and pressure for the two trials.

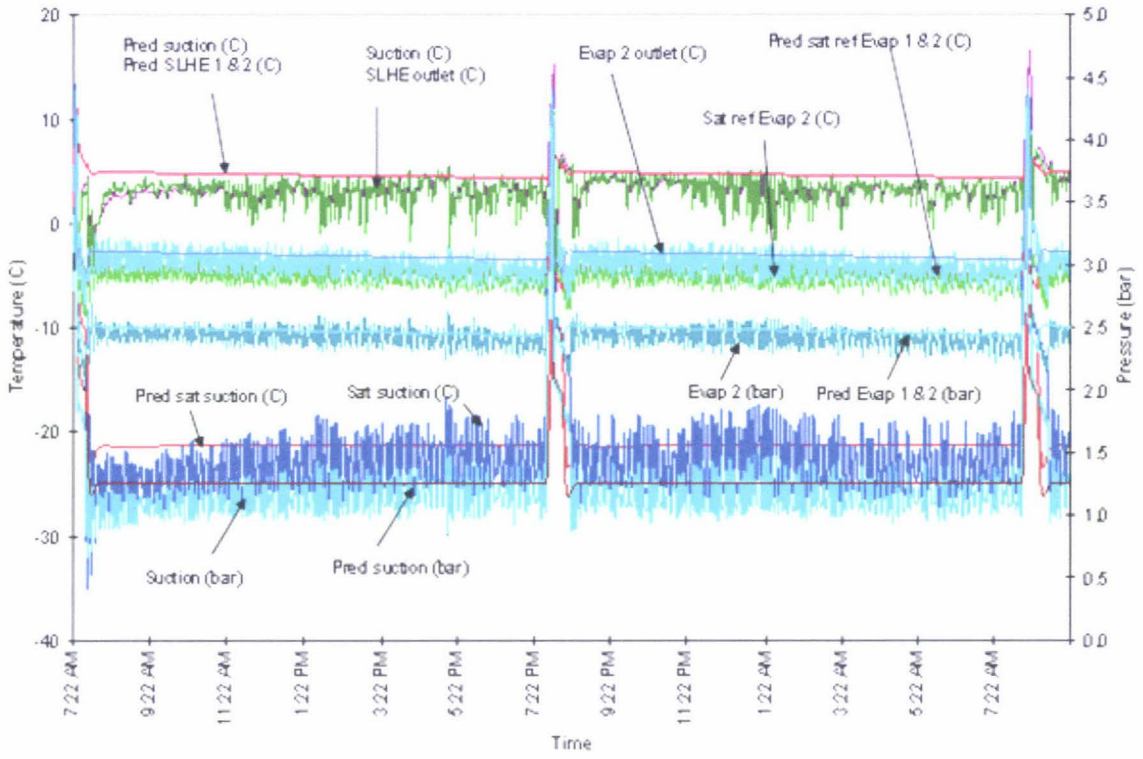

Figure 6-18: Comparison of predicted and measured refrigerant pressure and temperature for the low side for simulation 3 (experimental trial 2).

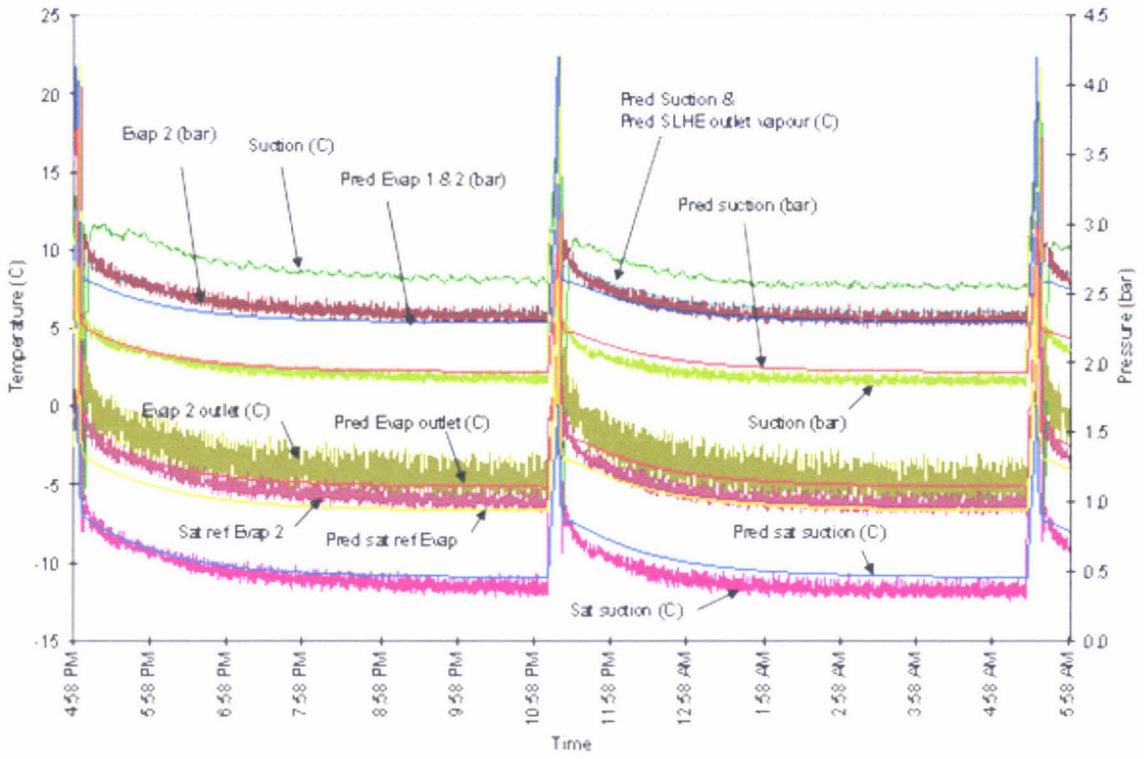

Figure 6-19: Comparison of predicted and measured refrigerant pressure and temperature for the low pressure side for simulation 2 (experimental trial 13).

Table 6-24: Average measured and predicted low pressure side refrigerant temperatures and pressures for simulation 3

		Measured Average	Predicted Average	Difference
Evaporator outlet temperature (°C)	Evap 1		-3.04	
	Evap 2	-3.92	-3.04	0.88
SLHE inlet (liquid) (°C)	SLHE 1		22.75	
	SLHE 2	22.27	22.75	0.47
SLHE outlet (liquid) (°C)	SLHE 1		16.13	
	SLHE 2	14.91	16.13	1.22
SLHE outlet (vapour) (°C)	SLHE 1		4.70	
	SLHE 2	3.07	4.70	1.62
Suction temperature (°C)		3.26	4.70	1.43
Saturated suction temperature (°C)		-22.85	-21.01	1.84
Evaporator pressure (bar, absolute)	Evap 1		2.48	
	Evap 2	2.44	2.48	0.04
Suction pressure (bar, absolute)		1.20	1.28	0.08

Table 6-25: Average measured and predicted low pressure side refrigerant temperatures and pressures for simulation 2.

		Measured Average	Predicted Average	Difference
Evaporator outlet temperature (°C)	Evap 1		-4.32	
	Evap 2	-3.62	-4.32	-0.70
SLHE inlet (liquid) (°C)	SLHE 1		32.19	
	SLHE 2	34.91	32.19	-2.72
SLHE outlet (liquid) (°C)	SLHE 1		25.24	
	SLHE 2	25.17	25.24	0.08
SLHE outlet (vapour) (°C)	SLHE 1		6.64	
	SLHE 2	7.44	6.64	-0.81
Suction temperature (°C)		8.66	6.64	-2.02
Saturated suction temperature (°C)		-10.59	-10.03	0.56
Evaporator pressure (bar, absolute)	Evap 1		2.37	
	Evap 2	2.43	2.37	-0.06
Suction pressure (bar, absolute)		1.97	2.01	0.04

6.2.2.3 Correction Factor for Condenser Heat Transfer

Figure 6-20 and Figure 6-21 compares the measured and predicted values for the refrigerant pressure and temperature for the high pressure side for the simulation 3 (low sensible heat load) and 2 (high sensible heat load). For the low sensible heat load trial the predicted discharge temperature was higher than the measured values; whereas for the high sensible heat load trial the predicted discharge temperature was lower than the measured values, but in both cases the difference was small. The measured values for both trials were cyclic due to the control effect of the TX valve. For simulation 3 the measured values were periodic indicating the influence of some variations in ambient conditions on the high pressure side heat transfer. Table 6-26 and Table 6-27 give the high pressure side average refrigerant temperature and pressure for the trials. The good overall agreement suggests that the condenser heat transfer correction factor chosen and compressor heat loss factor were reasonable.

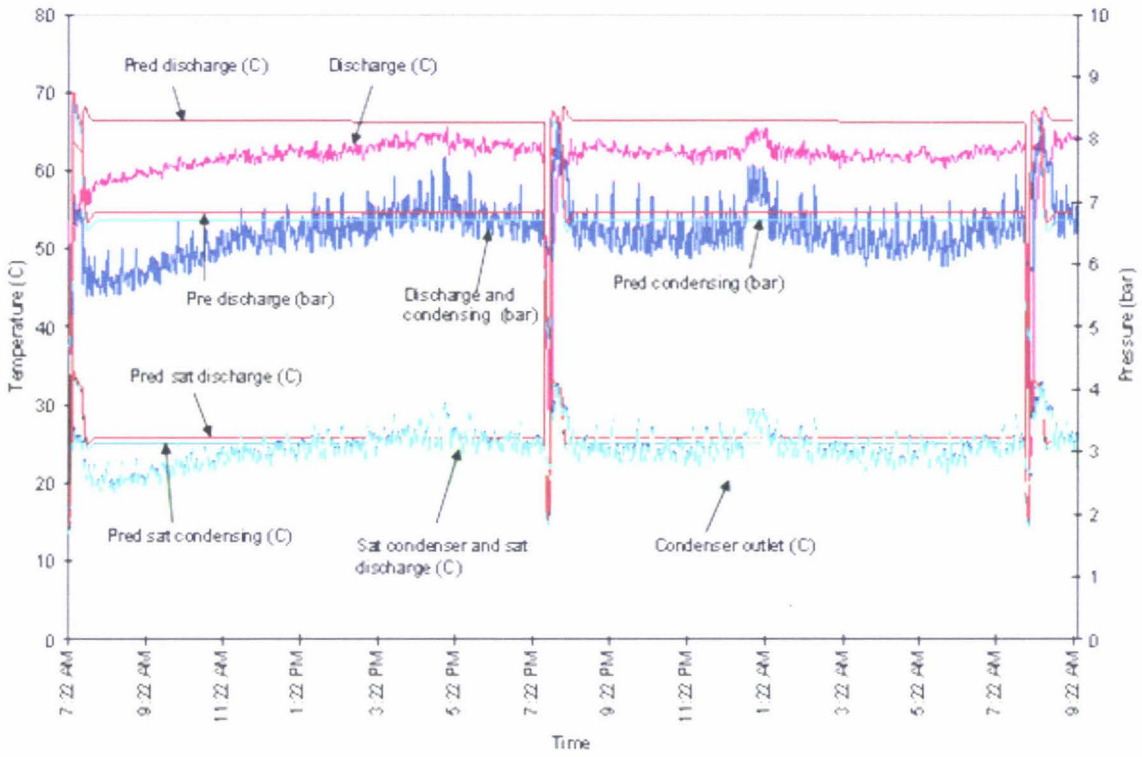

Figure 6-20: Comparison of predicted and measured refrigerant pressure and temperature for the high pressure side for simulation 3 (experiment trial 2).

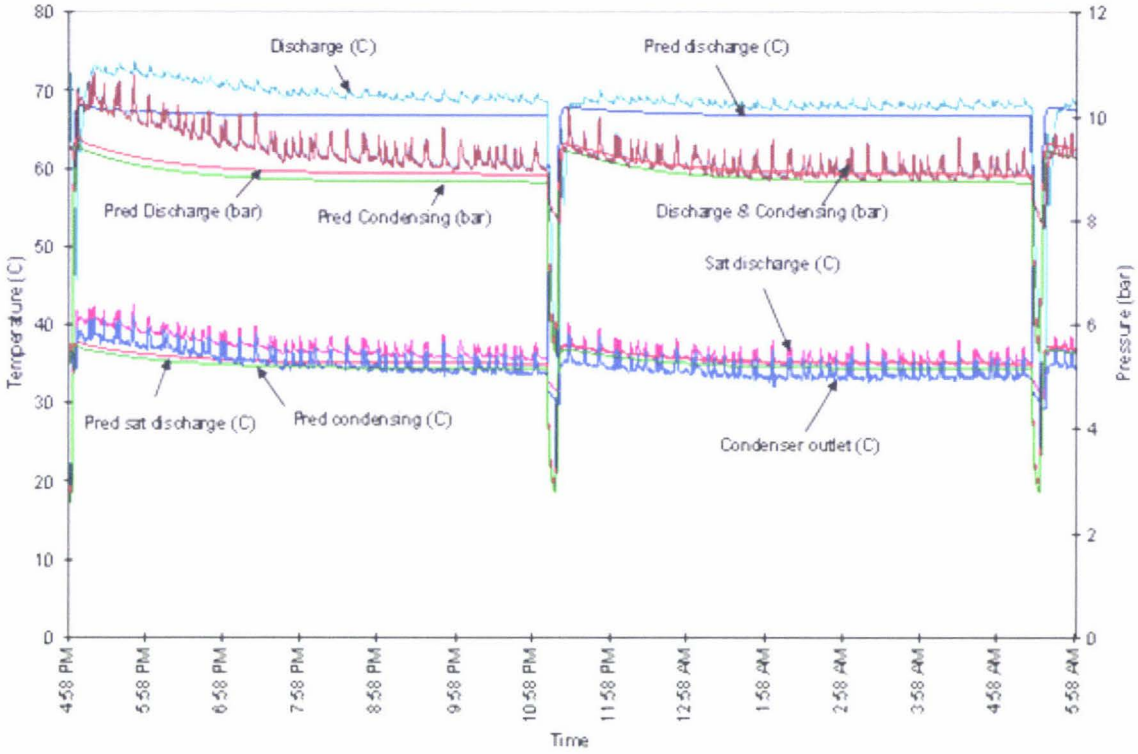

Figure 6-21: Comparison of predicted and measured refrigerant pressure and temperature for the high pressure side for simulation 2 (experiment trial 13)

Table 6-26: Average measured and predicted high pressure side refrigerant temperatures and pressures for simulation 3 (experiment trial 2).

	Measured Average	Predicted Average	Difference
Discharge temperature (°C)	61.52	65.68	4.16
Saturated discharge temperature (°C)	24.18	25.99	1.81
Condenser outlet temperature (°C)	22.18	22.75	0.57
Saturated condensing temperature (°C)	24.09	25.25	1.16
Discharge pressure (bar, absolute)	6.51	6.87	0.36
Condensing pressure (bar, absolute)	6.49	6.72	0.22

Table 6-27: Average measured and predicted high pressure side refrigerant temperatures and pressures for simulation 2 (experiment trial 13)

	Measured	Predicted	Difference
Discharge temperature (°C)	68.72	66.28	-2.44
Saturated discharge temperature (°C)	36.66	35.30	-1.36
Condenser outlet temperature (°C)	34.78	32.19	-2.59
Saturated condensing temperature (°C)	36.43	34.69	-1.74
Discharge pressure (bar, absolute)	9.31	8.97	-0.34
Condensing pressure (bar, absolute)	9.25	8.82	-0.43

6.2.2.4 Frost Deterioration Factor

The factor for evaporator heat transfer deterioration with frost accumulation was best calibrated for the trial with the longest time between defrosts simulation 4 (30 hour interval). The trial had 3.45 kW extra sensible heat load and moisture addition of 0.293 kg/hour.

Figure 6-22 compares the experimental values to the predicted values for the frosting factor of 7.5 for the room air temperature, evaporator surface temperature, air-on air-off evaporators, saturated refrigerant temperature in the evaporator and relative humidity air on to evaporator and relative humidity of room. The predicted evaporator saturated refrigerant temperature curves declines with a similar gradient to the measured curves apart from the cycling due to the effect of the evaporator TX valve control. Table 6-28 compares the average air side temperatures, RH and evaporation temperature for the trial. The measured RH was 3% higher than the predicted RH on average which is acceptable.

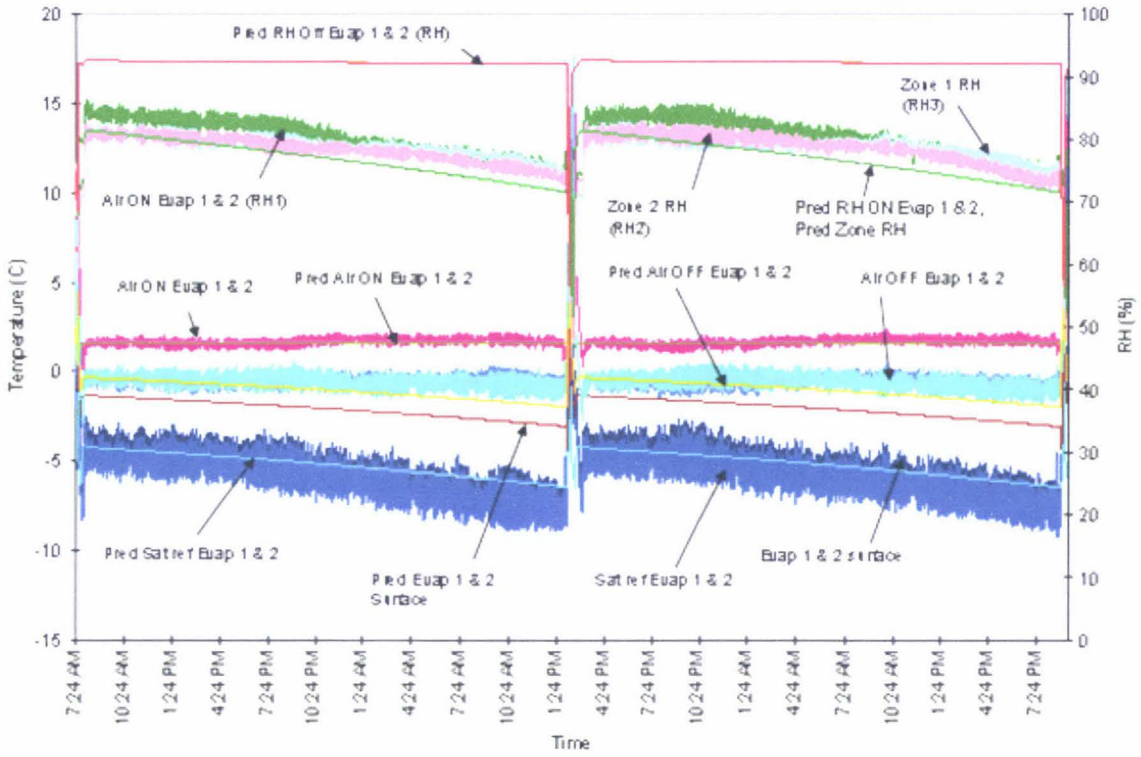

Figure 6-22: Comparison of predicted and measured air and refrigerant temperatures and air RH for simulation 4 (experimental trial 6).

Table 6-28: Average measured and predicted air side temperature, RH and evaporation temperature for simulation 4 (experimental trial 6).

		Measured Average	Predicted Average	Difference
Air off temperature (°C)	Evap 1	-0.38	-1.01	-0.63
	Evap 2	-0.37	-1.00	-0.63
Air on temperature (°C)	Evap 1	1.78	1.63	-0.14
	Evap 2	1.89	1.63	-0.26
Evaporator saturated refrigerant temperature (°C)	Evap 1		-5.18	
	Evap 2	-5.83	-5.18	0.65
Evaporator surface temperature (°C)	Evap 1		-2.06	
	Evap 2	-5.28	-2.06	3.23
	SLHE 2	15.41	15.49	0.08
Air on RH (RH1) (%)	Evap 1	80.00	76.82	-3.18
	Evap 2		76.81	-3.20
Evap 1 RH off (%)			92.12	
Evap 2 RH off (%)			92.10	
Zone 1 RH (RH3) (%)		78.56	76.84	-1.72
Zone 2 RH (RH2) (%)		78.16	76.78	-1.38

Figure 6-23 and Figure 6-24 shows the comparison of the experimental and predicted results for the refrigerant pressure and temperature for the low pressure and high pressure side for the simulation 4 (30 hour defrost interval). The predicted temperature and pressure for the low pressure and high pressure side also follow the experimental curves closely. The calibrated values for the evaporator and suction line heat exchanger give similar values to that of the measured values for evaporator outlet superheat conditions, suction temperature and suction line heat exchanger outlet superheated vapour. Similarly the calibrated values for the condenser and compressor gave similar condensing and discharge temperature and pressure to the measured values. The experimental curves follow a cyclic pattern probably due to imprecise TX valve control and the variation in ambient conditions (slow cycling) whereas the model assumes ambient conditions to be constant and perfect TX valve control.

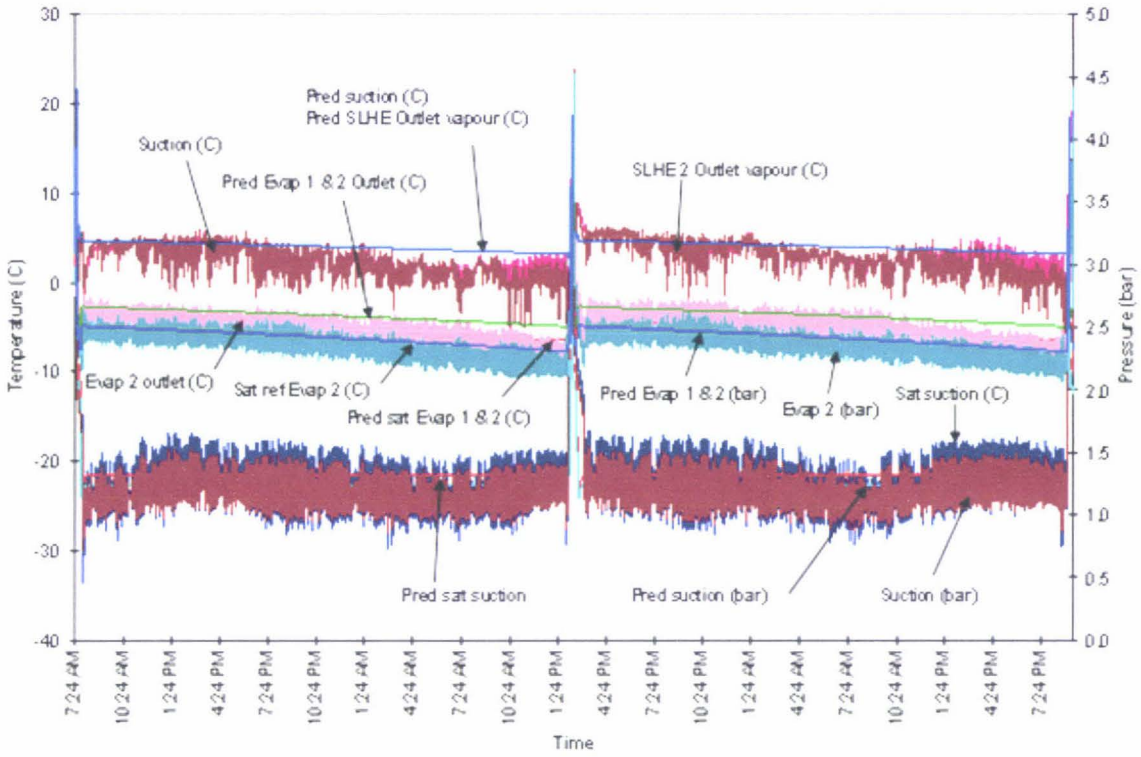

Figure 6-23: Comparison of predicted and measured refrigerant pressure and temperature for the low pressure side for simulation 4 (experimental trial 6).

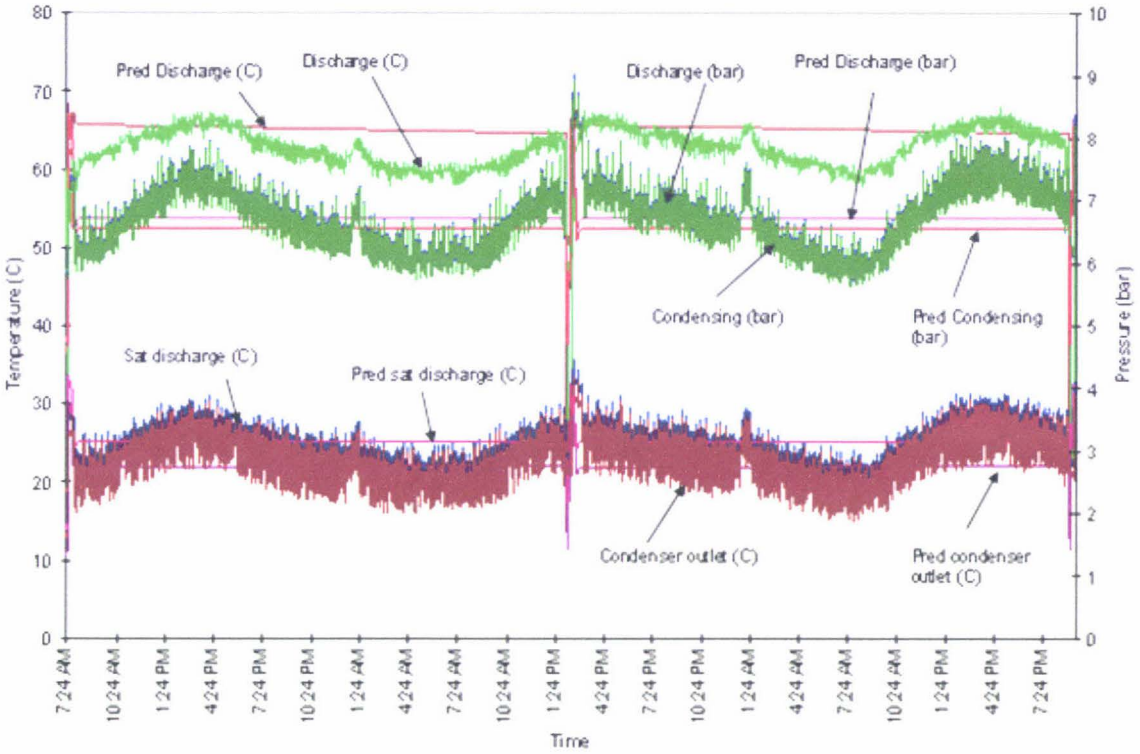

Figure 6-24: Comparison of predicted and measured refrigerant pressure and temperature for the high pressure side for simulation 4 (experimental trial 6).

Table 6-29 and Table 6-30 compare the measured and predicted average refrigerant temperature and pressure for the low and high pressure sides of the refrigeration system. Again, overall agreement is reasonable given uncertainty in the measured data and model parameter data but deficiencies in the model cannot be totally eliminated.

Table 6-29: Average measured and predicted low pressure side refrigerant temperatures and pressures for simulation 4 (experimental trial 6).

		Measured Average	Predicted Average	Difference
Evaporator outlet temperature (°C)	Evap 1		-3.68	
	Evap 2	-4.87	-3.68	1.19
SLHE inlet temperature (liquid) (°C)	SLHE 1		22.05	
	SLHE 2	23.45	22.05	-1.40
SLHE outlet temperature (liquid) (°C)	SLHE 1		15.49	
	SLHE 2	15.41	15.49	0.08
SLHE outlet temperature (vapour) (°C)	SLHE 1		4.04	
	SLHE 2	2.49	4.04	1.55
Suction temperature (°C)		3.05	4.04	0.99
Saturated suction temperature (°C)		-22.52	-21.35	1.17
Evaporator pressure (bar, absolute)	Evap 1		2.42	2.42
	Evap 2	2.36	2.42	0.06
Suction pressure (bar, absolute)		1.21	1.26	0.05

Table 6-30: Average measured and predicted high pressure side refrigerant temperatures and pressures for simulation 4 (experimental trial 6).

	Measured Average	Predicted Average	Difference
Discharge temperature (°C)	62.72	64.87	2.15
Saturated discharge temperature (°C)	25.26	25.31	0.05
Condenser outlet temperature (°C)	23.21	22.05	-1.16
Saturated condensing temperature (°C)	25.18	24.55	-0.62
Discharge pressure (bar, absolute)	6.73	6.73	0.00
Condensing pressure (bar, absolute)	6.71	6.58	-0.14

6.2.2.5 Evaporator Frost

Table 6-31 gives a comparison of the predicted and measured condensate collected and predicted evaporator frost accumulated on the evaporators for the three trials. For the simulation the evaporator frost was calculated excluding the defrosting periods and it is the sum of frosts on both evaporators and should be

equal to the condensate measured for the equivalent experimental trials unless condensation on other surfaces was significant.

Table 6-31: Comparison of predicted and measured evaporator frost and measured condensate collected for simulations 2, 3 and 4 (experimental trials 13, 2 and 6)

	Simulation 2	Simulation 3	Simulation 4
Experimental trials	13	2	6
Defrost intervals (hours)	6	12	30
Simulation time (Compressor switched ON to Compressor switched OFF) (hours)	12.4	24.6	61.5
Moisture added by humidifier (Experimental) (kg)	5.4	7.6	18
Measured condensate (corrected to simulation time) (kg)	5.7	6.5	18.5
Moisture added by humidifier and infiltration (simulation) (kg)	5.9	8.4	18.8
Frost accumulated on evaporators (simulation, condensate collected) (kg)	5.7	8.7	19.3

In case of condensate measured there were number factors affecting the measurements. These include splash from the tray and some amount of leakage from the tray itself. For simulation 2 and 4 measured condensate collected was slightly higher than moisture added by the humidifier, while for simulation 3 measured condensate collected was slightly less than moisture added. The predicted frost accumulation was higher than the moisture added (humidifier and infiltration) for simulation 3 and 4 and predicted frost accumulation was slightly lower than the moisture added (humidifier and infiltration) for simulation 2.

Overall, the differences were quite small which gives confidence in the calibrated model and its implementation as a computer programme.

6.3 MODEL VALIDATION

Two dynamic runs and one steady state run were use to validate the calibrated model simulations and to show the effect of model and actual coolstore behaviour with changes to different operating parameters. The operating parameters were extra sensible heat loads, amount of moisture added, fan speed and evaporator size and defrosting interval. For each set of conditions the plant was operated until steady state was reached.

6.3.1 Simulation 5

Figure 6-25 compares the measured and predicted values for temperature and RH for the trial. Table 6-32 and Table 6-33 compare the average measured and predicted values for RH and air side temperatures evaporator pressure and temperatures for the trial. As expected lowering the sensible heat load in the second period increased both the air-off temperature and air RH in the room. Similarly the evaporator surface temperature and evaporation temperature increased to adjust to the new sensible heat load. The air-on temperature did not change showing the refrigeration system control was working well. The difference between measured and predicted RH in the first 2 periods was about 3% for zone 1. For the second period the RH was about 7% higher. In the third period increasing the sensible heat load to original values restored RH, air-off temperature, evaporator surface temperature and evaporation temperature to the same conditions as the period one. There was a defrost in this period and air temperature rose rapidly at the same time RH dropped; similarly evaporator surface temperature and evaporation temperature rose rapidly. Once defrost was terminated and the pulldown period was complete, the temperature and RH quickly recovered. The measured RH in zone 2 was about 8% higher than for zone 1. No

reason for this difference was found although short term changes in sensor calibration due to condensation of moisture were suspected.

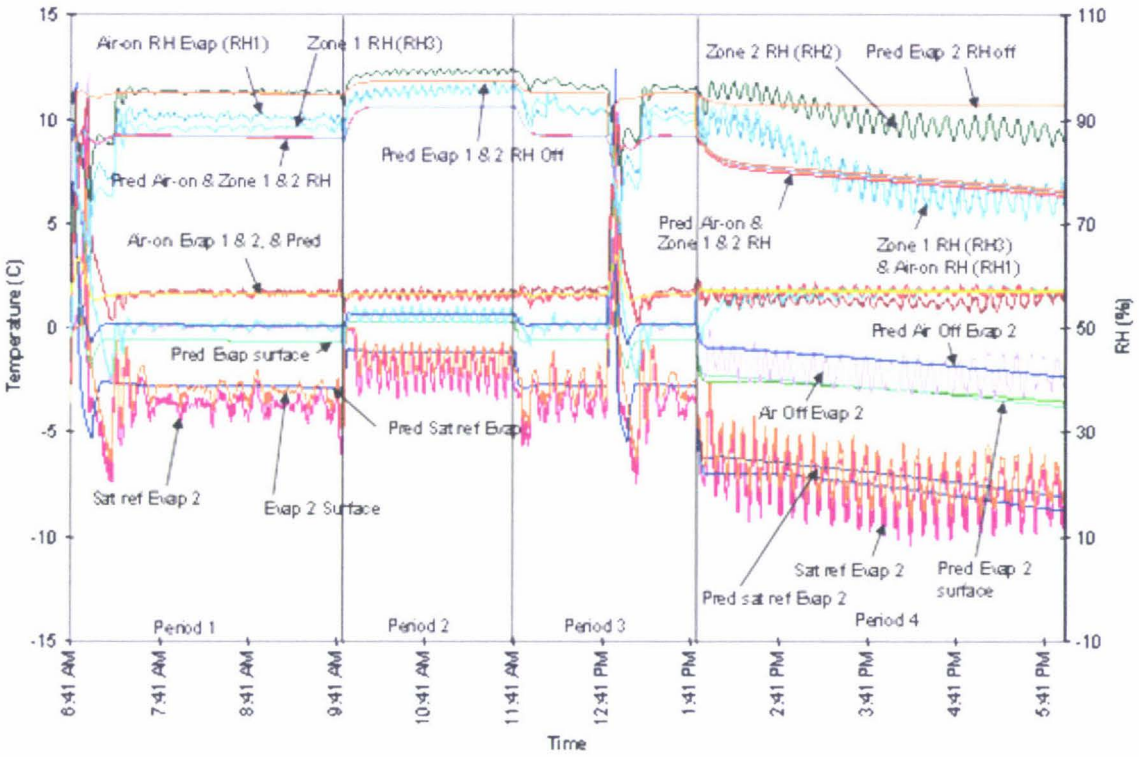

Figure 6-25: Comparison of predicted and measured temperature and RH for simulation 5 (experimental trial 14).

In the fourth period since the evaporator capacity was halved by switching off evaporator 1, RH lowered due to the larger temperature difference across the evaporator 2. Air-off temperature for evaporator 2 dropped to a low level whereas for evaporator 1 air-on and air-off were the same as expected. The predicted evaporators air-on RH and zone 1 & 2 RH declined rapidly similar to the measured air-on and zone 1 RH whereas measured RH in zone 2 had a slow decline. A likely reason for the rapid decline in measured RH for the evaporator air-on and zone 1 was due to the imperfect mixing in the room, the positioning of the heaters and the location of air-on RH sensor. Since evaporator 2 was rapidly frosting and evaporator 1 only circulated the air a slight hot spot was created in the zone 1. The

predicted air-off RH for evaporator 2 was higher than the predicted air-on RH indicating dehumidification on the evaporator 2 while air-off RH for evaporator 1 was same as air-on RH indicating that the air was not cooled passing through evaporator 1 and hence no moisture was removed. The predicted air-on and zone 1 RH was 1% lower than the measured whereas 11% lower than the measured for zone 2 RH. This probably was due to sensor positioning for air-off RH from the evaporator 2, imperfect mixing of the air zones although changes in sensor calibration may also have been significant. The cycling of the measured values were due to the imprecise control of the evaporator TX valves. The predicted air-on and air-off temperature for the evaporator's was in good agreement with the measured values throughout the trial.

Table 6-32: Average measured and predicted RH for the four periods for simulation 5 (experimental trial 14)

	Room Set Temperature (°C)		Air-on Evaporator RH (%)		Air-off Evaporator RH (%)		Zone RH (%)	
			1	2	1	2	1	2
Period 1	1.6	Measured	88.27				86.25	93.62
		Predicted	86.65	86.61	94.80	94.78	86.72	86.53
		Difference	-1.63	-1.66			0.47	-7.09
Period 2	1.6	Measured	95.45				95.18	99.08
		Predicted	92.32	92.29	97.26	97.24	92.40	92.21
		Difference	-3.12	-3.16			-2.79	-6.87
Period 3	1.6	Measured	89.63				89.12	94.79
		Predicted	86.50	86.46	94.32	94.33	86.58	86.39
		Difference	-3.13	-3.17			-2.54	-8.40
Period 4	1.6	Measured	79.87				79.81	90.78
		Predicted	78.95	79.18	78.95	92.86	78.50	79.64
		Difference	-0.92	-0.69			-1.31	-11.14

Table 6-33: Average measured and predicted air-on, air-off, evaporation, evaporator surface and evaporator outlet temperatures for the four periods for simulation 5 (experimental trial 14)

	Room Set Temperature (°C)		Air-on Evaporator (°C)		Air-off Evaporator (°C)		Evaporator Pressure (bar)		Evaporation Temperature (°C)		Evaporator Surface Temperature (°C)		Evaporator Outlet Temperature (°C)	
		Evaporator No.	1	2	1	2	1	2	1	2	1	2	1	2
Period 1	1.6	Measured	2.07	2.16	0.57	0.45		2.59		-3.40		-2.80		-2.59
		Predicted	1.65	1.65	0.20	0.20	2.67	2.67	-2.60	-2.60	-0.48	-0.48	-1.10	-1.10
		Difference	-0.42	-0.51	-0.37	-0.25		0.08		0.80		2.32		1.48
Period 2	1.6	Measured	1.52	1.69	0.63	0.54		2.72		-2.01		-1.39		-1.19
		Predicted	1.59	1.59	0.71	0.71	2.81	2.81	-1.12	-1.12	0.24	0.24	0.38	0.38
		Difference	0.07	-0.09	0.08	0.17		0.09		0.88		1.63		1.57
Period 3	1.6	Measured	1.93	2.20	0.51	0.43		2.61		-3.21		-2.58		-2.29
		Predicted	1.69	1.69	0.28	0.28	2.68	2.68	-2.53	-2.53	-0.41	-0.41	-1.03	-1.03
		Difference	-0.23	-0.50	-0.23	-0.16		0.07		0.68		2.17		1.26
Period 4	1.6	Measured	1.75	1.33	1.57	-2.00		2.21		-7.57		-6.82		-5.61
		Predicted	1.82	1.75	1.82	-1.52	2.21	2.26	-7.60	-6.97	-2.92	-2.90	-6.10	-5.47
		Difference	0.08	0.42	0.25	0.48		0.05		0.60		3.92		0.14

Figure 6-26 and Figure 6-27 shows refrigerant temperature and pressure for the low pressure side and high pressure side. Table 6-34 shows average refrigerant temperatures and pressures for the low pressure side and high pressure side. The predicted saturated refrigerant temperature for the evaporator and evaporator surface temperature follow the same trend as the measured with changes to the operating parameters.

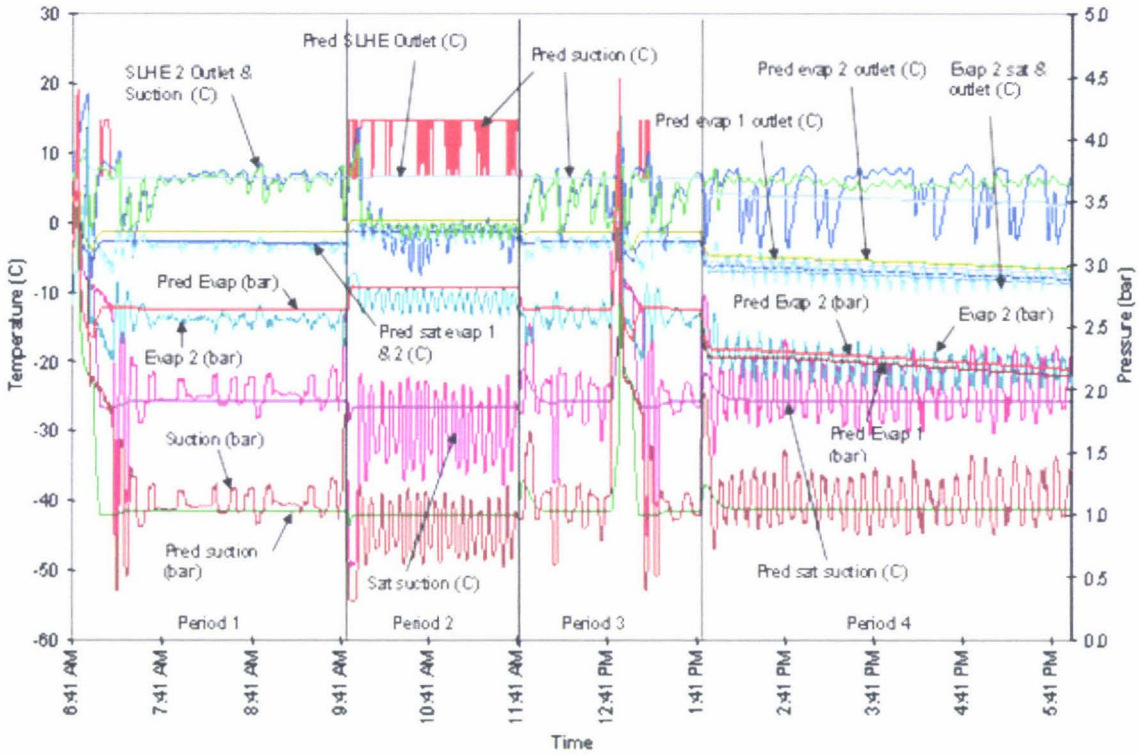

Figure 6-26: Comparison of predicted and measured refrigerant temperature and pressure for the low pressure side for simulation 5 (experimental trial 14)

The predicted saturated suction temperature, suction temperature and pressure follows the same trend as the measured values, except for the suction temperature and SLHE vapour outlet conditions for the period 2; this was due to imprecision of the hot gas bypass circuit liquid injection. Similarly the predicted discharge and condensing pressure and temperature followed a similar trend to that of the measured values. The predicted discharge temperature was about 6°C higher for

period 1, 2 and 3 and condensing and discharge pressures were lower than the measured values suggesting some of the input parameter values such as compressor heat losses might have considerable uncertainties. The measured values for temperature and pressure for the high side showed cyclic patterns. This may be due to the influence of ambient conditions and the imprecise control of the evaporator TX valves, whereas for the simulation ambient conditions were assumed constant and control was perfect.

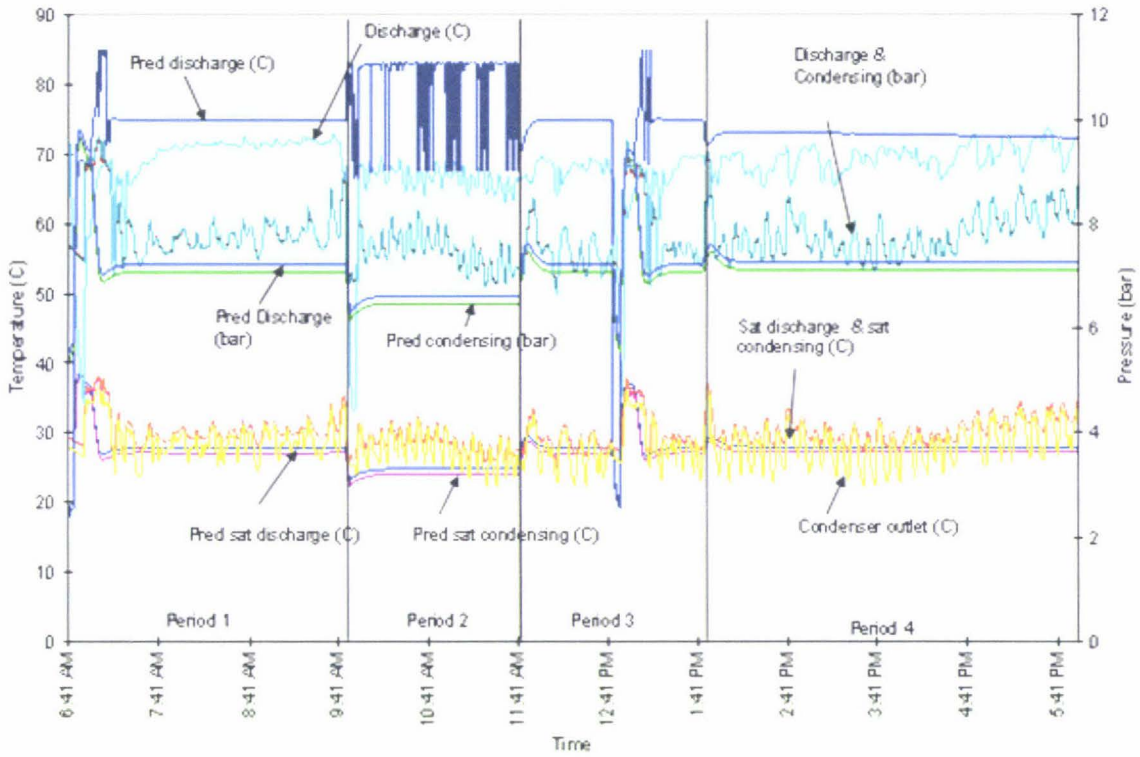

Figure 6-27: Comparison of predicted and measured refrigerant temperature and pressure for the high pressure side for simulation 5 (experimental trial 14)

Overall the predicted values to follow the same trend as the measured values for the air side temperature, relative humidity and the refrigerant low side and high side temperatures and pressures.

Table 6-34: Average measured and predicted refrigerant pressures and temperatures for the low pressure and high pressure side and compressor pressure ratios for the four periods for simulation 5 (experimental trial 14)

	Room Set Temperature (°C)		SLHE 1 (Inlet Liquid) (°C)	SLHE 2 (Inlet Liquid) (°C)	SLHE 1 (Outlet Liquid) (°C)	SLHE 2 (Outlet Liquid) (°C)	SLHE 1 (Outlet Vapour) (°C)	SLHE 2 (Outlet Vapour) (°C)	Suction Pressure (bar)	Suction Temperature (°C)	Discharge Pressure (bar)	Discharge Temperature (°C)	Condensing Pressure (bar)	Condensing Temperature (°C)	Compressor Pressure Ratio
Period 1	1.6	Measured		28.90		18.98		5.83	1.30	6.26	7.88	68.60	7.88	29.02	6.75
		Predicted	25.03	25.03	17.85	17.85	6.74	6.74	1.16	6.97	7.35	73.56	7.20	25.03	6.71
		Difference		-3.87		-1.13		0.91	-0.14	0.71	-0.53	4.96	-0.68	-3.99	-0.04
Period 2	1.6	Measured		27.50		17.81		0.12	0.86	-0.70	7.44	65.07	7.45	27.27	9.47
		Predicted	21.44	21.44	14.59	14.59	6.70	6.70	1.00	13.82	6.61	80.66	6.46	21.44	6.62
		Difference		-6.06		-3.22		6.58	0.14	14.52	-0.83	15.59	-0.99	-5.83	-2.85
Period 3	1.6	Measured		27.88		18.81		3.69	1.31	4.48	7.66	66.10	7.65	27.87	6.73
		Predicted	25.10	25.10	17.92	17.92	6.81	6.81	1.16	7.02	7.37	71.85	7.22	25.10	6.60
		Difference		-2.77		-0.89		3.12	-0.15	2.53	-0.29	5.75	-0.43	-2.77	-0.13
Period 4	1.6	Measured		28.85		20.35		5.81	1.14	4.51	7.81	69.42	7.81	28.19	7.00
		Predicted	24.75	24.75	17.29	17.32	3.15	3.60	1.05	3.60	7.27	72.81	7.12	24.75	6.91
		Difference		-4.10		-3.04		-2.22	-0.09	-0.92	-0.54	3.39	-0.69	-3.45	-0.09

6.3.2 Simulation 6

Figure 6-28 to Figure 6-30 compares the measured and predicted values for the air temperature, RH, refrigerant low and high side temperature and pressure for this trial. Table 6-35 and Table 6-36 compare the average measured and predicted values for RH and air side temperatures evaporator pressure and temperatures for the trial. Since the humidifier was switched off in the first period the RH was low, and switching on the humidifier in the second period caused the RH to increase similar to the measured values. The same sensible heat load was applied so the change in RH was due to the moisture load from the humidifier. There was little change in air-off temperature, evaporation and surface temperature.

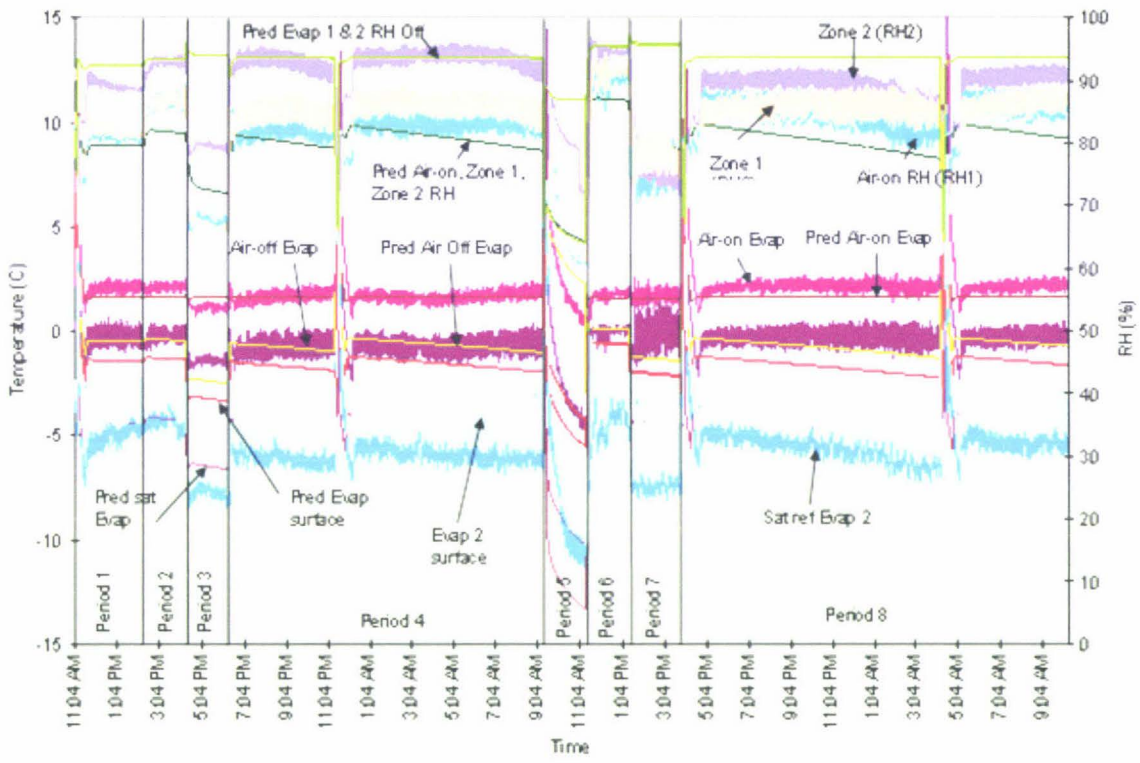

Figure 6-28: Comparison of predicted and measured temperature and RH for simulation 6 (experimental trial 15)

Table 6-35: Average measured and predicted RH for the eight periods for simulation 6 (experimental trial 15)

	Room Set Temperature (°C)		Air-on Evaporator RH (%)		Air-off Evaporator RH (%)		Zone RH (%)	
			1	2	1	2	1	2
Period 1	1.6	Measured	80.36				80.69	88.24
		Predicted	79.50	79.45	92.30	92.28	79.58	79.37
		Difference	-0.87	-0.91			-1.11	-8.86
Period 2	1.6	Measured	86.27				86.30	92.70
		Predicted	81.82	81.78	93.45	93.42	81.90	81.69
		Difference	-4.45	-4.49			-4.39	-11.01
Period 3	1.6	Measured	68.08				67.66	79.77
		Predicted	73.23	73.16	94.19	94.15	73.38	73.02
		Difference	5.15	5.08			5.71	-6.75
Period 4	1.6	Measured	82.76				84.83	92.64
		Predicted	80.59	80.54	93.40	93.37	80.68	80.45
		Difference	-2.17	-2.22			-4.14	-12.18
Period 5	1.6	Measured	66.39				66.04	78.90
		Predicted	66.29	66.65	66.38	86.36	65.57	67.38
		Difference	-0.10	0.26			-0.47	-11.52
Period 6	1.6	Measured	88.55				89.30	93.55
		Predicted	86.06	85.99	95.07	95.29	86.20	85.85
		Difference	-2.49	-2.56			-3.10	-7.70
Period 7	1.6	Measured	76.34				78.27	77.42
		Predicted	80.09	79.99	95.62	96.07	80.28	79.79
		Difference	3.75	3.65			2.01	2.37
Period 8	1.6	Measured	84.33				84.69	88.46
		Predicted	80.78	80.73	93.37	93.34	80.87	80.63
		Difference	-3.55	-3.60			-3.82	-7.83

Table 6-36: Average measured and predicted air-on, air-off, evaporation, evaporator surface and evaporator outlet temperatures for the eight periods for simulation 6 (experimental trial 15)

Trials	Room Set Temperature (°C)		Air-on Evaporator (°C)		Air-off Evaporator (°C)		Evaporator Pressure (bar)		Evaporation Temperature (°C)		Evaporator Surface Temperature (°C)		Evaporator Outlet Temperature (°C)	
		Evaporator No.	1	2	1	2	1	2	1	2	1	2	1	2
Period 1	1.6	Measured	2.07	2.16	0.57	0.45		2.59		-3.40		-2.80		-2.59
		Predicted	1.65	1.65	0.20	0.20	2.67	2.67	-2.60	-2.60	-0.48	-0.48	-1.10	-1.10
		Difference	-0.42	-0.51	-0.37	-0.25		0.08		0.80		2.32		1.48
Period 2	1.6	Measured	1.52	1.69	0.63	0.54		2.72		-2.01		-1.39		-1.19
		Predicted	1.59	1.59	0.71	0.71	2.81	2.81	-1.12	-1.12	0.24	0.24	0.38	0.38
		Difference	0.07	-0.09	0.08	0.17		0.09		0.88		1.63		1.57
Period 3	1.6	Measured	1.93	2.20	0.51	0.43		2.61		-3.21		-2.58		-2.29
		Predicted	1.69	1.69	0.28	0.28	2.68	2.68	-2.53	-2.53	-0.41	-0.41	-1.03	-1.03
		Difference	-0.23	-0.50	-0.23	-0.16		0.07		0.68		2.17		1.26
Period 4	1.6	Measured	1.75	1.33	1.57	-2.00		2.21		-7.57		-6.82		-5.61
		Predicted	1.82	1.75	1.82	-1.52	2.21	2.26	-7.60	-6.97	-2.92	-2.90	-6.10	-5.47
		Difference	0.08	0.42	0.25	0.48		0.05		0.60		3.92		0.14

Table 6-36: Continued

Trials	Room Set Temperature (°C)		Air-on Evaporator (°C)		Air-off Evaporator (°C)		Evaporator Pressure (bar)		Evaporation Temperature (°C)		Evaporator Surface Temperature (°C)		Evaporator Outlet Temperature (°C)	
		Evaporator No.	1	2	1	2	1	2	1	2	1	2	1	2
Period 5	1.6	Measured	4.15	3.17	3.91	-0.98		2.26		-4.95		-6.47		-4.10
		Predicted	3.45	3.35	3.42	-0.71	1.95	2.17	-11.03	-8.23	-3.82	-2.58	-9.53	-6.73
		Difference	-0.71	0.18	-0.48	0.27		-0.10		-3.28		3.90		-2.63
Period 6	1.6	Measured	1.40	1.57	-0.10	-0.31		2.56		-3.76		-3.16		-2.93
		Predicted	1.57	1.58	0.06	-0.04	2.64	2.64	-2.83	-2.82	-0.64	-0.71	-1.33	-1.32
		Difference	0.18	0.01	0.15	0.27		0.08		0.95		2.45		1.62
Period 7	1.6	Measured	0.87	1.68	-1.66	-0.25		2.33		-6.19		-5.70		-5.90
		Predicted	1.57	1.58	-1.32	-1.48	2.49	2.49	-4.40	-4.41	-1.99	-2.09	-2.90	-2.91
		Difference	0.70	-0.10	0.34	-1.23		0.16		1.79		3.61		2.99
Period 8	1.6	Measured	1.75	2.42	-0.27	0.05		2.48		-3.54		-3.88		-3.48
		Predicted	1.67	1.67	-0.60	-0.60	2.49	2.49	-4.41	-4.41	-1.52	-1.52	-2.91	-2.91
		Difference	-0.08	-0.75	-0.33	-0.65		0.01		-0.87		2.36		0.57

For period 1 and 2 the measured average air-on temperature for evaporator 2 was 2.3°C whereas for evaporator 1 was 1.8°C and the predicted values were 1.6°C. The difference in measured values indicates imperfect mixing of air zones or off-set in the temperature probes. The measured air-on RH for period 1 was 1% higher than the predicted value and for period 2 was 5%. Overall air zone RH was higher for period 1 and 2 especially for Zone 2 (9% higher).

In case of period 3 the sudden decrease in RH was due to reduction in fan speed from full speed to 50% of full speed, causing a large temperature drop across the evaporator coil which in turn reduced evaporation temperature, evaporator pressure and evaporator surface temperature. In the fourth period RH was restored to the level in the second period once the fans were switched back to full speed. In this period defrosting occurred. During defrosting RH dropped and air-on, air-off temperature, evaporation and evaporator surface temperature rose. After the end of defrost pull down RH was restored to the RH just prior to defrost. The difference between measured and predicted for the period 3 and 4 was 5% higher for air-on and zone 1 RH and 12% for zone 2 RH.

In the fifth period RH dropped due to defrosting and due to switching off evaporator 1. Again this was due to the larger temperature drop across the evaporator 2. Since the period was short steady state was not reached. Again predicted and measured values for zone 2 RH followed the same trend. Once the evaporator 1 was switched on in period 6 steady state control for the air-on, air-off, evaporation and evaporator surface temperature was regained. RH in this period was higher due to the low sensible heat load (reduced from 3 kW to 2 kW).

In seventh period the fan speed was reduced to 50% with 2.0 kW sensible heat load. The predicted RH was similar to period 1. The predicted air-on and zone RH were 4% higher than the measured for the period. In the last period (period 8) the operating conditions were same as period 2 and hence the predicted RH followed similar trend to period 2. The predicted air-on RH and Zone 1 RH were 4% lower

than the measured whereas for zone 2 it was 8% lower. For this period the measured average air-on temperature for evaporator 2 was 2.4°C whereas for evaporator 1 was 1.8°C and the predicted values were 1.7°C. Again this indicates imperfect mixing of air zones and temperature sensor offset.

Overall for this dynamic trial air-on and zone 1 RH were predicted reasonably accurately but for zone 2 RH it was consistently higher. Reasons for the RH difference could not be fully defined. Uncertainty in the sensor calibrations and imperfect mixing of the air zones probably contributed but deficiencies in the evaporator dehumidification model could not be fully eliminated.

Figure 6-29 and Figure 6-30 shows refrigerant temperature and pressure for the low pressure side and high pressure side. Table 6-37 shows average refrigerant temperatures and pressures for the low pressure side and high pressure side. It can be seen in Figure 6-24 the predicted evaporator outlet conditions and SLHE (vapour) outlet conditions for the trial follow similar trend to the measured values, except for suction pressure for the period 3 which is slightly lower than the measured values. The high side refrigerant temperature and pressure for the measured case is cyclic in nature. This was due to plant control and varying ambient conditions as for other trials.

Overall the simulation shows the predicted values followed the same trend as the experimental values for the air side temperature, relative humidity and the refrigerant low side and high side temperature and pressure.

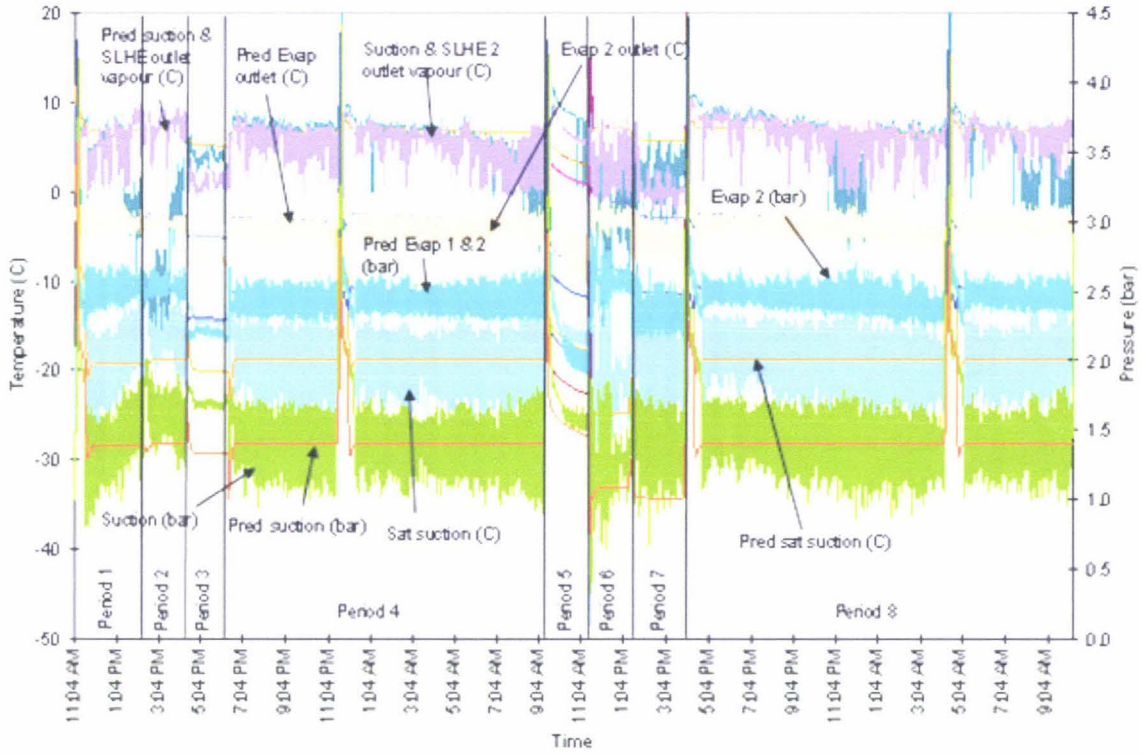

Figure 6-29: Comparison of predicted and measured refrigerant temperature and pressure for the low pressure side for simulation trial 6 (experimental trial 15).

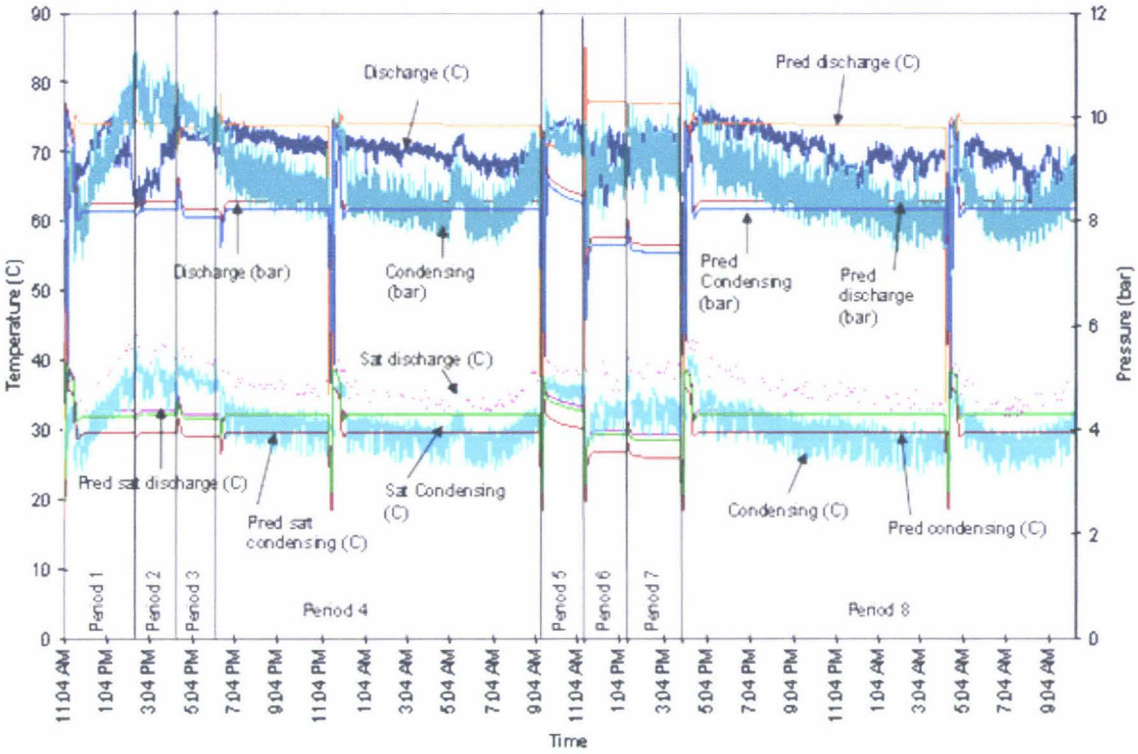

Figure 6-30: Comparison of predicted and measured refrigerant temperature and pressure for the high pressure side for simulation 6 (experimental trial 15).

Table 6-37: Average measured and predicted refrigerant pressures and temperatures for the low pressure and high pressure side and compressor pressure ratios for the eight periods for simulation 6 (experimental trial 15).

	Room Set Temperature (°C)		SLHE 1 (Inlet Liquid) (°C)	SLHE 2 (Inlet Liquid) (°C)	SLHE 1 (Outlet Liquid) (°C)	SLHE 2 (Outlet Liquid) (°C)	SLHE 1 (Outlet Vapour) (°C)	SLHE 2 (Outlet Vapour) (°C)	Suction Pressure (bar)	Suction Temperature (°C)	Discharge Pressure (bar)	Discharge Temperature (°C)	Condensing Pressure (bar)	Condensing Temperature (°C)	Compressor Pressure Ratio
Period 1	1.6	Measured		28.90		18.98		5.83	1.30	6.26	7.88	68.60	7.88	29.02	6.75
		Predicted	25.03	25.03	17.85	17.85	6.74	6.74	1.16	6.97	7.35	73.56	7.20	25.03	6.71
		Difference		-3.87		-1.13		0.91	-0.14	0.71	-0.53	4.96	-0.68	-3.99	-0.04
Period 2	1.6	Measured		27.50		17.81		0.12	0.86	-0.70	7.44	65.07	7.45	27.27	9.47
		Predicted	21.44	21.44	14.59	14.59	6.70	6.70	1.00	13.82	6.61	80.66	6.46	21.44	6.62
		Difference		-6.06		-3.22		6.58	0.14	14.52	-0.83	15.59	-0.99	-5.83	-2.85
Period 3	1.6	Measured		27.88		18.81		3.69	1.31	4.48	7.66	66.10	7.65	27.87	6.73
		Predicted	25.10	25.10	17.92	17.92	6.81	6.81	1.16	7.02	7.37	71.85	7.22	25.10	6.60
		Difference		-2.77		-0.89		3.12	-0.15	2.53	-0.29	5.75	-0.43	-2.77	-0.13
Period 4	1.6	Measured		28.85		20.35		5.81	1.14	4.51	7.81	69.42	7.81	28.19	7.00
		Predicted	24.75	24.75	17.29	17.32	3.15	3.60	1.05	3.60	7.27	72.81	7.12	24.75	6.91
		Difference		-4.10		-3.04		-2.22	-0.09	-0.92	-0.54	3.39	-0.69	-3.45	-0.09

Table 6-37: Continued.

	Room Set Temperature (°C)		SLHE 1 (Inlet Liquid) (°C)	SLHE 2 (Inlet Liquid) (°C)	SLHE 1 (Outlet Liquid) (°C)	SLHE 2 (Outlet Liquid) (°C)	SLHE 1 (Outlet Vapour) (°C)	SLHE 2 (Outlet Vapour) (°C)	Suction Pressure (bar)	Suction Temperature (°C)	Discharge Pressure (bar)	Discharge Temperature (°C)	Condensing Pressure (bar)	Condensing Temperature (°C)	Compressor Pressure Ratio
Period 5	1.6	Measured		34.49		25.44		7.08	1.84	8.30	9.47	69.44	9.45	35.67	5.44
		Predicted	30.56	30.56	23.06	23.15	2.50	4.46	1.59	4.42	8.58	67.83	8.43	30.56	5.46
		Difference		-3.93		-2.29		-2.62	-0.25	-3.89	-0.89	-1.61	-1.01	-5.11	0.03
Period 6	1.6	Measured		33.87		23.23		3.12	1.29	-0.46	8.98	68.86	8.97	33.87	7.63
		Predicted	26.50	26.50	18.96	18.96	7.02	7.03	1.07	6.57	7.65	76.19	7.50	26.50	7.18
		Difference		-7.36		-4.27		3.91	-0.22	7.03	-1.33	7.33	-1.47	-7.36	-0.44
Period 7	1.6	Measured		35.49		24.54		0.51	1.45	1.35	9.40	70.68	9.39	35.12	6.72
		Predicted	26.29	26.29	18.64	18.64	5.86	5.85	1.02	5.86	7.60	76.74	7.45	26.29	7.43
		Difference		-9.20		-5.90		5.34	-0.43	4.50	-1.80	6.06	-1.94	-8.84	0.71
Period 8	1.6	Measured		31.69		22.02		6.13	1.50	5.78	8.57	69.04	8.55	31.55	5.95
		Predicted	29.90	29.90	22.46	22.45	6.94	6.93	1.44	6.93	8.42	73.12	8.27	29.90	5.89
		Difference		-1.78		0.43		0.81	-0.07	1.15	-0.15	4.08	-0.28	-1.65	-0.06

6.3.3 Simulation 7

Figure 6-31 and Figure 6-32 compares the measured and predicted values for the air temperature, RH, evaporator surface temperature and evaporation temperature for the whole trial and the period during defrosting. The trial had very low sensible heat load and the room were pre-cooled to 1.6°C. The heat coming into the room was only through surfaces, fans, infiltration through door and from products. Due to low sensible heat load, RH was expected to be very high.

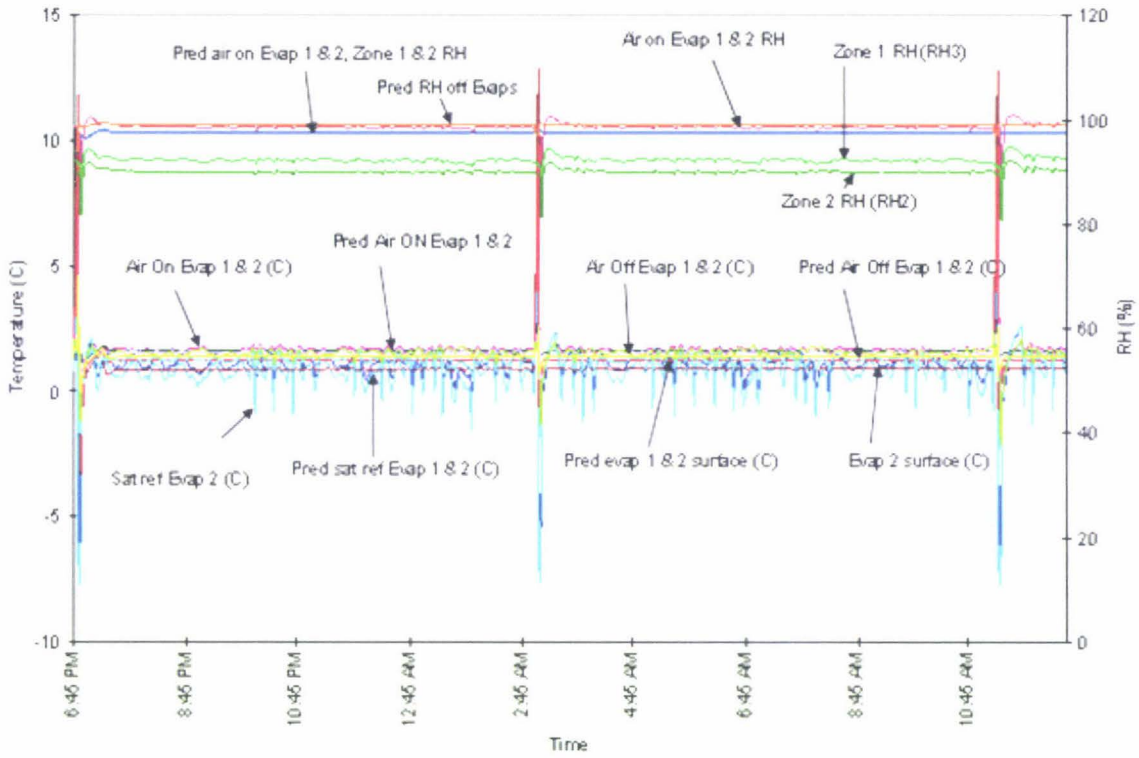

Figure 6-31: Comparison of predicted and measured temperature and RH for simulation 7 (experimental trial 15)

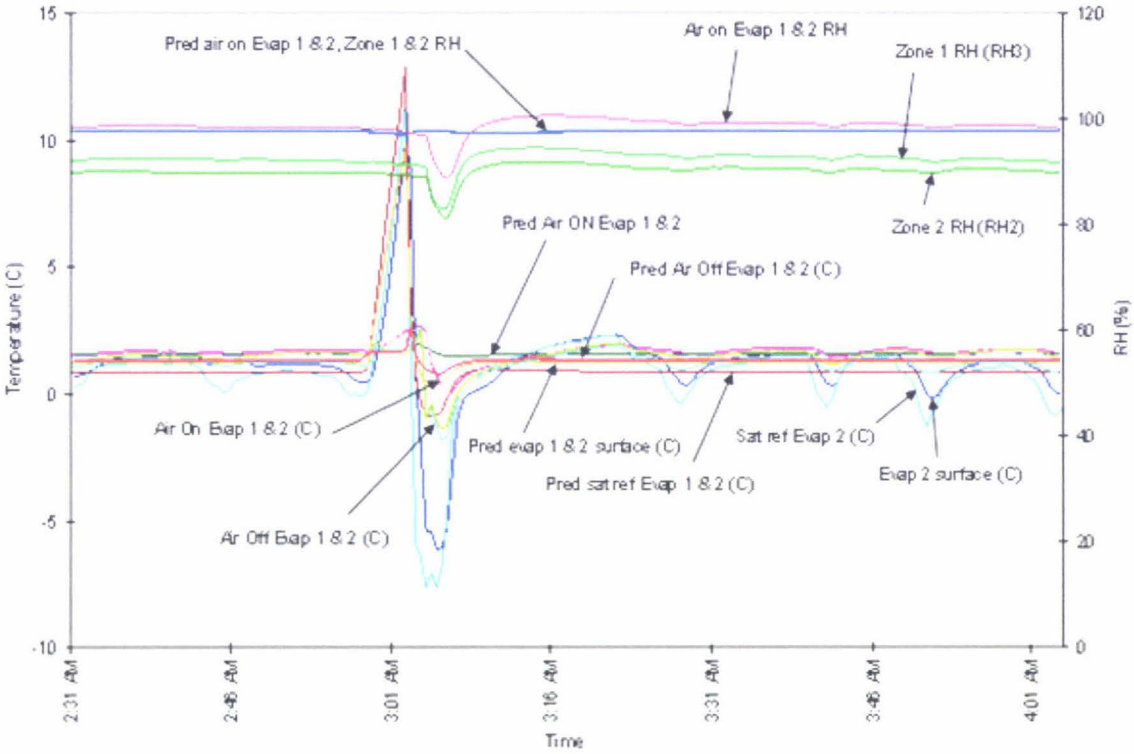

Figure 6-32: Comparison of predicted and measured temperature and RH for simulation 7 (experimental trial 16) before and after defrosting.

Table 6-38 compares the average measured and predicted air side temperatures, RH and evaporation temperature. Again the measured evaporation temperature and surface temperature fluctuated due to the expansion valve control. The predicted values were steady and were similar to the average measured values. There was little change in air-off temperature, evaporation and surface temperature. The measured and predicted air-on RH was close whereas for zone 1 & 2 RH the difference was high about 5% and 7% respectively.

During defrosting the predicted values closely followed the measured values. The defrost termination took same time for the predicted and measured cases. The measured evaporation temperature rapidly dropped during pull down to -7.6 °C and the predicted reached only -0.9 °C. This was probably due to the assumed

thermal buffering of the evaporator and suction pressure being higher than assumed in the predictions.

Table 6-38: Average measured and predicted air side temperatures, RH and evaporation temperature for simulation 7 (experimental trial 16).

		Measured Average	Predicted Average	Difference
Air off temperature (°C)	Evap 1	1.24	1.36	0.12
	Evap 2	1.52	1.36	-0.16
Air on temperature (°C)	Evap 1	1.67	1.60	-0.07
	Evap 2	1.57	1.60	0.03
Evaporator saturated refrigerant temperature (°C)	Evap 1		0.91	
	Evap 2	0.74	0.91	0.18
Evaporator surface temperature (°C)	Evap 1		1.26	
	Evap 2	1.09	1.26	0.17
Air on RH (RH1) (%)	Evap 1	98.59	97.56	-1.02
	Evap 2		97.55	-1.04
Evap 1 RH off (%)			99.13	
Evap 1 RH off (%)			99.12	
Zone 1 RH (RH3) (%)		92.23	97.59	5.37
Zone 2 RH (RH2) (%)		89.97	97.52	7.55

Figure 6-33 and Figure 6-34 compares the measured and predicted values for the low side refrigerant temperature and pressure for the whole run and the period immediately before and after defrosting. Table 6-39 compares the average measured and predicted refrigerant low side temperatures and pressures for the trial. The measured suction temperature and pressure was slightly higher than the predicted values and cyclic. Due to low sensible heat load the hot gas bypass circuit was activated. The predicted SLHE outlet on the vapour side was slightly higher than the measured. The predicted evaporator outlet conditions and SLHE outlet conditions were similar to the measured values. The predicted suction pressure and the saturated suction temperatures were lower than the measured values; due to the low setting of the hot gas bypass activation set point than modelled.

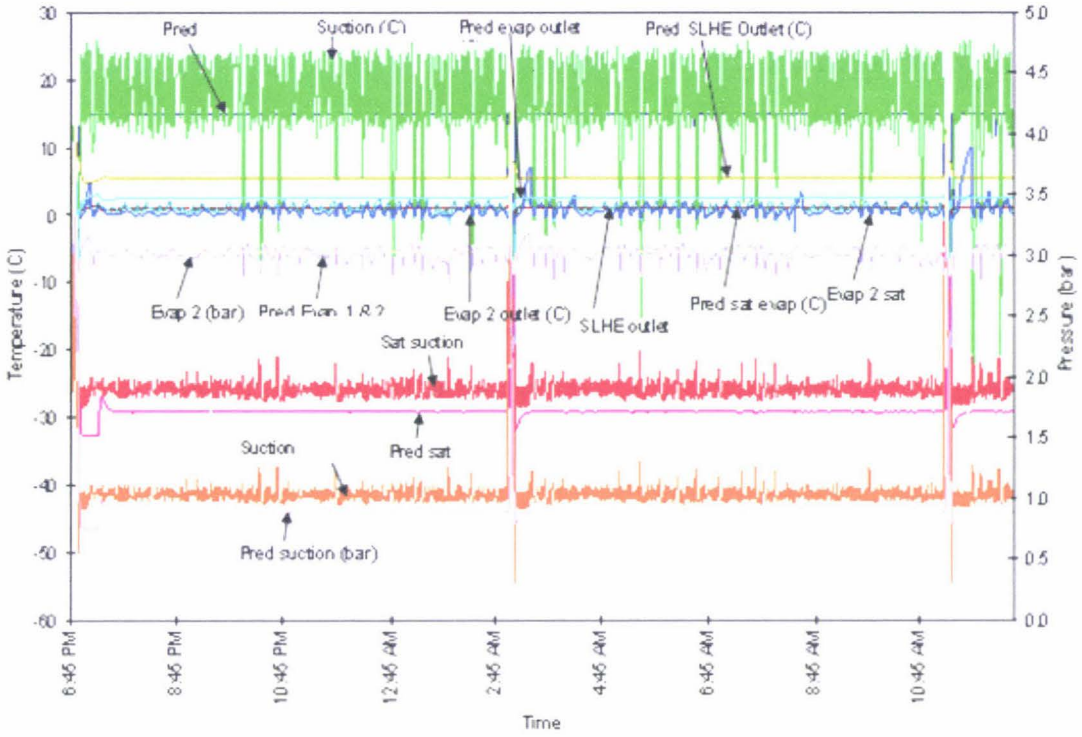

Figure 6-33: Comparison of predicted and measured refrigerant temperature and pressure for the low pressure side for simulation 7 (experimental trial 16).

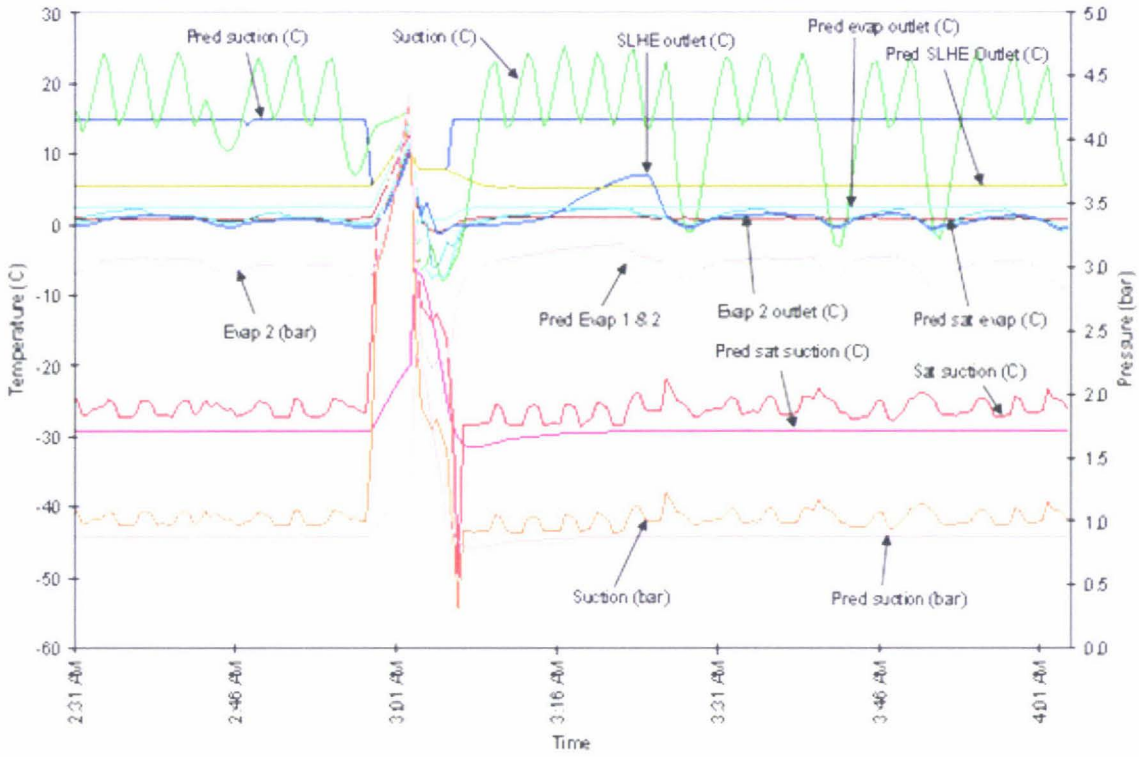

Figure 6-34: Comparison of predicted and measured refrigerant temperature and pressure for the low pressure side for simulation 7 (experiment trial 16) before and after defrosting.

Table 6-39: Average measured and predicted low side refrigerant temperatures and pressures for simulation 7 (experimental trial 16)

		Measured Average	Predicted Average	Difference
Evaporator outlet temperature (°C)	Evap 1		2.41	
	Evap 2	1.07	2.41	1.35
SLHE inlet temperature (liquid) (°C)	SLHE 1		12.92	
	SLHE 2	15.76	12.92	-2.84
SLHE outlet temperature (liquid) (°C)	SLHE 1		7.27	
	SLHE 2	8.40	7.27	-1.13
SLHE outlet temperature (vapour) (°C)	SLHE 1		5.57	
	SLHE 2	0.58	5.57	4.99
Suction temperature (°C)		17.02	14.90	-2.12
Saturated suction temperature (°C)		-25.62	-28.94	-3.32
Evaporator pressure (bar, absolute)	Evap 1		3.03	
	Evap 2	3.01	3.03	0.02
Suction pressure (bar, absolute)		1.05	0.90	-0.15

Figure 6-35 and Figure 6-36 compares the measured and predicted values for the high side refrigerant temperature and pressure for the whole trial and the period immediately before and after defrosting. Table 6-40 compares the average measured and predicted refrigerant high side temperatures and pressures for the trial. The predicted discharge temperature was higher than the measured values probably due to correction factor value for compressor surface heat transfer coefficient being too low. The predicted discharge pressure was slightly lower than the measured values. Again both measured and predicted discharge temperature cycled due to the effect of the activation of hot gas bypass and liquid injection into the suction line. The predicted condenser outlet temperature was very close to the measured values. Again, overall, the predicted trends were similar to the measured and differences were mostly explained by measurement uncertainty or control imprecision.

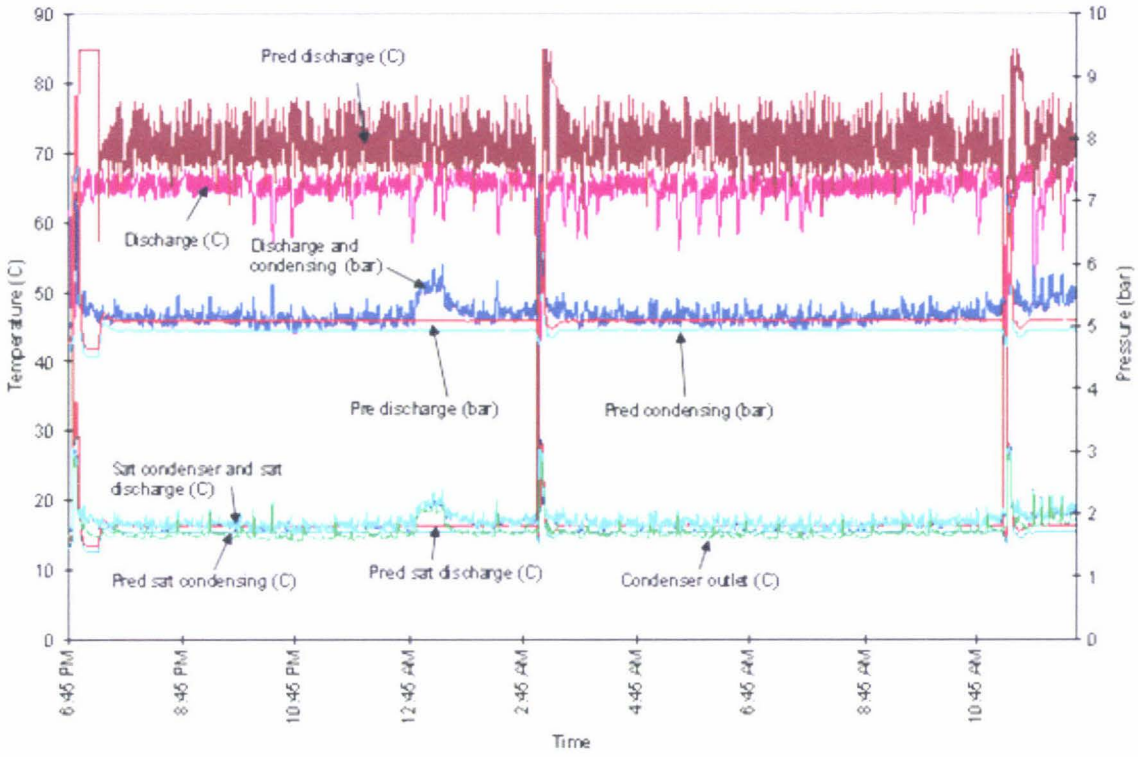

Figure 6-35: Comparison of predicted and measured refrigerant temperature and pressure for the high pressure side for simulation 7 (experimental trial 16).

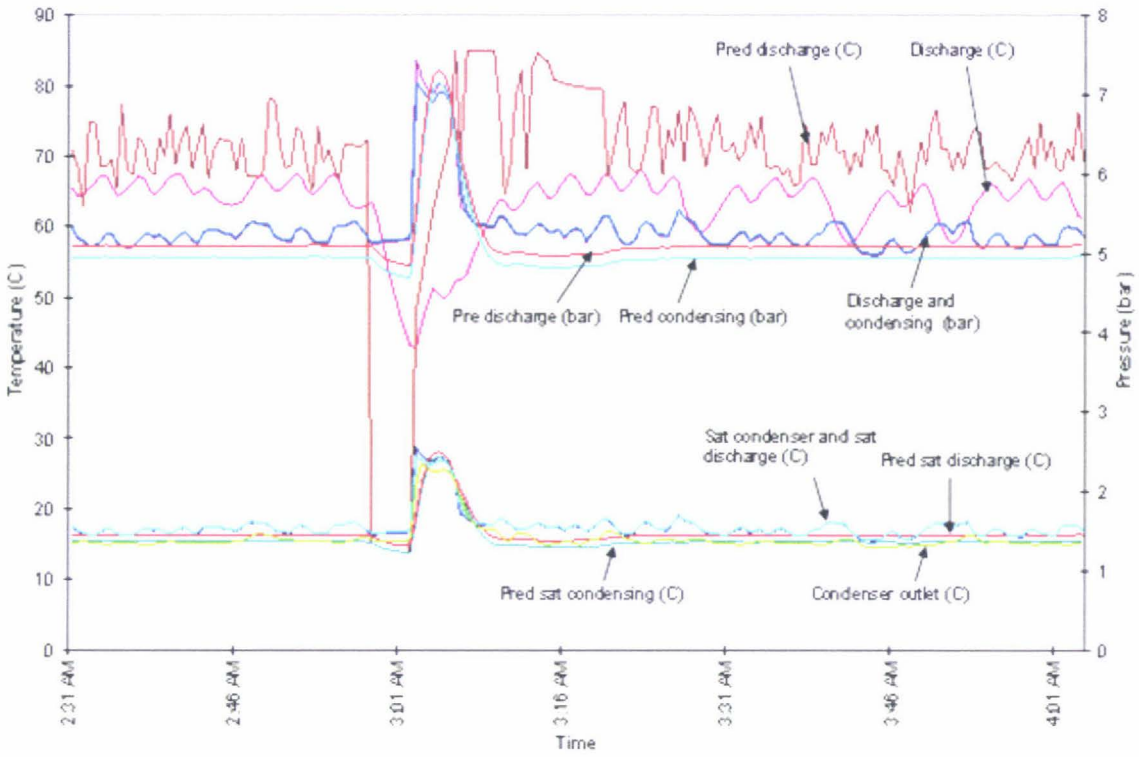

Figure 6-36: Comparison of predicted and measured refrigerant temperature and pressure for the high pressure side for simulation 7 (experimental trial 16) before and after defrosting.

Table 6-40: Average measured and predicted high side refrigerant temperatures and pressures for simulation 7 (experimental trial 16).

		Measured Average	Predicted Average	Difference
Discharge temperature (°C)		64.67	71.15	6.47
Saturated discharge temperature (°C)		16.87	16.36	-0.51
Condenser outlet temperature (°C)		15.34	12.92	-2.42
Saturated condensing temperature (°C)		16.93	15.42	-1.50
Discharge pressure (bar, absolute)		5.19	5.11	-0.08
Condensing pressure (bar, absolute)		5.20	4.96	-0.24

6.4 SENSITIVITY ANALYSIS

Time constraints meant that a comprehensive sensitivity analysis of all the important variables could not be undertaken. Therefore only a few variables were chosen to illustrate the principles. The values chosen were: air thermal buffering (affecting dynamics) and evaporator performance correction factor (affects balance between latent and sensible heat), overall to refrigerant side heat transfer coefficient ratio for the evaporator (affects amount of dehumidification) and sensible heat load (affects amount of dehumidification). Also it was decided to do one at a time analysis rather than a multi-variable analysis.

6.4.1 Thermal Mass of the Room Air

Figure 6-37 to Figure 6-39 compares measured and predicted values of air temperature, RH and the low and high side refrigerant temperatures and pressure for trials with changes to the air thermal buffering factor from 4.5 to 8.5.

As expected the rates of room air temperature pull down were significantly affected by changes to the thermal buffering factor but steady-state values were not

affected. There were small follow on effects on other variables due to the air temperature changes.

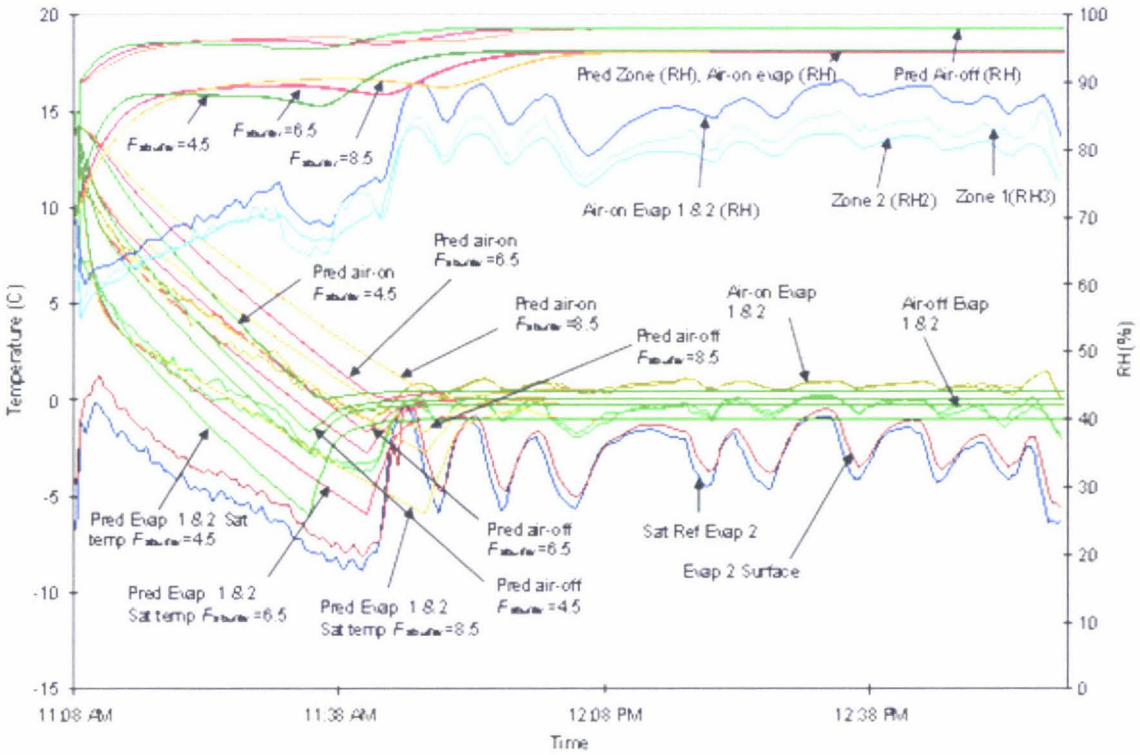

Figure 6-37: Comparison of predicted and measured temperature and RH with an air thermal buffering factor ($F_{a\ buffer}$) of 4.5, 6.5 and 8.5 for simulation 1.

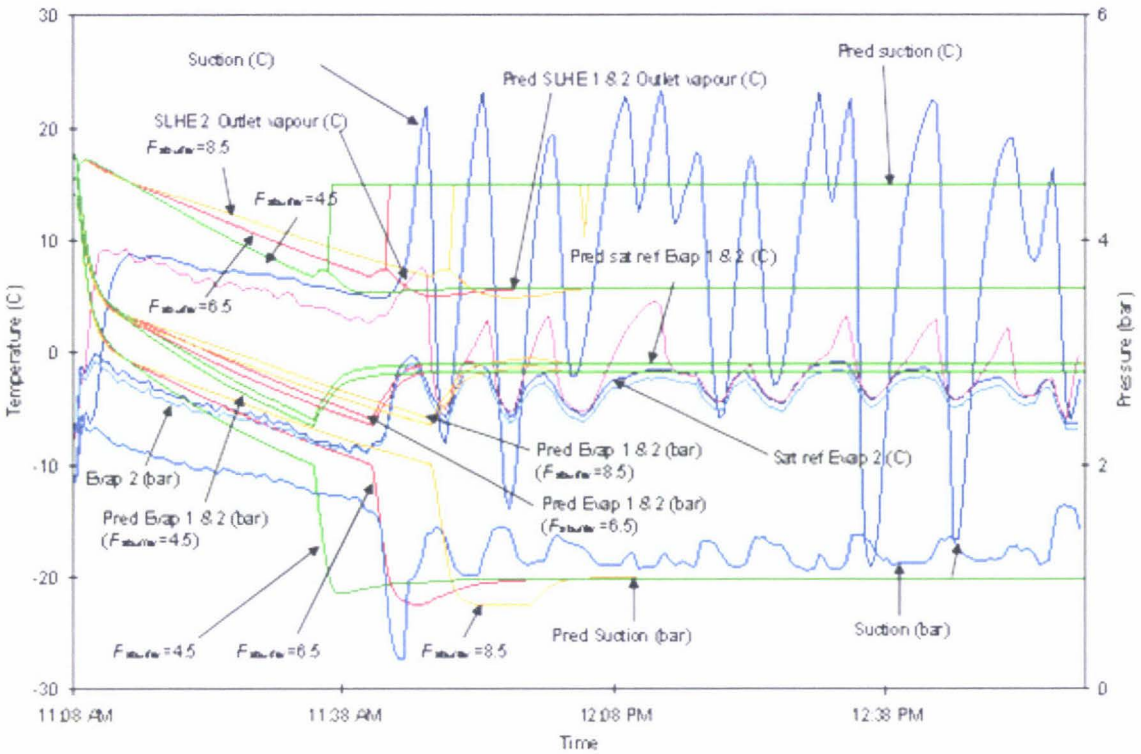

Figure 6-38: Comparison of predicted and measured temperature and pressure for the low pressure side with an air thermal buffering factor ($F_{a\ buffer}$) of 4.5, 6.5 and 8.5 for simulation 1.

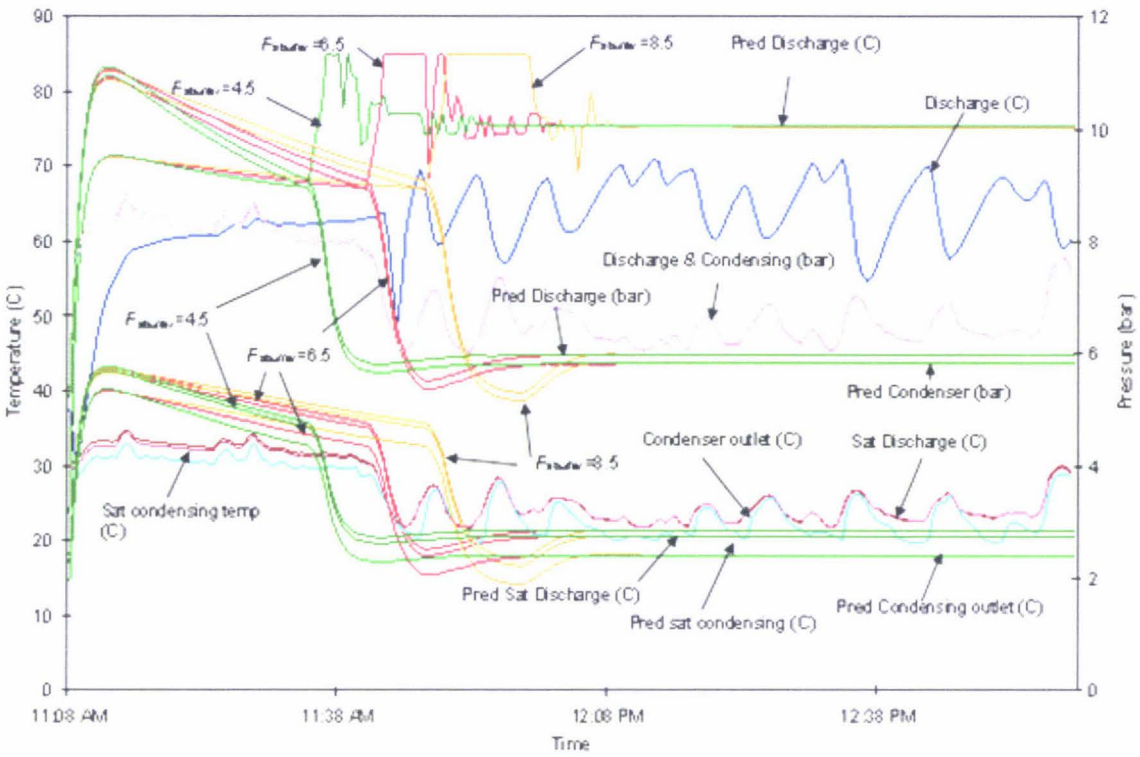

Figure 6-39: Comparison of predicted and measured temperature and pressure for the high pressure side with an air thermal buffering factor ($F_{a\ buffer}$) of 4.5, 6.5 and 8.5 for simulation 1.

6.4.2 Correction Factor for Evaporator Heat Transfer Performance

Figure 6-40 to Figure 6-42 compares predicted and measured values for the trials with changes to the correction factor of overall heat transfer value for the evaporator. The correction factor values were 0.7, 0.85 and 1.0; the manufacturer's nominal design value for the overall heat transfer value was 640 W/K. The value represents an uncertainty of about ±15% in the corrected evaporator heat transfer performance. This level of uncertainty is expected in practice.

Since there was no additional heat load added to the facility the air-off temperature for the evaporator did not change, but refrigerant evaporation temperature and the evaporator surface temperature were affected with the changes. With increased correction factor the refrigerant pressure, evaporation temperature and evaporator surface temperature all increased because a small temperature difference could remove the same amount of sensible heat.

The predicted RH decreased with decreasing in correction factor due to increased dehumidification by the coil as temperature difference increased. Due to the evaporator pressure regulator (EPR) valve control of air temperature, apart from affecting evaporator temperature and other low side conditions, other effects on the refrigeration operation conditions were minor (e.g. discharge temperature). Overall the selected value of 0.85 seemed reasonable.

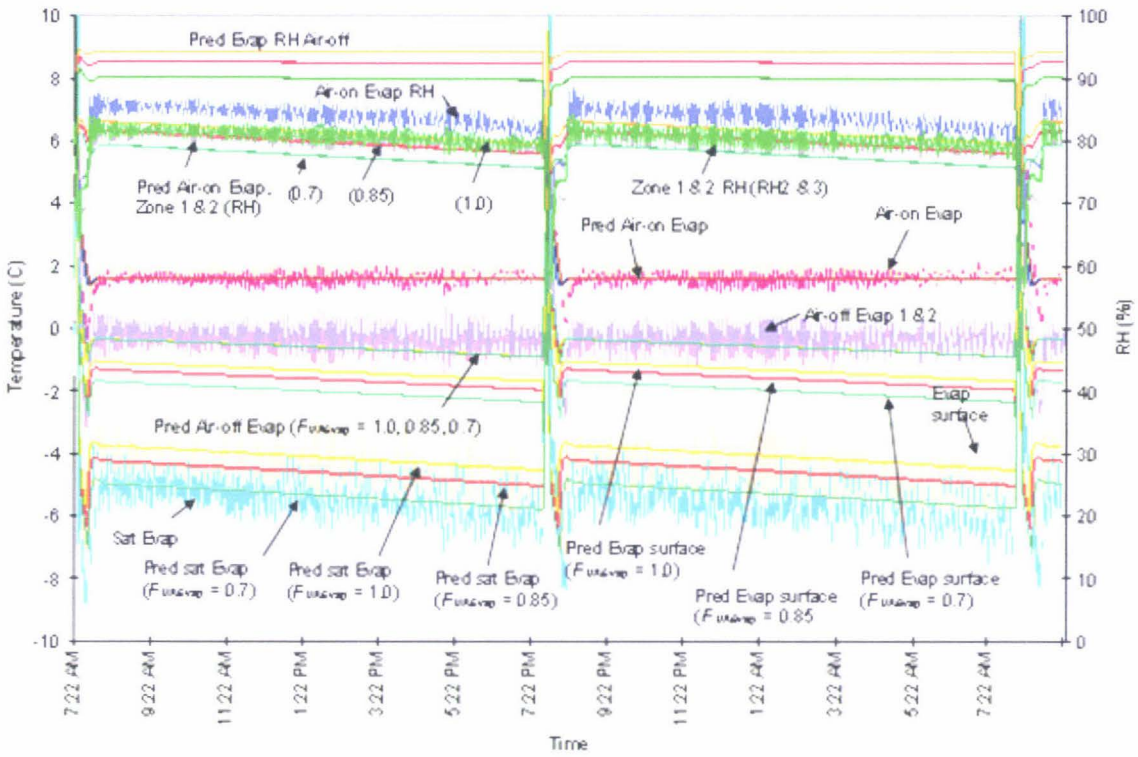

Figure 6-40: Comparison of predicted and measured temperature and RH with correction factor for heat transfer value for the evaporator (F_{UAEvap}) of 0.7, 0.85 and 1.0 for simulation 3.

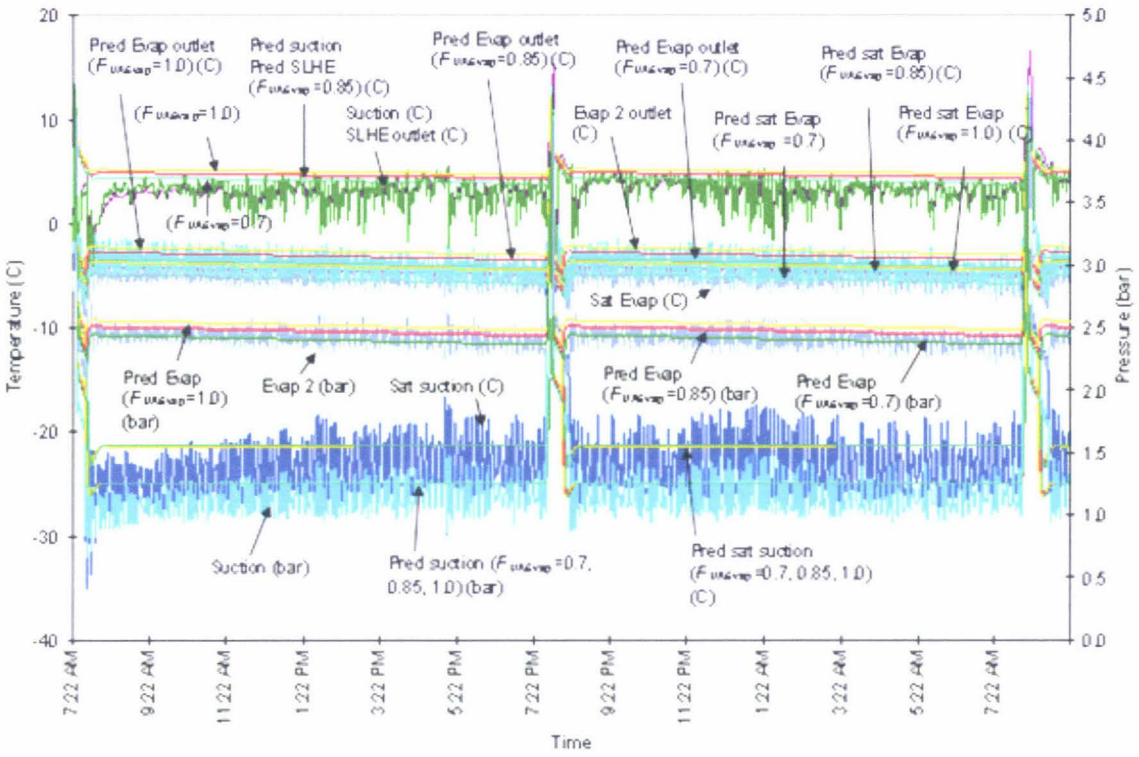

Figure 6-41: Comparison of predicted and measured temperature and pressure for the low side with correction factor for heat transfer value for the evaporator (F_{UAEvap}) of 0.7, 0.85 and 1.0 for simulation 3.

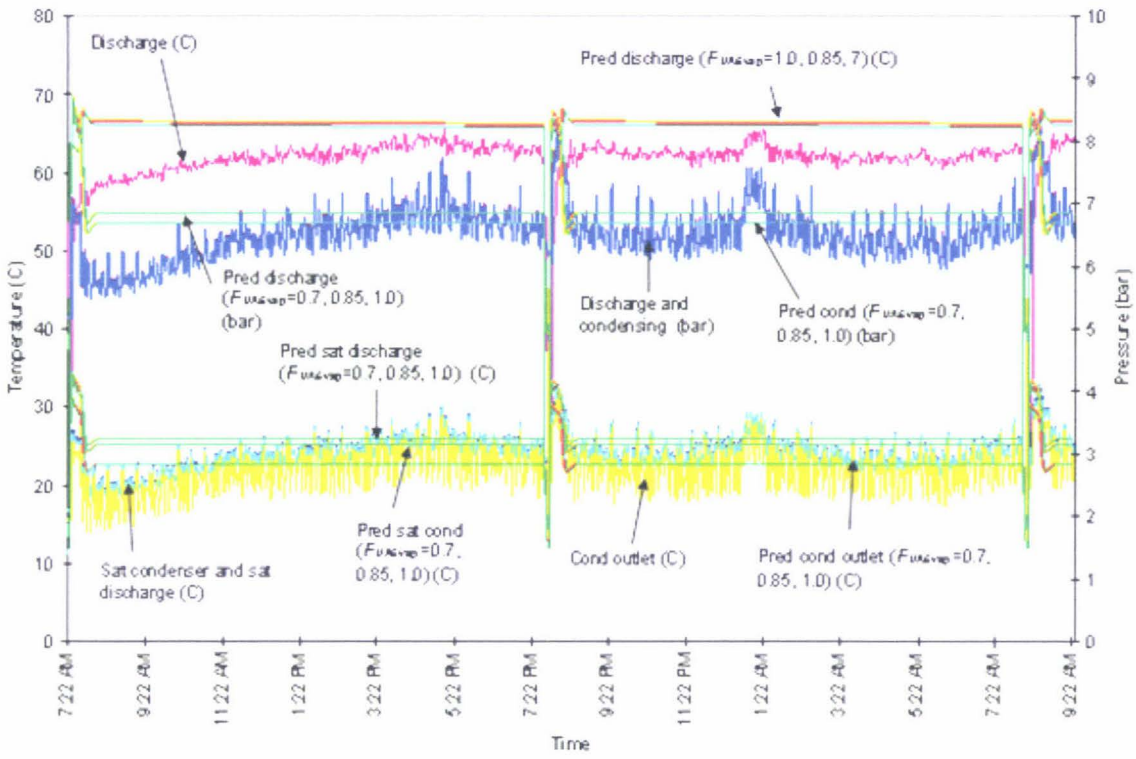

Figure 6-42: Comparison of predicted and measured temperature and pressure for the high side with correction factor for heat transfer value for the evaporator (F_{UAEvap}) of 0.7, 0.85 and 1.0 for simulation 3.

6.4.3 Overall to Refrigerant Side Heat Transfer Coefficient Ratio (*Ra*) for the Evaporator

Figure 6-43 to Figure 6-45 compares predicted and measured values for the trials with changes to the overall to refrigerant side heat transfer coefficient ratio value for the evaporator. The ratios used were 0.3, 0.4 and 0.5.

No additional sensible heat or moisture was added to the facility and the only parameter changed was overall to refrigerant side heat transfer ratio (*Ra*). With increased overall to refrigerant side heat transfer coefficient ratio (*Ra*) increases the air side heat transfer resistance, the evaporator surface temperature increases and this cause to decrease in dehumidification by the coil and predicted RH increases. Decreasing the overall to refrigerant side heat transfer coefficient ratio decreases the air side heat transfer resistance there by lowering the evaporator surface temperature. This increases the dehumidification of the coil and predicted RH decreases.

Due to the evaporator pressure regulator (EPR) valve control of air temperature apart from affecting evaporator temperature and other low side conditions, other effects on the refrigeration operation conditions were minor (e.g. discharge temperature). Overall the selected value of 0.5 was reasonable. This value indicates that refrigerant side and air side resistance to heat transfer are roughly balanced. Often the aim of evaporator designer's, when they add this to the air side is to ensure that the air side is not the controlling heat transfer resistance.

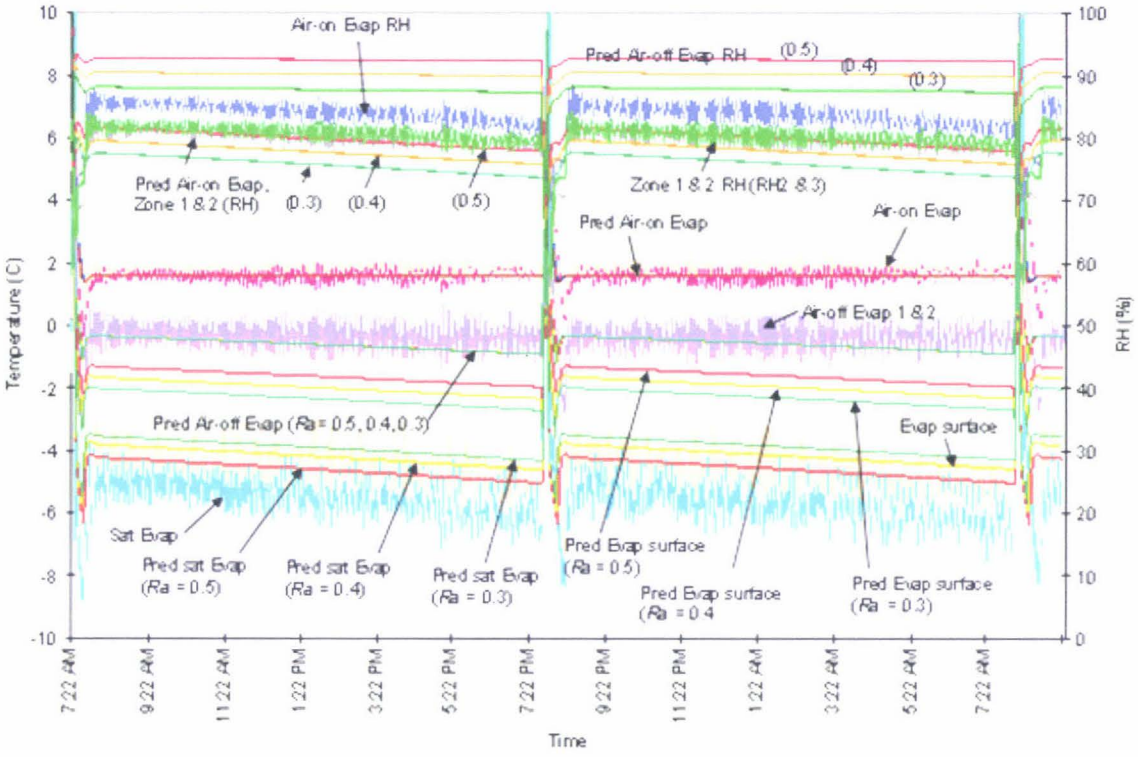

Figure 6-43: Comparison of predicted and measured temperature and RH with overall to refrigerant side heat transfer coefficient ratio for the evaporator (*Ra*) of 0.3, 0.4 and 0.5 for simulation 3.

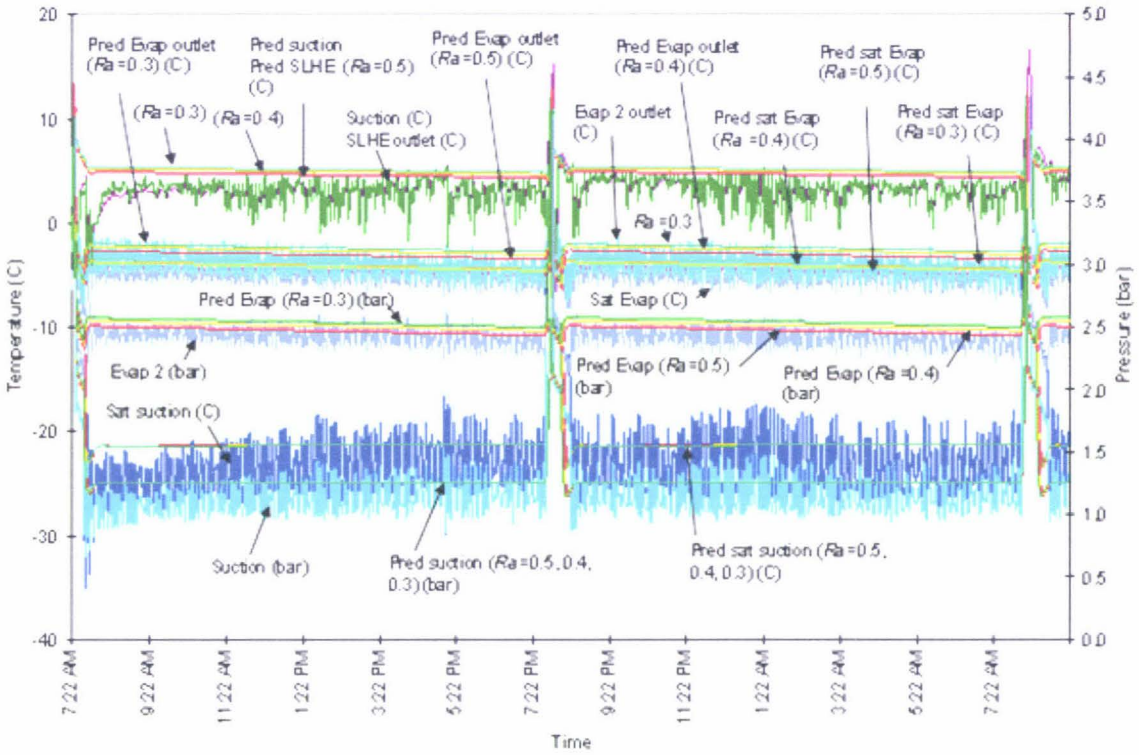

Figure 6-44: Comparison of predicted and measured temperature and pressure for the low pressure side with overall to refrigerant side heat transfer coefficient ratio for the evaporator (*Ra*) of 0.3, 0.4 and 0.5 for simulation 3.

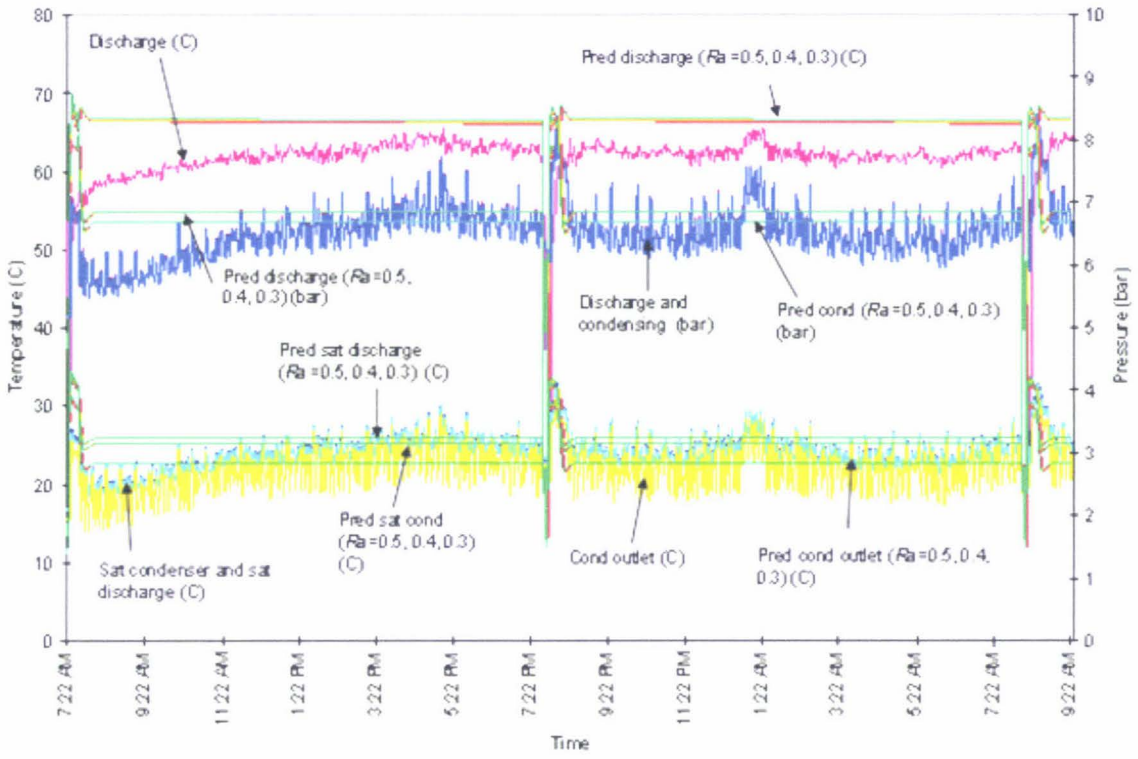

Figure 6-45: Comparison of predicted and measured temperature and pressure for the high pressure side with overall to refrigerant side heat transfer coefficient ratio for the evaporator (*Ra*) of 0.3, 0.4 and 0.5 for simulation 3.

6.4.4 Extra Sensible Heat Load

Figure 6-46 compares the predicted and measured three simulation runs with 90%, 100% and 110% of total extra sensible heat load (room lights plus electric heater loads) for the air temperature and RH. Since room light loads were estimated from the labelling on the fluorescent light tubes and half the tubes were working at any given time, a likely error for the sensible heat loads could be the load due to room lights and an error of ±10% in sensible load was considered likely.

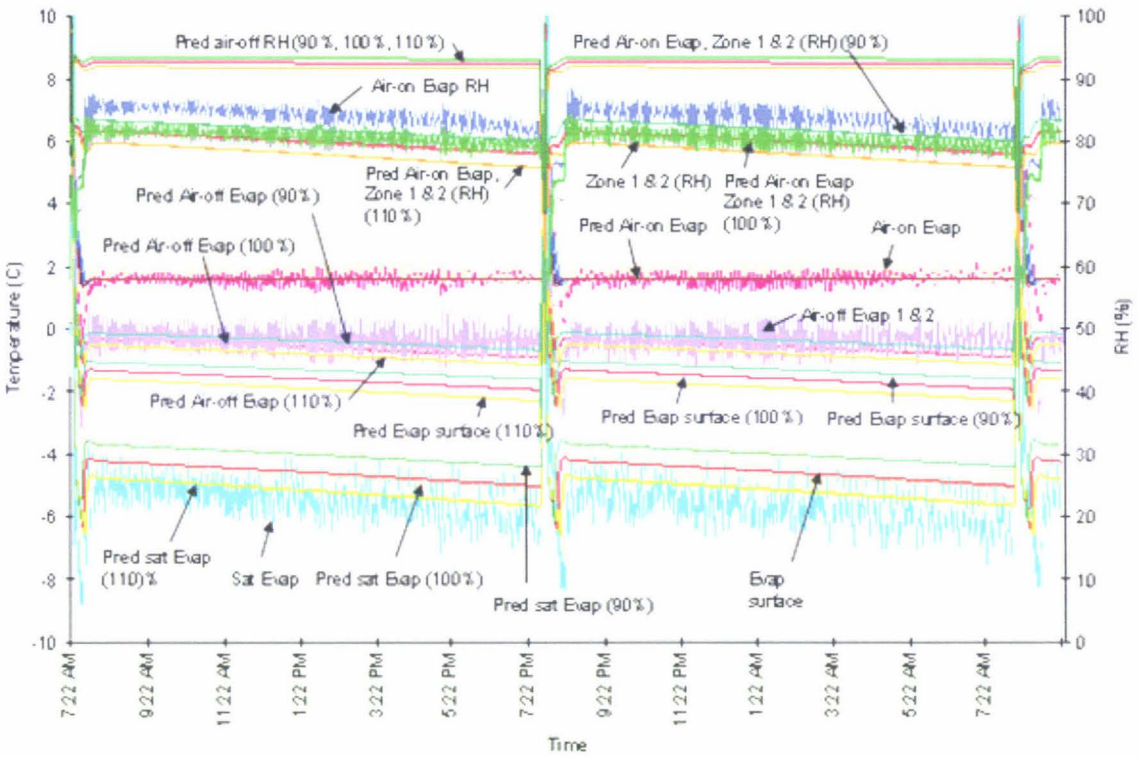

Figure 6-46: Comparison of predicted and measured temperature and RH with 110%, 100% and 90% of electric heater loads (room lights plus electric heaters) for simulation 3.

The air-off temperature lowers with increase in sensible heat load and RH follows a similar pattern. With sensible heat load of 90% the RH was highest and with

sensible heat load of 110% the RH was the lowest. This is consistent with greater dehumidification by the coil if the sensible load is greater.

Figure 6-47 and Figure 6-48 compares the measured and predicted value for low and high side refrigerant temperature and pressure. With increase in sensible heat load evaporator pressure drops there by lowering the evaporation temperature due to more evaporation of the refrigerant in the evaporator with more heat to absorb and hence suction, discharge and condensing conditions were affected.

Overall, the input value for the room lights and RH prediction was found to be reasonable.

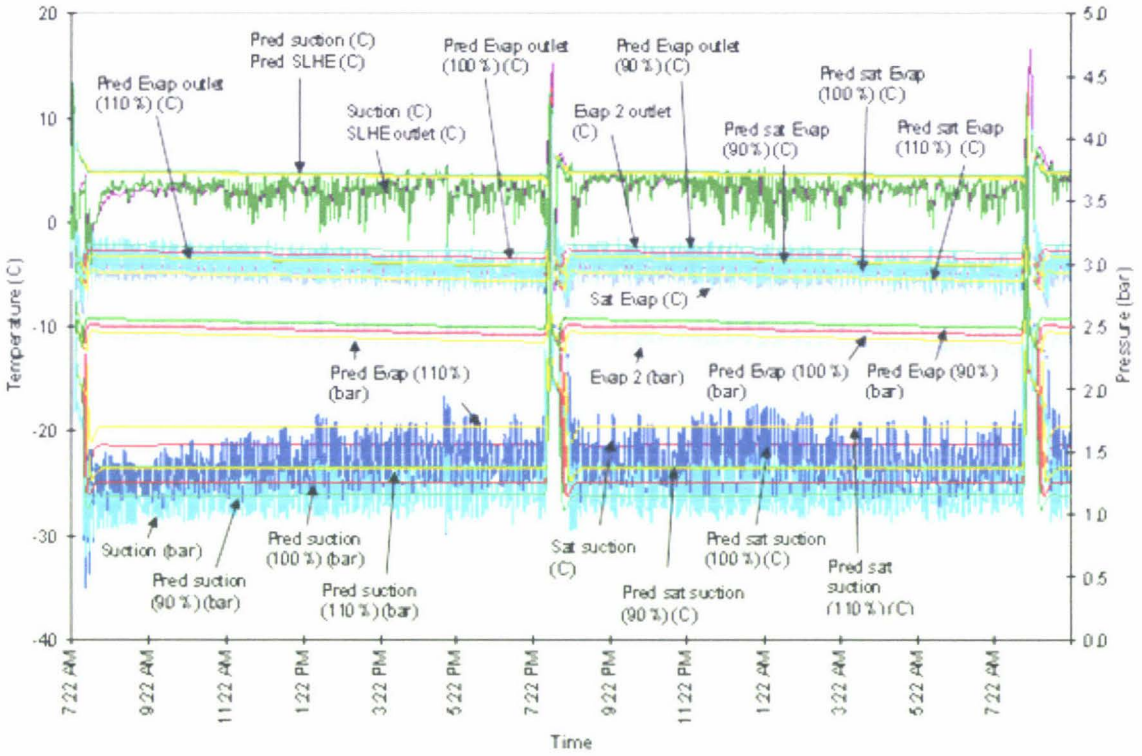

Figure 6-47: Comparison of predicted and measured low pressure side temperature and pressure with 110%, 100% and 90% electric heater loads (room lights plus electric heaters) for simulation 3.

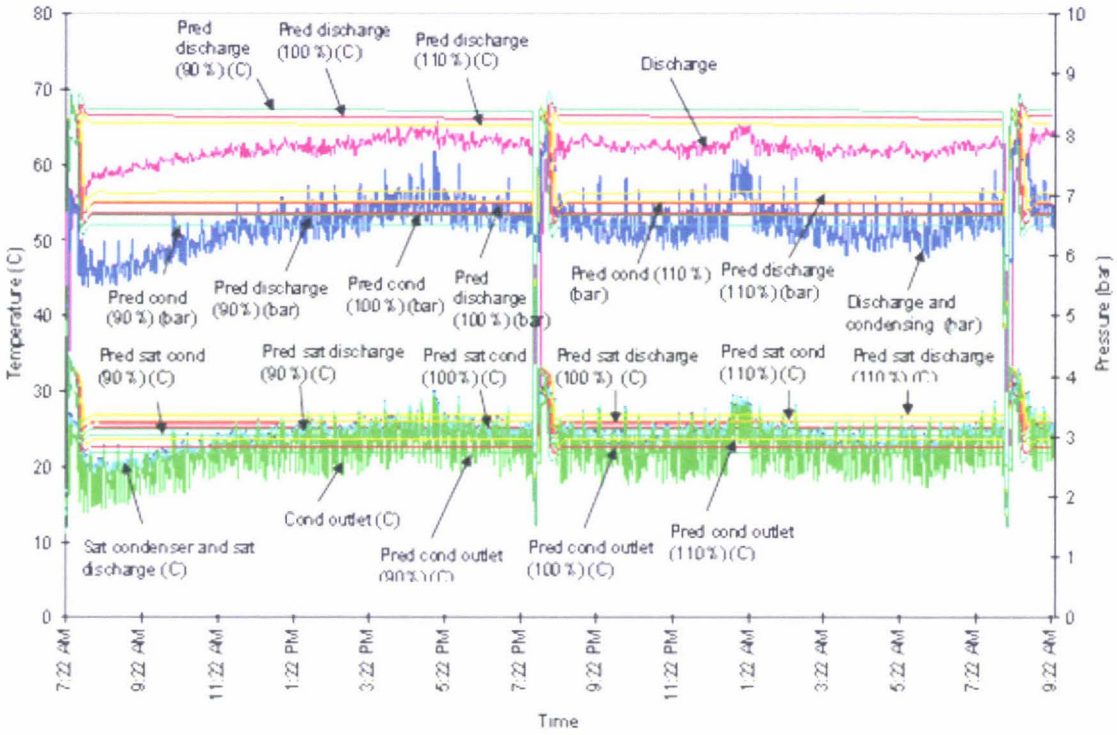

Figure 6-48: Comparison of predicted and measured high pressure side temperature and pressure with 110%, 100% and 90% electric heater loads (room lights plus electric heaters) for simulation 3.

7 EFFECT OF DEFROST FREQUENCY ON DEFROST EFFICIENCY

Figure 7-1 to Figure 7-3 gives a typical cyclic pattern for the defrost trials carried out for 24, 16 and 6 hourly defrosts intervals with 5 kW of electric heat and 0.41 kg/h moisture addition. During the defrosting period with the refrigeration system switched off, the air temperature of the room increased and hence the room RH decreased. After the defrosting period the refrigeration system operated at full capacity (pull down period) until temperature control is regained. This is followed by a period with relatively constant operating conditions with slow decline in refrigerant evaporation temperature as the coil became more heavily frosted and room RH declines. The performance of the coil is eventually lost due to heavy frosting and the air temperature increases. Once the air temperature increases above set point, RH drops rapidly until the next defrost was started and the cycle repeats.

Table 7-1 gives the details of the store performance for the different intervals between defrost. Infrequent defrost causes heavy frosting on the coils and therefore loss of temperature control due to the deterioration of the heat transfer between room air and the surface of the coil and longer time to complete the defrost. The average refrigerant evaporation temperature lowers leading to lower average air RH and potentially increases the energy consumption of the compressor depending upon the control method used for the plant. Frequent defrosting causes shorter defrosting time, higher temperature fluctuations and higher defrosting energy due to the heating up of all the coil metal even with little or no frost.

For the cool store studied a frost load of 4 kg at defrost initiation had the best temperature control and RH and energy use, this corresponds to 8 hourly defrost for higher latent load and 12 hourly defrost for lower latent load.

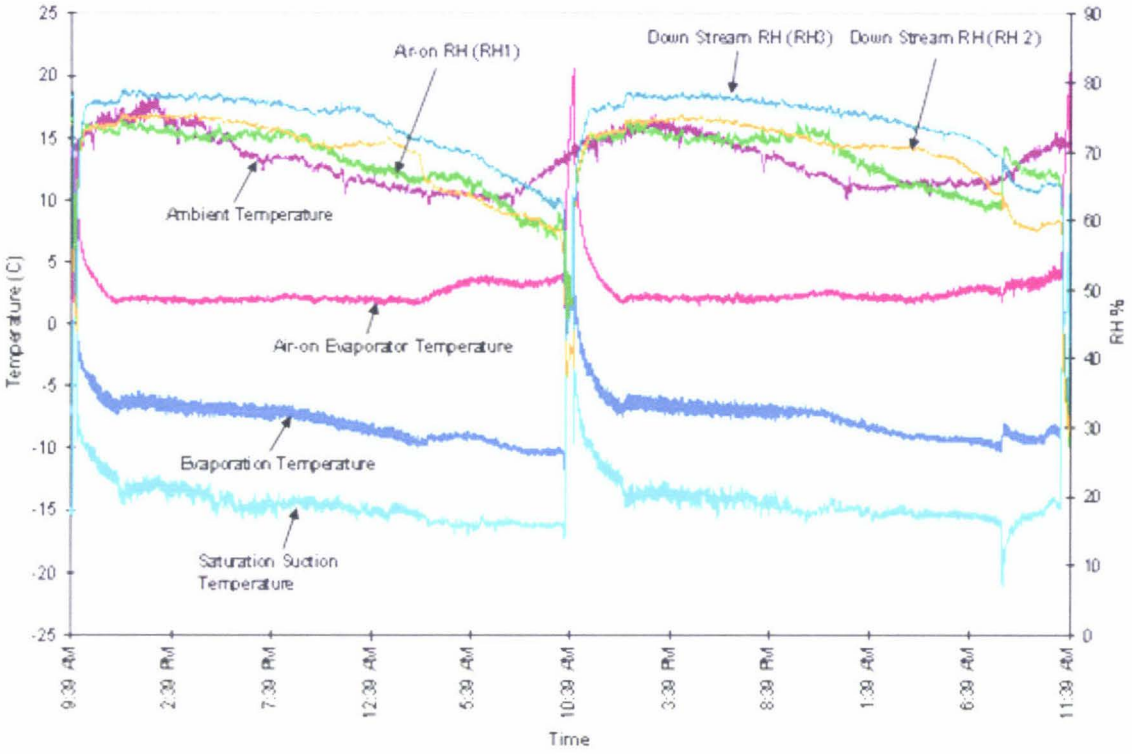

Figure 7-1: Measured ambient air, coil air-on, refrigerant evaporation and compressor saturated suction temperatures and air-on RH for the cool room with a 24 hour defrost interval with 5 kW of extra electric heat and 0.41 kg/h of moisture addition.

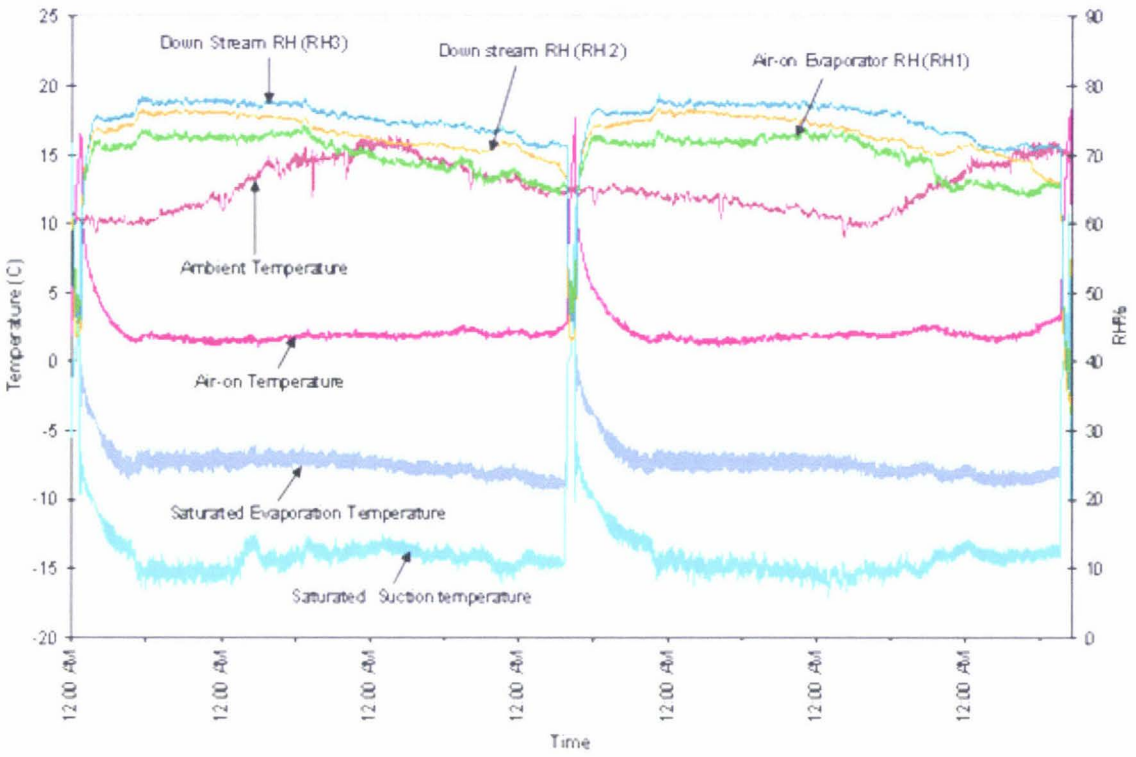

Figure 7-2: Measured ambient air, coil air-on, refrigerant evaporation and compressor saturated suction temperatures and air-on RH for the cool room with a 16 hour defrost interval with 5 kW of extra electric heat and 0.41 kg/h of moisture addition.

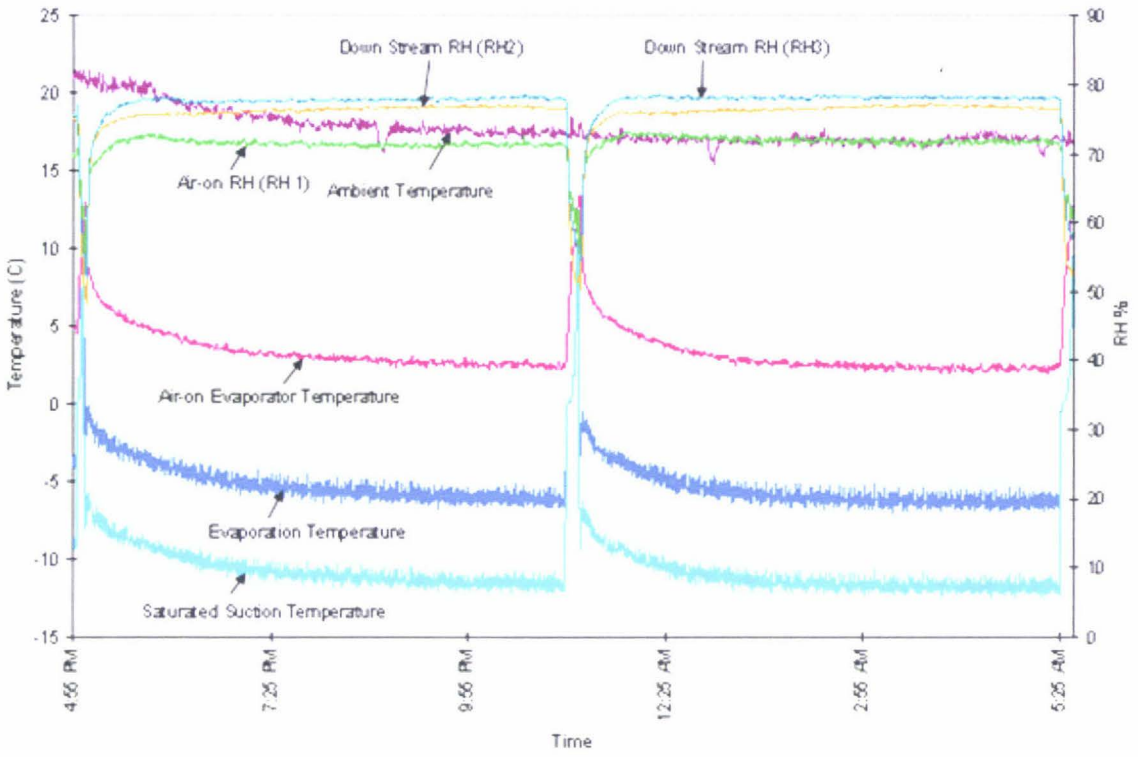

Figure 7-3: Measured ambient air, coil air-on, refrigerant evaporation and compressor saturated suction temperatures and air-on RH for the cool room with a 6 hour defrost interval with 5 kW of extra electric heat and 0.41 kg/h of moisture addition.

Table 7-1: The effect of defrost frequency on cool store operating conditions with air temperature set-point of 1.6°C.

Defrost Interval (hrs)	Av. Air Temp.[1] °C	Av. Air RH[1] %	Av. Te[1] °C	Coil Frost Load[2] (kg)	% Time >2.1 °C [1]	% Time >2.1 °C [2]	% Time >2.6 °C [1]	% Time >2.6 °C [2]	Defrost Time [2] (min)	Defrost Energy[3] (kWh)	Water Input Rate (kg/h)	Defrost Efficiency (%)	Av Defrost Heat Load (W)	Ratio of Defrost to Total Heat Load (%)	Overall Refrig. System Energy[3] (kWh)
3 kW extra sensible heat and 0.3 kg/hr water injection															
6	1.7	83	-4.9	1.81	3.5	5.8	2.9	5.1	77	5.9	0.29	23	91	2.2	139.6
8	1.7	84	-4.9	2.49	2.8	4.6	2.4	4.2	63	4.8	0.30	29	69	1.7	140.4
12	1.7	83	-5.1	3.94	2.4	3.6	1.9	3.1	52	3.9	0.31	37	50	1.2	139.0
16	1.7	83	-5.2	5.21	4.5	4.6	1.6	2.7	47	3.6	0.31	41	43	1.1	137.4
24	1.8	81	-5.6	7.29	4.1	4.6	1.2	2.0	40	2.9	0.29	46	32	0.8	138.0
30	1.7	80	-5.94	9.12	2.6	4.5	0.4	2.0	45	3.5	0.29	48	30	0.7	140.6
5 kW extra sensible heat and 0.4 kg/hr water injection															
6	3.3	72	-5.2	2.75	100.0	88.5	76.2	67.9	86	6.7	0.43	31	93	1.5	172.1
8	2.4	73	-6.3	3.71	26.9	26.7	15.9	13.7	76	5.9	0.45	35	77	1.3	166.7
12	2.4	72	-6.4	5.84	32.7	30.0	18.8	12.7	63	4.9	0.47	45	55	0.9	163.4
16	2.2	70	-7.3	6.86	31.4	26.5	14.6	12.3	54	4.3	0.41	45	48	0.8	164.1
24	2.7	69	-7.6	9.74	72.0	59.9	28.3	30.7	46	3.5	0.39	52	34	0.6	161.5
30	2.7	69	-8.5	12.77	52.8	47.6	46.4	37.8	27	2.1	0.41	57	29	0.5	159.8

[1] excluding defrost periods [2] prior to defrost [3] equivalent for 48 hour period.

Figure 7-4 shows the effect of defrost interval on the room air-on RH for the two frosting cases. With frosting case 2 (5 kW electric heater and 0.4 kg/h moisture addition) the RH is lower and declined rapidly above 12 hourly defrost, whereas for frosting case 1 (3 kW electric heater and 0.3 kg/h moisture) the room air-on RH was higher and a very slow decline with increased time between defrosting. The drop in RH for Case 2 was due to the high sensible heat load and the rapid decline of RH with increasing defrost interval was due to the more rapid frost build up due to the higher latent load. This is consistent with the theory of straight line approach of the air to the saturation condition at the evaporator surface temperature.

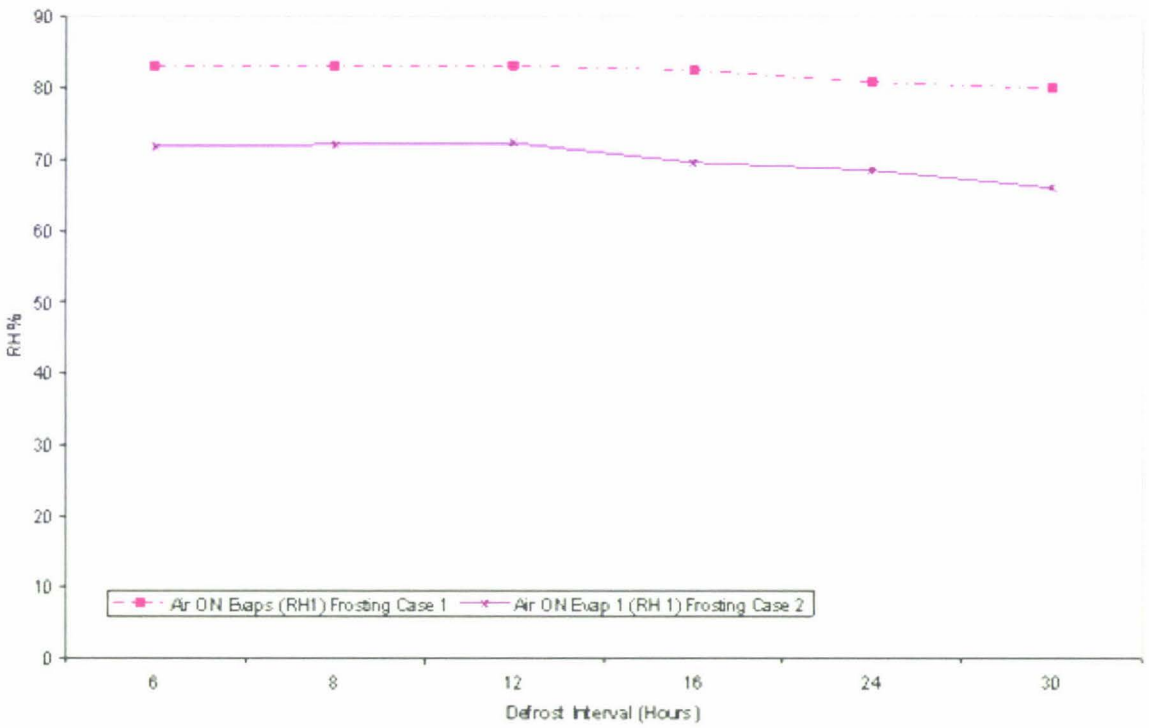

Figure 7-4: Measured air-on RH as a function of defrost intervals for frosting case 1 and case2

Figure 7-5 shows the effect of defrost interval on the defrosting efficiency and average time per defrost. With increase in defrost interval the defrost efficiency increased and average time per defrost increases for the two frosting cases. With

6 hourly defrost interval the defrost efficiency was found to be 20 to 30% whereas with 30 hourly defrost frequency the efficiency increased to 45 to 55%. The average time per defrost increased with defrost interval due the higher build up of frost on the evaporator.

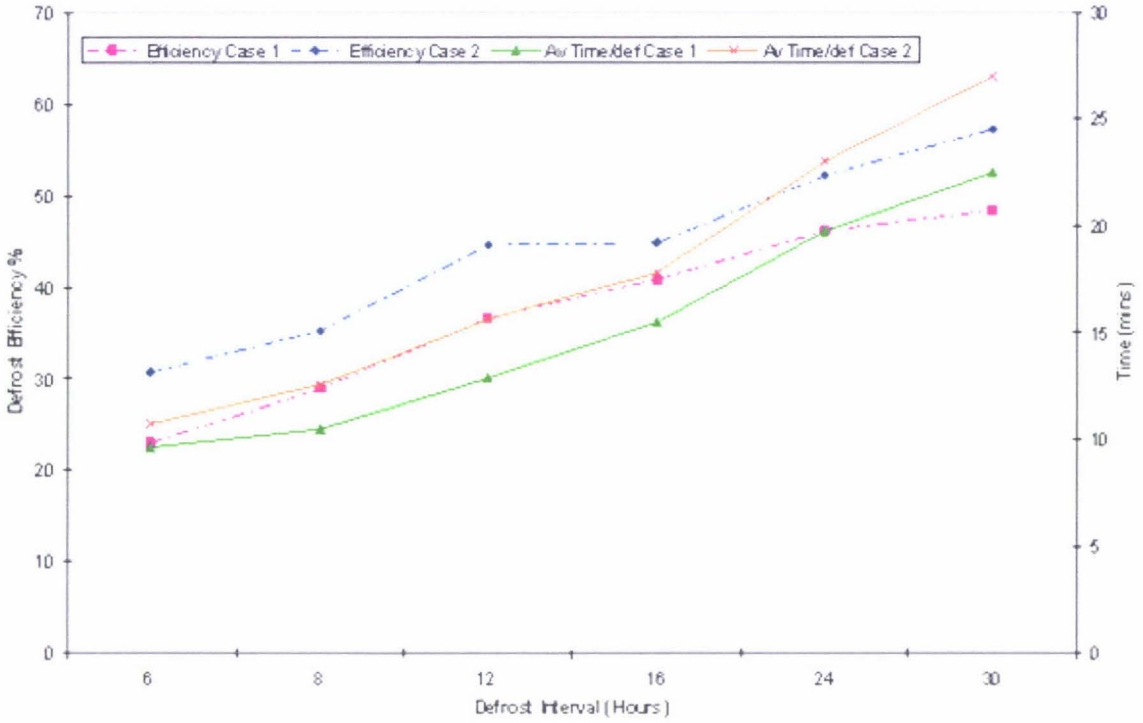

Figure 7-5: Measured defrost efficiency and average time per defrost as a function defrost interval for frosting case 1 and case2.

Figure 7-6 shows the effect of frost load at the start of defrosting on the defrost efficiency and average time per defrost. With increase in frost load both defrost efficiency and average time per defrost increases for the two frosting cases. The efficiency appear constant between frost load of 5.8 (kg) to 7.3 (kg) and increased rapidly at higher frost levels but this is probably data uncertainty than a real trend (more likely trend is a steady increase as frost load increases). The amount of heat to warm up the metal in the coil is constant and is independent of the frost load. With high frost load a greater fraction of defrost energy is required to melt the

given frost. Average time per defrost the relation was linear with increasing frost load increasing the average time for defrost.

Appendix C gives the paper presented at IIR/IRHACE Conference held at the University of Auckland, 2006 on the effect of defrost frequency on defrost efficiency .

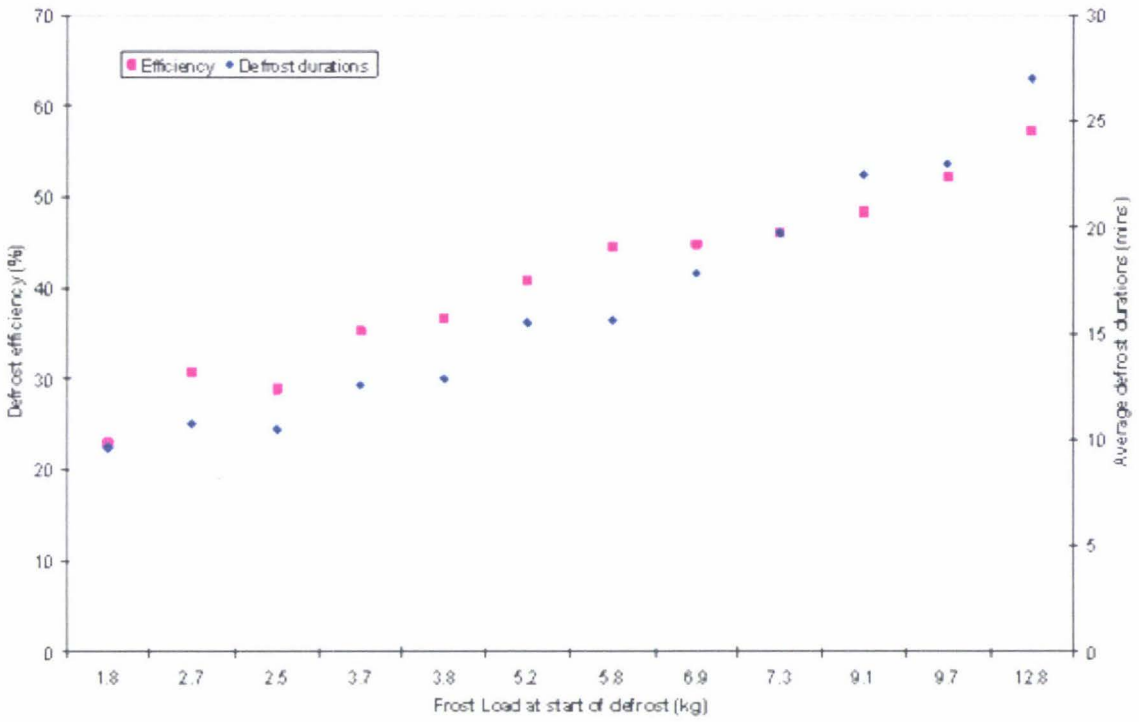

Figure 7-6: Measured defrost efficiency and average time per defrost as functions of frost load at start of defrost.

8 DISCUSSIONS

For simulations 1 to 7 (calibration and validation runs) the predicted and measured values were in reasonably close agreement. The main parameters compared were air-on, air-off temperatures, RH, evaporation temperature and evaporator surface temperature, low side and high side temperatures and pressures for the refrigeration system. Table 8-1 compares the measured and predicted average RH for the simulations 2 to 4 and 7. The differences between predicted and measured air-on RH was found to -4% to 1.5% whereas for the zones the difference was -4.5% to +7.5%. The highest error was for the simulation 7 where the measured air-on RH was 98.6%. For simulations 5 and 6 the maximum difference between measured and predicted air-on RH and zone 1 RH were 6% whereas for zone 2 the maximum difference was 12%. This suggests significant uncertainty of the zone 2 sensor calibrations or imperfect mixing of the air zones.

The RH was reasonably accurately predicted for the trials. The differences were mainly attributed to the uncertainty in sensor calibrations and input parameter values. The manufacturer's stated error was ±3% and sensors exposed to RH above 98% for long periods are known to be unreliable. Also the model assumed perfectly mixing of the air in each zone whereas in the room this was not the case. Of the model fitted parameters the biggest influence affecting RH was the overall to refrigerant side heat transfer coefficient ratio (*Ra*), which is dependent on the design of the cooling coil.

The control of air RH in refrigerated facilities can be optimised by applying engineering principles in a similar way to that currently performed for temperature control. Such methods allow RH control to be improved without unnecessary expense on dedicated humidity control equipment or advanced packaging systems.

The trials showed that the main methods to increase RH were:

- Reduced sensible heat loads (e.g. increased insulation, reduced lights and fan power).
- Larger evaporator surface area so it can operate with higher evaporation and surface temperatures.

Conversely, the methods to reduce RH were to increase sensible heat loads and design evaporator to operate with large temperature differences.

Table 8-1: Average measured and predicted RH for simulations 2 to 4 and 7.

Trials	Room Set Temperature (°C)		Air-on Evaporator RH (%)		Air-off Evaporator RH (%)		Zone RH (%)	
			1	2	1	2	1	2
Simulation 2	1.6	Measured	71.38				77.26	75.73
		Predicted	72.80	72.78	89.04	89.03	72.84	72.74
		Difference	1.42	1.40			-4.41	-2.99
Simulation 3	1.6	Measured	83.54				79.37	80.13
		Predicted	79.73	79.72	92.31	92.30	79.77	79.68
		Difference	-3.81	-3.82			0.40	-0.45
Simulation 4	1.6	Measured	80.00				78.56	78.16
		Predicted	76.82	76.81	92.12	92.10	76.84	76.78
		Difference	-3.18	-3.20			-1.72	-1.38
Simulation 7	1.6	Measured	98.59				92.23	89.97
		Predicted	97.56	97.55	99.13	99.12	97.59	97.52
		Difference	-1.02	-1.04			5.37	7.55

Table 8-2 compares average measured and predicted air temperatures, evaporation temperatures, evaporator surface temperatures, and evaporator pressures for the evaporator for simulations 2 to 4 and 7. The model prediction of the average evaporating pressure was fairly good agreement for all the trials. A maximum predicted pressure difference was 0.06 bar was noted for the simulation 4. In case of simulation 2 the average air-on temperature were found to be higher than the room set temperature of 1.6°C due to a combination of high sensible heat

load in the room, fast frost build up on the evaporator reducing the heat transfer in the evaporator, and the short defrosting interval not giving sufficient time to reach the steady state. For simulations 5 and 6 with different operating conditions, the predictions of evaporator pressure and air-on temperatures for both trials followed similar trends to the measured values within an acceptable range.

Table 8-3 compares average measured and predicted refrigerant temperatures and pressure for the simulations 2 to 4 and 7. The predicted outlet vapour of the SLHE was slightly higher than the measured average. Overall the predictions were acceptable given the simple model formulation. The average predicted discharge and condensing pressure were found to have reasonable agreement to the measured values, but in general discharge temperatures were found to be over predicted probably due to uncertainty in input data related to compressor heat losses.

The average predicted suction pressure and suction temperature were found to have reasonable agreement to the measured values with the differences mainly due to input parameters and how the hot gas by pass circuit was controlled and modelled. The model assumed a simple proportional controller for the hot gas bypass circuit, where as the actual control appeared more complex. Also it did not take in to account heat gained by the suction line due to varying ambient conditions.

Comparing the effects of different operating conditions on the low side and high side refrigerant temperatures and pressures for the simulations 5 and 6 shows that for both trials, predictions followed similar trends to the measured values within an acceptable range. The present work have shown that it was difficult to obtain an exact match between the simulation and the measured results due to large number of varying factors affecting the refrigeration system.

Table 8-2: Average measured and predicted air-on, air-off, evaporation, evaporator surface and evaporator outlet temperatures for simulations 2 to 4 and 7.

Trials	Room Set Temperature (°C)		Air-on Evaporator (°C)		Air-off Evaporator (°C)		Evaporator Pressure (bar)		Evaporation Temperature (°C)		Evaporator Surface Temperature (°C)		Evaporator Outlet Temperature (°C)	
		Evaporator No.	1	2	1	2	1	2	1	2	1	2	1	2
Simulation 2	1.6	Measured	2.99	3.40	-0.26	-0.25		2.43		-5.17		-4.31		-3.62
		Predicted	3.15	3.15	0.09	0.09	2.37	2.37	-5.82	-5.82	-1.45	-1.44	-4.32	-4.32
		Difference	0.16	-0.25	0.35	0.35		-0.06		-0.65		2.87		-0.70
Simulation 3	1.6	Measured	2.04	1.80	-0.34	2.12		2.44		-4.98		-4.43		-3.92
		Predicted	1.65	1.65	-0.54	-0.53	2.48	2.48	-4.54	-4.54	-1.57	-1.57	-3.04	-3.04
		Difference	-0.39	-0.15	-0.19	-2.66		0.04		0.44		2.86		0.88
Simulation 4	1.6	Measured	1.78	1.89	-0.38	-0.37		2.36		-5.83		-5.28		-4.87
		Predicted	1.63	1.63	-1.01	-1.00	2.42	2.42	-5.18	-5.18	-2.06	-2.06	-3.68	-3.68
		Difference	-0.14	-0.26	-0.63	-0.63		0.06		0.65		3.23		1.19
Simulation 7	1.6	Measured	1.67	1.57	1.24	1.52		3.01		0.74		1.09		1.07
		Predicted	1.60	1.60	1.36	1.36	3.01	3.03	0.91	0.91	1.26	1.26	2.41	2.41
		Difference	-0.07	0.03	0.12	-0.16		0.02		0.18		0.17		1.35

Table 8-3: Average measured and predicted refrigerant temperature and pressure for simulations 2 to 4 and 7.

Trials	Room Set Temperature (°C)		SLHE 1 (Inlet Liquid) (°C)	SLHE 2 (Inlet Liquid) (°C)	SLHE 1 (Outlet Liquid) (°C)	SLHE 2 (Outlet Liquid) (°C)	SLHE 1 (Outlet Vapour) (°C)	SLHE 2 (Outlet Vapour) (°C)	Suction Pressure (bar)	Suction Temperature (°C)	Discharge Pressure (bar)	Discharge Temperature (°C)	Condensing Pressure (bar)	Condensing Temperature (°C)	Compressor Pressure Ratio
Simulation 2	1.6	Measured		34.91		25.17		7.44	1.97	8.66	9.31	68.72	9.25	34.78	4.76
		Predicted	32.19	32.19	25.24	25.24	6.64	6.64	2.01	6.64	8.97	66.28	8.82	32.19	4.48
		Difference		-2.72		0.08		-0.81	0.04	-2.02	-0.34	-2.44	-0.43	-2.59	-0.28
Simulation 3	1.6	Measured		22.27		14.91		3.07	1.20	3.26	6.51	61.52	6.49	22.18	5.61
		Predicted	22.75	22.75	16.13	16.13	4.70	4.70	1.28	4.70	6.87	65.68	6.72	22.75	5.40
		Difference		0.47		1.22		1.62	0.08	1.43	0.36	4.16	0.22	0.57	-0.22
Simulation 4	1.6	Measured		23.45		15.41		2.49	1.21	3.05	6.73	62.72	6.71	23.21	5.67
		Predicted	22.05	22.05	15.49	15.49	4.04	4.04	1.26	4.04	6.73	64.87	6.58	22.05	5.36
		Difference		-1.40		0.08		1.55	0.05	0.99	0.00	2.15	-0.14	-1.16	-0.31
Simulation 7	1.6	Measured		15.76		8.40		0.58	1.05	17.02	5.19	64.67	5.20	15.34	5.13
		Predicted	12.92	12.92	7.27	7.27	5.57	5.57	0.90	14.90	5.11	71.15	4.96	12.92	5.74
		Difference		-2.77		-1.13		4.99	-0.15	-2.12	-0.08	6.47	-0.24	-2.42	0.61

9 CONCLUSIONS

Research into refrigeration system design and its applications in the past has been focused on heat transfer only and positional variation of air conditions was not considered; few models included models of water vapour transport in detail and these have been situation specific. A generic model has been developed that considers both heat and moisture transfer, models defrosting of the evaporator, and considers positional variation of air conditions.

Predicted values of RH and temperature for a small cool room were consistent with the measured values; indicating the model took account of most of the major heat and mass transfer mechanisms in a reasonably realistic manner. The condensate measurements and the predicted frost accumulated on the evaporators also closely agreed with measured data. Differences in predicted and measured RH could be explained by uncertainty in model input data, sensor calibration changes and imperfect mixing of the air in the cool store.

The predicted refrigerant temperature and pressure for the high pressure side and low pressure side were consistent with the measured values, indicating refrigeration system component models were adequate. Most differences were accounted for by uncertainty in thermostatic expansion valve performance (the actual control system being less precise than how it was modelled), uncertainty in measured data and uncertainty in model parameter values. Detailed testing of all the individual component models was not possible, because of the limited range of detailed experimental data.

The average room temperature and RH control by the refrigeration system was significantly affected by the defrost frequency. The defrost efficiency and duration of defrost was proportional to the defrost interval and defrost efficiency and duration doubled when defrost interval increased from 6 to 30 hours. The defrost

frequency had little effect on the total energy use by the refrigeration system due to the use of the EPR temperature control, and the low latent heat loads for the trials.

Further work may include investigating the effects on zone RH by varying the air flow pathways between zones and the number of air zones for the cool room and the way in which it affects the predicted localised conditions of the cool room.

In order to improve the accuracy of the model for predicting the flowrate of refrigerant through the evaporators more experimental data are needed. The simple evaporator model could further be developed to improve the predictions of cool room RH.

NOMENCLATURE

Main Variables

A	Area (m^2)
abs	Absolute
B	Number of product items per batch.
Bi	Biot number
Cond	Condensate (kg)
c	Specific heat capacity (J/kg K).
c_a	Specific heat capacity of air (J/kg K).
c_v	Specific heat capacity of water vapour (J/kg K).
c_w	Specific heat capacity of water (J/kg K).
c_{GAB}	GAB isotherm constant
D	Derivative response factor for the PID controller
DB	Deadband (°C).
E_{pro}	Effectiveness of door protection
Evap	Evaporator
F	Factor or fraction
forced	Forced draught fan
g	Gravitational acceleration (m/s^2).
H	Absolute humidity (kg water vapour / kg dry air).
HP	High pressure
h	Enthalpy (J/kg)
h_{fg}	Latent heat of vapourization of water vapour at 0.01 °C (J/kg).

h_L	Latent heat of sublimation of water ice (J/kg).
I	Integral response factor for the PID controller
k	Mass transfer coefficient for water vapour (kg/m^2 s).
k_{GAB}	GAB isotherm constant
L	Length (m).
LP	Low pressure
Mc	Thermal capacity (W/k).
M	Mass (kg).
MW	Molecular weight
m	Mass flow rate (kg/s).
max	Maximum
min	Minimum
N	Speed (rpm) or frequency (movements / hour) / Number of air zones.
NZones	Number of air zones
NSurfaces	Number of surfaces
NFloors	Number of floors
NStrucs	Number of structures
NEvaps	Number of evaporators
NFans	Number of fans
Ndoors	Number of doors
NProd	Number of stacks
P	Pressure (Pa).
P_g	Partial pressure of dry air (Pa).
P_t	Atmospheric pressure (Pa).
P_v	Partial pressure of water vapour (Pa).
P_w	Vapour pressure of water vapour (Pa).
Pf	Proportional response factor for the PID controller
Pr	Number of products.

PR	Ratio of discharge pressure to suction pressure
Q	Flow rate (m^3/s).
R	Universal gas constant (J / kg mole K)
Ra	Ratio of heat transfer from air to refrigerant for the evaporator
RH	Relative humidity (%).
R_Q	Rate of actual airflow rate decline with frost accumulation (1/kg).
R_{uA}	Rate of relative heat transfer decline with frost accumulation (1/kg).
SC	Sub cooling (°C).
SH	Super heating (°C).
SLHE	Suction line heat exchanger
SolRad	Solar radiation incident on the outside surface (W/m^2).
Switch	Switch to control.
T	Temperature (°C).
t	Time (s).
U	Overall heat transfer coefficient (W/m^2K).
u	Velocity (m/s).
V	Volume (m^3) or volts (V).
v	Specific volume (m^3/kg).
w	Door width (m).
X	Shortest distance
x	Thickness (m).
x_{mGAB}	GAB isotherm constant
y	Door height (m).

z	Ratio of warm air density to cold air density = $\rho_{a,out}/\rho_{a,i}$

Greek Letters

The following Greek letters are used in the equation developments.

α	Heat transfer coefficient (W/m^2 K).
ΔP	Pressure drop (Pa).
ϕ	Energy or heat flow (W).
ρ	Density (kg/m^3).
ε	Emissivity of the outside face of the surface or heat transfer effectiveness factor for heat exchanger.
λ	Thermal conductivity (W/m K).
η	Efficiency

Subscripts

The following subscripts are used in the equation developments.

a	Air
air	Air
airCon	Condenser air side
av	Average
am	Ambient
b	b^{th} component
bat	Batch
buffer	Thermal buffering
cl	Door closed
co	Correction

Com	Compressor
ComIsen	Compressor Isentropic
Comloss	Compressor losses
comdis	Compressor discharge
comp	Compression
comvol	Compressor volumetric
Con	Condenser
conc	Concrete
cond	Conduction
D	Number of doors
Drain	Drain
d	d^{th} door, or door
de	Defrost
dedur	Defrost duration
deRep	Defrost repeat
dis	Discharge
disline	Discharge line
dry	Dry
Evap	Evaporator
EPR	Evaporator pressure regulator valve
e	Evaporation
ef	Effective
ev	Evaporator
ex	External zone
ext	External zone
for	Forced convection
fin	Fin

fl	fl^{th} floor or floor
fr	Frost
full	Full
hg	hg^{th} Heat generator or heat generator
hotgpass	Hot gas bypass (refrigerant)
hotgpassMax	Maximum hot gas bypass (refrigerant)
hu	hu^{th} Humidifier or humidifier
hg	hg^{th} Heat generator or heat generator
i	i^{th} air zone or air zone
I	Number of air zones
in	In
ini	Initial
inf	Infiltration
ins	Inside
insu	Insulation
int	Internal zone
j	j^{th} evaporator
J	Number of evaporators
k	k^{th} fan
K	Number of fans
L	Liquid
la	latent heat
loss	losses
load	loaded
liqbypass	Liquid refrigerant bypass

nc	natural convection
n	n^{th} neighbouring air zones
N	Number of air zones
NEvaps	Number of evaporators
out	out or outside
off	off
on	air from air zone on to fan or evaporator
op	door opened
pack	external packaging
pr	pr^{th} product or product
pro	door protection
ref	refrigerant
refCon	Condenser refrigerant side
refer	reference
ro	room
S	Number of surfaces
SatSucCom	Saturated compressor suction
SatComdis	Saturated compressor discharge
Suc	Suction
SucCom	Compressor suction
SH	Super heat
SLHE	Suction line heat exchanger
s	s^{th} surface, or surface
sa	Saturated
sat	Saturated
se	seal

sen	sensible heat
set	set limit
sjdefrostoff	Evaporator surface setpoint for defrosting (temperature)
sp	Set point
so	soil
sol	Solar to air
st	st^{th} structures or structure
std	Standard
suc	Suction
sucSet	Suction setpoint
Tam	Tamm's equation
to	total
tr	forklift traffic
Vol	volumetric
v	vapour (water, refrigerant)
w	condensed water
→	Between

REFERENCES

Amos, N.D. (1995). *Mathematical Modelling of heat transfer and water vapour transport in apple coolstores*. PhD Thesis, Massey University.

Amos, N.D., Cleland, D.J., Cleland, A.C., & Banks, N.H. (1993a). The effect of coolstore design and operation on air relative humidity. *Proceedings of the International Conference for Agricultural Machinery & Process Engineering.* 433-438.

Amos, N.D., Cleland, D.J., Banks, N.H., & Cleland, A.C. (1993b). A survey of air velocity, temperature and relative humidity in a large horticultural coolstore. *"IIR Refrigeration Science and Technology Proceedings"*. Vol 1993-3. 414-422.

Amos, N.D., Cleland, D.J., & Banks, N.H. (1993c). Effect of pallet stacking arrangement on fruit cooling rates within forced-air pre-coolers. *Refrigeration Science and Technology*. Vol 1993-3. 232-239.

Argaud, T. (1999). Experimental comparison of two methods for triggering the defrosting of reversible air/water heat pumps. Time delay & air and evaporator temperature difference. *Proceedings 20th International Congress of Refrigeration, IIR/IIF Sydney.* Vol. 1999-3. (paper 201).

ASHRAE (2001). *ASHRAE Handbook – Fundamentals.* American Society of Heating, Refrigeration and Air-Conditioning Engineers Inc, Atlanta, GA.

ASHRAE (2000). *ASHRAE Handbook – Heating, Ventilating, and Air-Conditioning Systems and Equipment.* American Society of Heating, Refrigeration and Air-Conditioning Engineers Inc, Atlanta, GA.

Becker, M., Hasse, H., Grossmann, K., & Litz, L. (1995). Top-down model for dynamic simulation of cold storage plants. *Proceedings 19th International Congress of Refrigeration*. Vol.1995-IIIb, 743-750.

Bendapudi, S., Braun, J.E., Groll, E. A. (2005). Dynamic model of a centrifugal chiller system – model development numerical study, and validation. *ASHRAE Trans.* Vol. 2005-111, part 1, 1-17.

Brooks, R.W. (2001). *The use of refrigerated stores for electrical load management.* Ph.D. Thesis, University of Manchester.

Campanone, L. A., Giner, S.A., & Mascheroni, R.H. (2002). Generalized model for the simulation of food refrigeration. Development and validation of the predictive numerical method. *International Journal of Refrigeration,* Vol 2002-25, 975-984.

Cavallini, A., Col, D. D., Doretti, L, Longo, G.A., Rossetto, L. (2000). Heat transfer and pressure drop during condensation of refrigerants inside horizontal enhanced tubes. *International Journal of Refrigeration,* Vol 2000-23, 4-25.

Cerepnalkovski, I., & Cerepnalkovska, S. (1995). Relative humidity determination for its process control in air conditioning systems. *Proceedings 19th International Congress of Refrigeration*. Vol 1995-3. 775-781.

Chan, C. Y., Haselden, G.G. (1981a). Computer-based refrigerant thermodynamic properties. Part 1: Basic equations. *International Journal of Refrigeration.* Vol. 1981-4, 7-12.

Chan, C. Y., Haselden, G.G. (1981b). Computer-based refrigerant thermodynamic properties. Part 2: Program listings. *International Journal of Refrigeration.* Vol. 1981-4, 52-60.

Chan, C. Y., Haselden, G.G. (1981c). Computer-based refrigerant thermodynamic properties. Part 3: Use of the program in the computation of standard refrigeration cycles. *International Journal of Refrigeration.* Vol. 1981-4, 131-134.

Chan, K.Y., Tassou, S.A., Ge, Y.T.(1998). Control and optimisation of food retail refrigeration systems. *Refrigeration Science and Technology Proceedings*. Vol 1998-6, 645-651.

Chen, P., Cleland, D.J., Lovatt, S.J., & Basset, M.R. (2002). An empirical model for predicting air infiltration into refrigerated stores through doors. *International Journal of Refrigeration*. Vol 2002-25, 799-812.

Chua, H. T., Ng, K. C. & Gordon, J. M. (1996). Experimental study of the fundamental properties of reciprocating chillers and their relation to thermodynamic modelling and chiller design. *International Journal of Heat and Mass Transfer.* Vol 1996-39, 2195-2204.

Cleland, A. C. (1990). *Food Refrigeration Processes analysis, design and simulation*. Elsevier Science London.

Cleland, A.C. (1994). Polynomial curve-fits for refrigerant thermodynamic propertites: extension to include R134a. *International Journal of Refrigeration.* Vol.1994-17, 245-249.

Cleland, D.J., Cleland, A. C. (1989). Appropriate level of model complexity in dynamic simulation of refrigeration systems. *Refrigeration Science and Technology.* Vol. 1989-1, 261-268.

Cleland, A.C. (1986). Computer subroutines for rapid evaluation of refrigerant thermodynamic properties. *International Journal of Refrigeration.* Vol. 1986-9, 346-351.

Cleland, A.C. (1985a). RADS – a computer package for refrigeration analysis, design and simulation. *International Journal of Refrigeration.* Vol. 1985-8, 372-373.

Cleland, A.C. (1985b). Experimental verification of a mathematical model for simulation of industrial refrigeration plants. *International Journal of Refrigeration.* Vol. 1985-8, 275-282.

Cleland, A.C. (1983). Simulation of industrial refrigeration plants under variable load conditions. *International Journal of Refrigeration.* Vol. 1983-6, 11-19.

Cleland, D.J., & Boyd, N.S., (1982). A model for fish freezing and storage on board small New Zealand fishing vessels. *Refrigeration Science and Technology,* Vol. 1982- 1, 147-155.

Cleland, D.J., Cleland, A.C., & White, S.D. (2002). Cost Effective Refrigeration. Massey University, Palmerston North, New Zealand.

Cleland, D.J., Lovatt, S.J., Chen, P., & Basset, M.R. (2004). A modified model to predict air infiltration into refrigerated facilities through doorways. *ASHRAE Trans.,* Vol. 2004-110, paper T193-03, ASHRAE Winter Meeting, Anheim, January 2004.

Cleland, D.J., & O'Hagan, A.N. (2003). Performance of an air cooling coil under frosting conditions. *ASHRAE Trans.* Vol. 2003-109(2), paper 4623, ASHRAE Winter Meeting, Chicago, January 2003.

Cole, R.A. (1989a). Refrigeration loads in a freezer due to hot gas defrost and their associated costs. *ASHRAE Trans.* Vol. 1989-95(2), 1149-1154.

Cole, R. (1989b). Costing out hot gas defrost. *Engineered Systems.* Vol. 1989-May/June, 52-54.

Cornelius, M. (1991). *Refrigeration Analysis Design and Simulation Package: "RADS" – Notes for Users (revised), Release 3.1,* Food Technology Research Centre, Massey University, Palmerston North, New Zealand.

Crawford, R.R., Mavec, J.P., Cole, R.A. 1992. Literature survey on recommended procedures for the selection, placement and type of evaporators for refrigerated warehouses. *ASHRAE Trans.* Vol. 1992-89(1), 500-513.

Darrow, J.B., Lovatt, S.J. and Cleland, A.C., (1991). Assessment of a simple mathematical model for predicting the transient behaviour of a refrigeration system, *Proceedings 18th International Congress of Refrigeration*, Vol. 1991-3, 74-80.

Ditchev, S., Paunov, P., Angelov, N., & Lambrevr, Y. (1998). Frost formation and defrosting of dry air coolers as decisive factors for the efficiency of refrigeration units. *Refrigeration Science and Technology Proceedings*. Vol. 1998-6, 633-636.

Downing, C.C, Meffert, W.A. 1993. Effectiveness of cold-storage door infiltration protective devices, *ASHRAE Trans.*, Vol. 1993-99(2), 356-366.

Eagleton, D.G., & Marcondes, J.A. (1994). Moisture-sorption isotherms for paper based components of transport packaging for fresh produce. *Tappi Journal,* Vol.1994- 77(7), 75-81.

East, A. R., Cleland, D. J., Bassett, M. R., & Lovatt, S. J. (2002). Refrigerated buildings insulation quality and door air infiltration. *Proceedings IRHACE Technical Conference,* Christchurch. 134-140.

East, A. R., Jeffery, P.B, Cleland, D. J. (2003). Air infiltration into walk-in cold rooms. *Proceedings of the IRHACE Technical Conference,* Hamilton, New Zealand. 96-104.

Estrada-Flores, S., Cleland, A.C., & Cleland, D.J. (2001). Prediction of the dynamic thermal behaviour of walls for refrigerated rooms using lumped and distributed parameter models. *International Journal of Refrigeration*. Vol.2001-24, 272-284.

Estrada-Flores, S. (1996). *Evaluation of dynamic models for refrigeration system components*. PhD Thesis. Massey University, New Zealand.

Estrada-Flores, S., Cleland, A.C., & Cleland, D.J. (1995). Modelling of thermal behaviour of walls for low temperature applications: Sandwich panel type. Proceedings *19th International Congress of Refrigeration,* Vol. 1995-2, 73-80.

Fahlen, P.O. (1995). Frosting of air-coils. *Proceedings 19th International Congress of Refrigeration*. Vol. 1995- 3, 751-758.

Gosney, W.B., Olama, H.A.L. (1975). Heat and enthalpy gains through cold room doorways. *The Institute of Refrigeration, Faculty of Environmental Science and Technology, The Polytechnic of the South Bank, London*. Session 1975-1976, 1-9.

Gupton, G.W. (2001). Humidity control. *Heating, Piping, Air Conditionning,* Vol. 2001-73(3), 43-53.

Hasse, H., Becker, M., Grossmann, K., & Maurer, G. (1996). Top-down model for dynamic simulation of cold storage plants. *International Journal of Refrigeration*. Vol.1996-19, 10-18.

Hendrix, W.A., Henderson, D.R, Jackson, H.Z. 1989. Infiltration heat gains through cold-storage room doorways, *ASHRAE Trans.*, Vol. 1989-95(2), 1155-1168.

Hoffenbecker, N., Klein, S. A., Reindl, D. T. (2005). Hot gas defrost model development and validation. *International Journal of Refrigeration.* Vol. 2005-28, 605-615.

Houston, C. (2000). Fog humidification for industrial and commercial application. *Heating, Piping, Air Conditioning.* V. 2000-72(4), 47-53.

Incropera, F. P. & De Witt, D. P. (1985). *Fundamentals of Heat and Mass Transfer* J. Wiley & Sons, New York.

Jakobsen, A. (1995a). *Energy optimisation of refrigeration system. The domestic refrigerator- a case study.* PhD Thesis, The Technical University of Denmark.

Jakobsen, A. (1995b). Energy analysis and optimisation of a domestic refrigerator. *Proceedings Equipment and Processes.* Vol. 1995-3, 337-344.

Jakobsen, A. (1995c). Dynamic modelling and simulation of a domestic refrigerator. *Proceedings Equipment and Processes.* Vol. 1995-3, 345-352.

James, R.W., & Missenden, J.F. (1993). Control of refrigeration systems with the aid of analytical models. *Proceedings Cold chain refrigeration equipment by design.* Vol. 1993-3, 295-304.

Jamieson, D. J., Cleland, D.J. (1993). Modelling of bulk-stacked cheese cooling in cold store. *Proceedings Refrigeration Science and Technology.* Vol. 1993-3, 268-276.

Janssen, M.J.P., de Wit, J.A., Kuijpers, L.J.M. (1992). Cycling losses in domestic appliances: an experimental and theoretical analysis. *International Journal of Refrigeration.* Vol. 1992-15, 152-158.

Jia, X., Tso, C.P., Jolly, P., & Wong, Y.W. (1999). Distributed steady and dynamic modelling of dry-expansion evaporators. *International Journal of Refrigeration.* Vol. 1999-22, 126-136.

Jia, X., Tso, C.P., Chia, P.K., & Jolly, P. (1995). A distributed model for prediction of the transient response of an evaporator. *International Journal of Refrigeration.* Vol. 1995-18, 336-342.

Jolly, P. G., Tso, C. P.,Wong, Y. W., & Ng, S. M., (2000). Simulation and measurement on full-load performance of a refrigeration system in a shipping container. *International Journal of Refrigeration.* Vol. 2000-23, 112-126.

Jung, D., Radermacher, R., (1993). Prediction of evaporation heat transfer coefficient and pressure drop of refrigerant mixtures in horizontal tubes. *International Journal of Refrigeration,* Vol. 1993-16, 201-209.

Kallu, R.D.S, Cleland, A.C., & Lovatt, S.J. (1993). Time Variable modelling of total refrigeration demand in meat processing. *Proceedings Cold chain refrigeration equipment by design.* Vol. 1993-3, 224-231.

Kim, M. H., & Bullard, C. W. (2002). Air-side performance of brazed aluminium heat exchangers under dehumidifying conditions. *International Journal of Refrigeration.* Vol. 2002-25, 924-934.

Klein, F. H., Melo, C., & Marques, M. E.. (1999). Steady-state simulation of an all refrigerator. *Proceedings 20th International Congress of Refrigeration,* Vol. 1999-3, paper 073, Sydney, 1999.

Kondepudi, S.N., & O'Neal, D.L. (1993a). Performance of finned-tube heat exchangers under frosting conditions: I. Simulation model. *International Journal of Refrigeration.* Vol. 1993-16, 175-180.

Kondepudi, S.N., & O'Neal, D.L. (1993b). Performance of finned-tube heat exchangers under frosting conditions: II. Comparison of experimental data with model. *International Journal of Refrigeration.* Vol. 1993-16, 181-184.

Kondepudi, S.N., & O'Neal, D.L. (1989). Effect of frost growth on the performance of louvered finned tube heat exchangers. *International Journal of Refrigeration.* Vol. 1989-12, 151-158.

Koury, R.N.N., Machado, L., & Ismail, K.A.R. (1999). Numerical model of a vapour compression refrigeration system. *Proceedings 20th International Congress of Refrigeration,* Vol. 1999-3, paper 367, Sydney, 1999.

Koury, R.N.N., Machado, L., & Ismail, K.A.R. (2001). Numerical simulation of a variable speed refrigeration system. *International Journal of Refrigeration.* Vol. 2001-24, 192-200.

Lee, G. H., Yoo, J. Y. (2000). Performance analysis and simulation of automobile air conditioning system. *International Journal of Refrigeration,* Vol. 2000-23, 243-254.

Liang, S.Y., Wong, T.N., & Nathan, G.K. (2001). Numerical and experimental studies of refrigerant circuitry of evaporator coils. *International Journal of Refrigeration,* Vol. 2001-24, 823-833.

Lin, Z., Cleland, A. C., Serrallach, G. F. & Cleland, D. J. (1993). Prediction of chilling times for objects of regular multi-dimensional shapes using a general geometric factor. *Refrigeration Science and Technology.* Vol. 1993- 3, 259-267.

Lin, Z., Cleland, A. C., Cleland, D. J. & Serrallach, G. F. (1996a). A simple method for prediction of chilling times for objects of two-dimensional irregular shape. *International Journal of Refrigeration,* Vol. 1996-19, 95-106.

Lin, Z., Cleland, A. C., Cleland, D. J. & Serrallach, G. F. (1996b). A simple method for prediction of chilling times: extension to three-dimensional irregular shapes. *International Journal of Refrigeration,* Vol. 1996-19, 107-114.

Lovatt, S.J. (1992). A dynamic modelling methodology for simulation of industrial refrigeration system. PhD Thesis, Massey University, Palmerston North, New Zealand.

Lovatt, S. J., Merts, I. (1999). Recommended methods for food refrigeration process design. *Proceedings 20th International Congress of Refrigeration.* Vol. 1999-4, paper 350, Sydney 1999.

Machielsen, C. H. M., Kerschbaumer, H. G. (1989). Influence of frost formation and defrosting on the performance of air coolers: standards and dimensionless coeffients for the system designer. *International Journal of Refrigeration,* Vol. 1989-12, 283-290.

Mago, P., Sherif, S.A. (2005). Coil frosting and defrosting issues at low freezer temperature near saturation conditions. *ASHRAE Trans.* Vol. 2005-3, Part 1, paper 4742, ASHRAE Winter Meeting 2005.

Manske, K. A., Reindl, D. T., & Klein, S. A. (2001). Evaporative condenser control industrial refrigeration systems. *International Journal of Refrigeration,* Vol. 2001-24, 676-691.

Marinyuk.B.T. (1980). Heat and mass transfer under frosting conditions. *International Journal of Refrigeration.* Vol. 1980-3, 366-368.

Merts, I., Lovatt, S.J., and Lawson, C.R., (1998). Diffusivity of moisture in whole muscle meat measured by a drying curve method. *Proceedings Refrigeration Science and Technology,* Vol. 1998-6, 473-479.

Mithraratne, P., & Wijeysundera, N.E. (2001). An experimental and numerical study of the dynamic behaviour of a counter-flow evaporator. *International Journal of Refrigeration.* Vol. 2001-24, 554-565.

Mithraratne, P., Wijeysundera, N.E., & Bong, T.Y. (2000). Dynamic simulation of a thermostatically controlled counter-flow evaporator. *International Journal of Refrigeration.* Vol. 2000-23, 174-189.

Ng, C. K.$ Cleland, D.J., & Cleland, A. C. (1999). Effect of suction-line heat exchangers on the performance of direct expansion evaporators. *Proceedings 20th International Congress of Refrigeration.* Vol. 1999-3, paper 652, Sydney, 1999.

Niederer, D.H. 1976. Frosting and defrosting effects on coil heat transfer, *ASHRAE Trans.*, Vol. 1976-82 (1), 467-473.

O'Hagan, A.N. (1994). *The effect of favourable and unfavourable frost on air cooling coil performance*. Master of Technology Thesis, Massey University.

O'Hagan, A.N., Cleland, D.J., & Cleland, A. C. (1993). Air cooling coil performance under frosting conditions. Part 1: Performance measurement and results. *Refrigeration Science and Technology.* Vol. 1993- 3, 345-354.

O'Hagan, A.N., Cleland, D.J., & Cleland, A. C. (1993). Air cooling coil performance under frosting conditions. Part 2: Performance measurement and results. *Refrigeration Science and Technology.* Vol. 1993- 3, 355-362.

Pham, Q. T., Wee, H. K., Lovatt, S. J., Lindsay, D., & Kemp, R. M. (1993). A quasi-steady approach to the design of meat plant refrigeration systems. *Refrigeration Science and Technology.* Vol. 1993-3, 215-223.

Rossi, T., Braun, J.E. (1999). A real-time transient model for air conditioners. *Proceedings 20th International Congress of Refrigeration.* Vol. 1999-5, paper 743, Sydney, 1999.

Sanders, C. Th. (1974). *Frost formation the influence of frost formation and defrosting on the performance of air coolers.* PhD Thesis, Delft University of Technology, The Netherlands.

Shahid, B.E. (1995). Ultrasonic humidifiers offer advantages. *Air Conditioning Heating & Refrigeration News,* Vol. 1995-194(5), 36-37.

Smith, G.R. 1989. Theoretical cooling coil calculations at freezer temperatures to avoid unfavourable coil-frost. *ASHRAE Trans.* Vol. 1989-95(2), 1138-1148.

Smith, G.R. 1992. Latent heat, equipment-related load, and applied psychrometrics at freezer temperatures. *ASHRAE Trans.* Vol. 1992-11(1), 649-657

Stoecker, W. F. (1988). *Industrial Refrigeration.* Business News Publishing Company. Michigan.

Stoecker, W.F, Lux, J.J., Kooy, R.J. 1983. Energy considerations in hot-gas defrosting of industrial refrigeration coils. *ASHRAE Trans.* Vol. 1983-89(2), 549-568.

Sherif, S. A., Theen, R. S., Mago, P. J., Bilen, K., & Al-Mutawa, N. K. (2001). Psychrometrics in the supersaturated frost zone. *ASHRAE Trans.* Vol. 2001-107(2), paper 1094, ASHRAE 2001.

Sieres, J., & Fernandez-Seara, J. (2005). Simulation of compression refrigeration systems. *Computer Applications in Engineering Education,* Vol. 2005-14(3), 188-197.

Tanner, D. J., Cleland, A. C., Opara, L. U., & Robertson, T. R. (2002a). A generalised mathematical modelling methodology for design of horticultural food packages exposed to refrigerated conditions: part 1, formulation. *International Journal of Refrigeration,* Vol. 2002-25, 33-42.

Tanner, D. J., Cleland, A. C., & Opara, L. U. (2002b). A generalised mathematical modelling methodology for design of horticultural food packages exposed to refrigerated conditions: part 2, Heat transfer modelling and testing. *International Journal of Refrigeration,* Vol. 2002-25, 43-53.

Tanner, D. J., Cleland, A. C., & Robertson, T. R. (2002c). A generalised mathematical modelling methodology for design of horticultural food packages exposed to refrigerated conditions: part 3, mass transfer modelling and testing. *International Journal of Refrigeration,* Vol. 2002-25, 54-65.

Tanner, D.J. (1998). *Mathematical Modelling of Design of Horticultural Packaging.* PhD Thesis, Massey University.

Tassou, S. A., Datta, D. (1998). Frost formation and demand defrost of display cabinet evaporators. *Proceedings Refrigeration Science and Technology,* Vol. 1998-6, 626-632.

Tassou, S. A., Xiang, W. (1999). The application of computational fluid dynamics to the design of refrigeration systems. *Proceedings Recent Developments in Refrigeration and Heat Pump Technologies.* Vol. 1999-1, 61-78.

Tso, C. P.,Yu, S.C.M., Poh, H.J., & Jolly, P. G. (2002). Experimental study on the heat and mass transfer characteristics in a refrigerated truck. *International Journal of Refrigeration,* Vol. 2002-25, 340-350.

Tso, C. P.,Wong, Y. W., Jolly, P. G., & Ng, S. M. (2001). A comparison of hot-gas by pass and suction modulation method for partial load control in refrigerated shipping containers. *International Journal of Refrigeration*, Vol. 2001-24, 544-553.

Turaga, M., & Guy, R.W. (1985). Refrigerant side heat transfer and pressure drop estimates for direct expansion coils. A review of works in North America use. *International Journal of Refrigeration*. Vol. 1985-8, 134-142.

Witt, J. J., Cleland, D.J., Cleland, A.C. (1999). A simple model for the temperature-buffering effect of palletised product in refrigerated stores. *Proceedings 20th International Congress of Refrigeration.* Vol. 1999-4, paper 232, Sydney 1999.

Xia, Y., Hrnjak, P.S., Jacobi, A.M. (2005). Air-side thermal-hydraulic performance of louvered-fin, flat-tube heat exchangers with sequential frost-growth cycles. *ASHRAE Trans.* Vol. 2005-111(1), paper OR-05-1-2, ASHRAE Winter Meeting 2005.

Xiang, W., Tassou, S. A. (1998). A dynamic model for vertical multideck refrigerated display cabinets. *Proceedings Refrigeration Science and Technology.* Vol. 1998-6, 637-644.

Yaqub, M., Zubair, S. M., & Khan, J. R., (2000). Performance evaluation of hot-gas by-pass capacity control schemes for refrigeration and air-conditioning systems. *Energy.* Vol. 2000-25, 543-561.

Yun, R., Kim, Y., & Min, M. (2002). Modeling of frost growth and frost properties with airflow over a flat plate. *International Journal of Refrigeration.* Vol. 2002-25, 362-371.

APPENDIX A

Figure A 1 shows the 4 RH sensor calibration lines. The equations are given in terms of sensor output voltages and RH%.

$$RH1 = 32.402V - 41.67 \quad \text{(A-1)}$$

$$RH2 = 26.934V - 26.549 \quad \text{(A-2)}$$

$$RH3 = 25.276V - 20.994 \quad \text{(A-3)}$$

$$RH4 = 31.471V - 36.002 \quad \text{(A-4)}$$

Where:

V = Output voltage (volts).

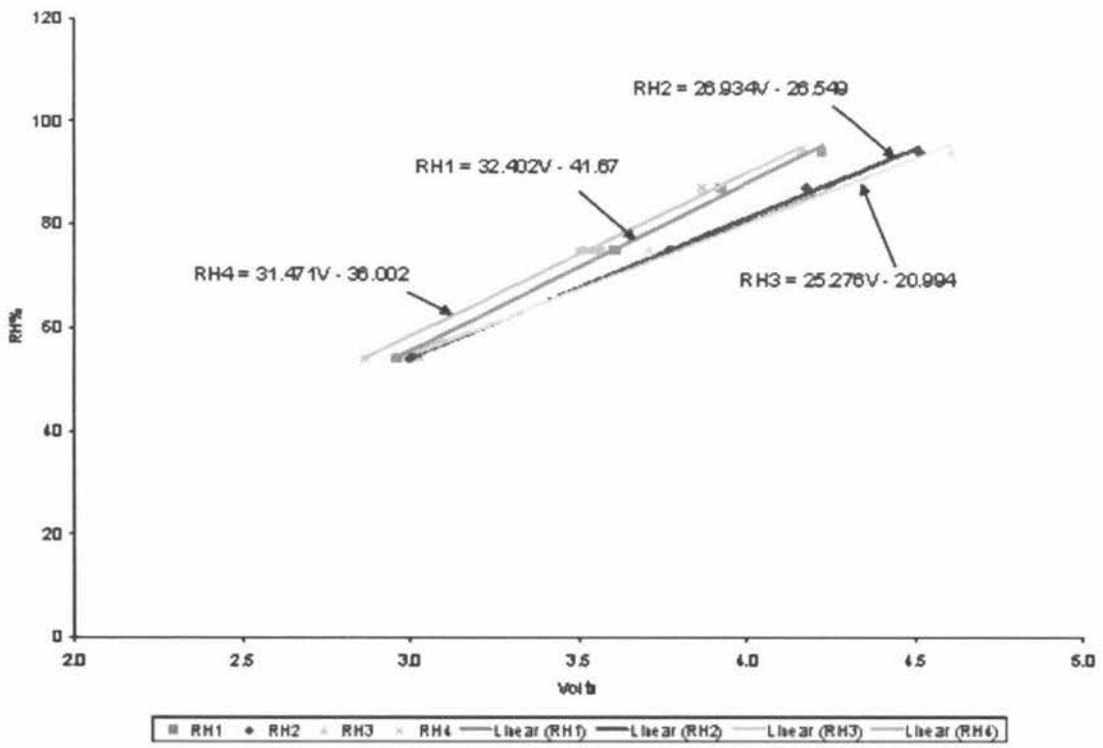

Figure A 1: RH sensor calibrations

APPENDIX B

Figure B 1 shows the calibration lines for the 3 low pressure sensors. The equations are given in terms of sensor output voltages and gauge pressure (bars).

$$LP1 = 1.7727V - 2.8215 \quad \text{(B-1)}$$

$$LP2 = 1.7664V - 2.81 \quad \text{(B-2)}$$

$$LP3 = 1.7607V - 2.7942 \quad \text{(B-3)}$$

Where:

V = Output voltage (volts).

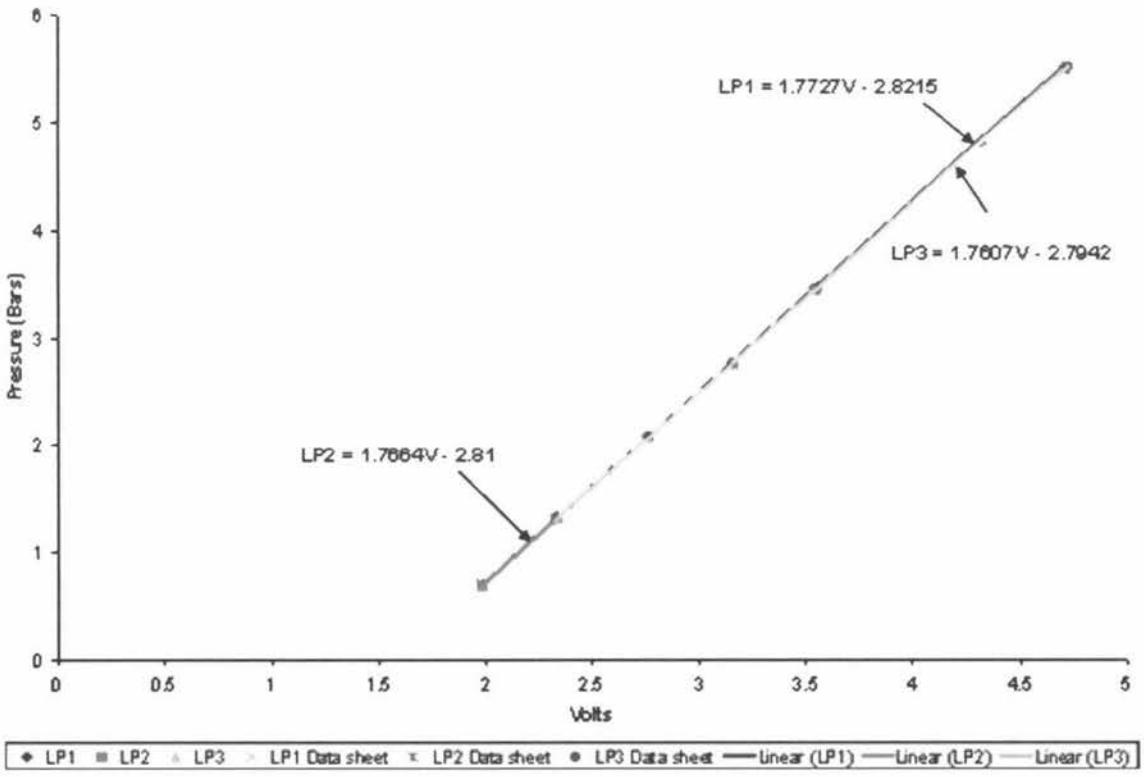

Figure B 1: Low pressure sensor calibrations

Figure B 2 shows the calibration lines for the 3 high pressure sensors. The equations are given in terms of sensor output voltages and gauge pressure (bars).

$$HP1 = 8.8382V - 9.9706 \quad \text{(B-4)}$$

$$HP2 = 8.8302V - 9.9531 \quad \text{(B-5)}$$

$$HP3 = 8.8216V - 9.9331 \quad \text{(B-6)}$$

Where:

V = Output voltage (volts).

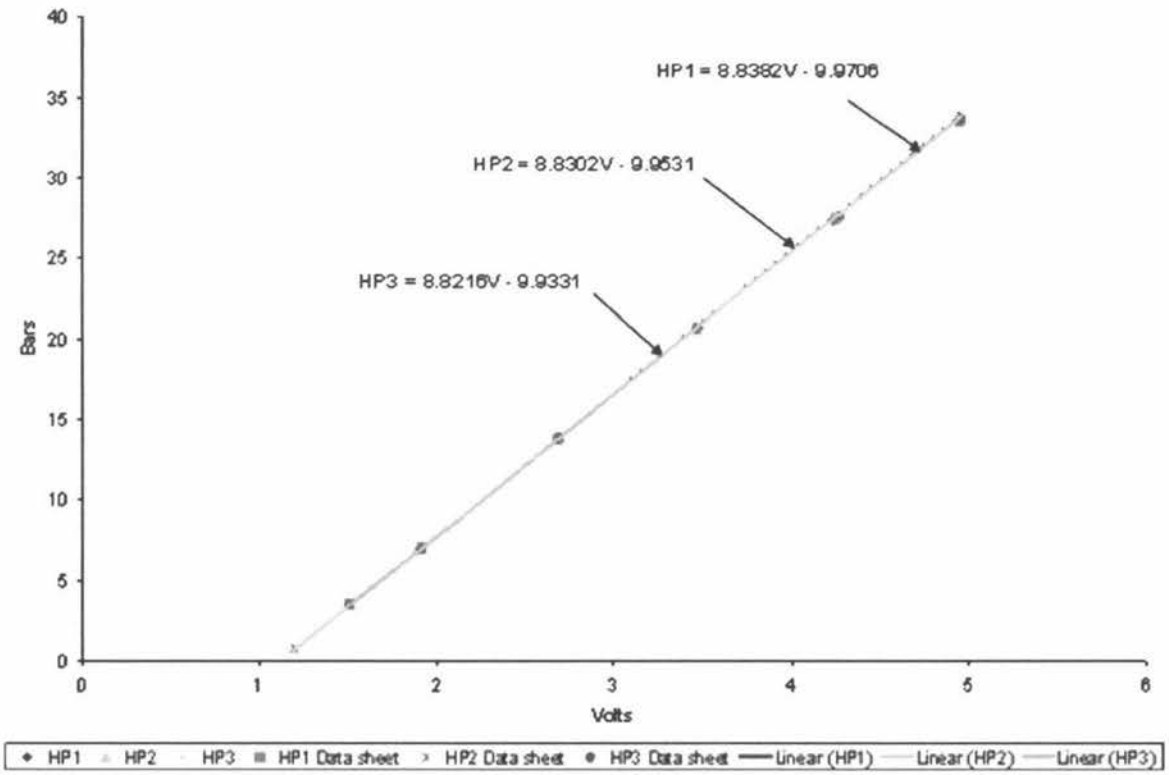

Figure B 2: High pressure sensor calibrations

APPENDIX C

Sujau *et al.* (2006), Proceedings of the IIR/IRHACE Conference, The University of Auckland, 2006, p 525-532.

EFFECT OF DEFROST FREQUENCY ON DEFROST EFFICIENCY, DEFROST HEAT LOAD AND COOLSTORE PERFORMANCE

M. SUJAU*, J.E. BRONLUND, I. MERTS, D.J. CLELAND
Centre for Postharvest and Refrigeration Research, Massey University,
Private Bag 11-222, Palmerston North, New Zealand
* M.Sujau@massey.ac.nz

ABSTRACT

The performance of a small walk-in cool store and its refrigeration system with temperature terminated electric defrost was measured for defrost intervals ranging from 6 hours to 30 hours for two different heat load regimes. Defrost efficiency and defrost duration were both proportional to defrost interval and approximately doubled as defrost interval increased from 6 to 30 hours. The main benefit of longer intervals arose from reduced heating of the coil mass. The change in overall system energy use with defrost interval was not significant because the system used EPR temperature control, and the latent and hence defrost heat loads were quite small compared with the total heat load. At short defrost intervals, cool store temperature control was poorer due to the pull-downs after each defrost. At long defrost intervals, cool store RH was lower and temperature control was poorer due to significant coil performance decline and longer duration defrosts. For the system and heat load conditions studied, a defrost frequency of 8 to 12 hours appeared optimal.

1. INTRODUCTION

If a refrigerated facility operates near or below 0°C, most entering moisture ultimately deposits on the evaporator coil surfaces as frost, decreasing the refrigeration system efficiency. In particular, the frost both reduces the air flow through the coil and insulates the coil heat transfer surface. The refrigeration system must either operate with a lower refrigerant evaporation temperature or for a greater percentage of the available time, or there may be loss of temperature control in the freezer. Longer run-time incurs energy use penalties. A lower evaporation temperature incurs both energy use and system capacity penalties. The reduction in air flow rate can also have important effects on uniformity of conditions and the desired rate of heat transfer in the facility, such as removal of heat from product. Periodically, the coils must be defrosted to remove the accumulated frost, incurring further energy costs, increasing the facility heat load, and causing increased risk of temperature fluctuations that may contribute to accelerated product quality deterioration.

From a design perspective two key aspects of defrost are: what is the extra heat load on the refrigeration system due to defrost, and what is the best defrost system type and configuration to install to ensure reliable and efficient operation? From an operational perspective, the key consideration is to optimise the frequency and duration of defrosting to minimise both energy use and the disruption to the air and product conditions in the freezer. Although the principles are well established, there are few quantitative guidelines to ensure efficient defrosting available to the designer and operator of industrial refrigeration systems (Machielsen & Kerschbaumer, 1989).

There are two heat load-related effects of defrost - extra heat added to the refrigerated space that is not removed with the melt water (some to heat the coil and some into the freezer air), and the loss of refrigeration effect while a coil is being defrosted (Cleland & Cleland, 2004). There is comparatively little information on heat loads due to defrost (Crawford *et al.*, 1992). Defrost heat load allowances used in industrial design vary from 0% to 25% of the other heat loads with about 5% and 15% or higher being common values for medium and low temperature applications respectively (ASHRAE,

2002). Loss of refrigeration effect is taken into account by designing the refrigeration system to remove the design heat load in less than the total available time. Some designers use both types of allowance, some only one or the other, some use neither and rely on the use of a combination of worst case design conditions to provide a safety factor for defrost. One measure of likely heat load is a defrost efficiency which is the ratio of the heat required to melt frost only to the total heat supplied to defrost the coil:

$$\eta_{defrost} = E_{melt} / E_{defrost} \tag{1}$$

where: $\eta_{defrost}$ defrost efficiency
E_{melt} energy in melt water (kJ)
$E_{defrost}$ energy input to coil during defrost (kJ)

Assuming that ice and melt-water sensible heat effects are small compared with latent heat effects, and that apart from the melt water all defrost heat input ends up in the refrigerated facility then the extra heat load due to defrost is given by (Cleland & Cleland, 2004):

$$\phi_{defrost} = 0.12\,\phi_{latent}\left(1 - \eta_{defrost}\right)/\eta_{defrost} \tag{2}$$

where: $\phi_{defrost}$ average defrost heat load (kW)
ϕ_{latent} average facility latent heat load (kW)

For hot-gas systems, a partially theoretical analysis suggested efficiencies less than 20% (Stoecker *et al.*, 1983; Cole, 1989). For other types of defrost there is even less heat load information available.

Operation of defrost systems in terms of frequency and duration can have a significant effect on the cost of defrost and the degree of disruption to the refrigerated facility. Defrosting too often or for too long is very disruptive and energy inefficient (as the whole coil is heated irrespective of the amount of frost), whilst infrequent and/or short defrosts result in incomplete melting and the refrigeration system will operate well below peak efficiency for a large fraction of the time.

Traditionally most defrost systems have been initiated on a fixed time basis, and use a combination of time or temperature termination because such systems are simple and reliable. The initiation and termination settings are often independent of the operating conditions that the refrigeration system is experiencing. However, it has been found that the effect of frost on coil performance is highly dependent on the conditions under which the coil is operating and the coil design (Smith, 1989; Cleland & O'Hagan, 2003; Mago & Sherif, 2005). For example, Mago & Sherif (2005) measured hot gas defrost efficiency to be a strong function of coil face velocity. Therefore the optimal defrost schedule will depend on these factors as well as the inherent efficiency of the defrost system. On-demand defrost initiation systems (e.g. ice thickness sensor, adaptive timer algorithms) have been developed but their uptake has been limited, in part because their economic benefits have not been demonstrated quantitatively and independently, but also they have often proved unreliable unless they are regularly maintained and adjusted (Tassou & Datta, 1998).

A number of models of coil frosting and defrost have been developed (e.g. Machielsen & Kerschbaumer, 1989; Kodepudi & O'Neal, 1993a, 1993b; Le Gall *et al.*, 1997). Unfortunately either these models have not been validated against measured data or they are so complex that they are impractical for use by industrial practitioners.

In summary, there remains a need for more data on defrost efficiencies and heat loads as a function of design and operating conditions, leading to development of practical guidelines for the design and operation of coils under frosting conditions. The objective of this paper was to investigate the effect of coil defrost frequency on defrost efficiency, defrost heat load, uniformity of storage conditions and store performance for a small walk-in cool store with electric defrost.

2. EXPERIMENTAL

Figure 1 shows the cool store and instrumentation used for the experimental trails. The cool store was 3.3 m wide by 4.4 m long by 3.0 m high, was constructed of 150 mm polystyrene sandwich panel with a 1.2 m by 2.4 m hinged door protected by a strip curtain, and had 448 W of lighting. An air-cooled HFC-134a refrigeration system, with a nominal cooling capacity of 7.6 kW at -10°C evaporation and 40°C condensation, cooled the store via two cooling coils. Each coil had a nominal sensible heat transfer rating of 690 W/K, two 73 W fans, 2.3 kW electric defrost elements, a suction line heat exchanger and was controlled with a thermostatic expansion (TX) valve. Store air temperature was controlled by an electronic evaporation pressure regulating (EPR) valve. The refrigeration system operated continuously except during defrost and a hot gas bypass system with liquid injection cooling was used to prevent suction pressure going below about 1.5 bar.g. Defrost was initiated by a time clock and terminated based on coil surface temperature.

During the trials, the store held very small amounts of kiwifruit. There were few door openings and little personnel activity. To mimic different design and operating conditions up to 5 kW of electric heaters and an ultrasonic humidifier (Stulz ENS 1200; maximum output of 0.47 kg/h) were used to provide extra sensible and latent heat loads.

The store was operated with defrost intervals (time between defrosts) of 6, 8, 12, 18, 24 or 30 hours for the maximum of 48 hours or 2 defrost cycles. The air temperature set-point was 1.6°C and the extra heat loads were either 3.1 kW of electric heat and 0.29 to 0.31 kg/h water injection from the ultrasonic humidifier (latent load of about 230 W), or 5.1 kW of electric heat and 0.39 to 0.47 kg/h of extra water injection (latent load of about 340 W). The ambient conditions were about 15°C and 55% relative humidity (RH) during the trials. The heat load through the insulation and doors during the trials was estimated to be approximately 190 W. Overall, the sensible heat ratio for both sets of operating conditions was about 0.94.

Figure 1 shows the positions of the sensors used to monitor air temperature and RH, refrigerant pressure and temperature, refrigeration system energy use, and the mass of introduced water and coil defrost melt water. Temperatures were measured using PT1000 and type T thermocouple probes; air RH was measured with a Michell Series 3000 dewpoint meter or Carel SSDOHH and Hycal Ceramic SIL capacitance probes; refrigerant pressure was measured using Danfoss AKS 32 transmitters; energy was measured using Carrel T-1W3 and T-1LC sensors; while masses were measured using standard laboratory scales. All sensors were calibrated prior to the trials to within ±0.1°C, ±3% RH, ±0.1 bar, ±0.1 kW and ±0.01 kg respectively.

For most trails, humidifier water use and measured coil frost melt water agreed within 3%. For two trials the melt water collected was 10% and 15% less than that added but for these trials there was a leak in the defrost tray. Therefore data analysis was based on the measured humidifier water use.

3. RESULTS AND DISCUSSION

Figures 2 and 3 give the full temperature and RH profiles for 6 and 24 hours defrost intervals with the higher latent heat load. The cyclic patterns were typical of all the defrost trials. During defrost there

was a short-term increase in air temperature (with a corresponding drop in RH) while the refrigeration system was off. Following defrost there was a pull-down in temperature as the refrigeration operated at full capacity until it regained temperature control. Then there was a period where operating conditions were relatively constant with a slow decline in refrigerant evaporation temperature as the coil became more heavily frosted. Corresponding to the drop in evaporation temperature there was a decline in RH. Eventually for long defrost intervals, the loss of coil performance due to frosting became great enough that the refrigeration could not maintain air temperature control (Figure 3). As air temperature started to rise above the set-point, RH dropped more rapidly until the next defrost was initiated and the cycle started again. Note that the step change in conditions towards the end of the period shown in Figure 3 was due to the cool store door being open for a significant period of time.

Table 1 summarises the store performance for the different defrost intervals. If the defrost was too infrequent then frosting of the coil led to extended loss of temperature control (e.g. the last 7 hours before defrost in Figure 3). Additionally, defrost took longer, the pull-down following a defrost was longer, and the average refrigerant evaporation temperature was lower leading to lower average air RH and the potential for increased refrigeration system energy use depending on the compressor control method used. If the defrost was too frequent then, although each defrost was shorter, the high number of defrosts meant that the temperature fluctuations due to defrost became more significant and defrost energy use increased (the coil mass must be heated even if there was little frost to be melted).

Table 2 gives the defrost efficiency and the heat load due to defrost calculated using Eq. (1) and (2). Figure 4 gives defrost efficiency and defrost duration as a function of the amount of frost at the start of each defrost which is directly related to latent load and defrost interval. Data for both latent loads follows a consistent pattern. As expected defrost efficiency and defrost duration were roughly proportional to the amount of frost on the coil at the the onset of defrost. However the advantage of higher efficiency for longer defrost interval is offset by the loss of coil performance and ultimately loss of temperature control at higher levels of frosting.

The effect of defrost frequency on overall system energy use was not significant (Table 2). EPR temperature control meant that any impact of frost on coil performance, compressor suction condition, and hence energy use, would be small unless the refrigeration system became grossly overloaded. Also, even with the low defrost efficiencies, the sensible heat ratio was high meaning that the defrost heat load was less than 3% of the total heat load so a large effect on energy use was not expected. For a system with on/off temperature control and/or operating with lower sensible heat ratio then the impact would be greater. In particular, for longer defrost intervals loss of coil performance would be expected to result in lower compressor suction conditions and therefore higher energy use.

For the cool store studied it appeared that a frost load of about 4 to 7 kg at defrost initiation gave the best overall outcome in terms of both temperature and RH uniformity and energy use. This corresponded to an 8 hour defrost cycle for the higher latent load condition and a 12 hour cycle for the lower latent load condition.

4. CONCLUSION

Defrost frequency had a significant effect on the quality of temperature and RH control for the cool store. The total energy use by the refrigeration system was not significantly affected by defrost frequency due to the use of EPR temperature control and the low latent heat load. Defrost efficiency and duration were roughly proportional to the defrost interval and hence the amount of frost at the onset of defrost. Increasing defrost interval from 6 to 30 hours approximately doubled defrost efficiency and duration. Optimal frequency primarily depends on the size of the latent load and the design of the air-cooling coils.

Table 1: The effect of defrost frequency on cool store storage and operating conditions.

Defrost Interval (hrs)	Water Input Rate (kg/h)	Av. Air Temp.[1] (°C)	Av. Air RH[1] (%)	Av. Evap. Temp.[1] (°C)	Coil Frost Load[2] (kg)	% Time > 2.6°C	Defrost Time[3] (min.)	Defrost Energy[3] (kWh)
3.1 kW extra electric heat and 0.29 to 0.31 kg/h water injection								
6	0.29	1.71	83	-4.9	1.81	5.1	73.6	5.6
8	0.30	1.66	84	-4.9	2.49	4.2	60.5	4.6
12	0.31	1.70	83	-5.1	3.94	3.1	49.7	3.8
16	0.31	1.70	83	-5.2	5.21	2.7	44.9	3.4
24	0.29	1.76	81	-5.6	7.29	2.0	38.3	2.9
30	0.29	1.69	80	-5.8	9.12	2.0	34.9	2.7
5.1 kW extra electric heat and 0.39 to 0.47 kg/h water injection								
6	0.43	3.31	72	-5.2	2.75	67.9	81.7	6.3
8	0.45	2.43	73	-6.3	3.71	13.7	72.6	5.6
12	0.47	2.41	72	-6.4	5.84	12.7	60.1	4.7
16	0.41	2.15	70	-7.3	6.86	12.3	51.6	4.1
24	0.39	2.66	69	-7.6	9.74	30.7	44.5	3.4
30	0.41	2.65	64	-8.5	12.77	46.3	41.8	3.2

[1] excluding defrost periods [2] prior to defrost [3] equivalent for a 48 hour period

Table 2: The effect of defrost frequency on defrost efficiency, defrost heat load and overall refrigeration system energy use.

Defrost Interval (hrs)	Water Input Rate (kg/h)	Defrost Efficiency (%)	Av. Defrost Heat Load (W)	Ratio of Defrost to Total Heat Load (%)	Overall Refrig. System Energy[3] (kWh)
3.1 kW extra electric heat and 0.29 to 0.31 kg/h water injection					
6	0.29	23	91	2.2	139.6
8	0.30	29	69	1.7	140.4
12	0.31	37	50	1.2	139.0
16	0.31	41	43	1.1	137.4
24	0.29	46	32	0.8	138.0
30	0.29	48	30	0.7	140.6
5.1 kW extra electric heat and 0.39 to 0.47 kg/h water injection					
6	0.43	31	93	1.5	172.1
8	0.45	35	77	1.3	166.7
12	0.47	45	55	0.9	163.4
16	0.41	45	48	0.8	164.1
24	0.39	52	34	0.6	161.5
30	0.41	57	29	0.5	159.8

[3] equivalent for a 48 hour period

5. REFERENCES

1. ASHRAE 2002. *ASHRAE Handbook - Refrigeration*. ASHRAE. Atlanta. Georgia.
2. Cleland, A.C., Cleland, D.J. 2004. *Cost-Effective Refrigeration*. Massey University. Palmerston North. New Zealand.
3. Cleland, D.J., O'Hagan, A.N. 2003. Performance of an air-cooling coil under frosting conditions. *ASHRAE Trans.*, Vol. 109 (1) 243-250.

4. Cole. R.A. 1989. Refrigeration heat loads in a freezer due to hot gas defrost and their associated costs. *ASHRAE Trans.* Vol. 95(2): 1149-1154.
5. Crawford. R.R., Mavec. J.P., Cole. R.A. 1992. Literature survey on recommended procedures for the selection, placement and type of evaporators for refrigerated warehouses. *ASHRAE Trans.* Vol. 89(1) 500-513.
6. Kondepudi. S.N., O'Neal. D.L. 1993a. Performance of finned tube heat exchangers under frosting conditions: I. Simulation Model. *Int. J. Refrig.* **16**: 175-180
7. Kondepudi. S.N., O'Neal. D.L. 1993b. Performance of finned tube heat exchangers under frosting conditions: II. Comparison of experimental data with model. *Int. J. Refrig.* **16**: 181-184.
8. Le Gall. R., Grillot. J.M. & Jallut. C. 1997. Modelling of frost growth and densification. *Int. J. Heat Mass Transfer* Vol. 40: 3177-3187.
9. Machielsen. C.H.M., Kerschbaumer. H.G. 1989. Influence of frost formation and defrosting on the performance of air coolers: standards and dimensionless coefficients for the system designer. *Int. J. Refrig.* Vol. 12: 283-290.
10. Mago. P., Sherif. S.A. 2005. Coil frosting and defrosting issues at low freezer temperatures near saturation conditions. *ASHRAE Trans.*, Vol. 111(1). Paper 4742.
11. Smith. G.R. 1989. Theoretical cooling coil calculations at freezer temperatures to avoid unfavourable frost. *ASHRAE Trans.* Vol. 95(2): 1138-1148.
12. Stoecker. W.F. Lux. J.J., Kooy. R.J. 1983. Energy considerations in hot-gas defrosting of industrial refrigeration coils. *ASHRAE Trans.* Vol. 89(2): 549-568.
13. Tassou. S. A., Datta. D. 1998. Frost formation and demand defrost of display cabinet evaporators. *Proceedings Refrigeration Science and Technology*, Vol. 1998-6: 626-632.

ACKNOWLEDGEMENTS

The support of the New Zealand Foundation of Research Science and Technology through research contract MAUX0213 is gratefully acknowledged.

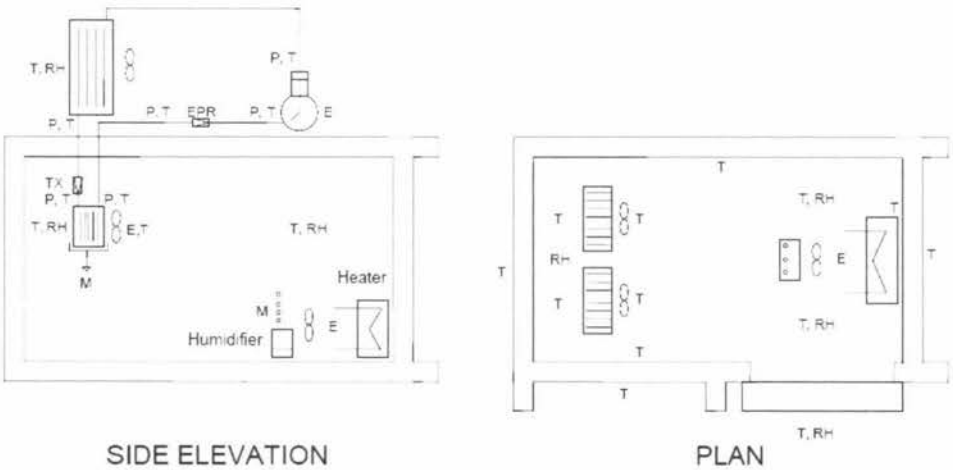

Figure 1: Schematic diagram showing the side elevation and a plan view of the small walk-in cool store that was monitored during normal operation and defrost cycles. Temperature (T), RH, pressure (P), energy use (E) and mass (M) measurement positions are indicated.

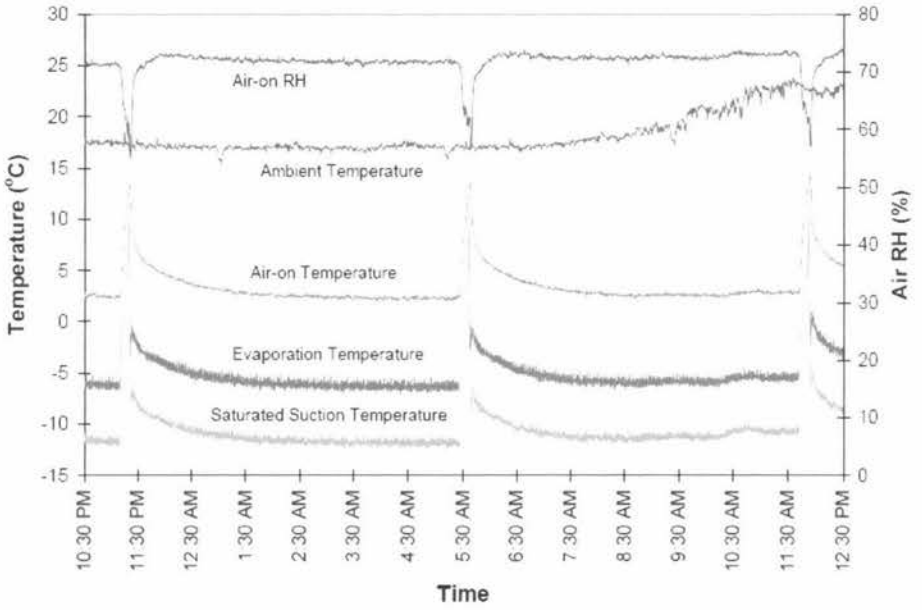

Figure 2: Measured ambient air, coil air-on, refrigerant evaporation and compressor saturated suction temperatures and air-on RH for a small walk-in cool store with a 6 hour defrost interval, 5.1 kW of extra electric heat and 0.43 kg/h of water injection.

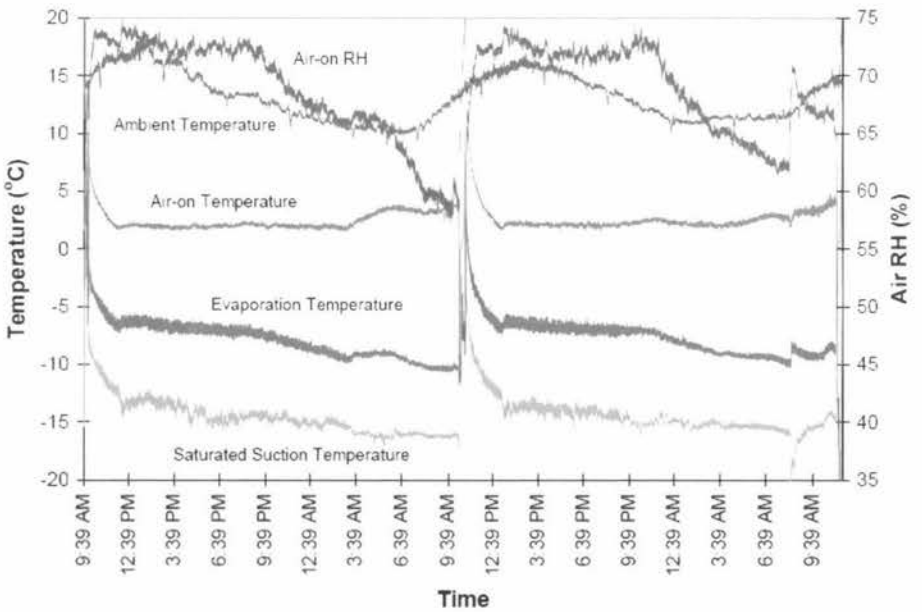

Figure 3: Measured ambient air, coil air-on, refrigerant evaporation and compressor saturated suction temperatures and air-on RH for a small walk-in cool store with a 24 hour defrost interval, 5.1 kW of extra electric heat and 0.39 kg/h of water injection.

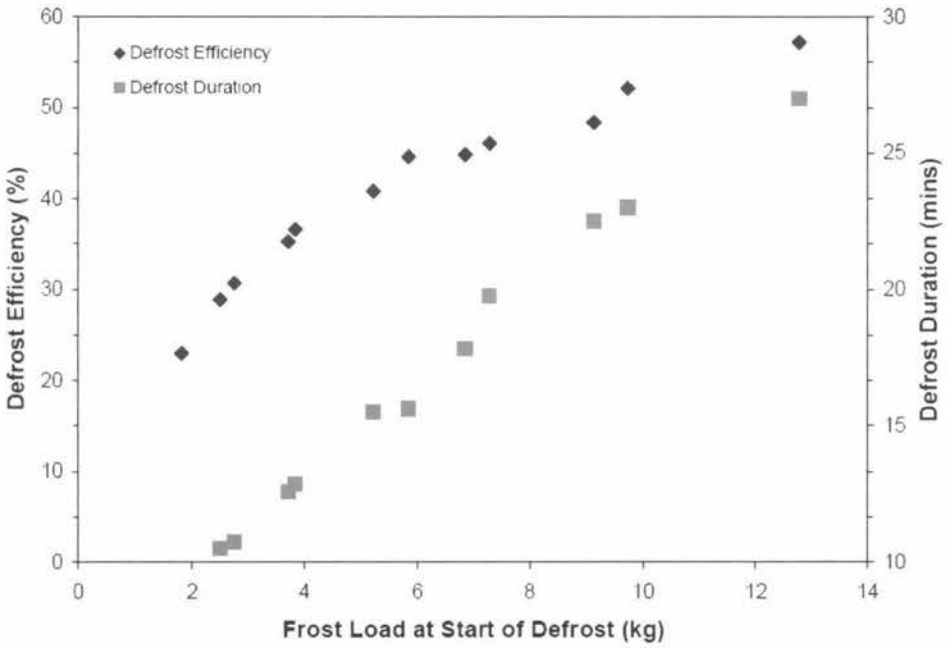

Figure 4: Effect of frost load at the onset of defrost on defrost efficiency and defrost duration.